International
Progress Report

IPR-06-10

Äspö Hard Rock Laboratory

Temperature Buffer Test

Evaluation modeling – Field test

Edited by

Mattias Åkesson
Clay Technology AB

March 2006

Svensk Kärnbränslehantering AB
Swedish Nuclear Fuel
and Waste Management Co
Box 5864
SE-102 40 Stockholm Sweden
Tel 08-459 84 00
+46 8 459 84 00
Fax 08-661 57 19
+46 8 661 57 19

Äspö Hard Rock
Laboratory

Report no.
IPR-06-10
Author
Mattias Åkesson
Checked by
Bertrand Vignal
Approved
Anders Sjöland

No.
F12K
Date
March 2006
Date
April 2006
Date
2006-08-15

Äspö Hard Rock Laboratory

Temperature Buffer Test

Evaluation modeling – Field test

Edited by

Mattias Åkesson
Clay Technology AB

March 2006

Keywords: Buffer, Bentonite, THM, Modeling, Full scale, Test, Temperature, Hydration, Stress, Strain

Résumé

TBT (Test de Barrière ouvragée en Température) est un projet mené dans le Hard Rock Laboratory d'Äspö en Suède par SKB et l'ANDRA, soutenu par ENRESA et DBE, qui vise à comprendre et modéliser le comportement thermo-hydro-mécanique de barrières ouvragées à base d'argile gonflante soumises à des températures élevées (> 100°C) pendant le processus de leur hydratation.

Depuis le début du projet, différentes tâches de modélisation ont été continûment développées. Les calculs de dimensionnement et les modélisations prédictives de la désaturation initiale du test *in situ* ont été antérieurement rapportés.

Le présent rapport traite de l'évaluation de la modélisation réalisée en 2004 qui a concerné deux tâches successives :

- I) l'effet d'un accroissement de la charge thermique de la sonde supérieure,
- II) la compréhension de l'évolution hydro-mécanique inattendue observée dans la bentonite autour de la sonde chauffante supérieure.

Les résultats de la première tâche indiquent qu'accroître la puissance de 1500 à 2250 W n'affecterait que modérément le processus d'hydratation. Ce fait et l'intérêt de conserver des conditions aux limites aussi stables que possible ont motivé la décision de ne pas accroître la puissance, comme envisagé.

Les résultats de la seconde tâche montrent que les évolutions inattendues observées, avec hausse des valeurs de succion et baisse des pressions totales, ont été la conséquence d'un manque temporaire d'alimentation en eau du filtre à sable (en périphérie de la bentonite).

Abstract

TBT (Temperature Buffer Test) is a joint project between SKB/ANDRA, supported by ENRESA and DBE, carried out in granitic rock at Äspö Hard Rock Laboratory, Sweden.

The test aims at understanding and modeling the thermo-hydro-mechanical behavior of buffers made of swelling clay exposed to high temperatures (over 100°C) during the water saturation process.

Since the beginning of the project, different modeling tasks have continuously been carried out. Previously, scoping design calculations and predictive modeling of initial field test desaturation have been reported.

The present report covers the evaluation modeling task carried out during 2004. Two issues were addressed within this framework:

- Step I. Analysis of effect of an increased heat load from upper heater.
- Step II. Evaluation of unexpected HM-trends around upper heater.

Results from the first task showed that a power increase from 1500 W to 2250 W would affect the hydration process to a minor extent only. This and the notion that boundary conditions should be kept as constant as possible motivated a decision not to increase the power.

Results from the second task showed that the deviating trends, with temporarily increasing suction values and decreasing stresses, were a consequence of a lack of water in the sand filter.

Sammanfattning

TBT (Temperature Buffer Test) är ett gemensamt SKB/ANDRA projekt, med deltagande av ENRESA och DBE, vilket utförs i granitiskt berg vid Äspö HRL i Sverige. Syftet är att öka förståelsen för, och att modellera, de termiska, hydrauliska och mekaniska processerna i en buffert av svällande lera som utsätts för höga temperaturer (över 100°C) under bevätningsfasen.

Olika modelleringsinsatser har utförts kontinuerligt sedan projektet startades. Tidigare har inledande beräkningar (scoping design) samt prediktiva modelleringar av den initiella uttorkningen rapporterats.

Den föreliggande rapporten omfattar utvärderingsmodelleringar utförda under 2004. Två frågor har behandlats inom denna ram:

- Steg I. Konsekvensanalys av en effektökning från den övre värmaren.
- Steg II. Utvärdering av oförutsedda HM-trender kring den övre värmaren.

Resultat från den första insatsen visade att en effektökning från 1500 W till 2250 W endast skulle påverka hydratiseringsprocessen i en begränsad omfattning. Tillsammans med uppfattningen om att randvillkoren skall hållas konstanta motiverade detta ett beslut om att inte genomföra den tänkta effektökningen

Resultaten från den andra insatsen visade att de avvikande trenderna, med tillfälligt ökande suction-värden och minskande spänningar, orsakades av ett underskott på vatten i sandfiltret.

Contents

1 Introduction and background

TBT (Temperature Buffer Test) is a joint project between SKB/ANDRA, supported by ENRESA and DBE, carried out in granitic rock at Äspö Hard Rock Laboratory, Sweden.

The test aims at understanding and modeling the thermo-hydro-mechanical behavior of buffers made of swelling clay exposed to high temperatures (over 100°C) during the water saturation process.

Two identical canisters (each 3 m long, 0.6 m diameter) and their bentonite buffer material are stacked in an 8 meters deep and 1.8 m diameter deposition hole, confined by a plug on top.

- The lower canister is directly surrounded by a bentonite buffer.
- Around the upper canister, an annular sand shield is placed between the canister and the bentonite buffer (composite barrier).

The sand shield will reduce the temperature to which the bentonite will be exposed. Without the sand shield, the bentonite will be exposed to temperatures well over 100°C.

Both options are tried in the TBT experiment.

The test started in March 2003, with heating of each canister using internally-located electric heaters set to 1500 W power output and implementing of an artificial wetting of the clay using a pressurized water source.

Prior to test initiation, a Predictive Modeling Program was specified and a number of modeling teams made blind predictions based on the specifications in that program. The results are found are in a predictive modeling report (Hökmark, 2005).

For ANDRA, the main concern is to improve the understanding of engineered barrier THM behavior under high temperature conditions. For the evaluation modeling phase there are the following general objectives:

1. Improve the fit between calculations and measurements by considering the present-day experiment status, new or updated information regarding material properties, boundary conditions etc.
2. Apply the updated, or improved, modeling approach to a case in which a significant change is done to the experimental conditions. This means that a new set of blind predictions shall be made. The change done to the test is suggested to be an increase of the power of the upper heater.
3. Based on the outcome of the improved simulations and blind predictions, evaluate relevance and discuss the relevance and validity of the conceptual models used in the numerical representation.

The *first step* in this evaluation modeling phase addressed the possible effects of 750 W power increase of the upper heater, tentatively scheduled for June 2004 (day 433). Of particular interest was the question whether or not the bentonite surrounding the sand-shield would dehydrate when subjected to elevated temperatures and heat fluxes. This task was thus of a predictive character, corresponding to the second point above.

Since the models showed that the saturation process wouldn't be reversed with the suggested power increase, this option was abandoned. Instead, in the *second step* of the evaluation modeling phase, the focus shifted to hydro-mechanical issues. In particular, the unexpected evolution of suction and stress in the bentonite surrounding the sand-shield in the upper part of the experiment was addressed. This task was thus of an improving character, corresponding to the first point above.

2 Step I – Analysis of effect of an increased heat load

The task addressed the possible effects of a 750 W power increase of the upper heater. A modeling program (Appendix Ia) was distributed in March 2004. Contributions were presented in May 2004 from UPC (Appendix Ib) and ClayTech (Appendix Ic).

Calculations were made for two different schemes of overheating for the upper heater. In both cases, the overheating was supposed to start at day 433 (June 2004) from 1500 W, and increasing thereafter up to 2250 W. In the slow case, the increase was made during a period of 30 days, whereas in the rapid case, the increase was made in 6 days.

Both UPC and ClayTech used Code_Bright and large quasi-3D thermo-hydraulic models for the problem. The geometries are shown in Figure 1. It can be noted that the geometry employed by UPC was significantly larger that the ClayTech geometry, incorporating rock well above the level of the tunnel floor.

The boundary conditions and the material properties used in the models displayed many similarities, although some significant differences existed. For instance, the retention properties of the sand were in the ClayTech model approx. one order of magnitude lower than in the UPC model, which implied that the sand tended to be very dry in the ClayTech case. This in turn, led to a lower thermal conductivity.

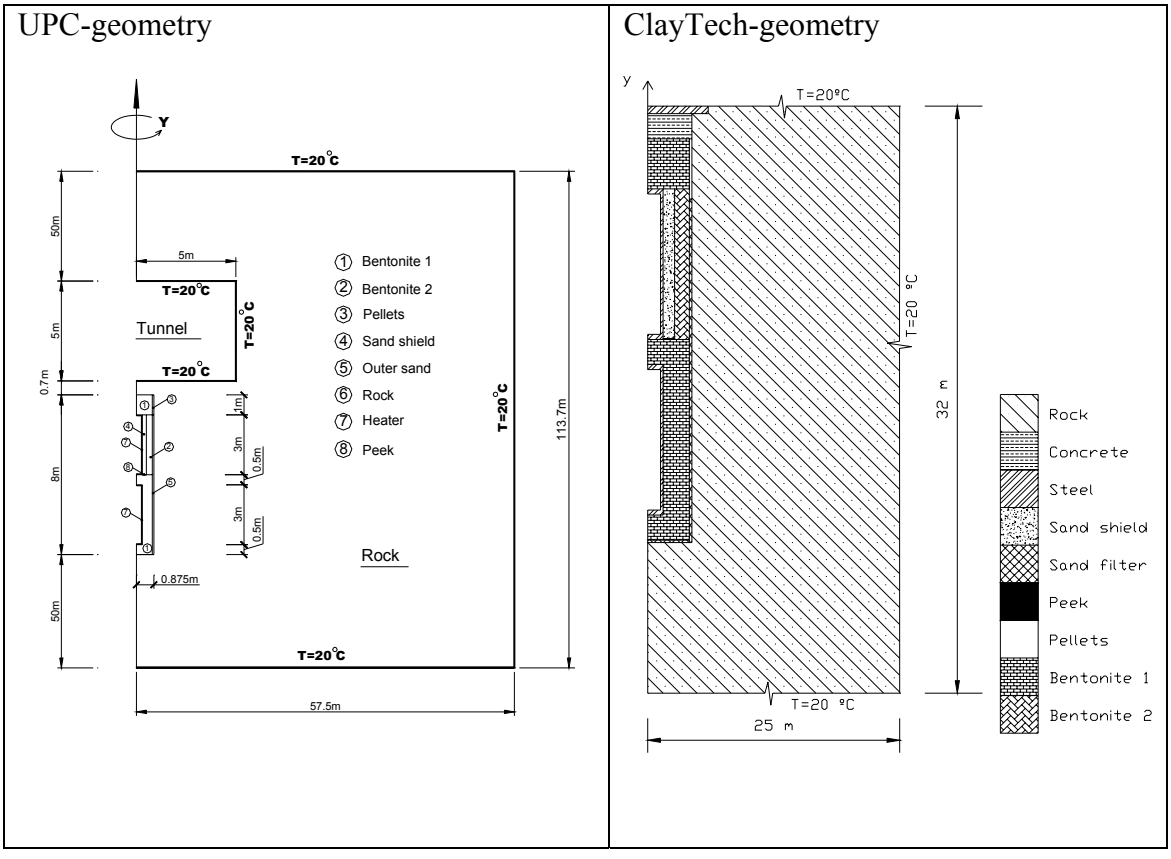

Figure 1. *Model geometries.*

From this it can be expected that the temperature at the surface of the upper heater would be higher in the ClayTech model than in the UPC model. Details of the models are given in the appendices.

Results were presented for a number of scan-lines, parameters and moments in time. The most important are shown in Figure 2 below. These are radial scan-line for the mid-height section around the upper heater regarding temperature and degree of saturation. The results shown are for the rapid heating scheme. It can be noted for both models that the overheating would lead to a higher temperature level, but with a negligible impact on the saturation of the bentonite buffer. Both models displayed quite different temperature level, which can be explained by the differences in the thermal conductivities of the sand.

Due to the low impact of the overheating scheme on the saturation process, it was decided to abandon the option of overheating.

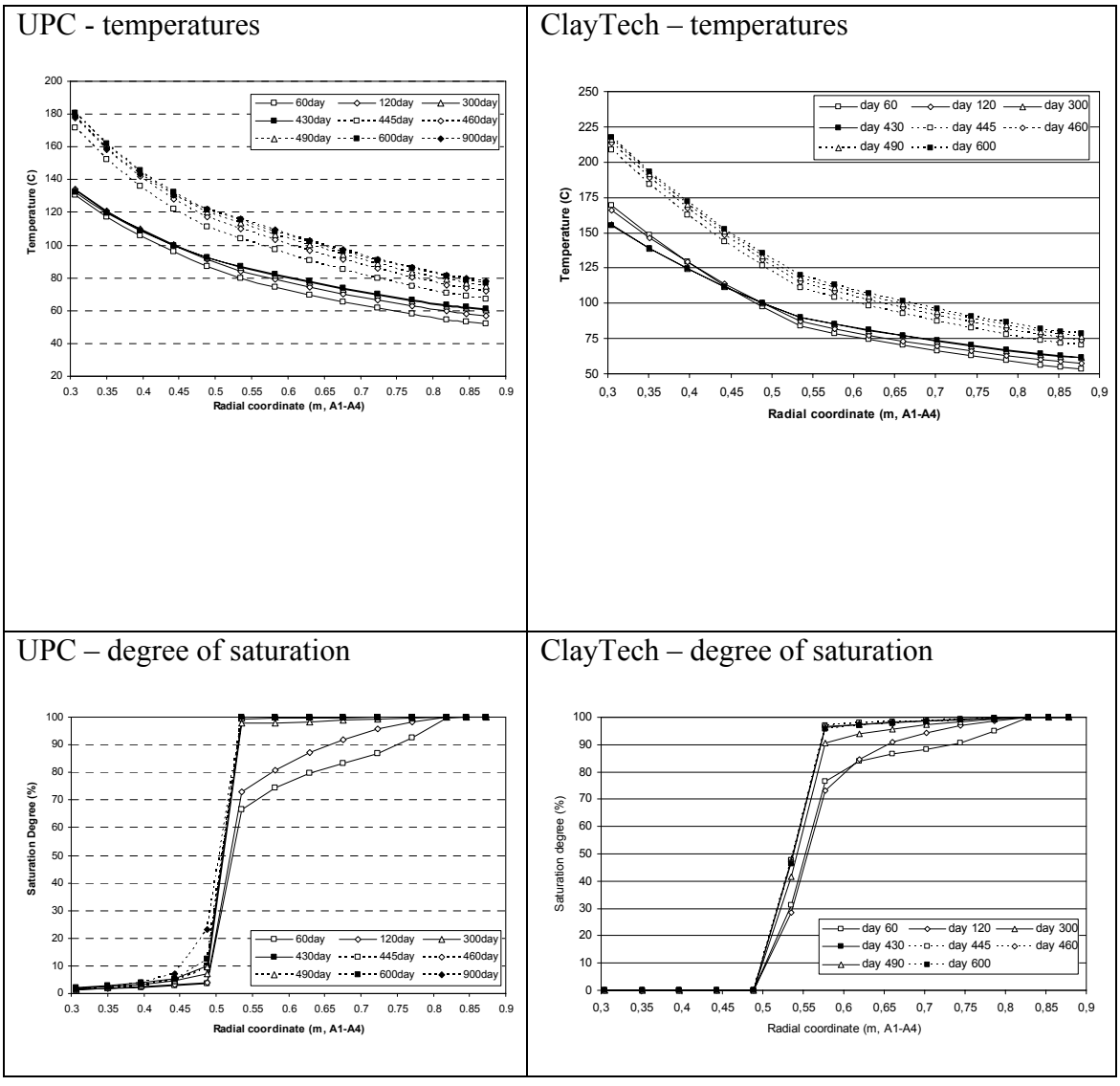

Figure 2. *Model results of temperature and saturation degree for a rapid heating scheme.*

3 Step II – Evaluation of unexpected HM-trends

The task addressed the hydro-mechanical developments around the upper heater, and aimed at explaining the unexpected trends observed in this part.

A modeling program (Appendix IIa) was distributed in August 2004. Contributions were presented in December 2004 from UPC (Appendix IIb) and ClayTech (Appendix IIc). The UPC team elaborated their model a bit further during the following year. Their updated contribution is included in this report.

Both UPC and ClayTech used Code_Bright for their work. The geometry of the UPC model was identical to the model used in Step I. ClayTech, on the other hand, used smaller geometries covering only a 1D section around upper heater (see Figure 3).

UPC presented results for three cases, all fully coupled THM models. The main difference between the cases was the implementation of the hydraulic boundary conditions (BC). In case 1, the BC followed the experimental water inflow, while in case II, the BC followed the experimental injection pressure. The third case was a combination of the previous two approaches, with a transition from flow BC to pressure BC at day 456.[1]

ClayTech presented results for seven models, both HM and TH models, but no fully coupled THM model. The hydraulic boundary condition were handled as a constant atmospheric liquid pressure from day 36 and onwards, except for an intermediary period, between day 234 and day 373, during which the pressure were set to either -45 or -8 MPa. One TH model was treated as hydraulically closed during this period. Otherwise, the models differed with respect to different mechanical properties and the temperature level of the HM models.

Details of the models are given in the appendices.

Results were presented for a number of history-graphs, scan-lines and parameters. The most important are shown in Figure 4 and 5 below. In the first one, the developments of stresses at the sensor positions in Ring 9 are compared with the experimental results. In the second figure, model suction values are compared with experimental results from Ring 10. Both UPC and ClayTech results are shown.

[1] It should be noted that pressure sensors were installed for each individual injection point at day 562. Prior to that day, there are no reliable data for the actual pressure in the sand filter, since the filter tips of the injection points appear to have developed a significant flow resistance.

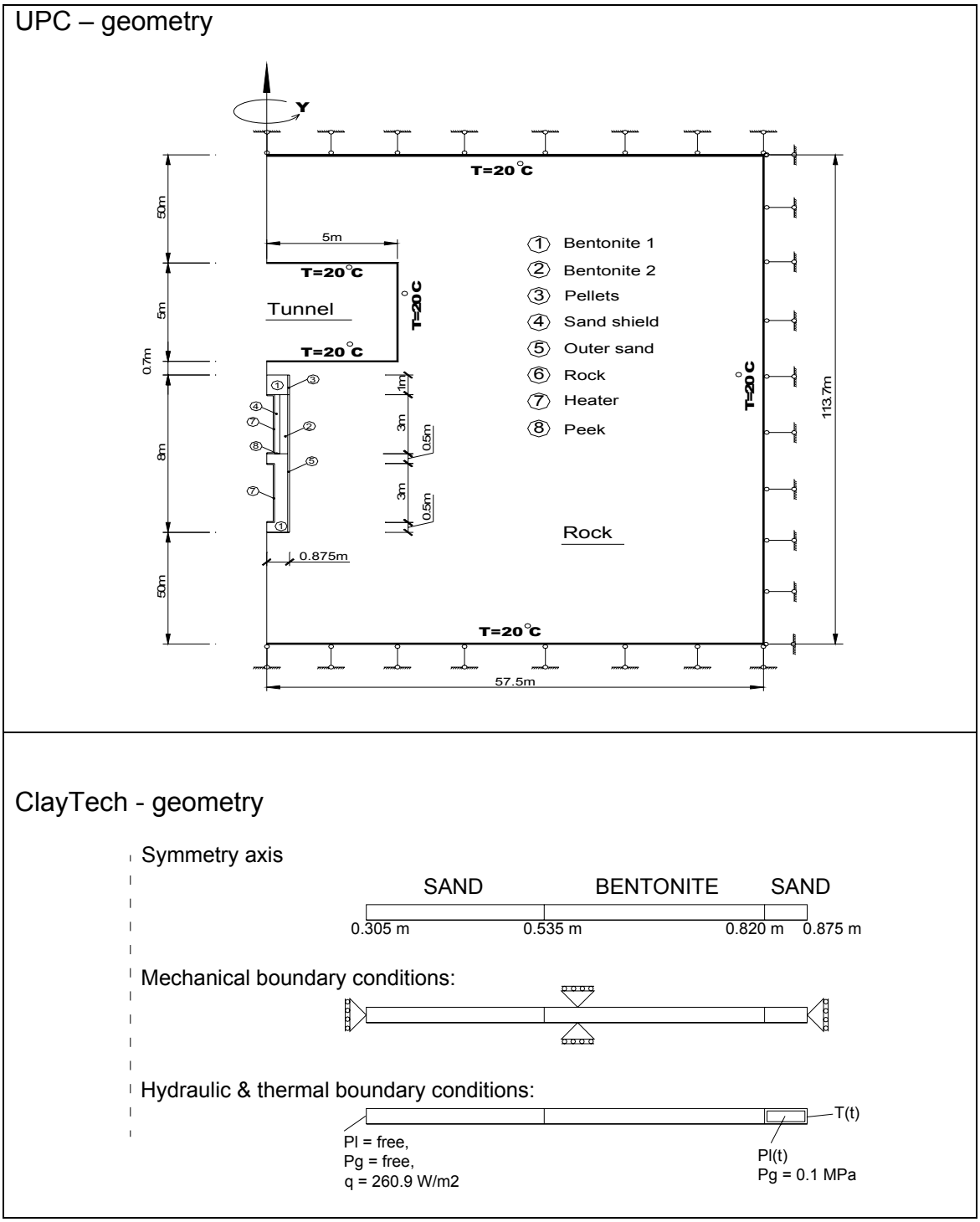

Figure 3. *Model geometries.*

UPC – radial stresses

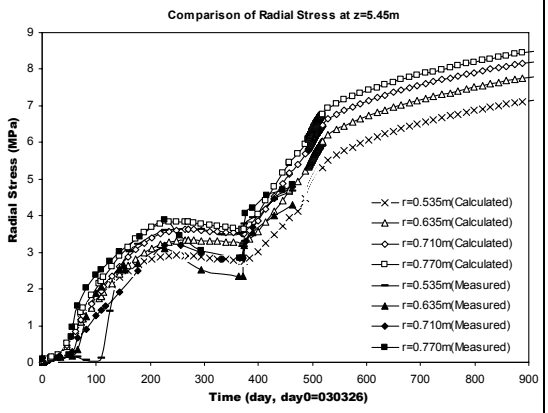

ClayTech – radial stresses

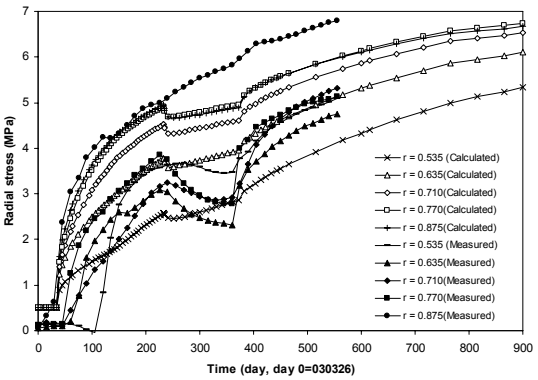

UPC – axial stresses

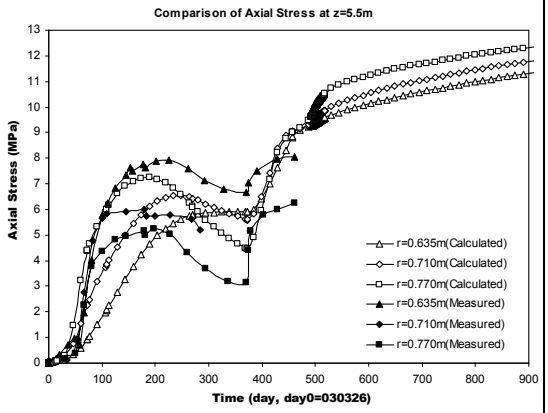

ClayTech – axial stresses

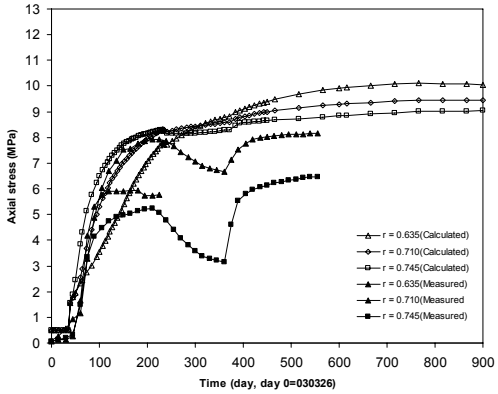

UPC – tangential stresses

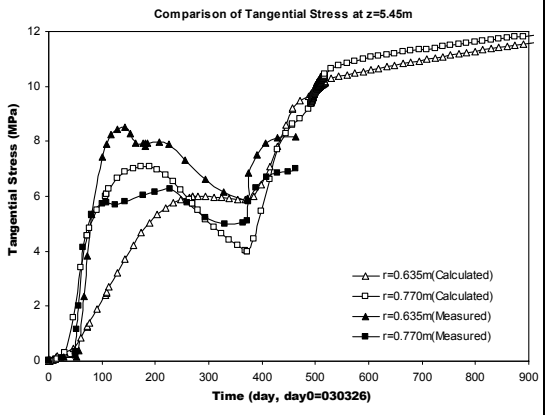

ClayTech – tangential stresses

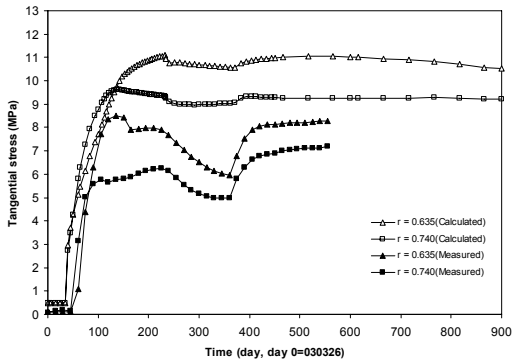

Figure 4. *Model results of stresses (UPC: Case 3; ClayTech: Model No3).*

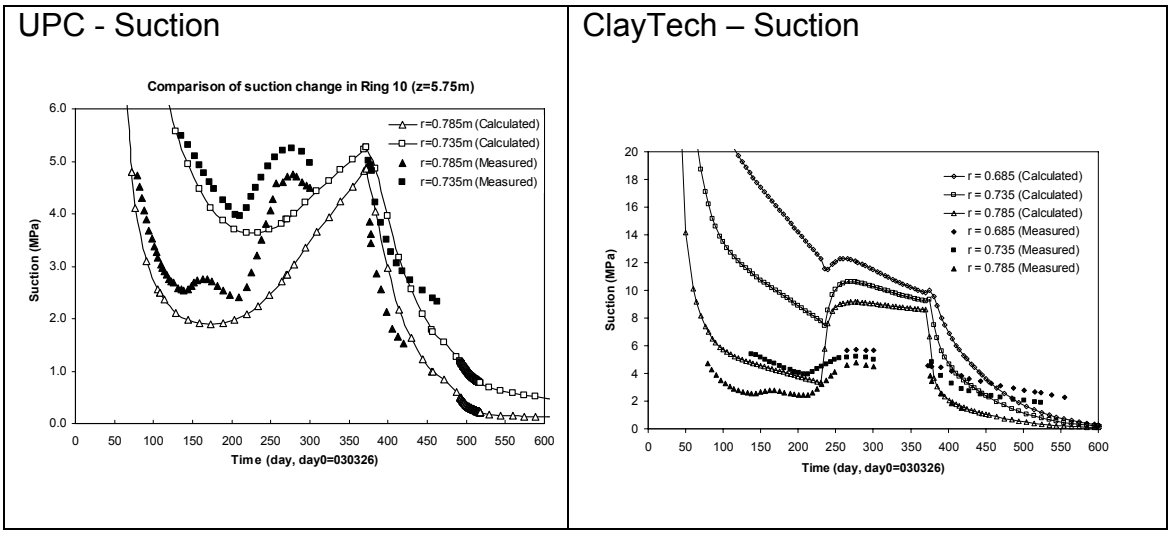

Figure 5. *Model results of suction (UPC: Case 3; ClayTech: Model No4).*

Both the UPC and the ClayTech models captured the general trends well. The UPC model was especially successful in reproducing the intermediary disturbance, while the ClayTech boundary conditions may have been too simplistic. The ClayTech description of the bentonite mechanical behavior managed nevertheless to capture the plastic shear strains that appear to have occurred during the initial phase.

Both models imply that the stress/suction disturbance was a consequence of an insufficient supply of water. The results don't lend support to the alternative explanation that the disturbance was triggered by a mechanical phenomenon which in turn affected the hydrodynamic conditions.

Clay Technology AB

Ideon Research Center

Lund, Sweden

TBT - Evaluation Modeling Program

March 2004

Harald Hökmark

Billy Fälth

Mattias Åkesson

Contents

1 TBT experiment

ANDRA is performing a Temperature Buffer Test in granitic rock at Äspö Hard Rock Laboratory, Sweden. The overall objective of the experiment is to investigate how well the bentonite buffer can endure the high temperatures expected to be found around Vitrified Waste canisters of about 0.6 m diameter, deposited in pits of about 1.8 m diameter and with bentonite buffer material in the annular space between canister and pit walls. For the Vitrified Waste concept, two possibilities are considered by ANDRA:

- Composite barrier with sand shield between canister and bentonite buffer
- Bentonite buffer only.

The sand shield will reduce the temperature to which the bentonite will be exposed. Without the sand shield, the bentonite will be exposed to temperatures well over 100°C.

Both options are tried in the TBT experiment. A drawing of the experiment set-up is provided in Figure 1.

After completion of the experiment, the bentonite will be sampled and its status analyzed with respect to mineralogical alterations and changes in rheological properties. To be able to do a fair evaluation of the effects of a realistic thermal shock, it is essential that the temperature is sufficiently high during the experiment and that, at the end of the experiment, the bentonite will have reached a high degree of saturation in all parts, also in the hottest ones.

To ensure that the temperature condition above will be met, a target temperature of about 100° at 0.5 m radius has been specified for the experiment. The power output of the two heaters was dimensioned to meet that condition. To meet the saturation condition, arrangements for artificial groundwater pressurization were made.

The experiment includes an extensive instrumentation to monitor temperatures, total pressures, pore pressures, relative humidities, etc. /Goudarzi et al., 2003/.

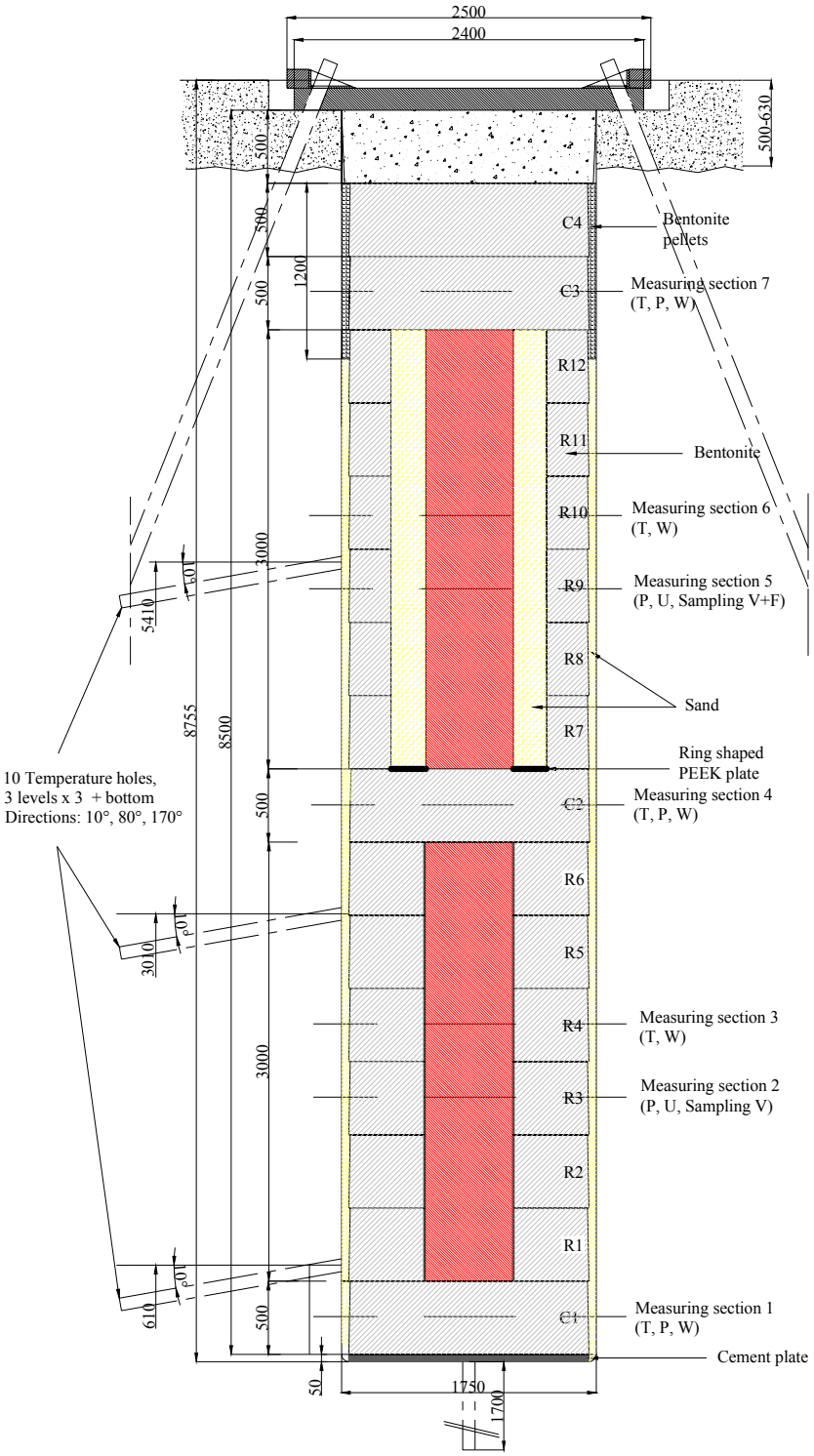

Figure 1-1. *TBT experiment set-up. T= temperature (thermocouples); P = total pressure (radial, tangential and axial stress); W = RH (capacity sensors and psychrometers); U = pore pressure (including option to sample gas or fluid).*

2 Predictive modeling phase

The experiment (heat generation) started in March 2003 and has been producing data for about 1 year up to the present day. Prior to test start, a Predictive Modeling Program was specified /Hökmark and Fälth, 2002/. A number of modeling teams made blind predictions based on the specifications in that program. The results are found are in a predictive modeling report.

A preliminary comparison between a selection of predicted results and corresponding measured values was compiled for the Sitges Workshop on large-scale field experiments in granite, November 2003 /Hökmark, 2003/.

Some reflections were:

- After 200 days there is a systematic dehydration of the inner, hottest part of the bentonite surrounding the lower heater. That dehydration took place soon after test start. During the period of time being covered in the compilation, there were little or no signs of resaturation of that inner part.
- For the bentonite surrounding the sand-shield around the upper heater and for the bentonite at radial distances larger than 0.2 m from the lower heater surface, the state of saturation seemed less clear. The slope of the thermal gradients, which were minutely recorded at mid-height of the two heaters, did not appear to change much after the initial moisture redistribution, which could be interpreted as no or very slow changes in the state of saturation. On the other hand, the RH readings suggested that there were changes, at least around the upper heater.

The comparison of modeling results seemed to point to the possibility that the assumptions made regarding gas escape or gas confinement could be part of the explanation for the differences found regarding the extent of dehydration. The gas escape issue (and the role of gas pressures in general) is consequently an area that needs more attention in the future, in particular for systems where high temperatures are expected.

3 Overview of results

3.1 General

All instrument readings up to February 20 are shown graphically in Appendix 1 in the format used in the sensor data reports (e.g. Goudarzi et al., 2003). Figure numbers with a leading 'A' (Axx) given here refer to that appendix.

3.2 Total inflow of water

The sand filter was filled through four tubes ending at the bottom of the sand filter. The accumulated water inflow up to day 82 was measured to 1.165 m^3 and from day 50 and onwards, the pressure in these tubes was measured to 0.8 MPa (Figure A1). However, that pressure was not effective continuously, but dropped to zero in periods. At day 82, water began to flow through tubes connecting the uppermost parts of the sand filter with the atmosphere, indicating that the sand filter was filled after about 80 days. At present (March 2004) approximately 1.3 m^3 has been injected into the system. During the first 75 days the inflow was about $1.7 \cdot 10^{-7}$ m^3/s. After 100 days the inflow had dropped to about $9.5 \cdot 10^{-9}$ m^3/s. Table 3-1 shows the inflow data and the average hydraulic conductivity of the sand filter, calculated assuming the pressure drop to be uniformly distributed over the height of the column. Table 3-2 shows the pore space available at the beginning of the test and the space remaining now (March 2004).

Table 3-1: Total inflow rate and estimated average sand filter conductivity

Time period	Total inflow [m^3/s] (from Fig A1)		Apparent sand filter conductivity [m/s]
Day 0- 75	$1.7 \cdot 10^{-7}$	(average)	$1 \cdot 10^{-7}$ (at the end of the period)
Day 100 and onwards	$9.5 \cdot 10^{-9}$	(when pressure was effective)	$5 \cdot 10^{-9}$
	0	(when pressure was zero)	
Lab data, compressed filter sand			$5 \cdot 10^{-7}$

The apparent sand filter conductivity at test start was only 20 % percent of the lab value, probably because of flow restrictions around the filter tips. In the period between 75 and 100 days, the apparent hydraulic conductivity decreased by a factor of about 20. The reason may be sand filter compression combined with bentonite intrusion and/or clogging of the filter tips.

Table 3-2: TBT Pore space

	Available at test start [m3]		Injected water [m3]	Remaining [m3]
Sand filter	0.77		0.77	0.00
Pellets filling	0.24	1.38	0.53	0.85
Bentonite	1.08			
Heater/bentonite clearance	0.06			
Sand shield	0.55		0.00	0.55
Total	2.70		1.30	1.40

3.3 Temperatures

Temperatures are monitored by use of thermocouples in three cylinders (Cyl 1, 2 and 3) and two rings (Ring 4 and 10), cf. Fig. 1-1. In addition, temperature readings are provided by the capacity RH sensors (Figure A21-A26). In general, the temperature results exhibit regular trends up to maximum values after about 200 days (Figure A2 – A10). A few exceptions have occurred for inner parts in Cyl 2 and the inner sand shield at Ring 10, where the maximum temperatures were reached after only about 40 and 60 days, respectively (Figure A6 – A7).

A minor temperature decrease has also been recorded at the innermost points in these sections. Similar trends are found on the heater surfaces and in the interior of the heaters. For the upper heater the trend is very clear (Figure A19 – A20) and can be explained by the delayed wetting of the upper parts of the sand filter (not completed until after 80 days). The gentle decrease in heater temperature after completion of the sand filter saturation may be due to compression of the sand shield and following increase in sand shield thermal conductivity. Details in these trends may be due to successive and slow changes in the heat flow organization around the heaters.

The temperature readings are compiled in table 3-3 below. It can be noted that the highest temperatures in the bentonite blocks are found in Ring 4, whereas the lowest can be found in Cyl 3. It should also be noted that the 120° isotherm appears to narrow in between the heaters in Cyl 2.

Table 3-3: Temperature distribution (°C) at day 295.

Radius (mm):	150	200	250	300	350	400	450	500	550	600	650	700
Cyl 3	52				49	48	47	46	45	44	43	42
Ring10					137	120	**110**	**98**	**89**	**83**	78	74
Cyl 2	120				**109**	**104**	**98**	**90**	**88**	**82**	79	75
Ring 4					125	**119**	**108**	**103**	**95**	**92**	**86**	**81**
Cyl 1	**113**				**92**	**87**	**82**	76	72	68	65	62

Legend: < 80° | 80 - 100° | 100-120° | >120°

The TBT experiment is located 6 m from the CRT experiment. The latter was initiated approximately 850 days before the start of the TBT experiment and has therefore affected the surrounding rock temperature. In general, recorded temperatures in the rock follow the same trend as in the bentonite blocks, but on a lower level (Figure A11 – A14). A compilation of the initial and the recently measured temperatures at different levels, depths and azimuths is presented in table 3-4 below. It can be noted that the current rock surface temperatures towards the CRT (Az 10°) are 5°C higher than the corresponding temperatures on the opposite side (Az 170°). The initial difference was not more than 3°C.

Table 3-4: Rock temperatures at the walls of the experiment hole

Time (d)	Level (m)	Temp.(°C) - rock surface Az:10°	Az:170°	Temp.(°C) - 1,5 m in rock Az:10°	Az:170°
0	5,41	21	19	24	17
	3,01	22	19	26	18
	0,61	22	19	25	18
295	5,41	64	63	44	38
	3,01	71	66	47	40
	0,61	61	57	41	35

Azimuth 0° is towards the CRT experiment.

Sporadic irregularities in the temperature trends, especially around the lower heater, can be attributed to a number of power failures (Figure A15 – A16).

Figure 3-1 shows Azimuth 90° temperatures measured in Ring 4 and 10. The effect of the wetting of the sand filter outside Ring 10 is obvious: After 60 days the temperature drop across the filter disappeared.

Figure 3-2 and 3-3 below illustrate changes in apparent thermal conductivity. The results are based on the slopes of temperature-distance curves derived from thermocouple readings in rings 10 and 4 (Fig. 3-1), and on the assumption of a constant radial heat output at heater mid-height. There are systematic increases that indicate that saturation may be proceeding at a reasonably high rate (as opposed to the findings from the preliminary evaluation). This is consistent with Table 3-2, i.e. that the bentonite (blocks, canister/block clearance and pellet filling) has taken up about 40% of the amount required for full saturation. There is also an apparent increase in the sand shield conductivity, in particular in the period between 60 and 145 days.

Figs 3-2 and 3-3 should be interpreted with some caution: some of the changes may be due to variation of the mid-height heat flux, and some may be due to dislocation of individual sensors.

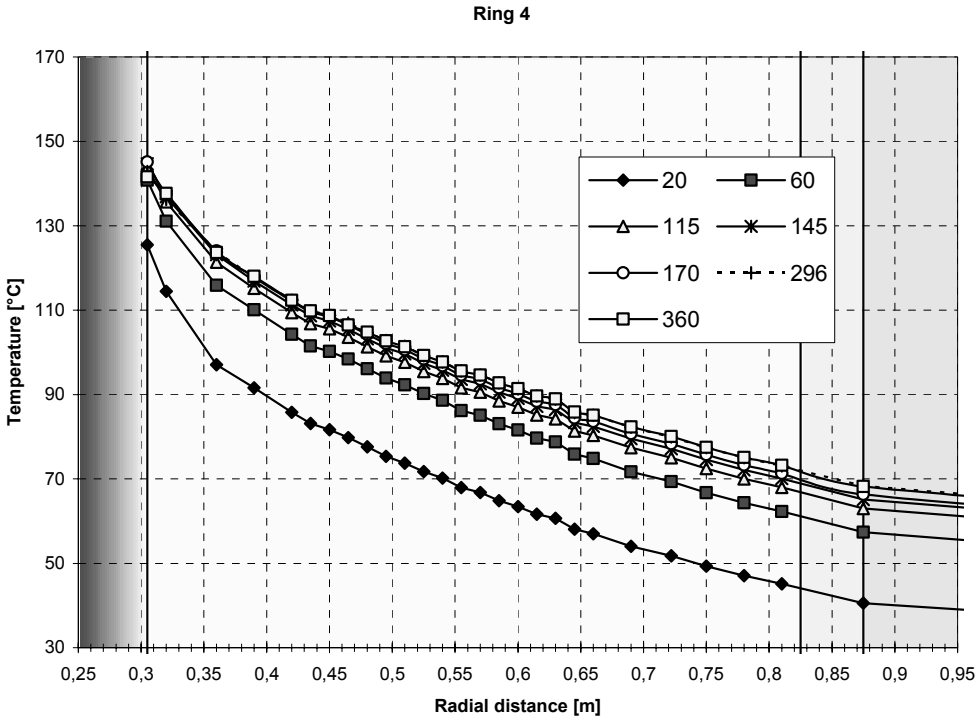

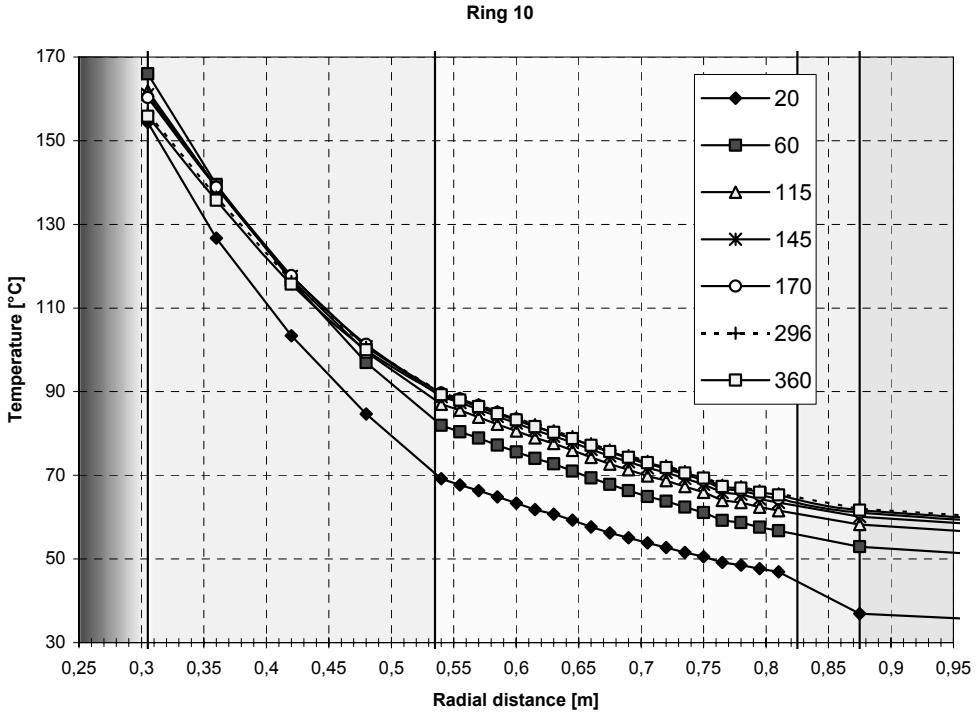

Figure 3-1. *Temperatures measured at mid-height of heater 1 (Ring 4) and heater 2 (Ring 10).*

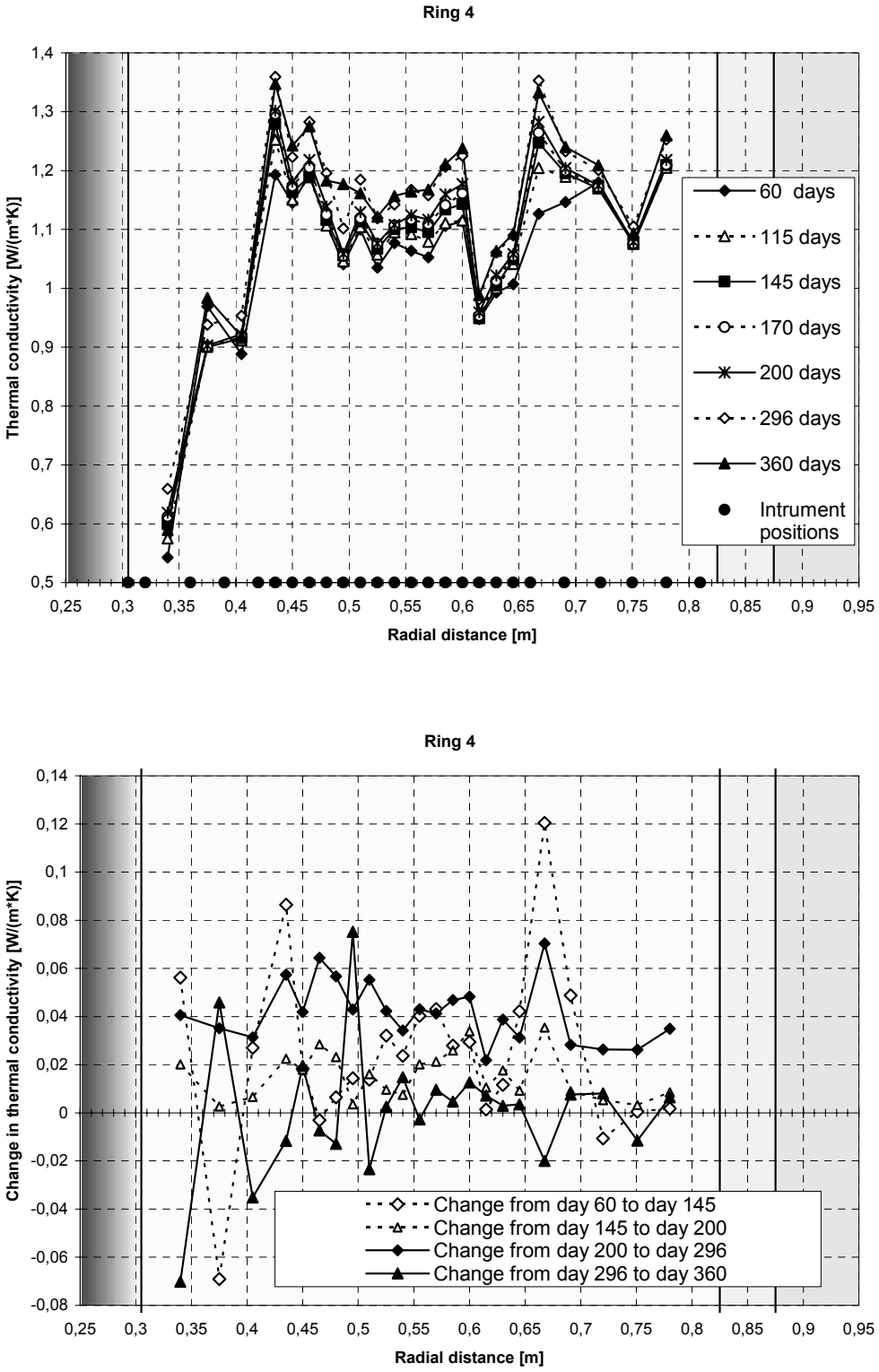

Figure 3-2. *Upper: Thermal conductivity in ring 4 as computed from slopes of distance-temperature relation. Lower: Change in thermal conductivity during four time intervals. Day 60 data are slightly affected by the transient heating effect.*

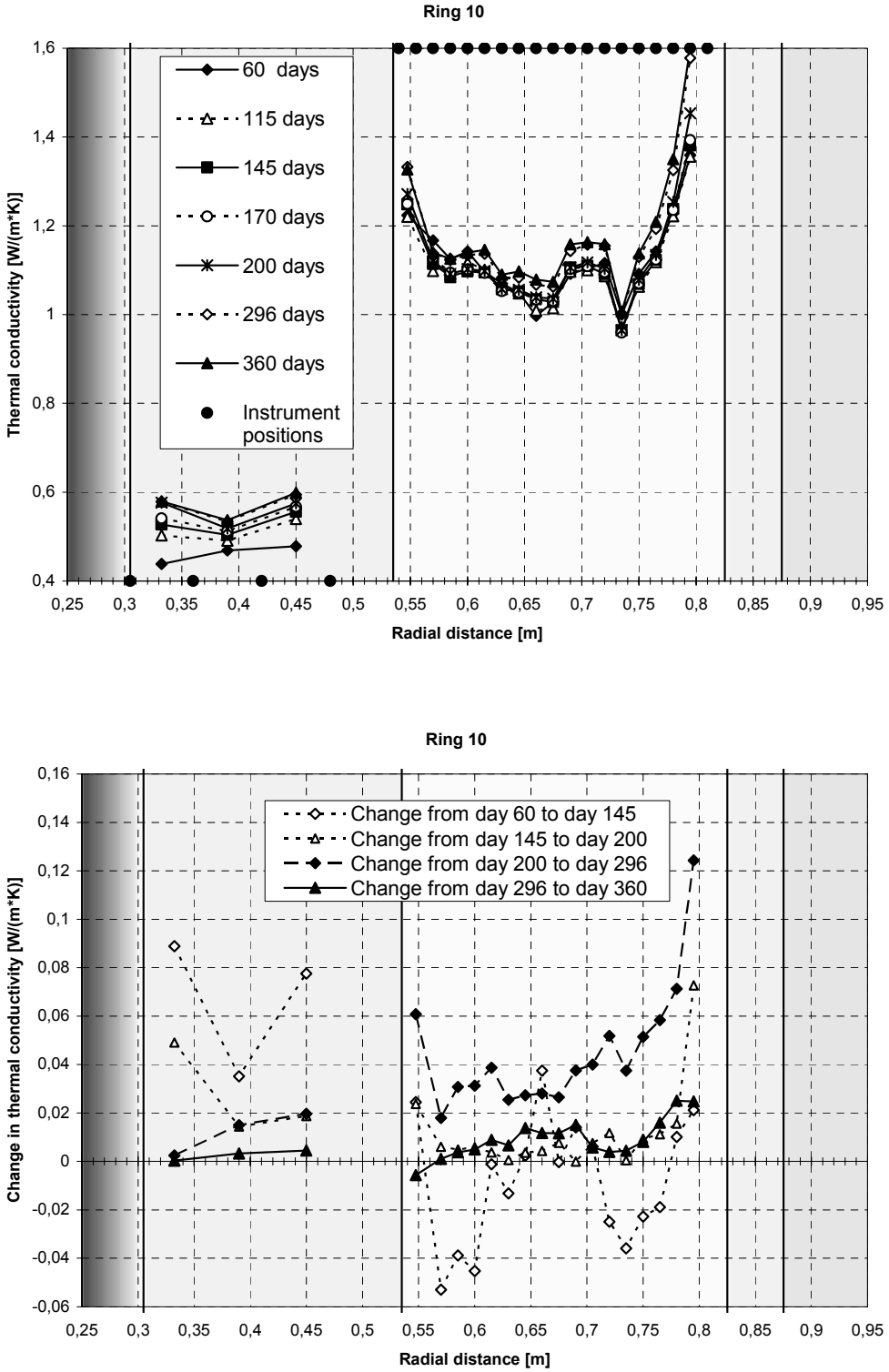

Figure 3-3. *Upper: Thermal conductivity in ring 10 and in sand shield as computed from slopes of distance- temperature relation. Lower: Change in thermal conductivity during four time intervals.*

3.4 Relative humidity/suction

Recorded RH values and suctions indicate that moisture contents generally increase: RH from 72 to maximum 100 % (Figure A21 – A26); suction between 6 and 2 MPa (Figure A27 – A31). A significant exception is the suction increase in Ring 10 at radius 785 and 735 mm after day 225 (Fig. A30). There are no indications that this suction increase is related to any changes in the water supply or to movement of water away from the sensors. Rather, the suction increase seems to be correlated to a general decrease in stresses in parts of Ring 9, probably triggered by an episode of vertical load transfer (for instance from the blocks to the sand shield). The suction increase would then be consistent with theories positing that stresses are traded for suction if the bentonite is not too far from saturation.

An indication of drying within 150 mm from the lower heater (Ring 4), measured by a RH sensor at radius 360 which failed around day 140 (Figure A22), has previously been derived through calculation of thermal conductivities (Figure 3-2, upper; /Sandén et al, 2003/).

A compilation of sensors indicating saturated conditions is presented in Table 3-5 below. They are arranged in time intervals. As can be noted, the minimum radius that has reached saturation so far is 635 mm (cf. the thermal conductivity plot in Figure 3-2, which shows a maximum just outside r = 0.65 m).

An observation that can be made is that Cyl 2, closely followed by Ring 4, seems to have gone through a rapid saturation of the outermost parts. The relatively fast saturation here may be an effect of vapor diffusing outwards from the hot, desaturated, parts close to the heater.

Table 3-5: Occurrence of saturation* in different sections.

Time interval from start (days):

	0 - 19	20 - 39	40 - 59	60 - 79	80 - 99	100 - 119	120 - 139	140 - 159	160 - 179	180 - 199	200 - 219	220 - 239	240 - 259	260 - 279
Cyl 3											W785			V785
Ring 10				W785 V785			W735			V685				W685
Ring 9														
Cyl 2		V785	W785						W635					
Ring 4		W785			W710 V710						W635			
Cyl 1				W785	V785									

* W = Wescor sensor generating data, indicating saturation > approx. 95%

V = Vaisala/Rotronic sensor indicating saturation (RH ≈ 100 %)

Number = Radius (mm)

3.5 Total pressure

Results from pressure monitoring are shown in Figures A32 – A40.

Figure 3-4 below shows the axial stress in different sections. Figure 3-5 shows the vertical buffer force transfer calculated by use of the measured axial stresses, assuming that the forces are transferred within a 0.275 m annular region just inside the sand filter. The total cable force is shown for comparison. The assumed annular force transfer area and the positions of the axial pressure transducers are shown in the right part.

The following can be observed:

- Although the annular transfer cross section area is probably underestimated rather than overestimated, the force transfer in the lower parts is significantly larger than the force taken up by the cables after 330 days. This indicates that the force balance is maintained by considerable shear stresses in the bentonite/sand filter interface.
- The increase in the cable forces was much more rapid than the pressure build-up in the bentonite. This is an effect of thermal volume expansion, in particular that of the two heaters: A 100°C temperature increase will result in about 7 mm increase in total heater length. Some of the axial heater expansion was probably absorbed by low-stiffness interfaces between cylinders and heaters, but some may have contributed to the straining of the cables, see Fig. A42. (The heater temperatures have increased by much more than 100°C, cf. Figs A19 and A20, but the increase relative to the rock is of that magnitude).
- Some 100 or 120 days after test start, the axial stress in Ring 9 did not increase any further. This seems to coincide with the appearance of radial stresses in the sand shield (Fig. A37). A possible explanation is that the buffer was successively plasticized as result of the change in properties following the wetting and that the plastication front reached the vicinity of the sand/buffer interface at this time. The failure of the bentonite block brought about an inward movement and established a supporting lateral pressure on the sand shield. (An attempt to model this in a very simplistic way is shown in Appendix 2.) The process may have transferred some of the axial forces from the buffer to the sand.
- After about 225 days, most stresses in Ring 9 began to decrease very significantly. A possible explanation is that there was an additional period of changes in the axial load transfer, perhaps triggered by further plastication. The change in axial stress found in Cylinder 3 after about 225 days may be correlated to this.
- There was a sudden (local) loss of axial stress in Cylinder 3 after about 80 days. This is probably an effect of brittle block failure. It could also be caused by a temporary malfunctioning of the total pressure sensor, as none of the two other sensors in Cylinder 3 indicated anything at that time.

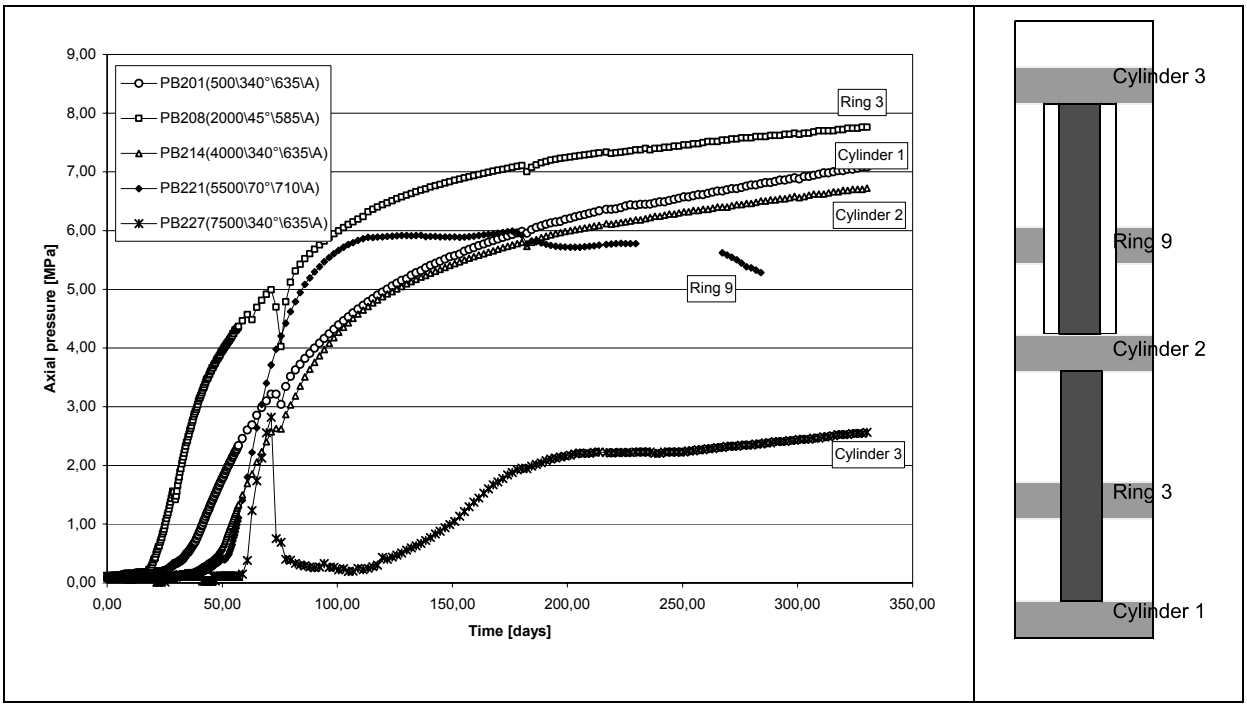

Figure 3-4. *Axial pressure measured in different sections*

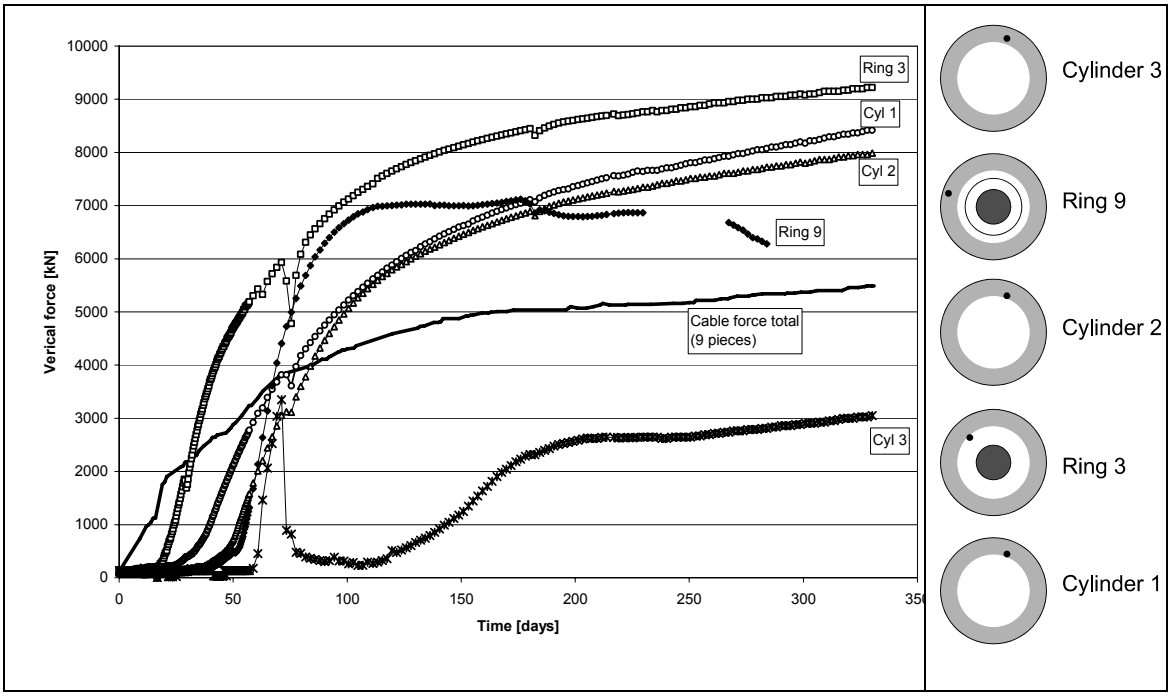

Figure 3-5. *Axial pressure measurement translated into vertical forces, assuming annular region shown to the right (grey-shaded) to be involved in force transfer. The black dots show the stress measurement positions.*

Figure 3-6 shows a schematic of the vertical forces acting on the package. The force balance seems to require that shear stresses in the periphery are significant. The pattern of the internal vertical force transfer is complicated and will vary over time as a result of creep movements in the peripheral parts (leading to reduced shear reactions), swelling, failure of individual blocks and temperature changes. Probably part of the variations in stress and suction readings is due to such changes in the axial force transfer, and not only to differences in wetting rate.

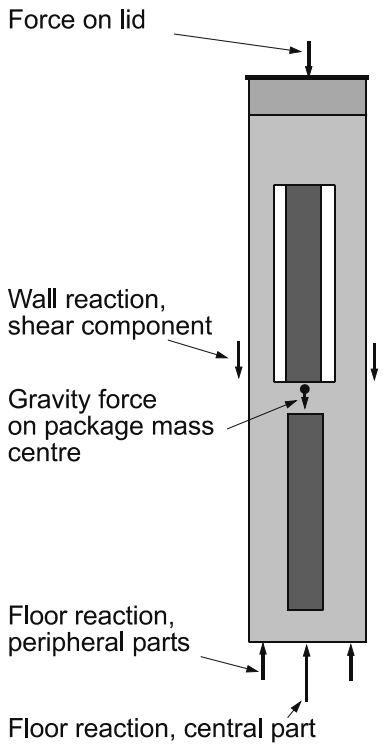

Up		Force [kN]
↑	Floor reaction, peripheral parts (estimated from cylinder 1 axial stress measurement, cf. Fig. 3-5)	8500
	Floor reaction, central part (should be high because of thermal heater expansion)	?
	Total	>>8500
Down		Force [kN]
↓	Force on lid (measured cable forces, cf. Fig. 3-5)	5500
	Gravity force (heaters, bentonite, sand, concrete plug, lid)	500
	Shear reaction	>>2500
	Total	>>8500

Figure 3-6. *Schematic of vertical forces acting on the package*

3.6 Pore pressure

There was no increase in pore pressure measured within the first 300 days of the experiment (Figure A43 - A44). This could indicate that the system is not gas-tight. However, the bentonite has not yet reached full saturation.

4 Evaluation modeling phase

For ANDRA, the main concern is to improve the understanding of engineered barrier THM behavior under high temperature conditions. For the evaluation modeling phase the objectives are to:

- Improve the fit between calculations and measurements by considering the present-day experiment status, new or updated information regarding material properties, boundary conditions etc.
- Apply the updated, or improved, modeling approach to a case in which a significant change is done to the experimental conditions. This means that a new set of blind predictions shall be made. The change done to the test is suggested to be an increase of the power of the upper heater.
- Based on the outcome of the improved simulations and blind predictions, evaluate relevance and discuss the relevance and validity of the conceptual models used in the numerical representation.

4.1 Present-day experiment status

The data obtained so far from the TBT experiment has given much information such that trends of the experiment now are visible, as shown in the previous chapter. However, the result and the trends are not easily interpreted. Some aspects of the development may be related to experimental conditions that result from unintended and/or stochastic processes or events.

4.2 New or updated information

4.2.1 Hydraulic boundary

4.2.1.1 From test start to the end of March 2004

The sand filter between bentonite cylinders/rings and rock was not filled completely with water until some 80 days after test start. It was necessary to apply a considerable pressure to inject water into the filter, while it was expected that the permeable sand should get saturated at a low (atmospheric) pressure and that it would be necessary to restrict the water supply in order to control the filling rate. It is not clear if the flow resistance is due to:

- clogging of the filters at the tips of the inflow pipes just above the bottom of the sand filter, or
- increase of flow resistance because of sand filter compression and/or bentonite intrusion.

Both processes could be responsible. The hydraulic conductivity of the sand filter can be approximated to $5 \cdot 10^{-7}$ m/s (lab value, c.f. Table 3-1) after compression from 1700 to 1870 kg/m^3 dry density. The left part of Fig. 4-1 shows results from an oedometer test of the sand filter material. It is not likely that the pressure exerted by the swelling bentonite blocks can have compressed the sand filter to much higher densities than that. Given the high fraction of fines in the sand (right part of Fig. 4-1), it does not seem likely that bentonite intrusion is an important process. Therefore the hypothesis of clogging around the filter tips is proposed as the main reason for the high flow resistance. This would mean that the boundary ground water pressure in the sand filter is low (approximately atmospheric) and fairly uniform along the height of the column.

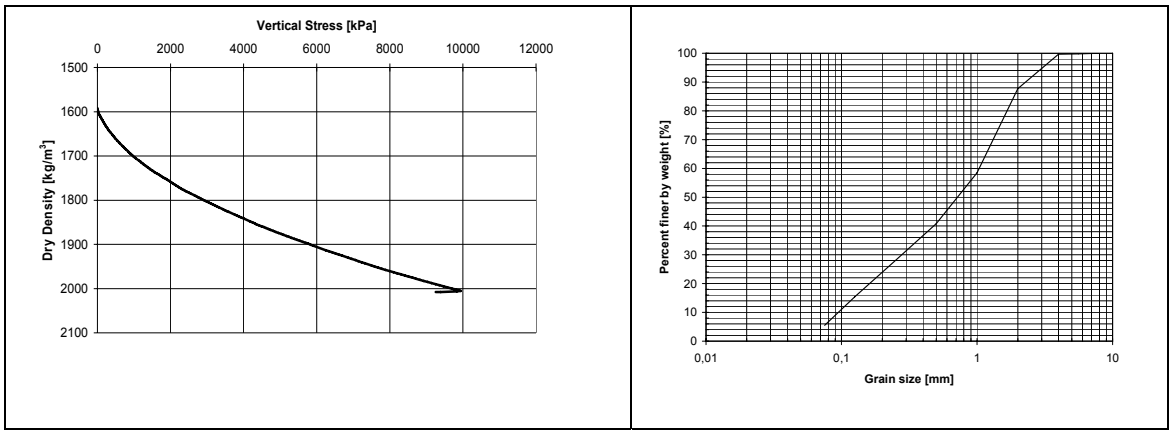

Figure 4-1. *Sand used in filter and shield. Left: compression test result. Right: grain size distribution.*

4.2.1.2 From April 2004 and onwards

From April 2004, water will be supplied to the tubes terminating in the upper parts of the sand filter. A small initial pressure will be applied, and then ramped to 0.8 MPa. The pressure ramping will be performed as gently as required to avoid sudden flow rate changes and piping. The details of the ramping scheme are not decided, but will have little importance to the modeling.

There are two reasons for this change:

- Reduce uncertainties regarding the hydraulic boundary pressure. It will be relevant to assume 0.8 MPa in the entire sand filter.
- Improve gas tightness of the system.

4.2.2 Pellets/sand filter

The sand/pellets interface is 200 mm below the top of Ring 12 (cf. Fig. 1-1). In the original design shown in the predictive modeling program, the pellet filling extended just to the top of Ring 12.

4.2.3 Rock heat conductivity

The rock heat conductivity specified in the predictive modeling program was 2.7 W/(m·K). That value should be reduced because of temperature dependence. Most crystalline rocks will loose about 0.1% of heat conductivity per °C /Kukkonen and Lindberg, 1995/. Therefore a more relevant value would be 2.6 W/(m·K) (cf. calculation example in next section).

4.2.4 Rock initial temperature

The initial temperature at the rock wall should be 20°C (c.f. Table 3-4) rather than the values suggested by the pre-test measurements presented in the predictive modeling program.

4.2.5 MX-80 thermo-hydraulic properties

New experiments on MX-80 bentonite have been performed by C. Gatabin, CEA /Gatabin and Robinet, 2003/. Two cylindrical bentonite samples, 200 mm in height and 200 mm in diameter, were confined in steel cells with fixed 20°C temperature at the top and variable temperature (22°C to 150°C) at the base.

The two samples, THM1G_Cell1 and THM1G_Cell2, had initial liquid saturations of 75.5% and 89.7%, respectively. Void ratios were 0.48 and 0.53. The cells were closed hydraulically, but not completely gas-tight. The temperature at the cell bases was increased from 22°C to 150°C in steps.

Figure 4-2 shows the relative humidity as function of distance from the heated base.

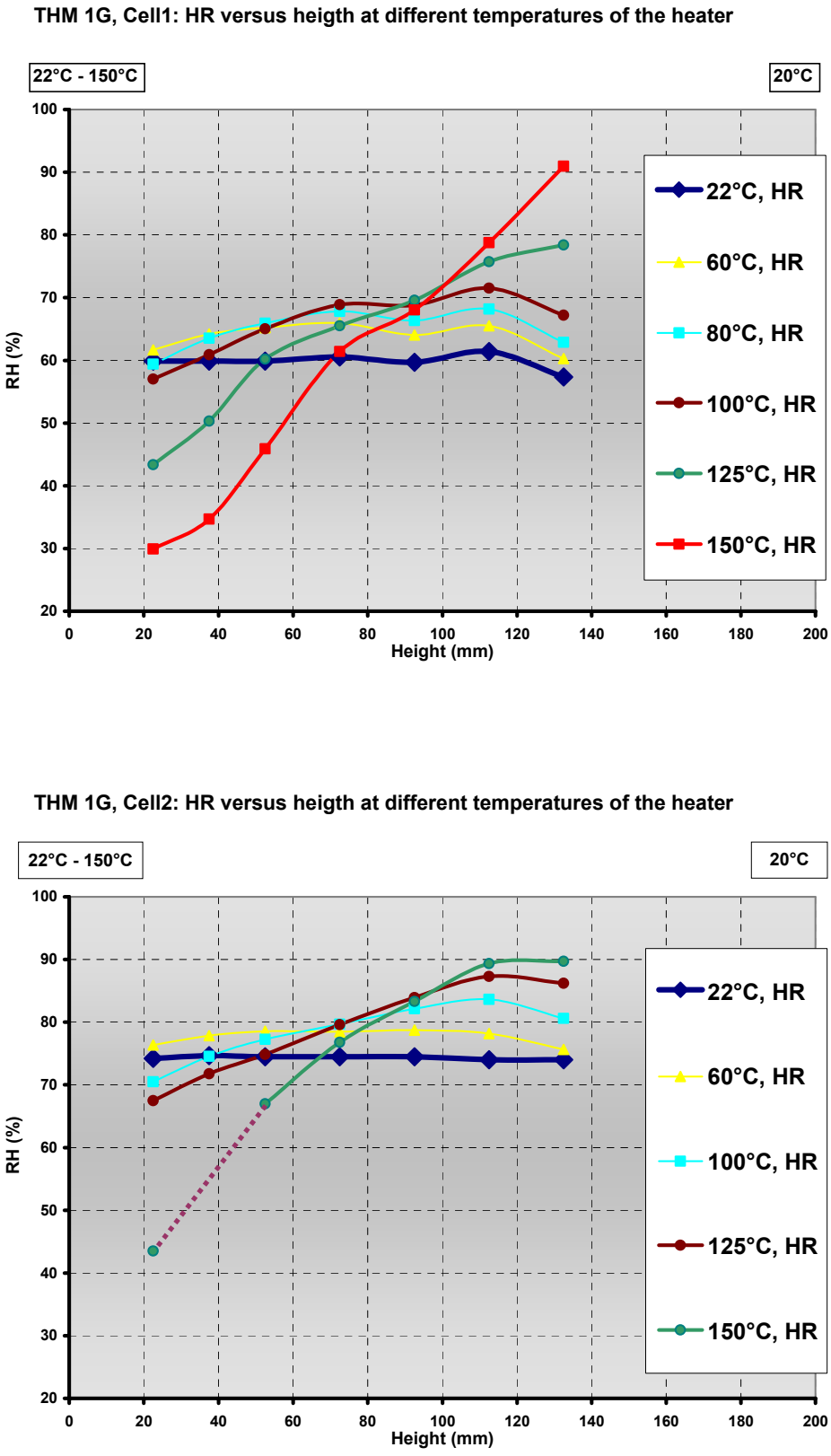

Figure 4-2: *Relative humidity as function of distance from the heated base. From /Gatabin and Robinet, 2003/.*

4.2.6 MX-80 Retention

Fig. 4-3 shows suction values based on work being conducted presently at Clay Technology. The new experimental data indicate that the suction is considerably higher than the values proposed in the predictive modeling program.

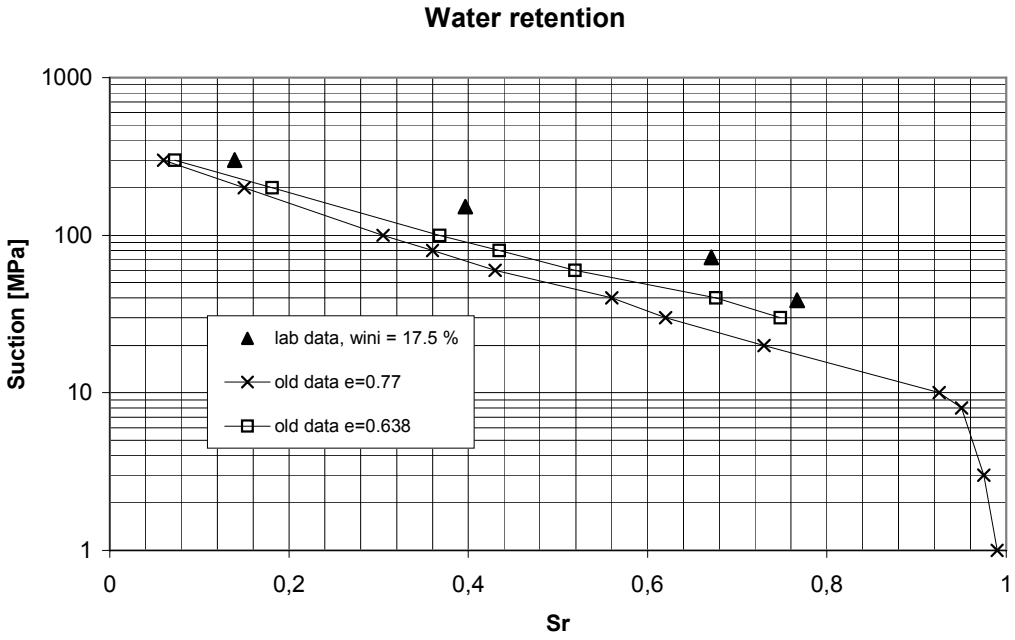

Figure 4-3: *Suction curves. "Old data e = 0.77" is the information given in the predictive modeling program for a void ratio of 0.77. "Old data e = 0.638" are these values translated to a relevant void ratio. Note that the translation is made only in saturation ranges where effects of swelling and confinement are small. The "lab data" are derived from measurements of suction as function of water ratio under un-confined conditions and have been converted here to apply for a void ratio of 0.638.*

4.2.7 Sand shield

In the predictive modeling program, the sand shield thermal conductivity was estimated to be 0.4 W/(m·K). The results obtained so far suggest that the conductivity is a higher: about 0.6 W/(m·K) (cf. Fig. 3-3).

In the predictive modeling program, the initial sand shield saturation was set at 3%. In reality, the sand was dried below that value. The resulting saturation was close to 0%.

4.3 Change in experimental conditions

The suggested course here is to increase the power of the upper heater. If the bentonite around the sand shield is exposed to high temperatures, similar to those now found in the bentonite around the lower heater, it will be possible to examine, for instance, the drying process further.

4.3.1 Estimate of effects on the temperature

An estimate of the thermal effects of a 750 W increase of Heater 2 power can be obtained using analytical line source solutions as shown in Fig. 4-4. The technique is described in the TBT design studies /Hökmark, 2001/. Figure 4-5 shows calculated and measured rock temperatures prior to the power increase. It appears that the rock conductivity should be set at 2.6 W/(m·K) rather than 2.7 W/(m·K) as suggested in the predictive modeling program. A probable reason is the temperature dependence of the rock thermal conductivity.

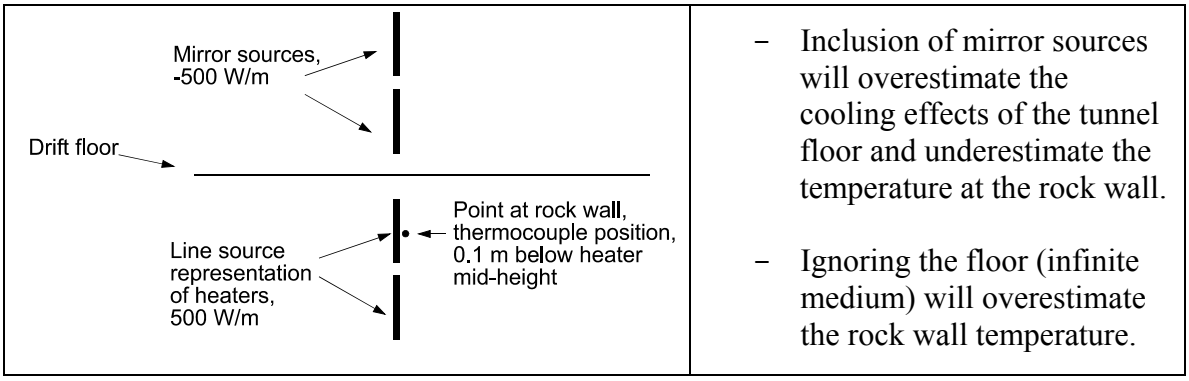

Figure 4-4. *Superposition of line sources to calculate rock wall temperature. The negative mirror sources are added to include effects of the tunnel floor.*

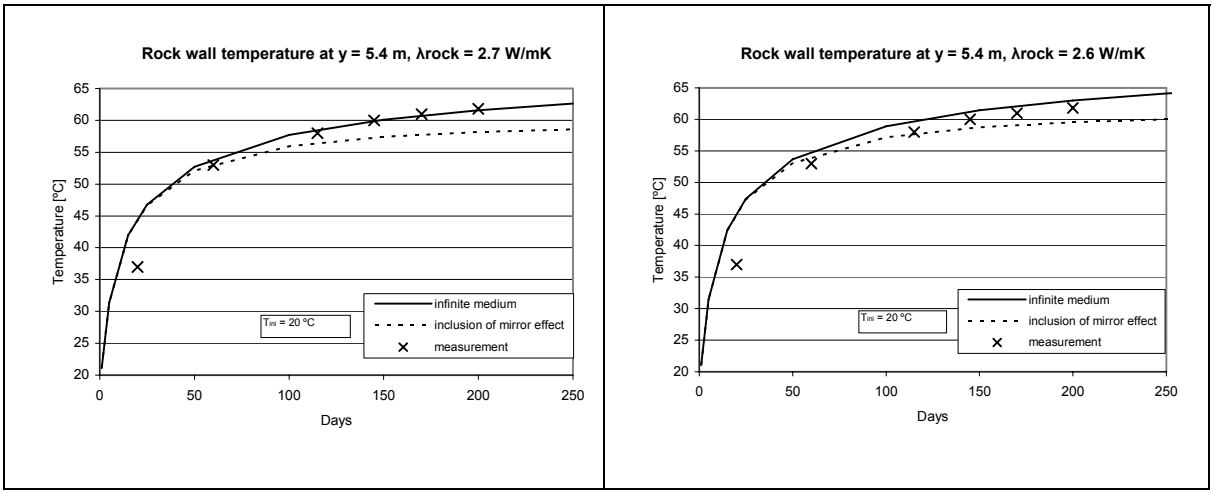

Figure 4-5. *Temperature at rock wall (position of thermocouple TR233) calculated by use of line source solution for two assumptions of the rock heat conductivity and assuming initial rock temperature to be 20 °C. The thermocouple readings are shown for comparison. The best fit (measured values intermediate to mirror source solution and infinite medium solution) is obtained assuming the rock conductivity to be 2.6 W/(mK).*

Figure 4-6 shows analytically calculated temperatures at two positions: at the level of measuring section 6 (Ring 10) and at heater mid-height. The results regard the case of a 750 W increase of the upper heater (lower heater kept at 1500 W). The results indicate that the 750 W power increase will give a temperature of about 120 - 125 °C at the sand/bentonite interface. At heater mid-height, the heater surface temperature will be close to the 225°C limit.

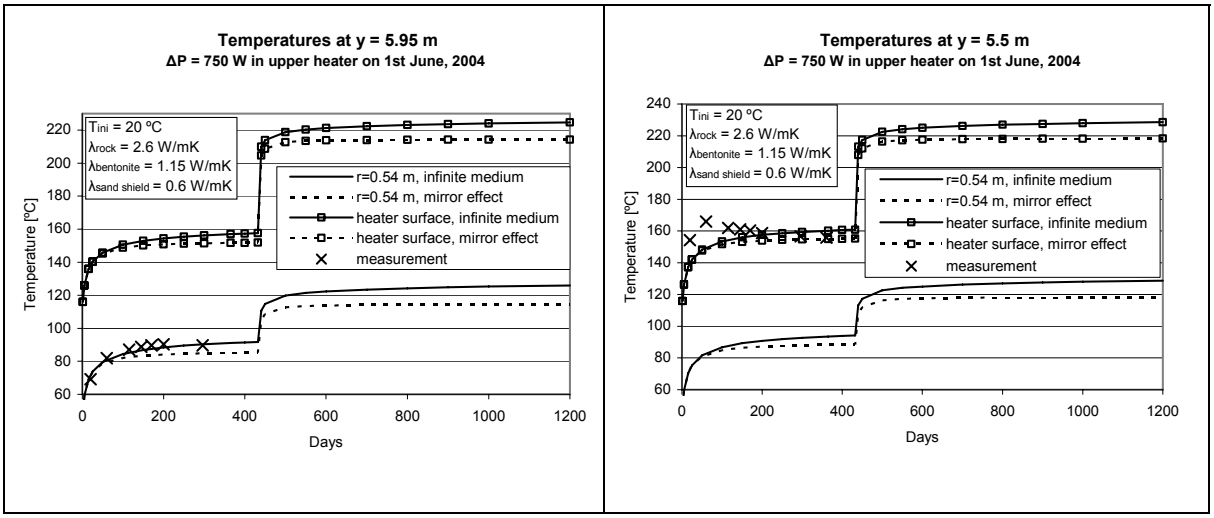

Figure 4-6. *Analytically calculated temperatures at the heater surface and at the sand/bentonite interface before and after 750 W increase of heater 2 power. Left: instrumented section in Ring 10. Right: Heater mid-height.*

4.3.2 Suggested course of action

Two different protocols of increasing the power from 1500 W up to 2250 W (canister surface temperature limited to 225 °C) are considered:

- A ‘sudden increase’ lasting 6 days, with 125 W power increase each day.
- A ‘step by step’ increase lasting 30 days, with 25 W increase each day.

Predictions of effects of both protocols should be modeled for mid-May. Depending on these prediction results, a procedure will be chosen and implemented from June 1, 2004.

The action suggested here, i.e. to increase the power of the upper heater only, will generate unbalance between the upper and lower parts of the experiment. This may well turn out to be an advantage: Around the lower heater the temperature will increase, but the radial thermal gradient at heater mid-height will change very little. This may give useful information on the relative importance of the thermal gradient and the absolute temperature level. The alternative, i.e. to increase the power of both heaters, would preserve some of the balance of the experiment, but not offer this opportunity. In addition, the bentonite temperatures around the lower heater would increase above levels that are relevant to repository concepts and, possibly, alter the bentonite material irreversibly such that subsequent sampling and testing may turn out to be inconclusive.

5 Modeling

5.1 General

The scan-lines referred to below are those defined in the predictive modeling program, i.e. according to Figure 5-1.

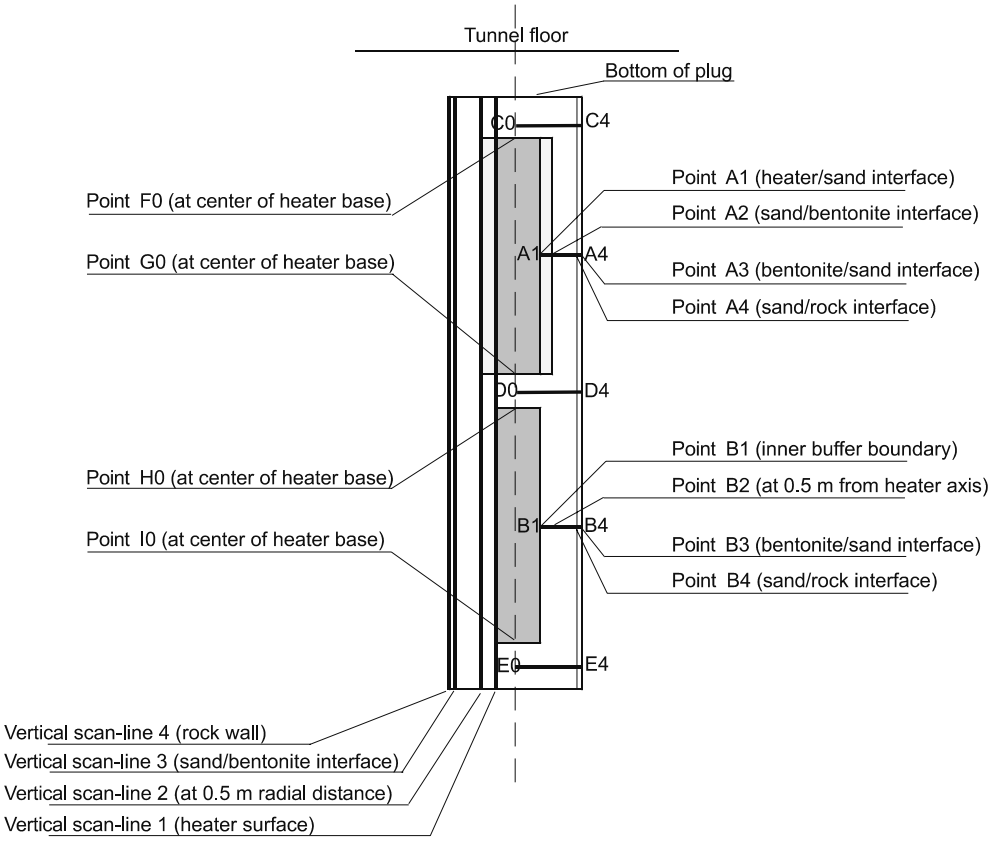

Figure 5-1. *Schematic of TBT with scan-lines.*

5.2 Program, 2004

The modeling will include elements of prediction as well as efforts to fit measured results. Below the term “prediction” is used for both. The following modeling program is proposed for 2004.

For mid-May 2004:

- Prediction of temperature, saturation, RH on scan-line A1-A4.
- Prediction of temperature, saturation, RH on scan-lines B1-B4 (2nd priority)
- Prediction of temperature on vertical scan-lines 1 (heater surface), 2 (at 0.535 m radial distance) and 4 (rock wall) (3rd priority).

For the mid-May predictions, the course of action suggested above should be assumed, which means ramping of heater 2 power from 1500 W to 2250 W by steps beginning June 1, 2004. Two cases are to be considered:

- 6 days power increase duration, with 125 W step each day,
- 30 days power increase duration, with 25 W step each day

The final decision on power changes and on details in the test control will be based on the outcome of the mid-May predictions. A complete modeling of the test should not be commenced until after these decisions are at hand. The complete modeling should be reported by the end of November 2004.

For the end of November 2004:

- Prediction of temperature, saturation, RH, porosity, stresses and displacements on scan-lines A1-A4, B1-B4, C0-C4, D0-D4 and E0-E4
- Prediction of temperature on vertical scan-lines 1 (heater surface), 2 (at 0.535 m radial distance) and 4 (rock wall)
- Prediction of accumulated total inflow vs. time
- Analysis of radial stress development in Ring 9
- Prediction of total cable force vs. time (2^{nd} priority)

The above points define the numerical output in a preliminary sense. Further precisions will be given an Addendum to the present program, scheduled to be issued late August 2004. The evaluation modeling work should result also in statements regarding the validity of the conceptual models used in the predictions, e.g. models used for heat and moisture transport in general and in the high temperature range in particular. The format for this part of the work will be proposed in the Addendum.

Scan-line output (mid-May predictions)

The test started on March 26, 2003. The power change is scheduled to begin June 1, 2004, i.e. 430 days after test start.

Results should be given for the following days after TBT start:

60, 120, 300, 430, 445, 460, 490, 600, and 900.

Scan-line output (end of November predictions)

The end of November time-table as well as the output format will be detailed in the late August Addendum.

References

Bäck R., 2004. Temperature Buffer Test. Report for retaining plug and anchoring. SKB IPR-02-64

Gatabin C., Robinet J-C, 2003. Mock-up for studying THM behaviour of swelling clay MX80 at temperature > 100°C. CEA/EuroGeomat

Goudarzi R., Börgesson L., Sandén T., Barcena I., 2003., 2004. Temperature Buffer Test. Sensors data report (Period 030326-031001). Report No:1. SKB IPR-04-02

Hökmark H, 2001. Test of vitrified wastes. Study 1 – thermal. One-dimensional radial heat flow in cavity interior. Clay Technology.

Hökmark H, 2003. Temperature Buffer Test – comparison of modeling results and experimental findings: causes of differences. Sitges Workshop on large-scale field experiments in granite. UPC, Barcelona.

Hökmark H., Fälth B., 2002. Predictive modeling Program,. Clay Technology

Kukkonen I., Lindberg A., 1995. Thermal conductivity of rocks at the TVO investigation sites Olkiluoto, Romuvara and Kievetty. Report YJT-95-08, Nuclear Waste Commission of Finnish Power Companies, Helsinki.

Sandén T., De Combarieu M., Hökmark H., 2003. Description of the instrumentation installed in Temperature Buffer Test. Sitges Workshop on large-scale field experiments in granite. UPC, Barcelona.

Thorsager P., 2002. Temperature Buffer Test. Detailed design materials. Foundation and artificial saturation. SKB IPR-02-62

Appendix 1 – Complete set of graphs

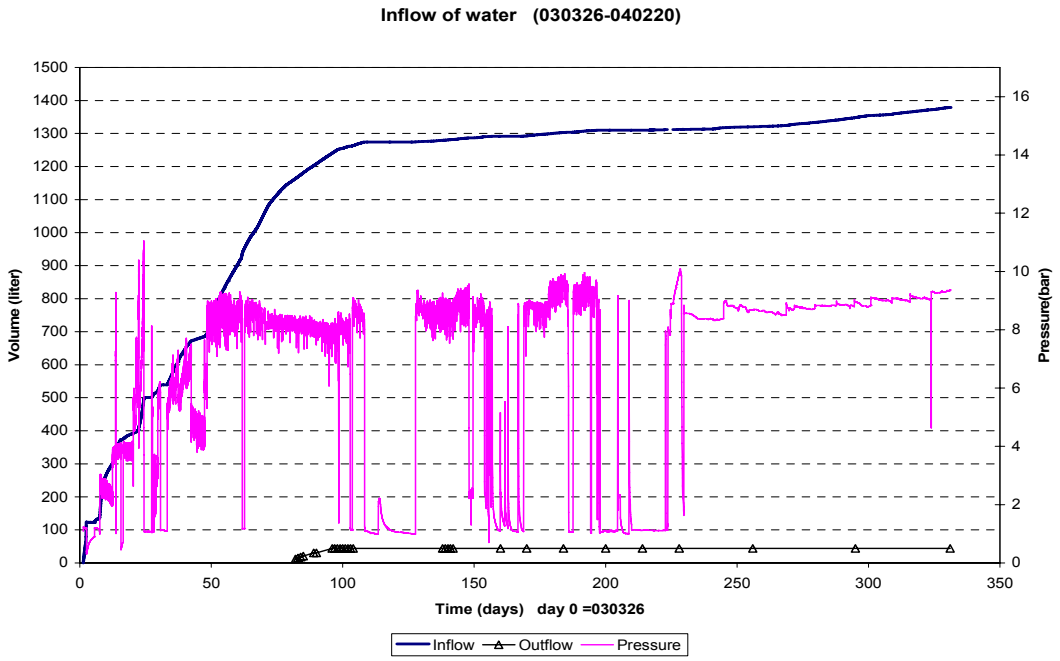

Figure 1. *Water inflow and water pressure in the sand filter.*

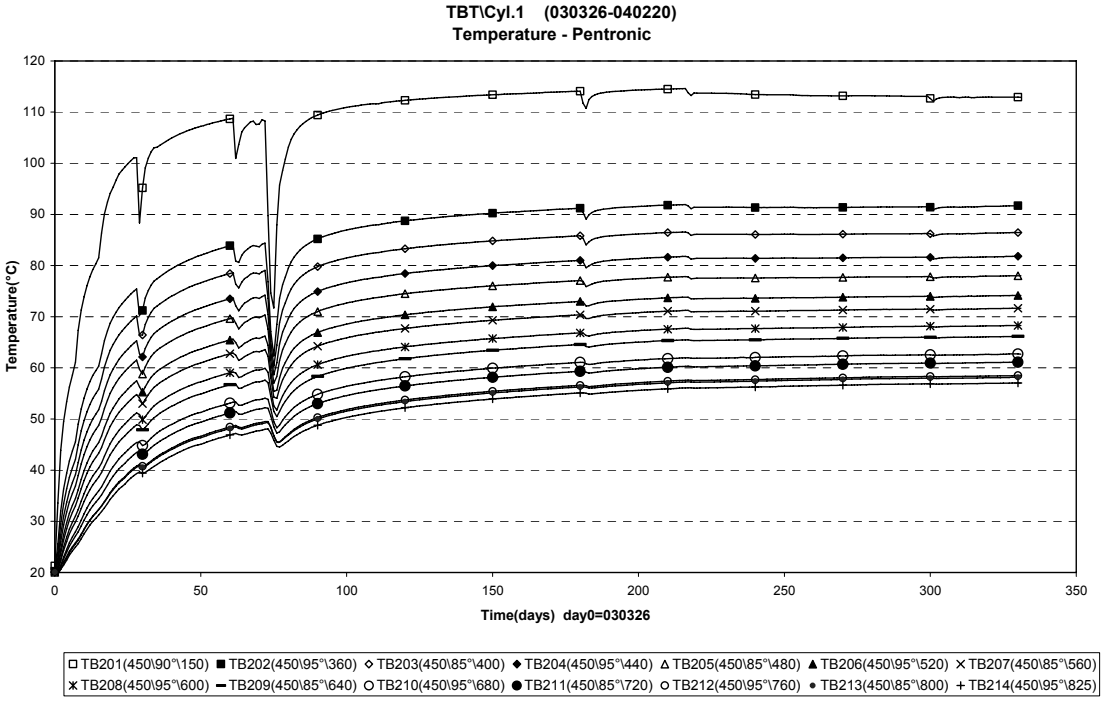

Figure 2. *Temperature – Cylinder 1.*

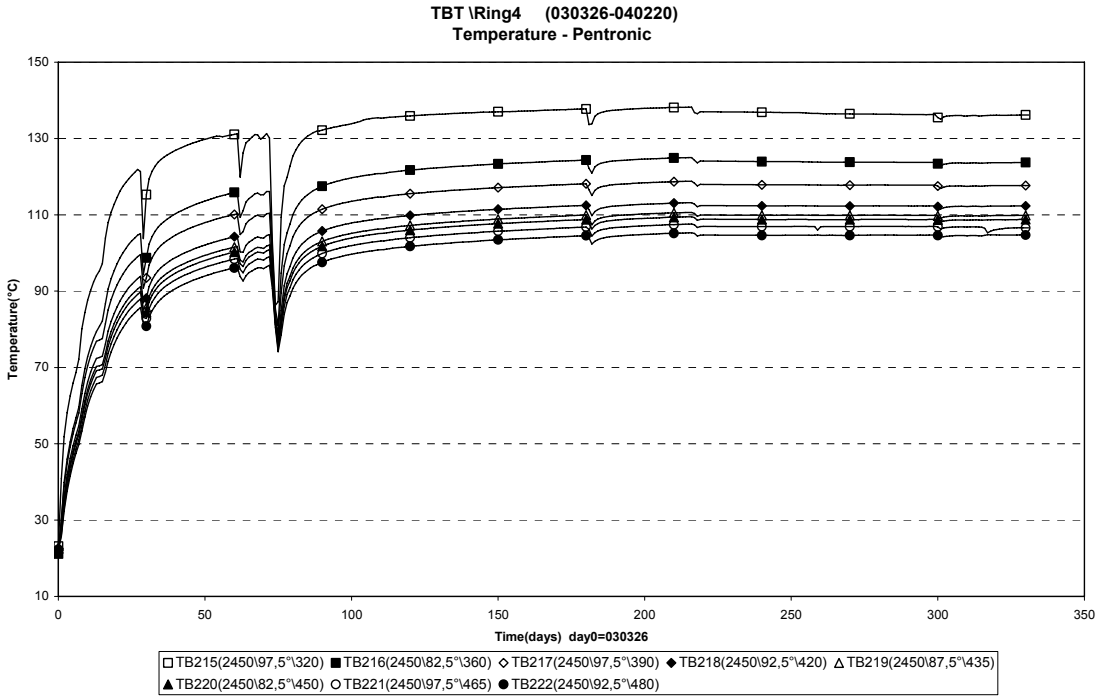

Figure 3. *Temperature – Ring 4, Radius 320 – 480.*

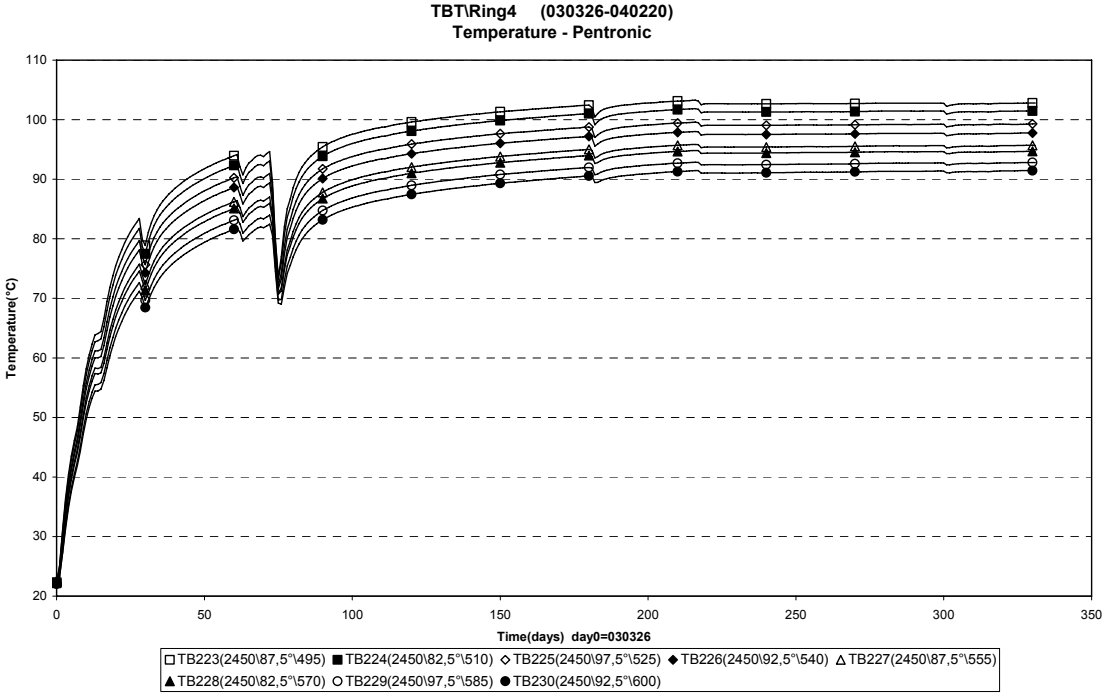

Figur 4. *Temperature – Ring 4, Radius 495 – 600.*

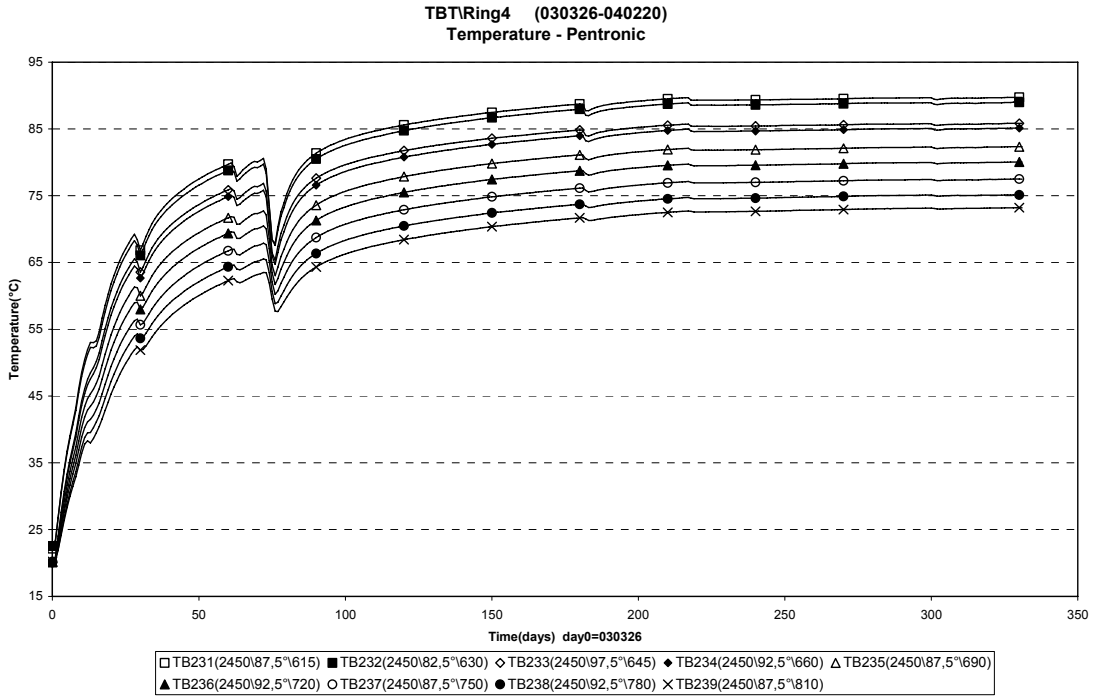

Figure 5. *Temperature – Ring 4, Radius 615 – 810.*

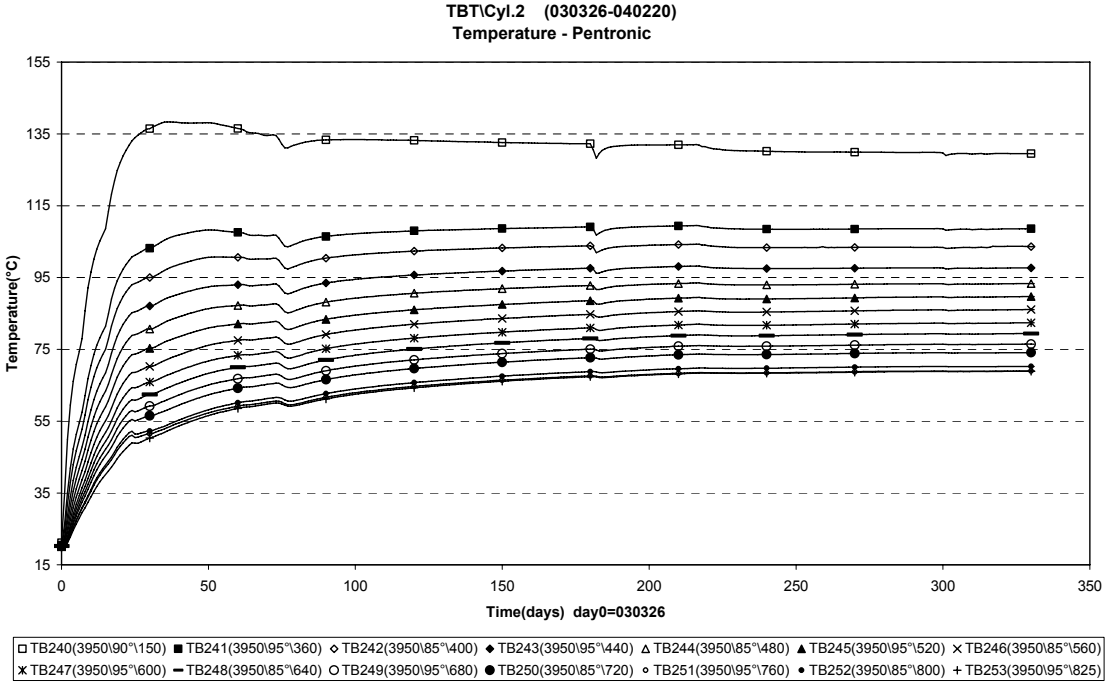

Figure 6*. Temperature – Cylinder 2.*

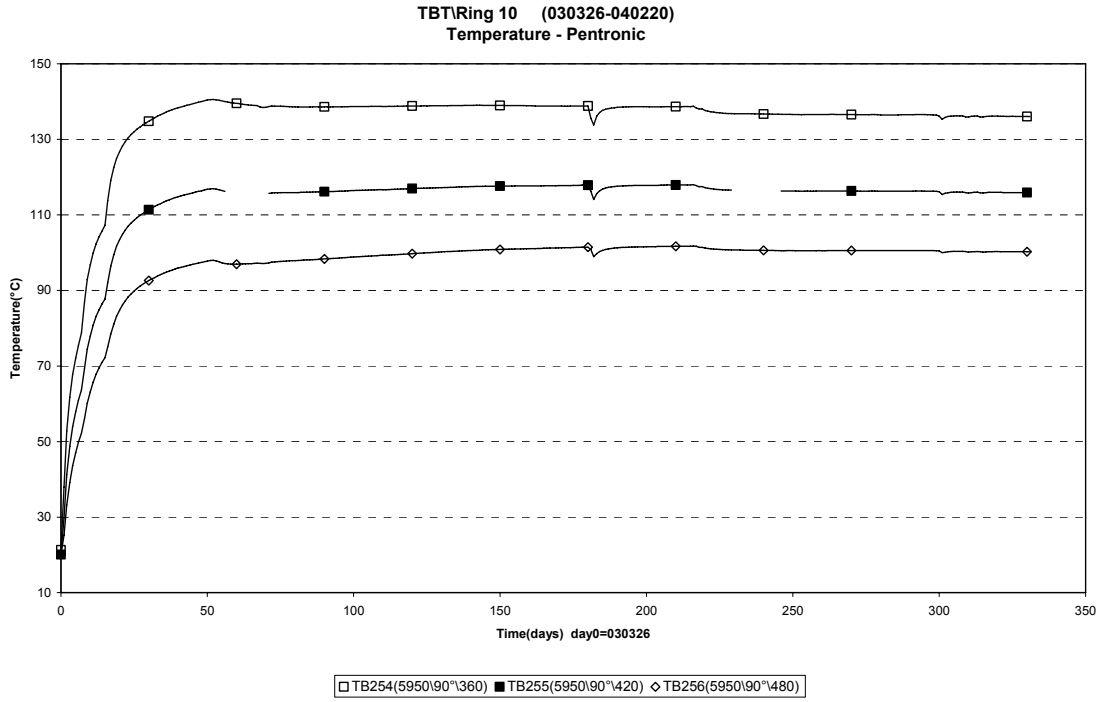

Figure 7. *Temperature – Ring 10, Radius 360 – 480.*

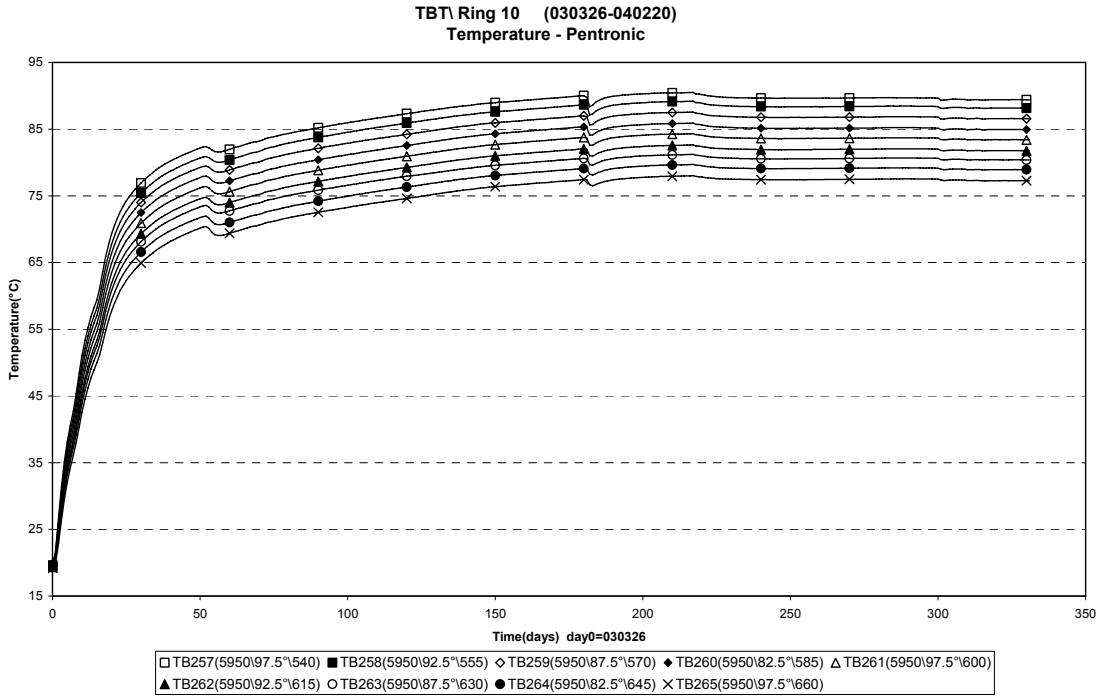

Figure 8. *Temperature – Ring 10, Radius 540 – 660.*

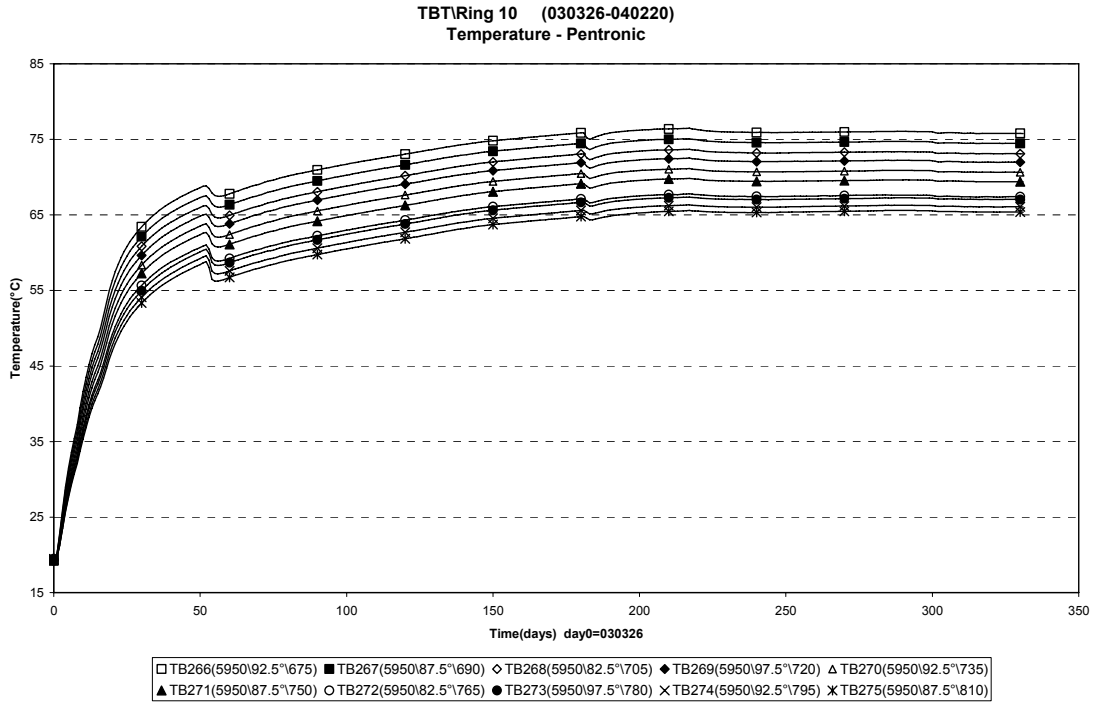

Figure 9. *Temperature – Ring 10, Radius 675 – 810.*

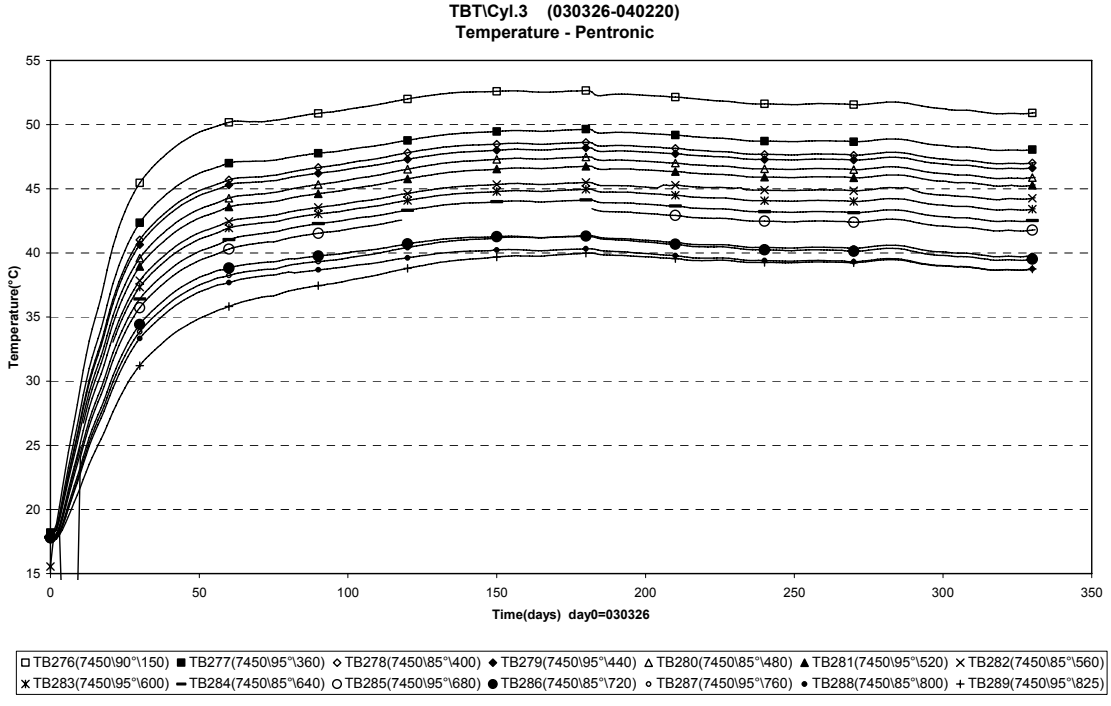

Figure 10. *Temperature – Cylinder 3*

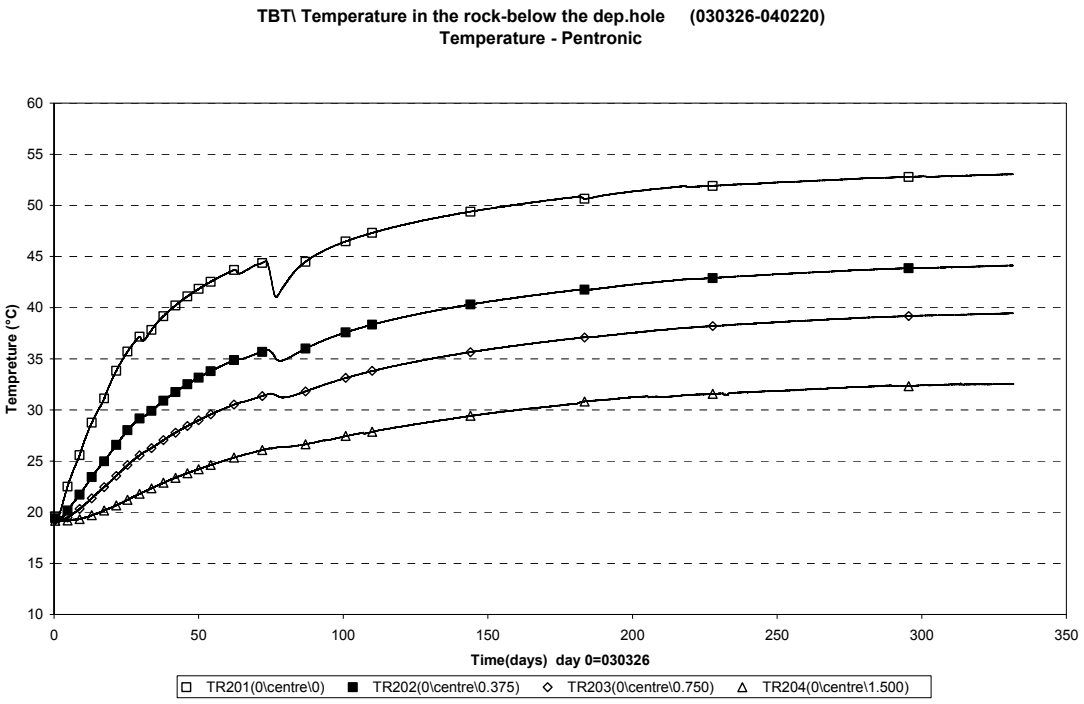

Figure 11. *Rock temperature – below hole.*

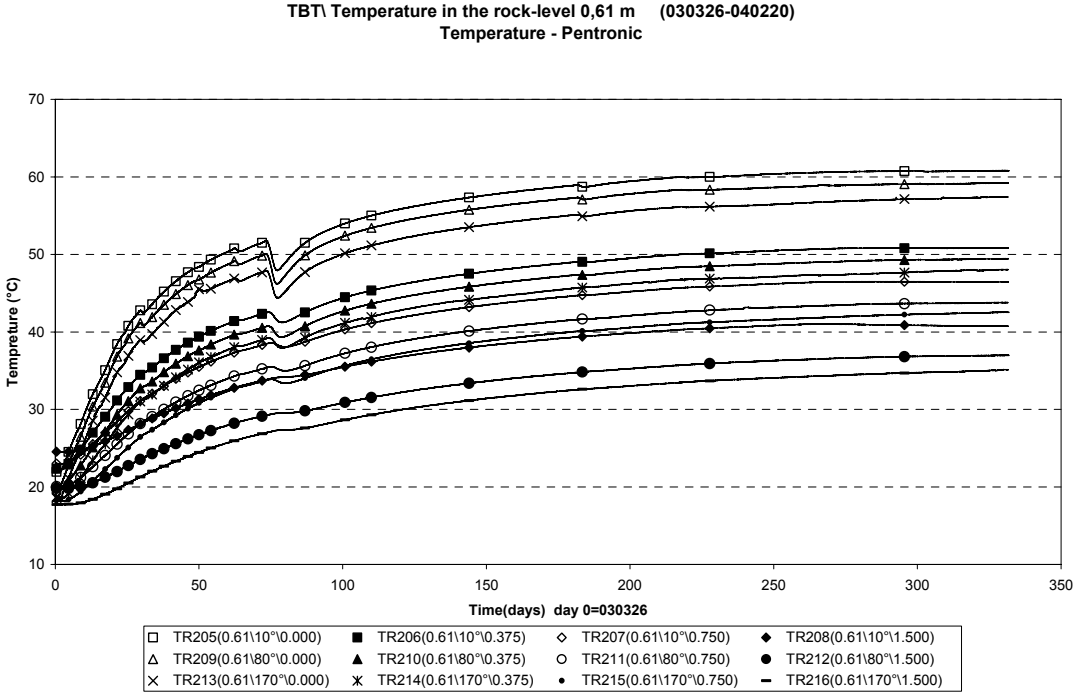

Figure 12. *Rock temperature – Level 0.61 m.*

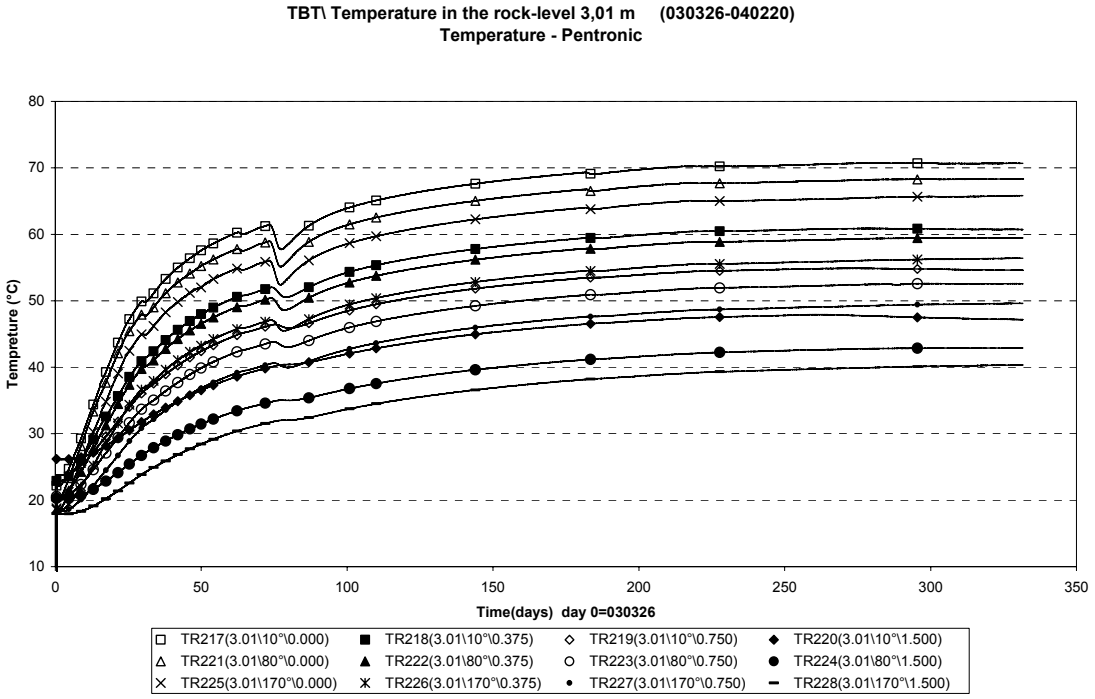

Figure 13. *Rock temperature – Level 3.01 m.*

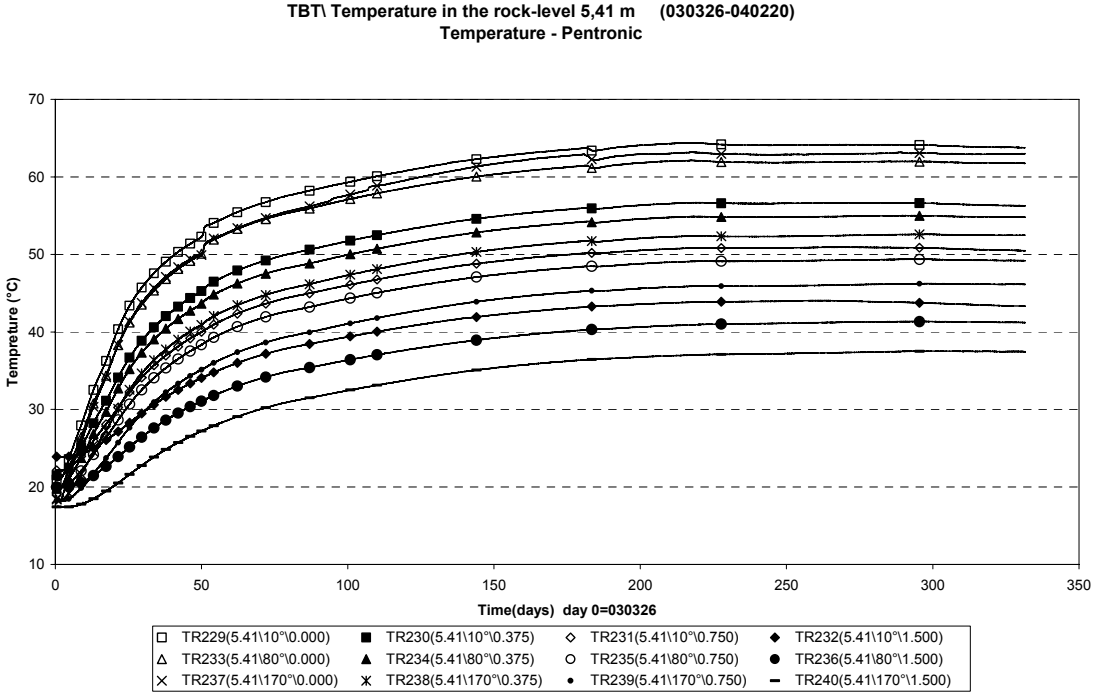

Figure 14. *Rock temperature – Level 5.41 m.*

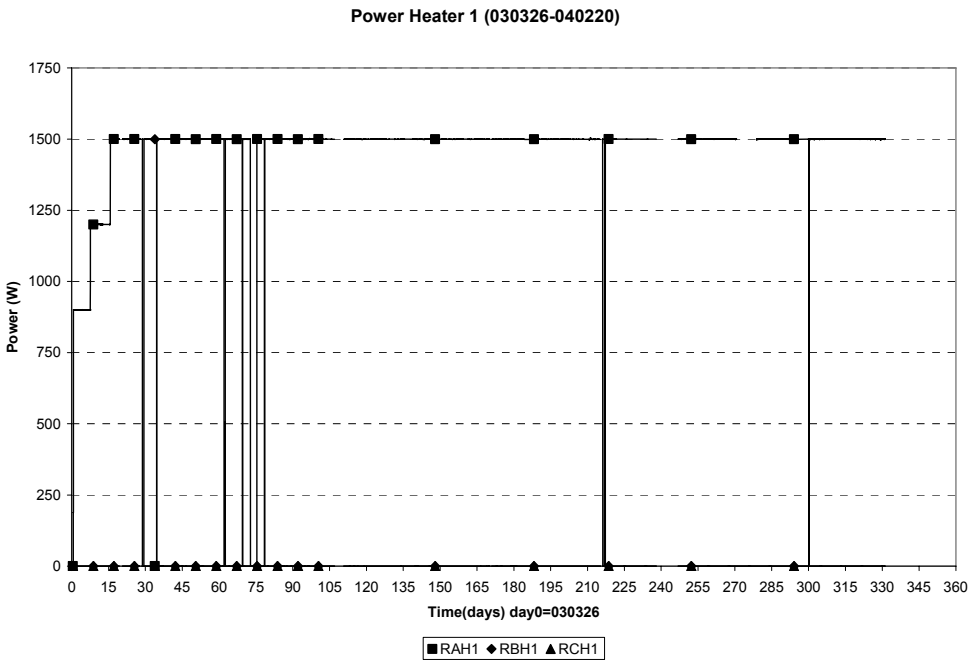

Figure 15. *Power – Heater 1.*

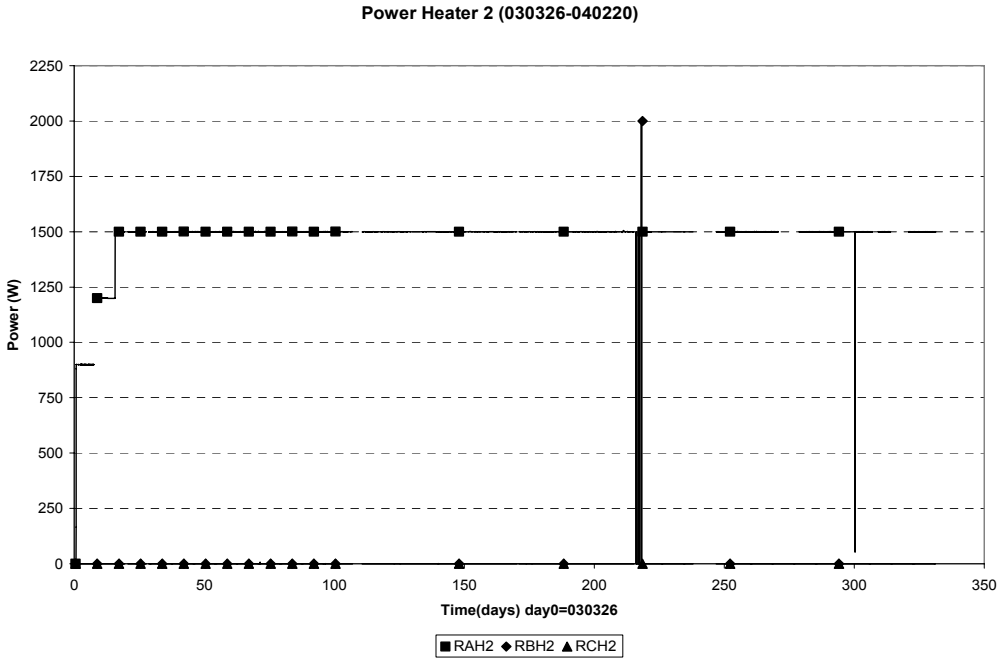

Figure 16. *Power – Heater 2.*

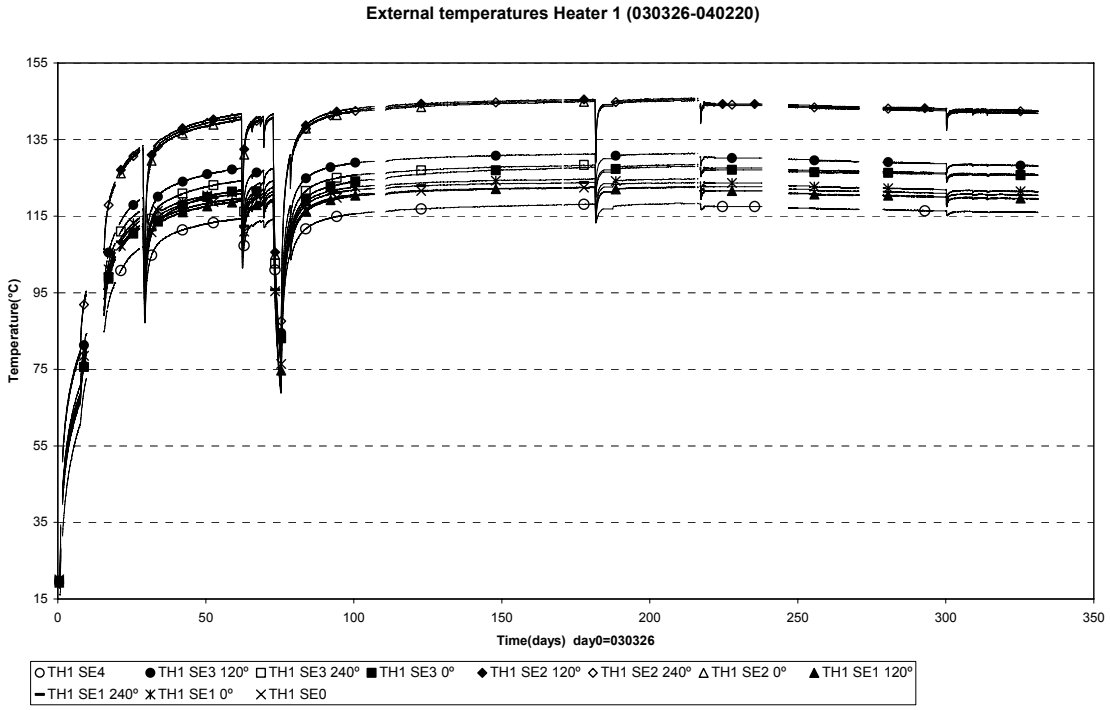

Figure 17. *External temperature – Heater 1.*

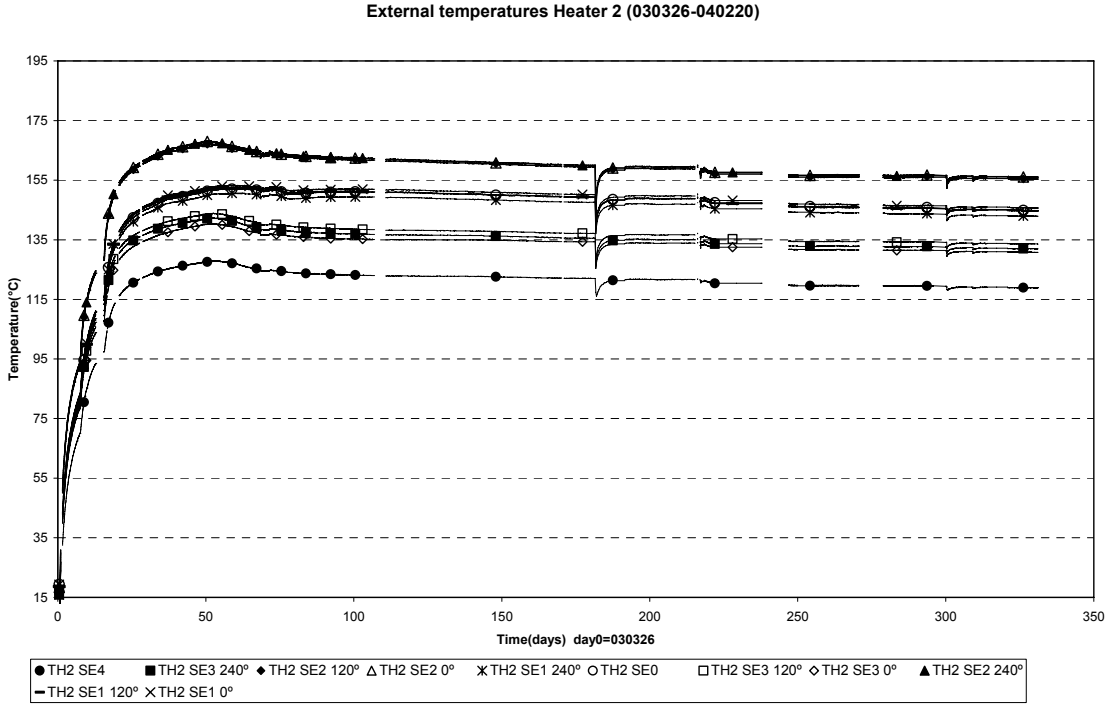

Figure 18. *External temperature – Heater 2.*

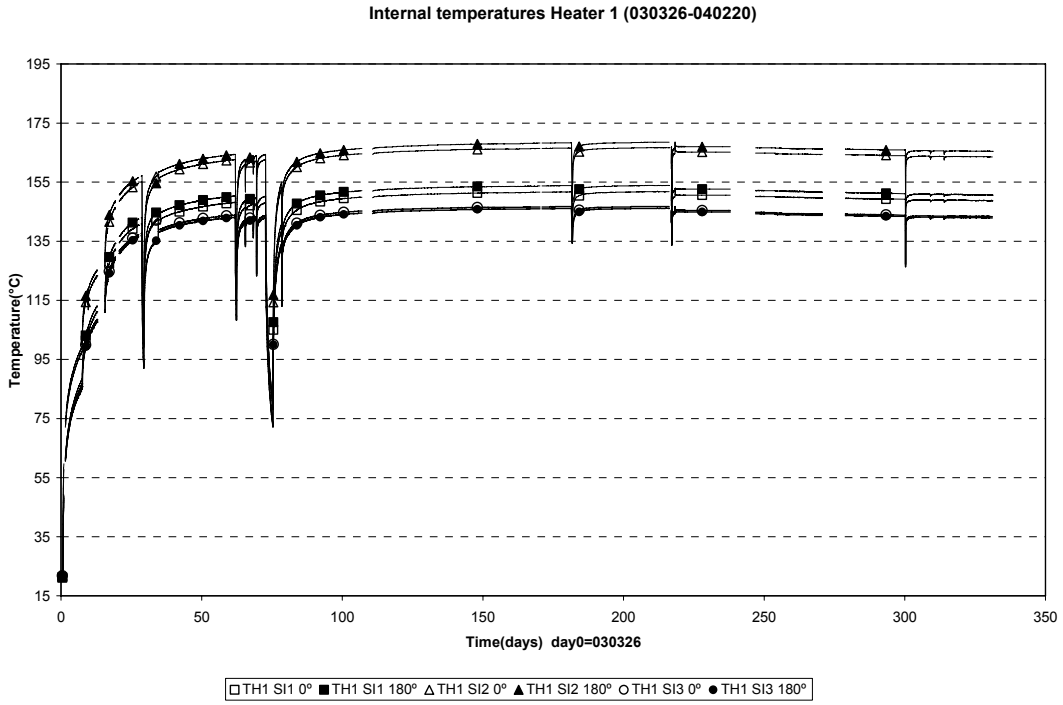

Figure 19. *Internal temperature – Heater 1.*

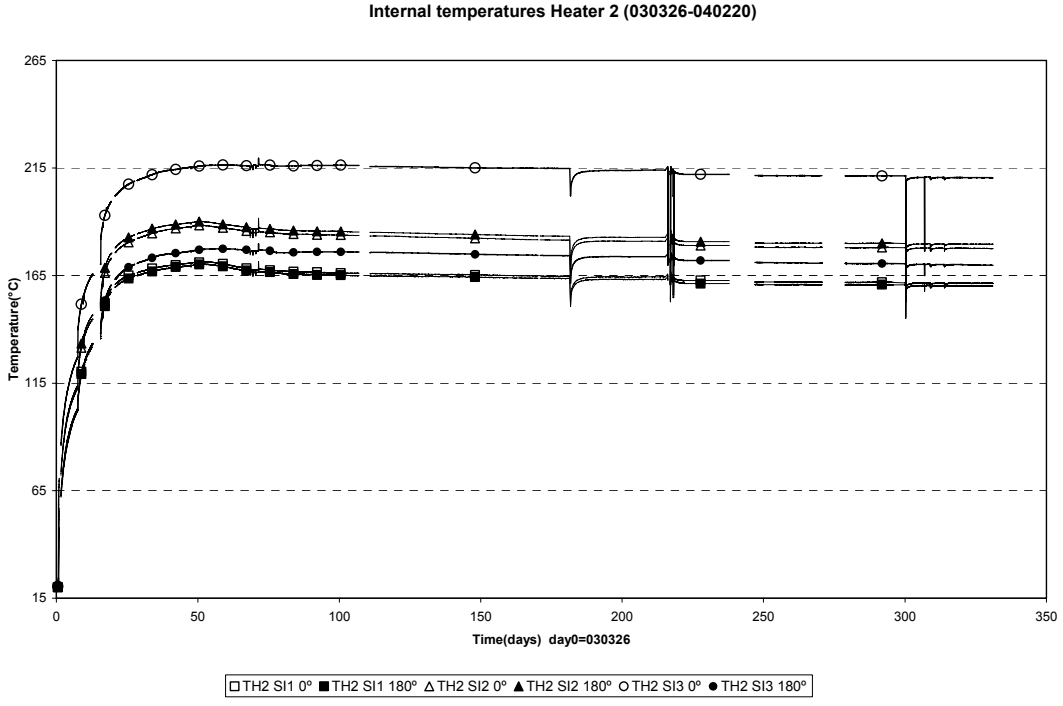

Figure 20. *Internal temperature – Heater 2.*

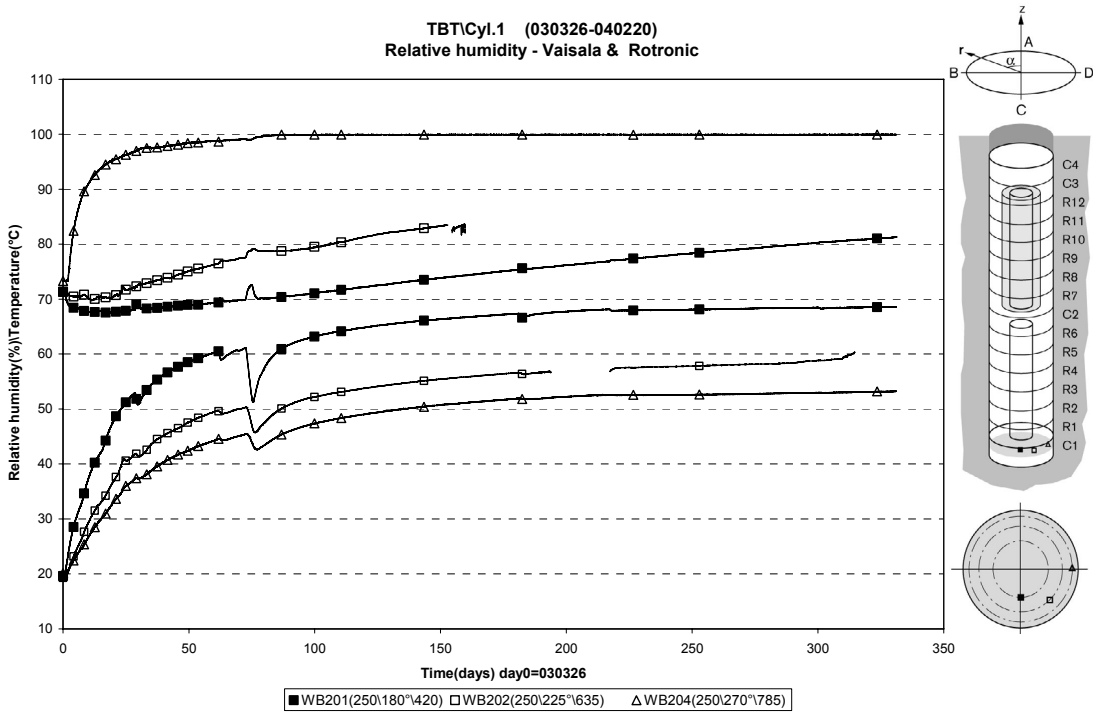

Figure 21. *Relative humidity - Cylinder 1.*

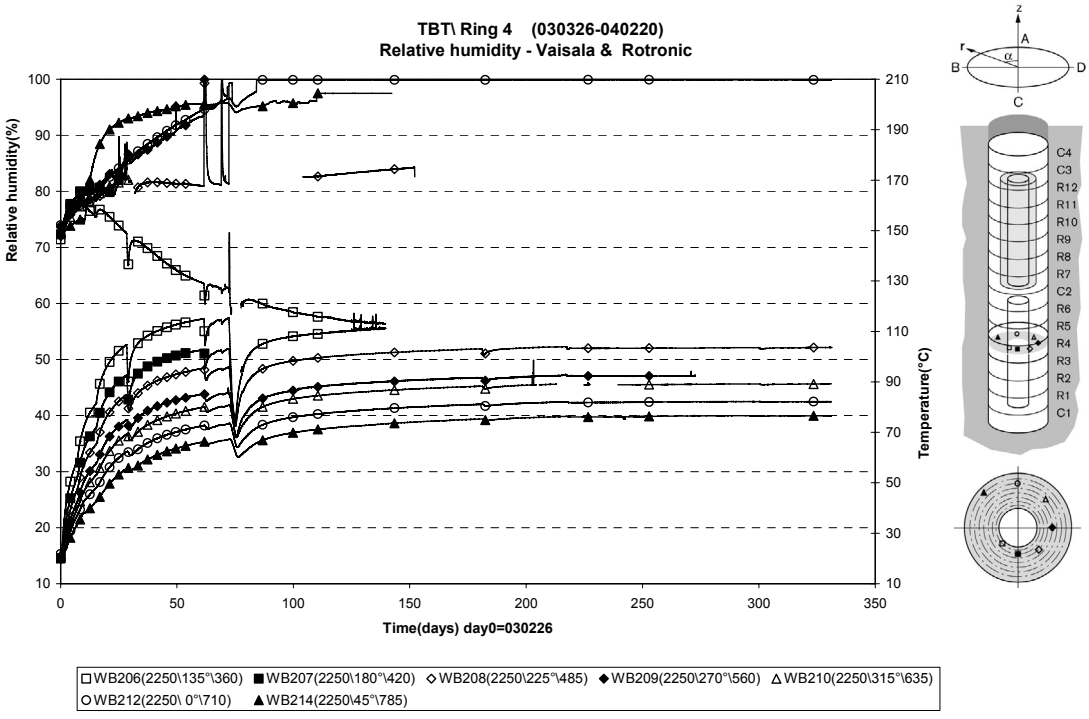

Figure 22. *Relative humidity - Ring 4.*

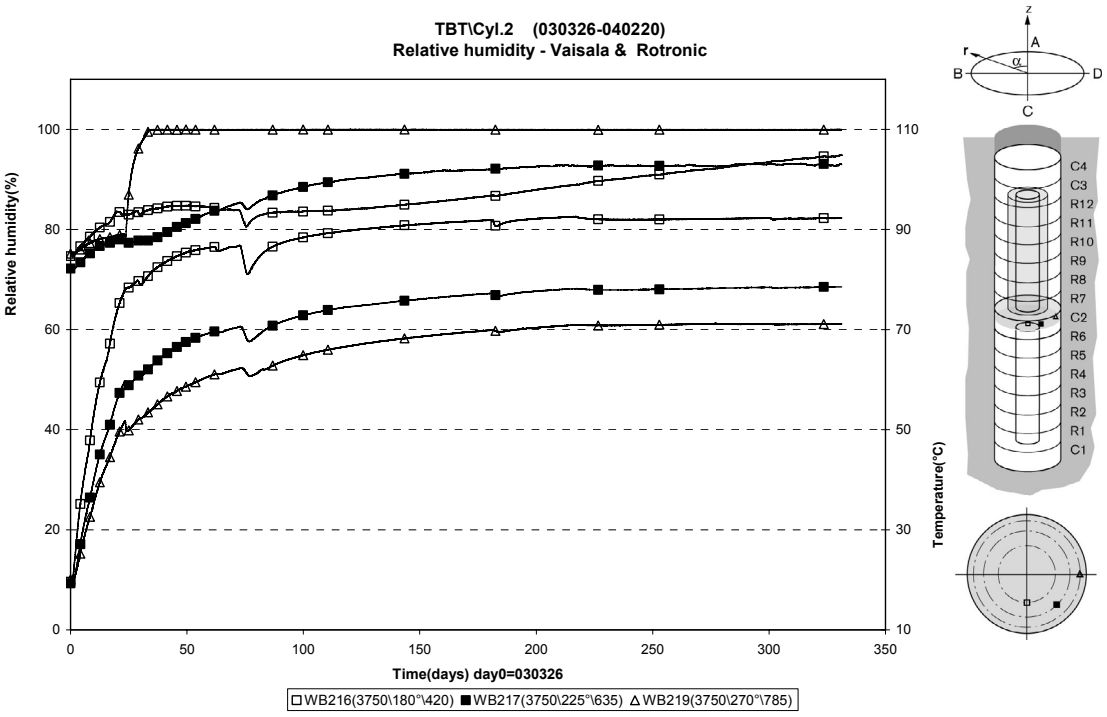

Figure 23. *Relative humidity - Cylinder 2.*

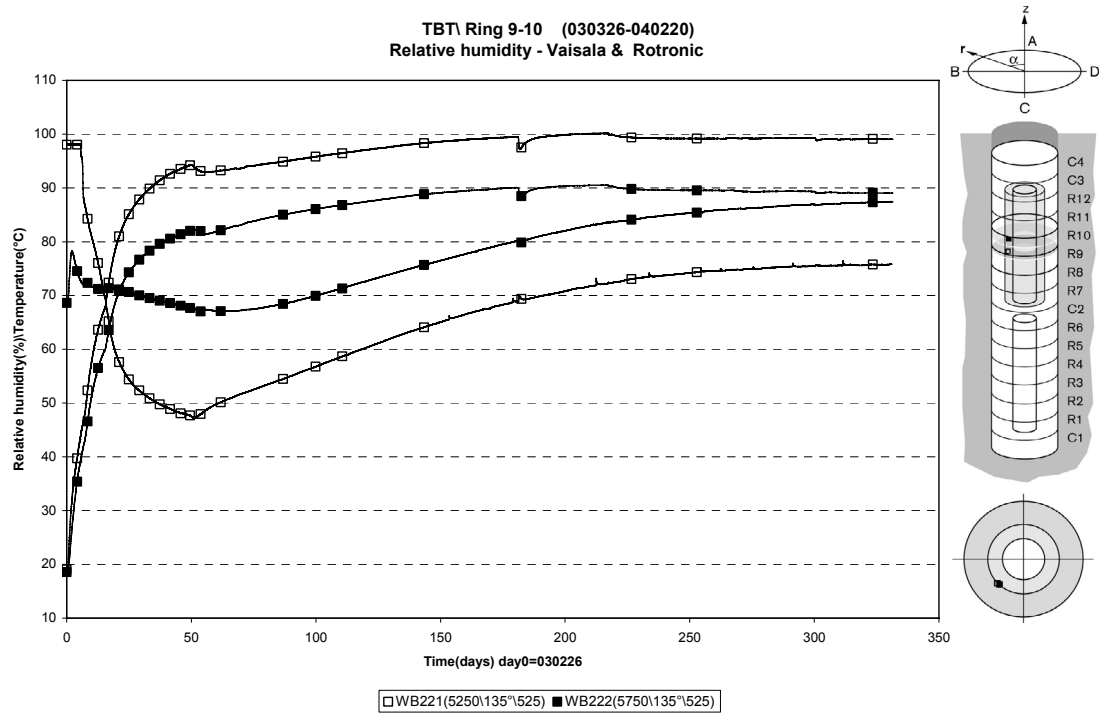

Figure 24. *Relative humidity - sand shield inside Ring 9-10.*

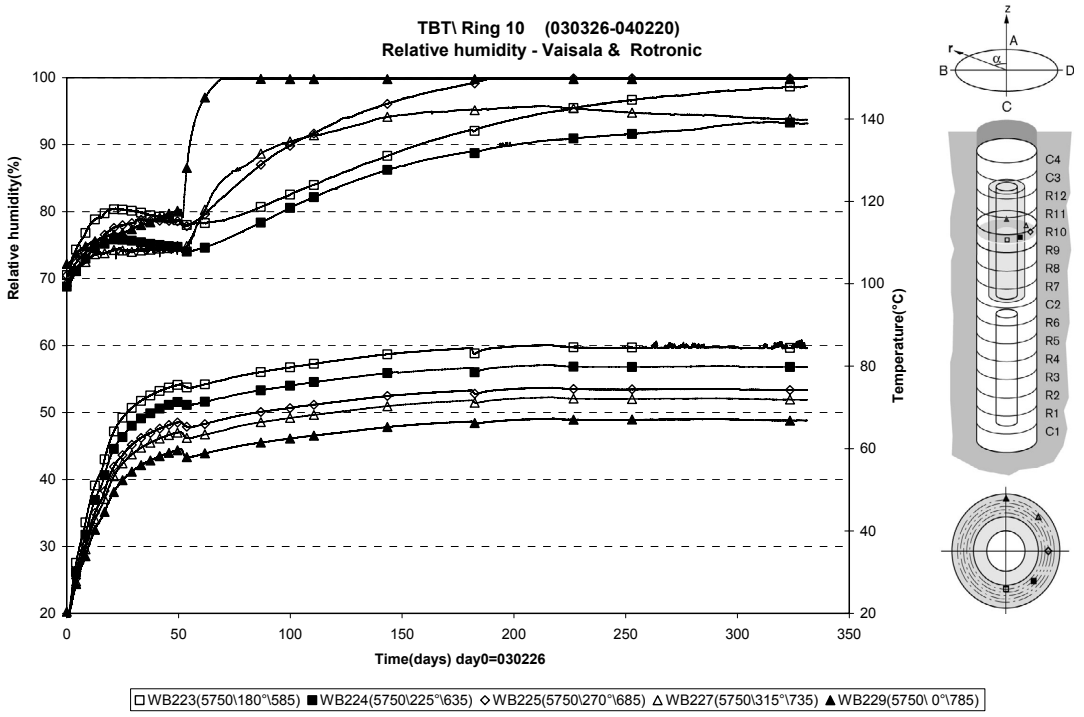

Figure 25. *Relative humidity - Ring 10.*

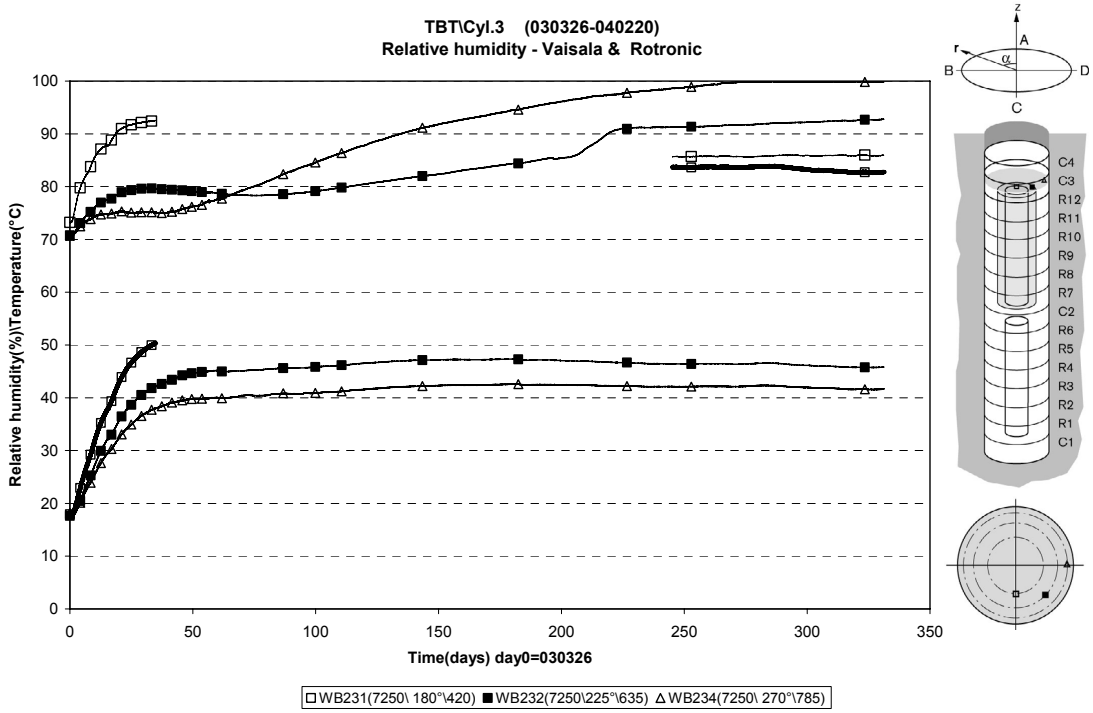

Figure 26. *Relative humidity - Cylinder 3.*

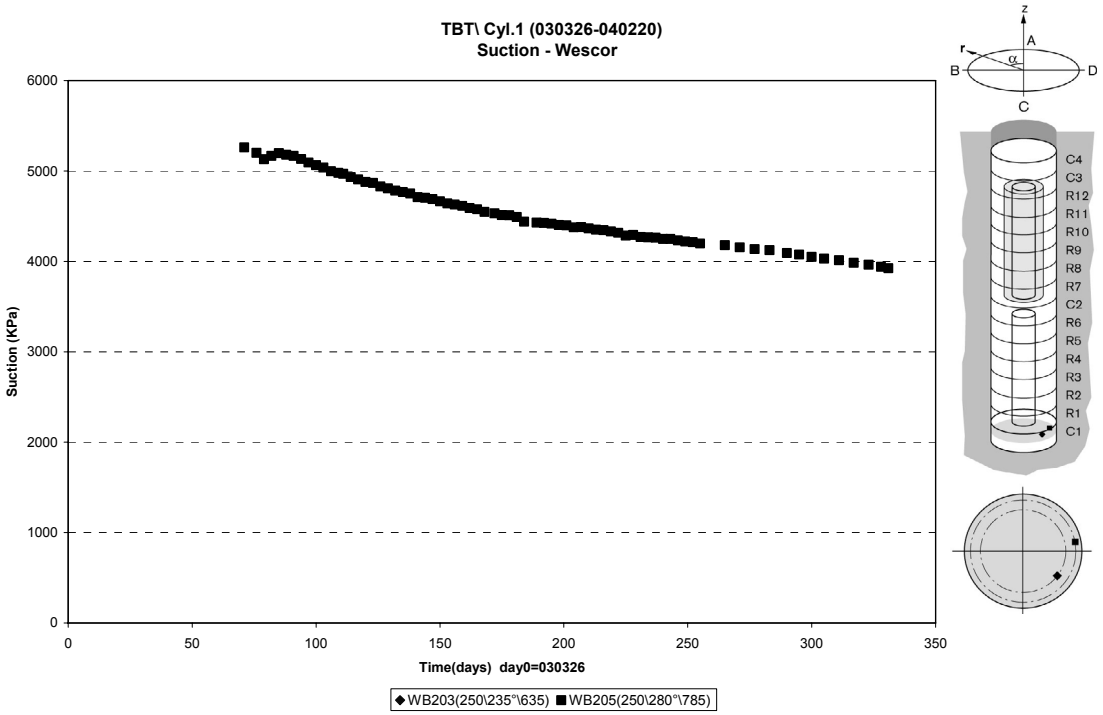

Figure 27. *Suction - Cylinder 1.*

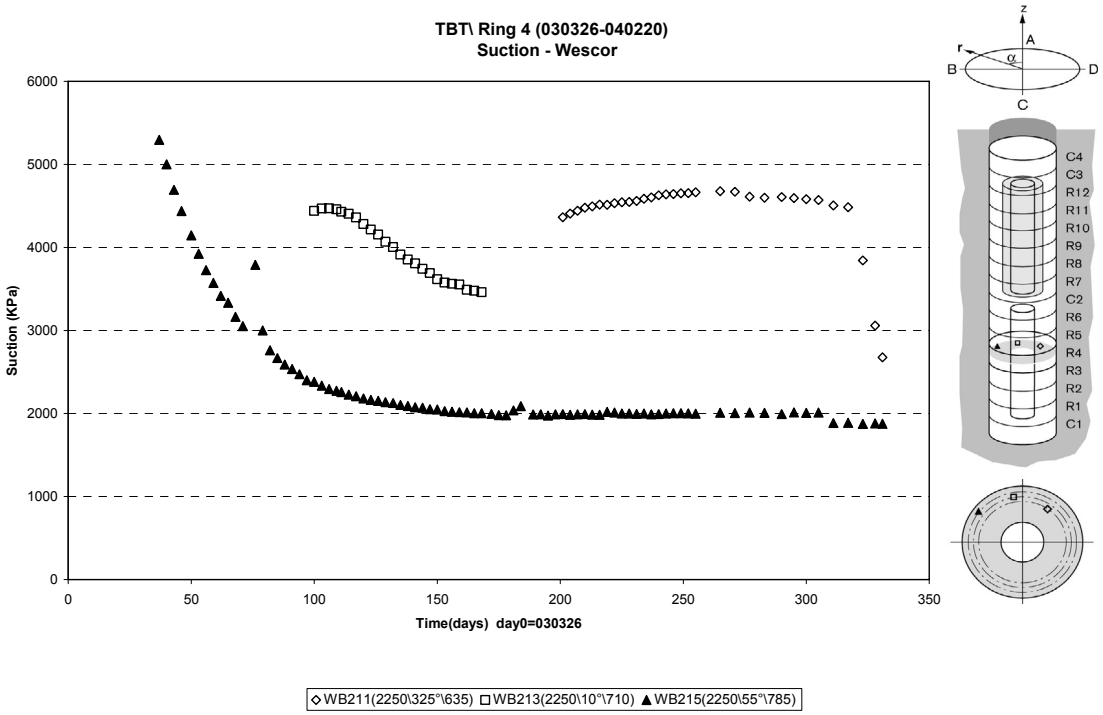

Figure 28. *Suction - Ring 4.*

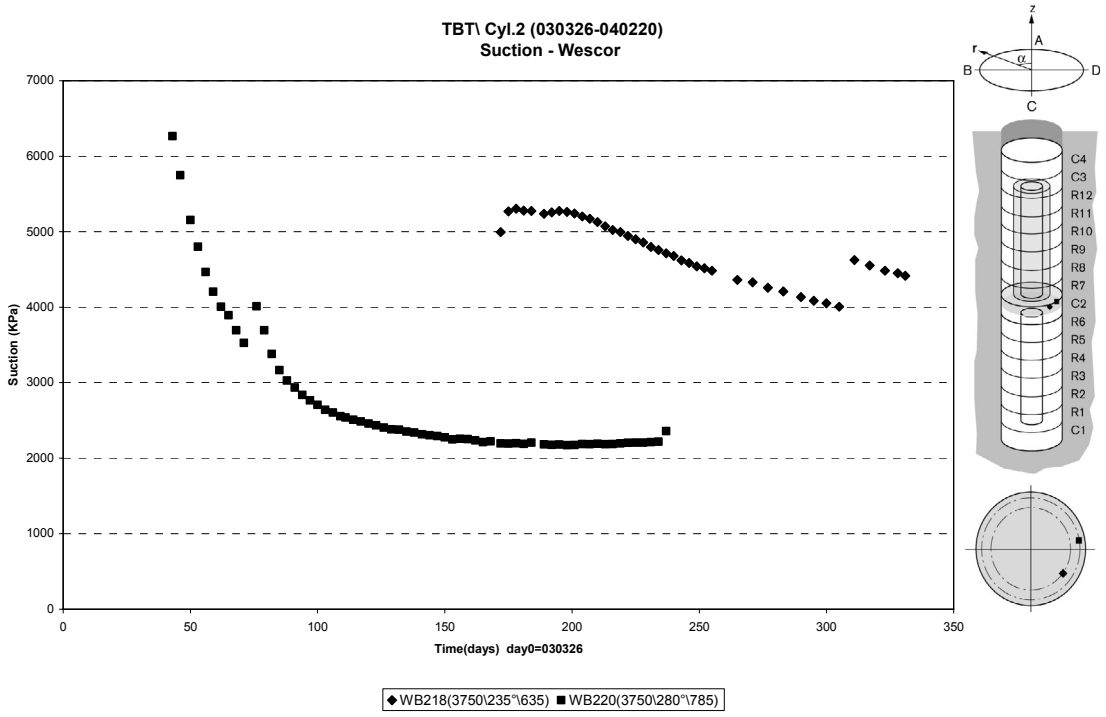

Figure 29. *Suction - Cylinder 2.*

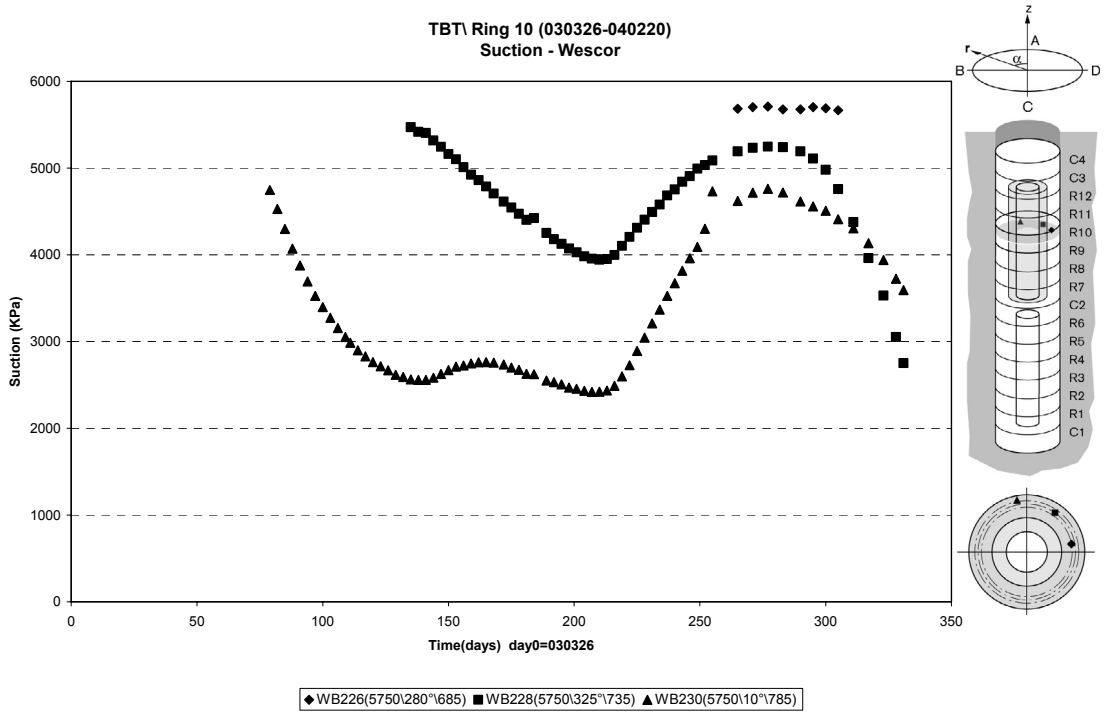

Figure 30. *Suction - Ring 10.*

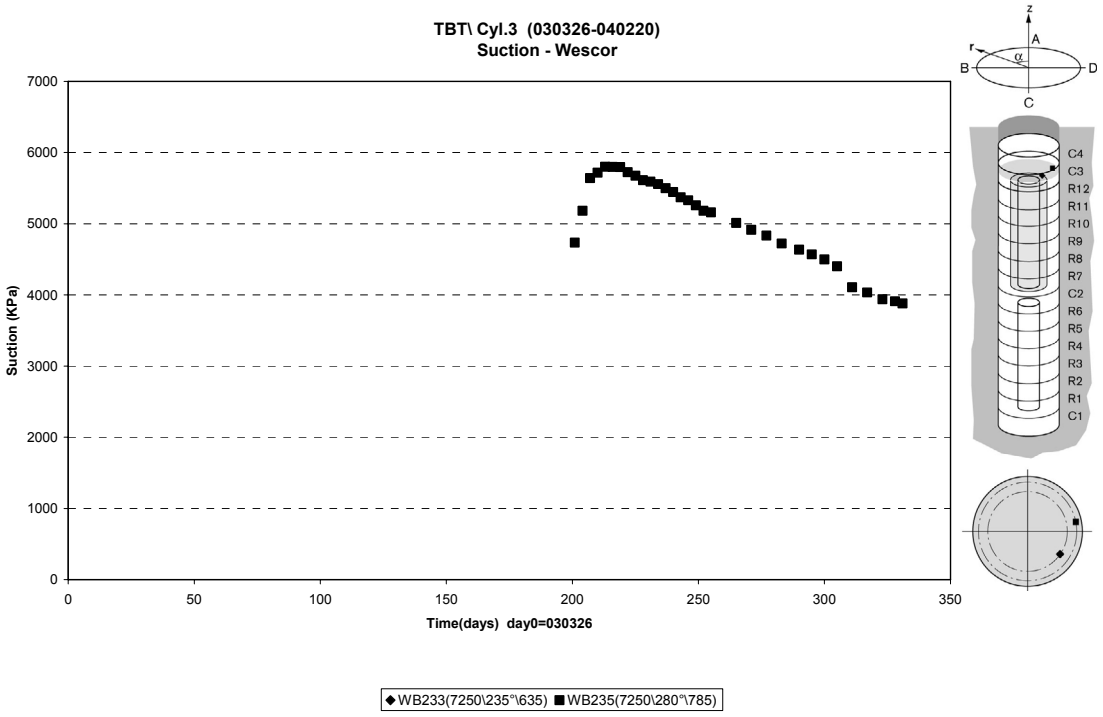

Figure 31. *Suction - Cylinder 3.*

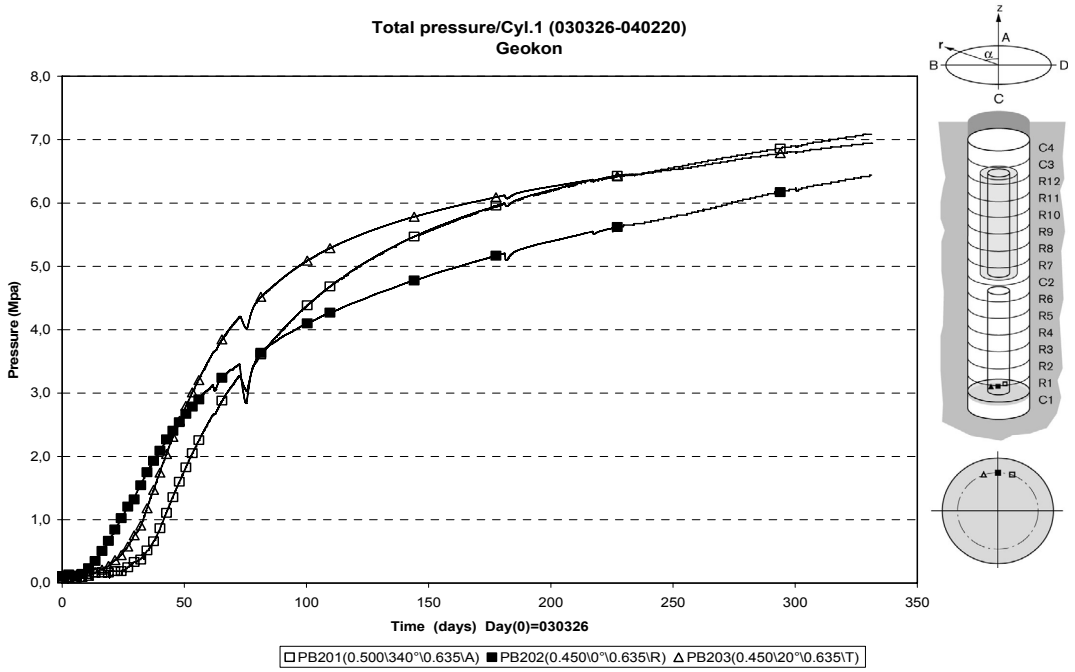

Figure 32. *Pressure - Cylinder 1.*

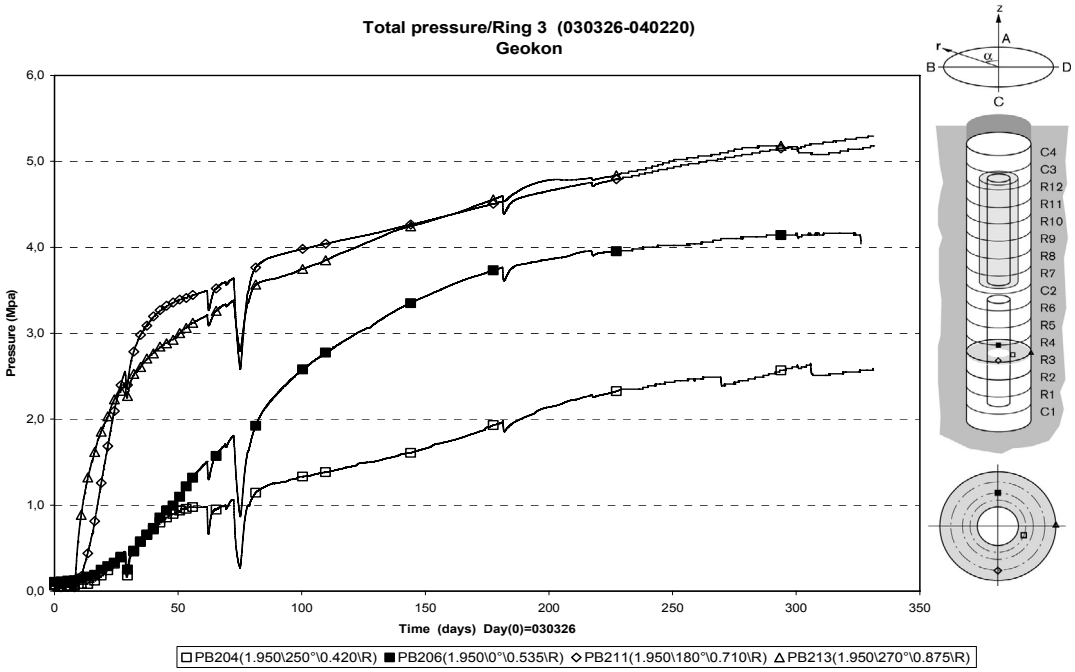

Figure 33. *Pressure - Ring 3, Radial.*

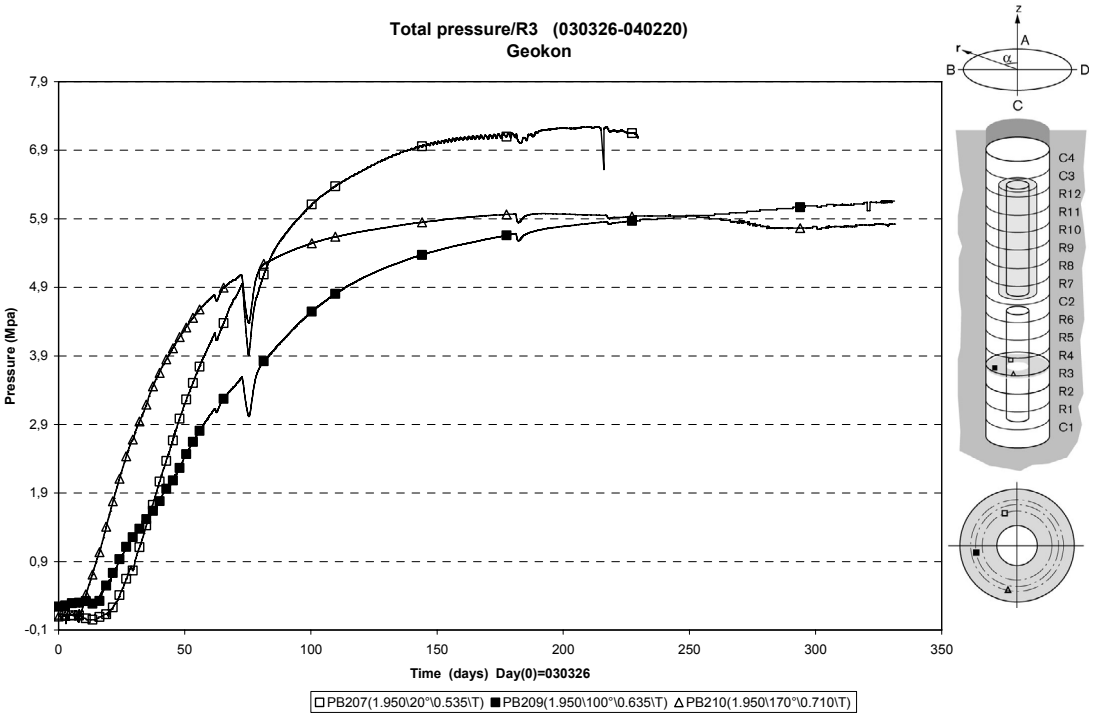

Figure 34. *Pressure – Ring 3, Tangential.*

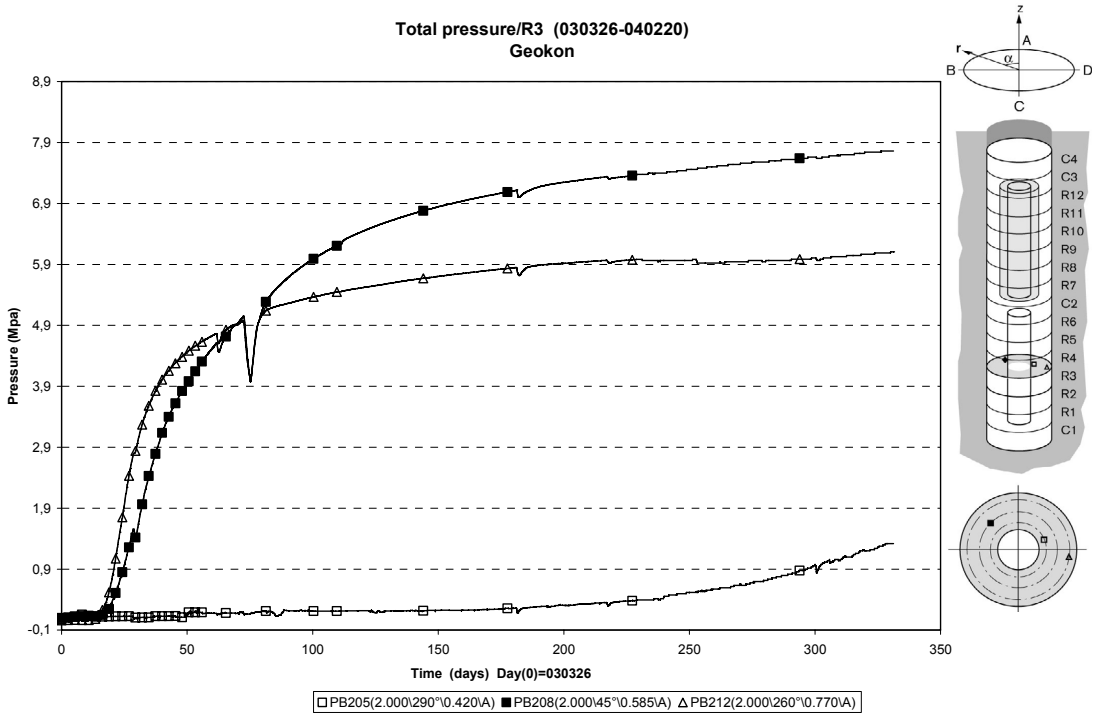

Figure 35. *Pressure – Ring 3 Axial.*

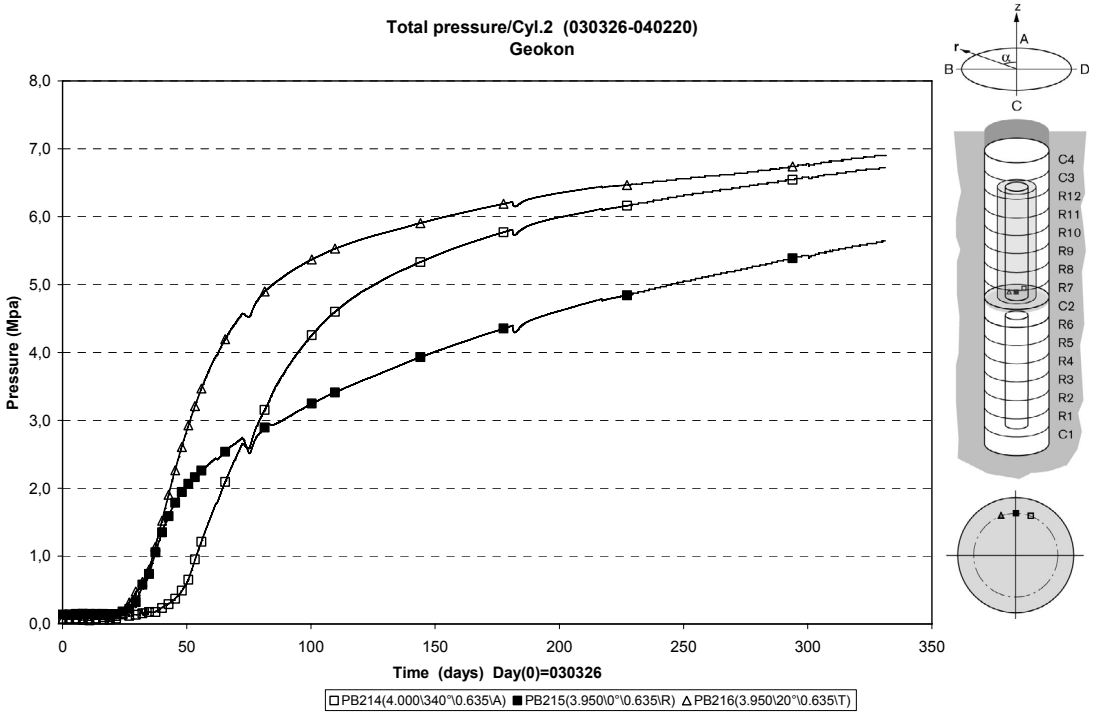

Figure 36. *Pressure - Cylinder 2.*

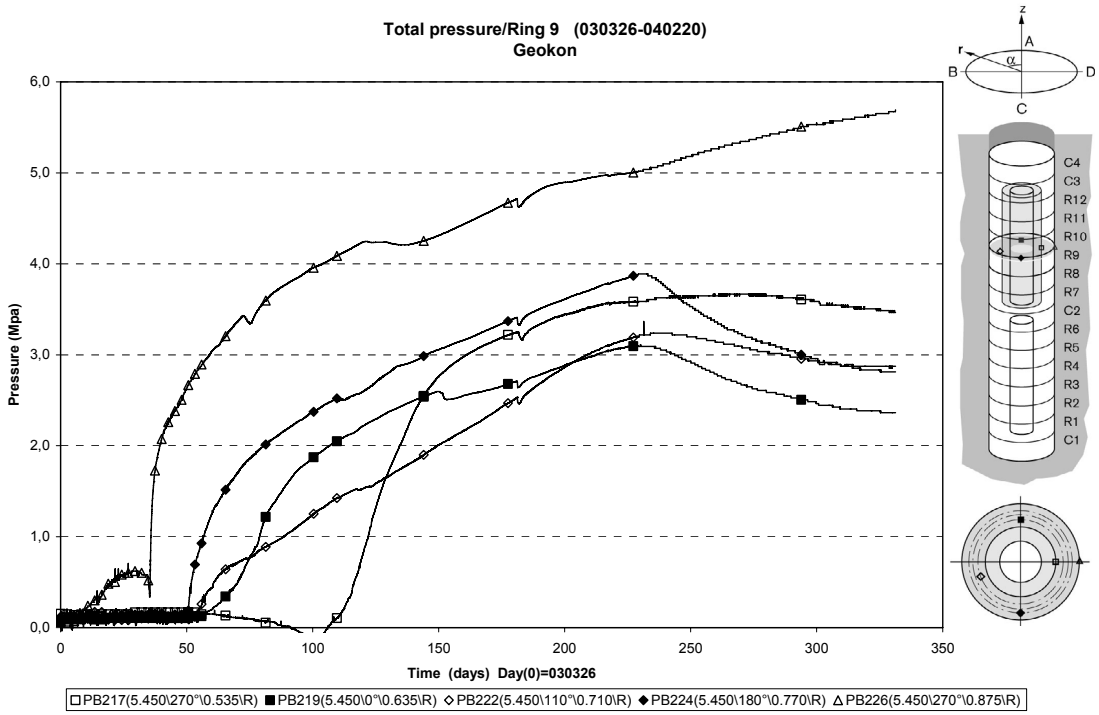

Figure 37. *Pressure - Ring 9, Radial.*

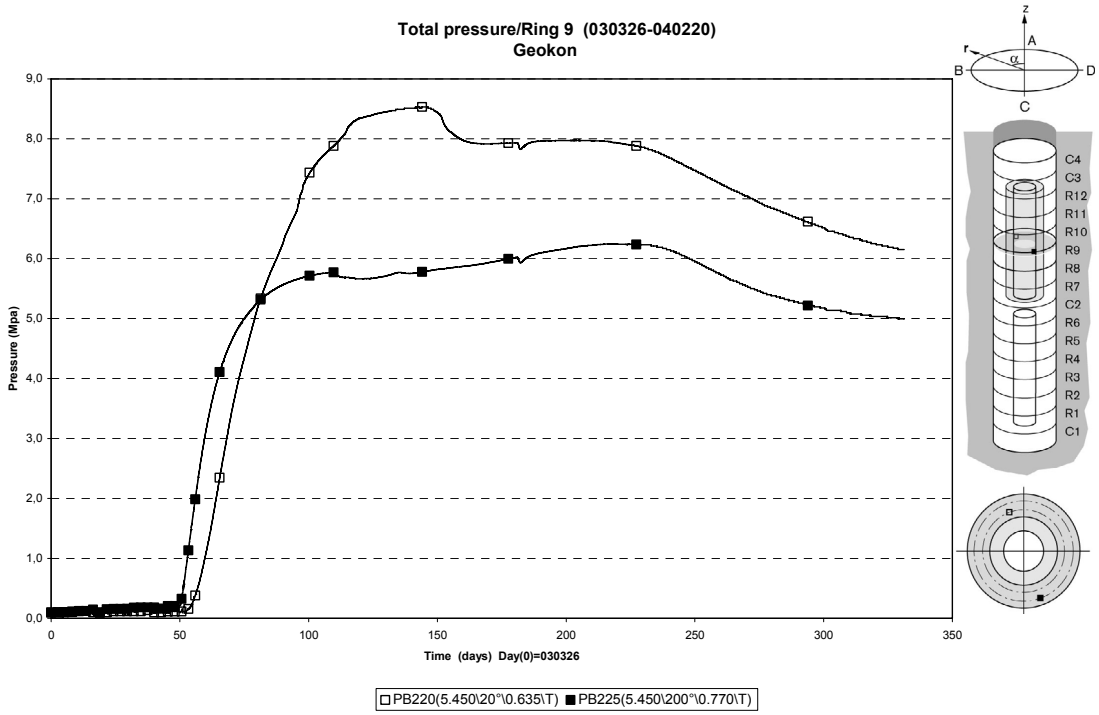

Figure 38. *Pressure – Ring 9, Tangential.*

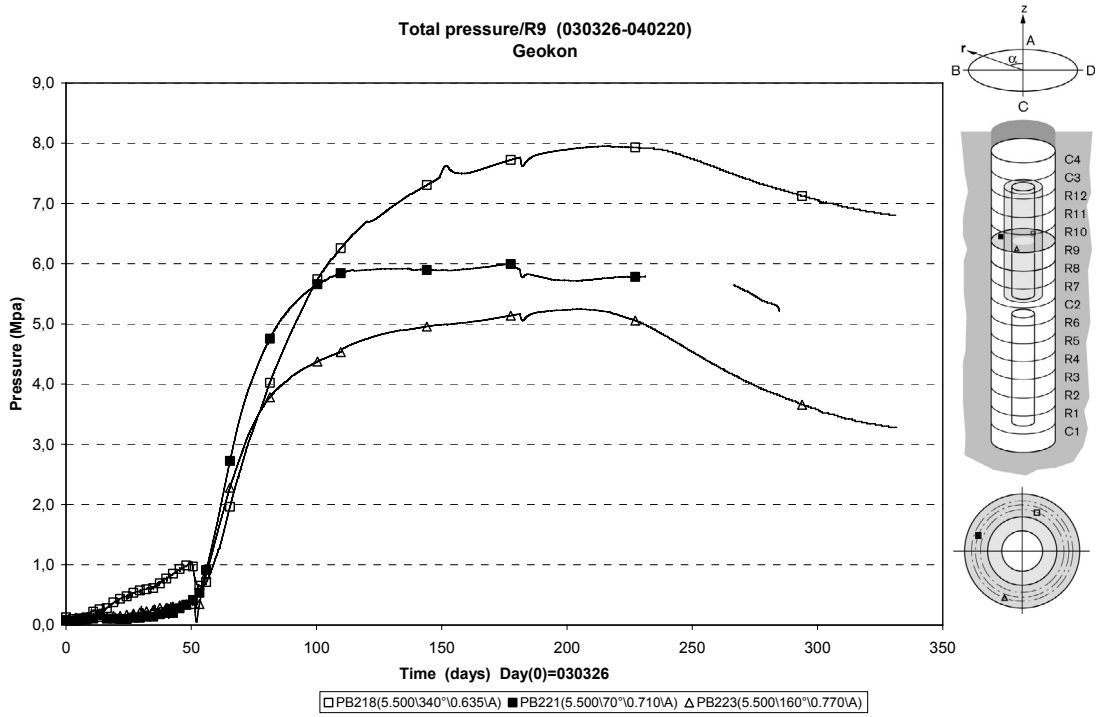

Figure 39. *Pressure – Ring 9, Axial.*

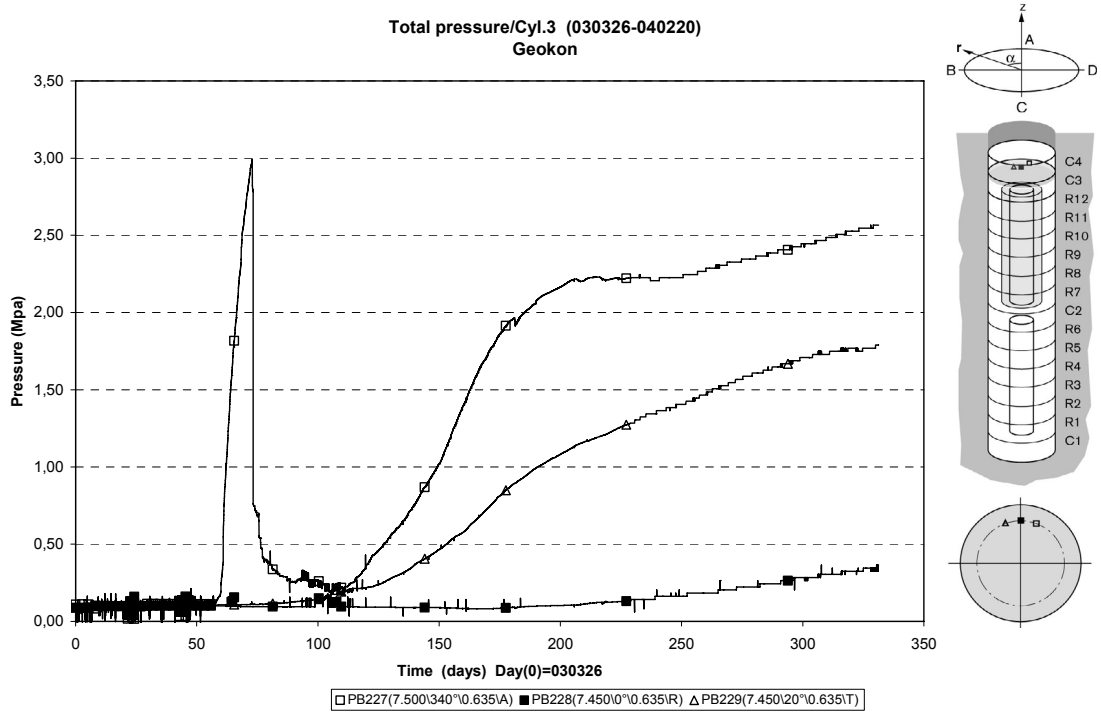

Figure 40. *Pressure - Cylinder 3.*

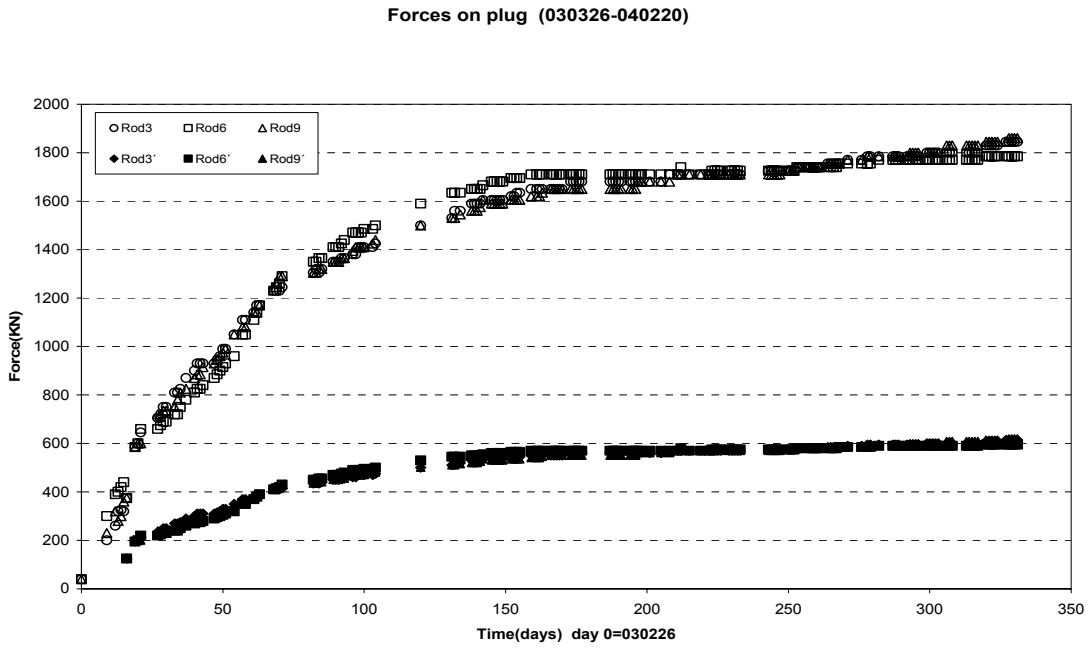

Figure 41. *Plug forces.*

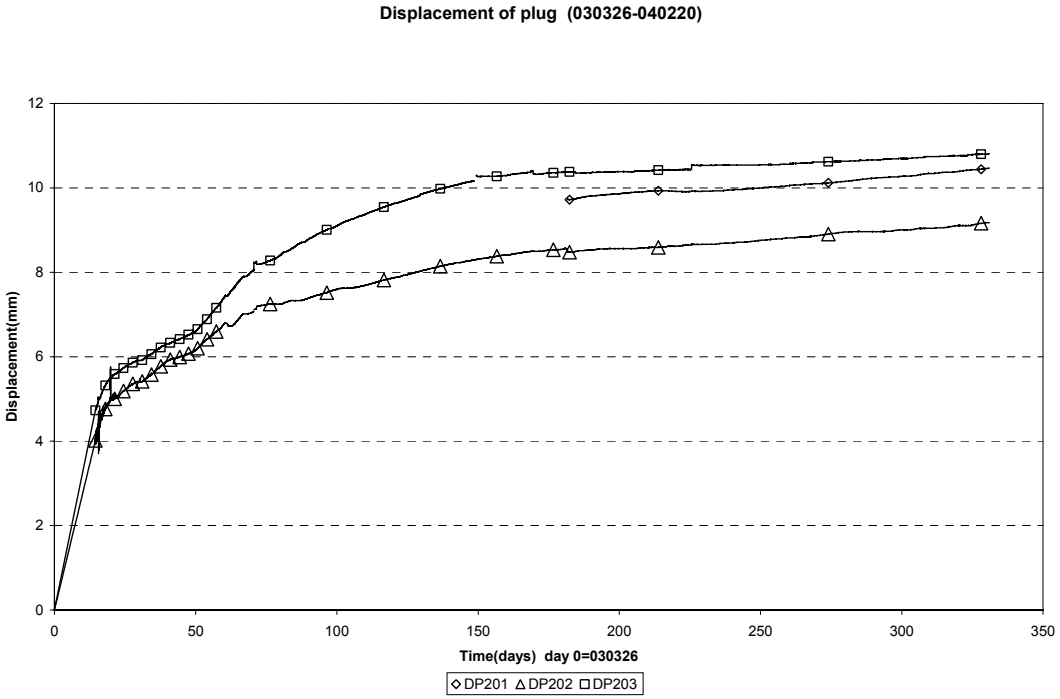

Figure 42. *Plug displacement.*

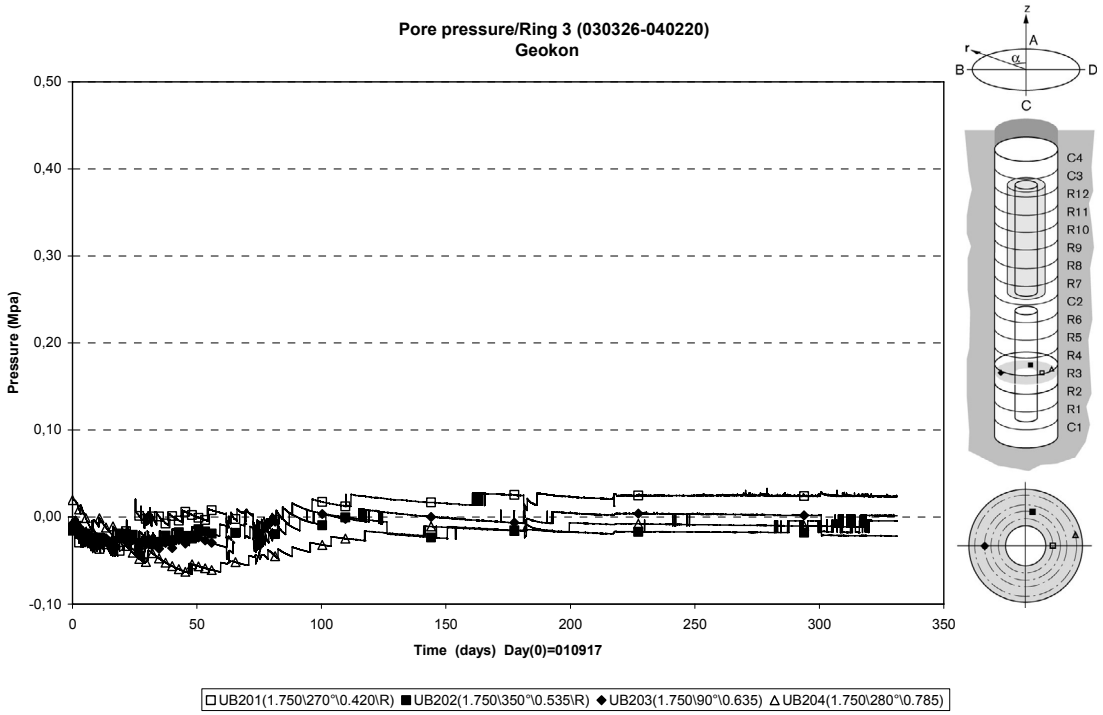

Figure 43. *Pore pressure – Ring 3.*

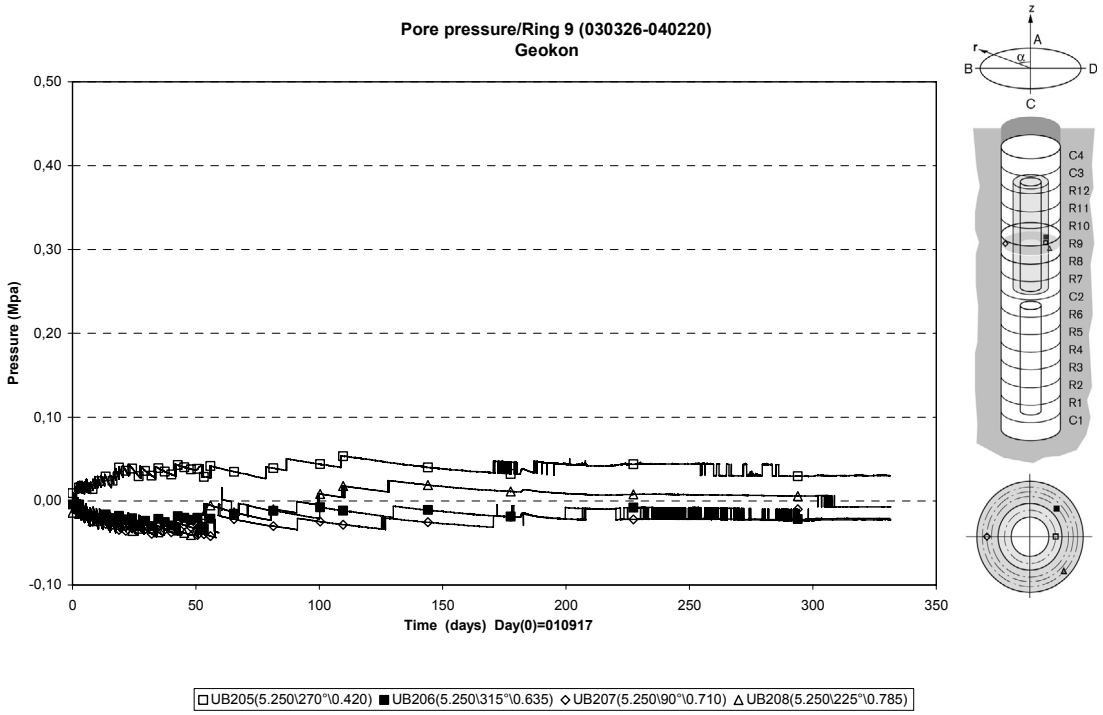

Figure 44. *Pore pressure – Ring 9.*

Appendix 2 – A simple model of radial stress development in Ring 9

Mattias Åkesson & Harald Hökmark, Clay Technology AB

Background

The development of radial stresses in Ring 9 around the sand shield may deserve some specific attention. The stress increase started at the filter/bentonite interface as soon as the sand filter had been saturated up to the level of Ring 9. At smaller radial distances, radial stresses appeared later. At the sand bentonite/shield interface, the radial stress appeared 110-130 days after test start (Figure 1 below).

While the stress increase at the outer part was correlated with wetting and a fast increase of the relative humidity to 100% (cf. Fig A25), this was not the case for the bentonite/shield interface at about 0.5 m radial distance. Some 100 or 130 days after test start, the relative humidity at the shield/bentonite interface was not more than 60-70% (cf. Fig A24). The stress increase here is therefore likely to be an effect of stress transfer from outer swelling parts rather than of local swelling. The 3 or 4 MPa radial stress increase found at 0.5 m radial distance corresponds to a 5% compression of the sand shield, according to sand compression data.

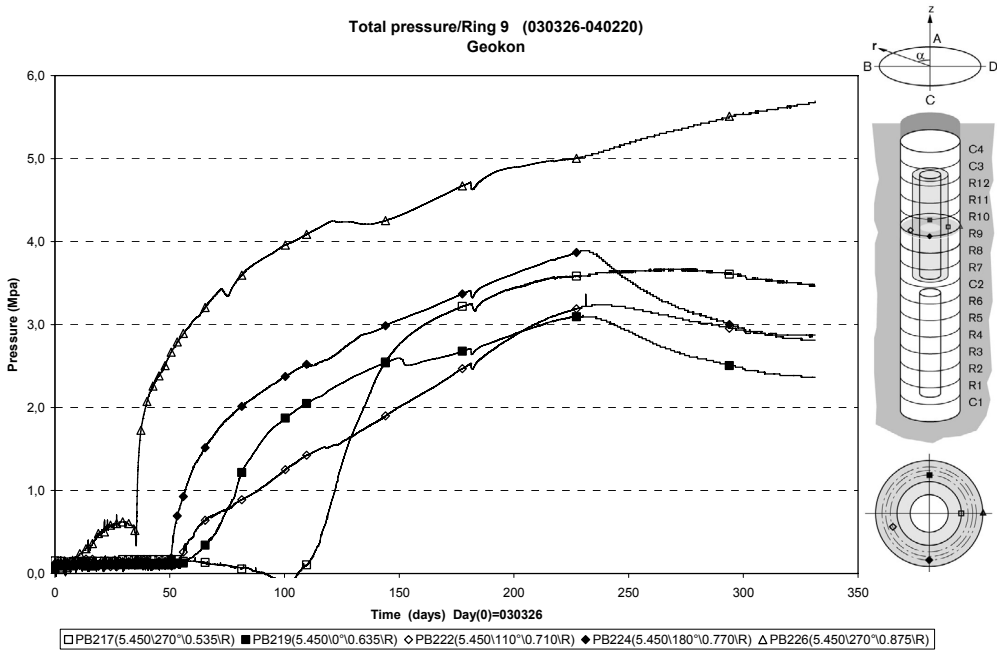

Figure 1. *Radial stresses in Ring 9 in TBT experiment.*

An attempt to capture some aspects of the mechanism behind the radial stress development was made using a Mohr-Coulomb plasticity model and the FLAC software. Figure 2 shows the conceptual model: The sand shield is stress-free up to about 110 days after test start. The bentonite blocks are largely in an elastic state with a high cohesion, in particular the portions close to the sand shield (upper). Because of wetting and increased loading, the bentonite block fails and compresses the sand shield (lower).

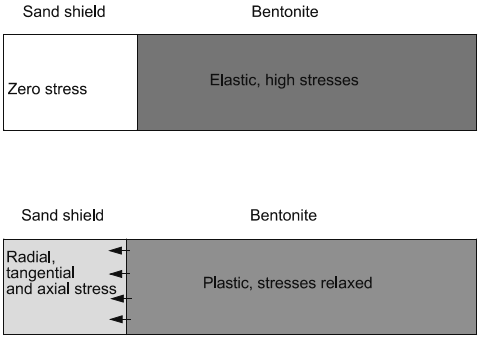

Figure 2. *Conceptual model. Sand and bentonite block before plastication (upper) and after plastication (lower).*

FLAC model

The investigated model was an axis symmetric rectangle divided into 31 elements in the radial direction and two elements in the axial direction. The radial width of each element was increased geometrically with the radius (see Figure 3).

The inner 19 elements were assigned properties corresponding to sand, whereas the outer 12 elements were given properties matching those of bentonite (Table 1).

Bentonite block properties were estimated from the literature /Kalbantner and Johanneson, 2000/. Values for the sand were estimated from compression test results.

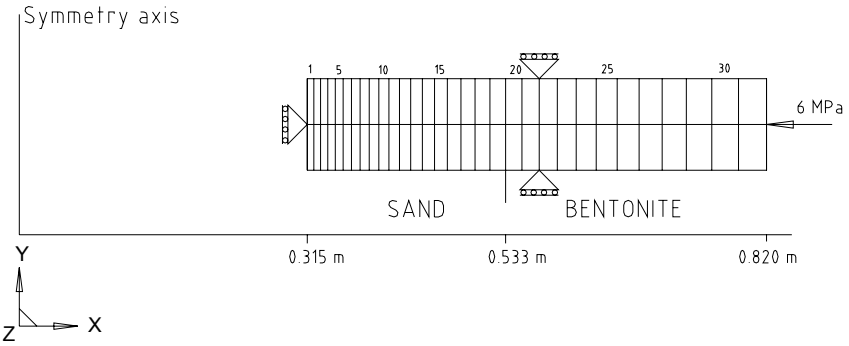

Figure 3. *Model geometry*

Table 1. material properties

Material	Bulk modulus (MPa)	Shear modulus (MPa)	Cohesion (MPa)	Friction (°)	Tension (MPa)	Density (kg/m^3)
Sand	30	6	0	30	0	2.500
Bentonite before plastication	30.000*	6.000*	5	30	6	2.500
Bentonite after plastication	300	60	0.1	30	0	2500

* Artificially high values set to suppress movement during initial equilibrium calculation.

The inner, upper and the lower boundaries were fixed in the normal direction. At the outer boundary, a constant radial stress of 6 MPa was applied.

Initial equilibrium state

The FLAC software performs mechanical calculations from an arbitrarily specified initial state to a state of equilibrium. Some calibration may be required in order to generate a given target equilibrium state. In the present model, each bentonite element was assigned initial stresses: 18 MPa in the radial direction and 15 MPa in the tangential and axial directions. The resulting equilibrium stresses are shown in Figure 4a. The straining up to this point was almost purely elastic.

Plastic deformation

After the initial equilibrium was achieved, plastic deformations were induced by reducing the bentonite cohesion (Table 1). The bentonite stiffness parameters were set at reasonably relevant values (Table 1). The FLAC model was run until a new equilibrium state was achieved, Figure 4b.

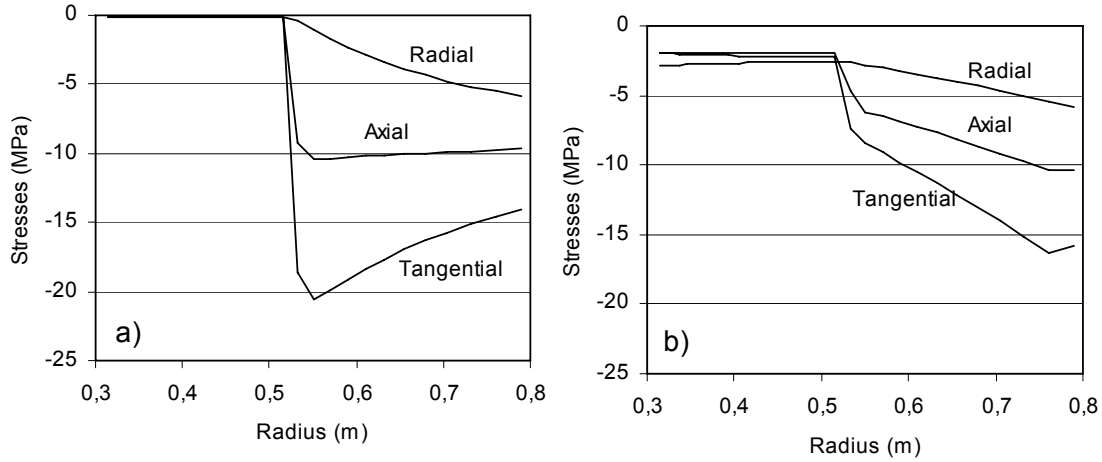

Figure 4. *Stresses at initial equilibrium (a) and after plastication (b).*

Summary

The transition from a state at the bentonite-sand interface with no radial stresses to a stress state of 2 – 3 MPa, similar to the test results in Figure 1, could be reproduced in principle. The model used here ignores the fundamental controlling process, i.e. the successively increased wetting. However, it provides a rough and qualitative illustration of the effects of that wetting, i.e. plastication of the bentonite block and following compression of the sand shield.

Reference

Kalbantner P., Johanneson L-E., 2000. Strength calculations of a bentonite buffer made up of uniaxially compacted bentonite bodies. SKB R-00-42 (In Swedish)

Temperature Buffer Test

Evaluation Modelling performed by

ENRESA

May 2004 report

ENRESA Contribution
A. Ledesma, G.J. Chen, A. Jacinto (UPC)
M. Velasco (DM Iberia)
F. Huertas (ENRESA)

Contents

1 Introduction

This report presents the modelling work performed by the team coordinated by ENRESA (Spain) regarding the evaluation modelling of the "TBT" experiment defined by ANDRA (France) and conducted at Äspö Hard Rock Laboratory (Sweden). The work refers to the following tasks:

a) Comparison between calculations and measurements for the measured variables during last year.
b) Prediction of the effects of an overheating in the upper part of the experiment, after day 430.

The indications included in the document "TBT – Evaluation Modeling Program" by Hökmark, Fälth and Åkesson (Clay Technology, March 2004) have been followed. It is important to point out that the analyses presented here constitute a modelling attempt performed within the short period of time available. Further calculations are expected to be performed for a more comprehensive understanding of the experiment by November 2004.

The code CODE_BRIGHT has been used in all cases. Only the T-H capabilities have been considered, and therefore, there is not a prediction of the mechanical variables involved in the test. That will be considered in the November report, as suggested by Clay Technology guidelines. In the T-H formulation, the gas equation has been always taken into account, due to the relevance of the gas pressure in the test.

The procedure used for the analyses presented here is similar to the one described in the "Predictive modelling report" presented by ENRESA last May 2003. Now some parameters have been updated and some physical laws improved, basically taking into account the information provided in the document by Clay Technology. However, the comparison between computations and measurements indicate that there is still room for further improvements, as there are some measured patterns that are difficult to reproduce in the simulations. Also, some of the difficulties in that task come from the problems encountered with some transducers in the test, and with the control of the boundary conditions (i.e. the tightness to gas of the whole experiment).

One of the events that required special attention is the cycle of suction and the corresponding decrease in total stresses around days 200 and 250. That happened in the upper heater and was totally unexpected. Next section indicates a possible explanation for that event in a qualitative manner, although it is concluded that further analyses should be performed to provide a definite and quantitative answer.

Section 3 summarizes the parameters and the conditions considered in the analyses for this report, whereas section 4 presents a comparison of computed and measured variables using those parameters. Section 5 compiles the predictions required in this exercise, that is, the effect of an overheating in the upper part, either in 6 or in 30 days, after June 2004. Finally, some conclusions about the convenience of this action and about the modelling work are included in section 6.

2 Stress reduction observed in the experiment

One of the interesting aspects of the experiment is the unexpected change in the trends observed for stresses (total pressures) and suction around day 200 – 250 in ring 9, that is, around the central area of the upper heater. During last weeks, some effort has been devoted to the analysis of that event, and the results are not satisfactory yet. Most probably there are several explanations of that unexpected behaviour, but at least one is presented here. The quantitative aspects are not fully developed, but a qualitative explanation is presented instead.

In the Clay Technology Report including the guidelines of this modelling exercise, we received an appendix with a possible explanation for that event ("A simple model of radial stress development in Ring 9", Akesson & Hokmark, Clay Technology). This is a good qualitative analysis of the problem, and the explanation included here shares some aspects of that work. Perhaps we have found more evidences that may complement that view of redistribution of stresses around ring number 9.

In fact, as the unexpected measurements involve stresses, most probably the key issue is the mechanical behaviour of that ring in the upper heater. In addition to that the mechanical aspects are related to the hydration of the bentonite and that provides the time scale to the problem. That also may explain why suction measurements show an unexpected pattern as well. In order to remind those unexpected trends, figure 1 shows the evolution of radial stresses against time. Tangential and axial stresses have shown a similar pattern, decreasing at some locations after day 200 or 250, whereas some points still increase the pressure. Figure 2 presents the suction evolution in this ring during the duration of the experiment. Note that hydration of the bentonite can only explain the decrease of suction, but not that cycle.

This process could accept different interpretations. If a mechanical explanation is considered, the stress release is directly related to a movement of the inner sand – bentonite contact. The outer sand filter would play a less important role. This effect has not been detected in the lower heater. In fact sand shield seems to behave as loose sand that allows the inner boundary of the bentonite to move towards the heater. Sand has been compressed to a value around 3 – 4 MPa and that implies an important reduction of its volume (5% according to the information provided by Clay Technology). That explains why radial stress decrease at a particular point. Timing is controlled by the saturation of the outer part of the bentonite block.

The decrease in radial stress while keeping tangential and axial stresses at usual high values for saturated bentonite may lead to a situation where deviatoric stresses become important. Figure 3 presents the measured total stresses at Ring 9, depicted in a mean stress – deviatoric stress graph. A similar plot for Ring 3 is presented in figure 4. The measured data allow analyzing the stress path of two bentonite points. Measurements at the beginning of the experiment may not be reliable in cell pressure transducers. However, after a minimum stress value, measurements are usually consistent.

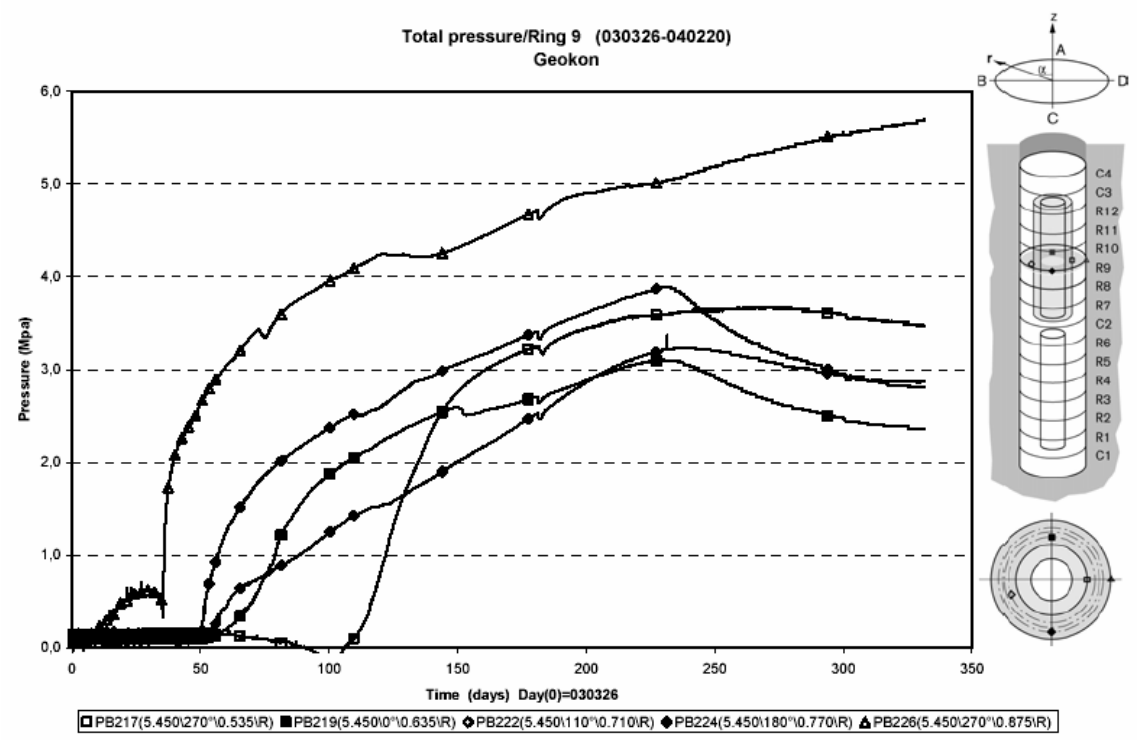

Figure 1. *Radial stresses evolution – Ring 9 (Clay Technology Report)*

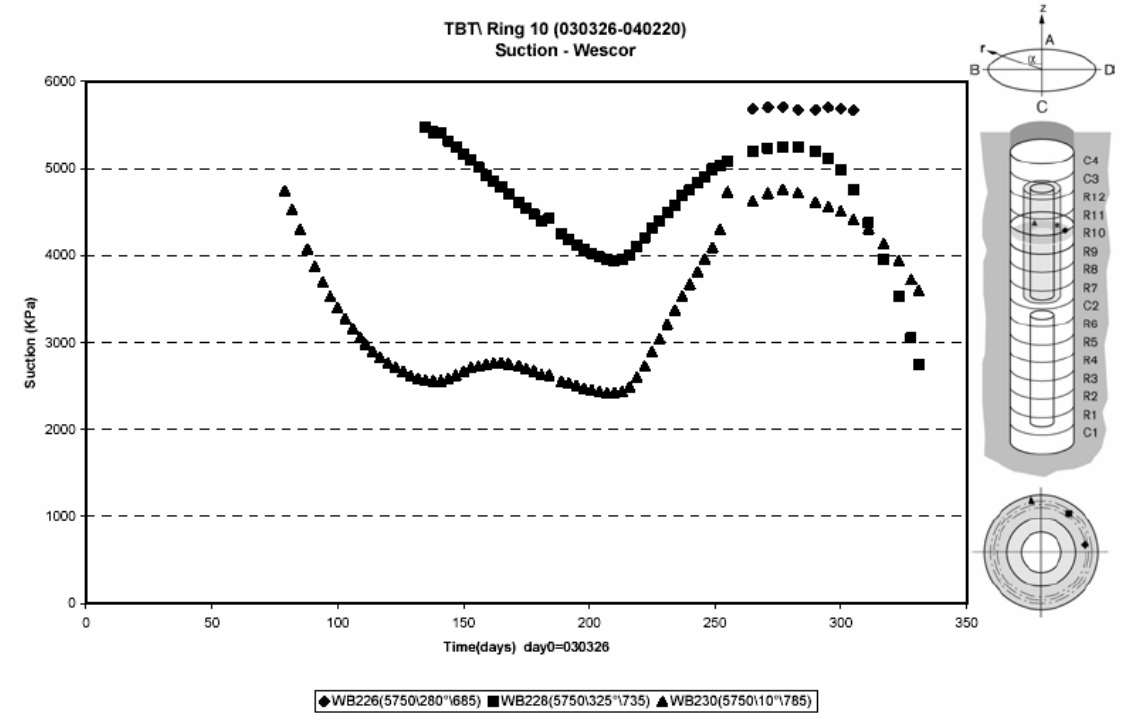

Figure 2. *Suction evolution – Ring 10 (Clay Technology Report)*

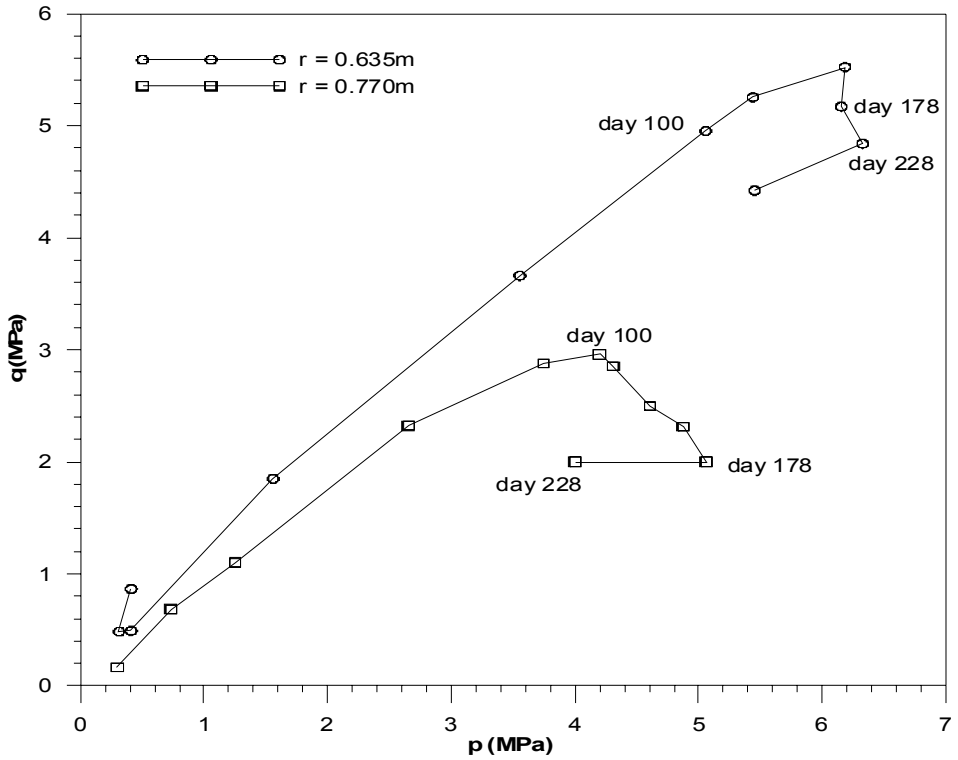

Figure 3. *Stress path (Mean stress "p" – Deviatoric stress "q") for two points in bentonite Ring 9*

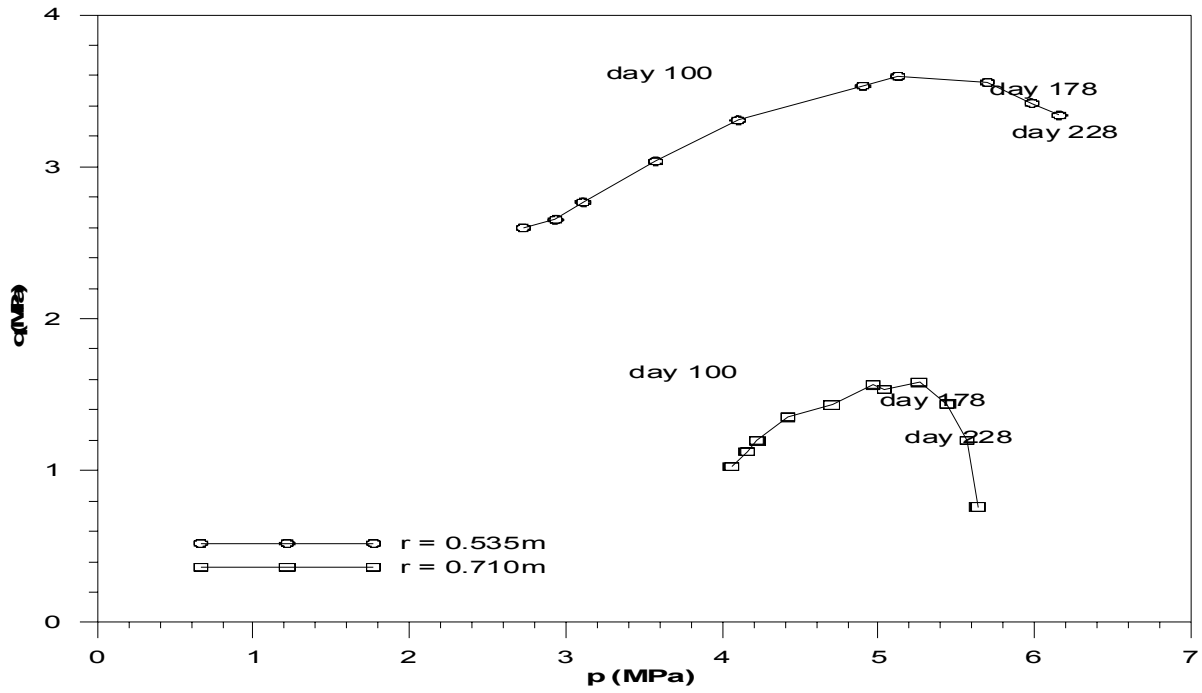

Figures 4. *Stress path (Mean stress "p" – Deviatoric stress "q") for two points in bentonite Ring 3. Note: Axial stresses for point at r=0.535 m were obtained from measurements at r=0.585. For point at r=0.710 axial stresses were measured at r=0.770.*

Figure 3 suggests that deviatoric stresses are quite important in this context and they seem to reach the extended Mohr-Coulomb envelope. This failure envelope takes into account the effect of unsaturation, basically by assigning an apparent cohesion to the material which is suction dependent (Fredlund and Rahardjo, 1993). This is also consistent with the standard elastoplastic models developed for unsaturated soils (Alonso et al, 1990).Thus bentonite at Ring 9 seems to develop plastic shear strains. This effect seems to be less important (although not negligible) at the bentonite surrounding the lower heater, where stresses are more homogeneous. Note that the slopes in the p-q path are smaller in Figure 4 than in figure 3.

This explanation comes from an attempt to understand what happened at Ring 9, but future work is required to complete that picture and to disregard other explanations. So far it seems that sand shield (and perhaps also sand filter) constitutes a "flexible" boundary for the bentonite blocks that may induce anisotropy in the stress distributions and therefore the possibility of a "shear failure". The consequences of that "shear failure" of the bentonite, if confirmed, should be analyzed in detail in the context of the project. Most probably, due to the confinement of the system, that will not constitute a fundamental drawback. In any case, the dismantling of the test will help in the understanding of this event.

As an academic exercise, we tried to reproduce changes in stresses considering the HM behaviour of a system sand-bentonite-sand. Several 1D analyses were performed with the objective of understanding the mechanisms involved in the distribution of stresses in that system. The thermal problem was not considered in order to simplify the analyses, and because it is assumed not relevant in this event. The geometry was the same of the experiment at the upper heater zone. Elastoplastic models were adopted for the bentonite and for the sand, and the parameters had to be defined according to the information available. Some of them were defined by guess. Boundary conditions were defined as in the actual experiment.

Figure 5 and 6 present typical results obtained for a point in the bentonite regarding the evolution of tangential and axial stresses. The purpose of the analysis is to show that a cycle in the stress evolution may be simulated by taking into account the flexibility of the sand layers surrounding the bentonite. The cycle of suction has not been reproduced yet; only very small variations have been obtained in this analysis, but not as large as the one shown in figure 2. That indicates that further work is left for the future. In addition to that, new evidences may come from the measurements in the near future, and when dismantling the experiment.

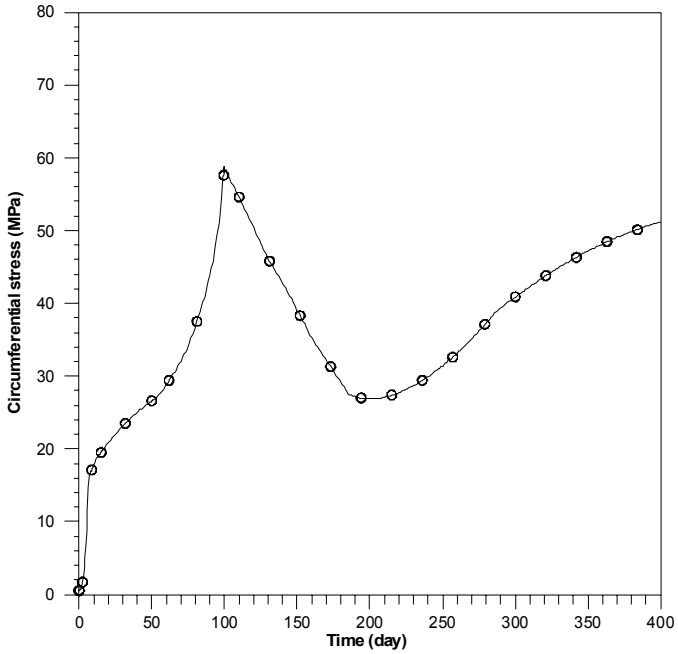

Figure 5. *Tangential stresses evolution for the 1D HM academic analysis*

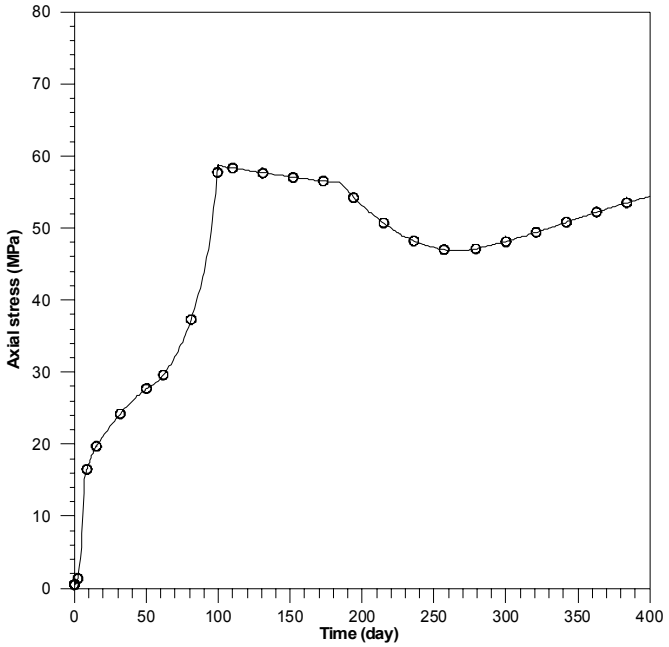

Figure 6. *Axial stresses evolution for the 1D HM academic analysis*

3 Parameters and physical laws used

Figure 7 presents a diagram of the geometry involved in the experiment, including the materials considered. Note that bentonites used in the buffer of heater 1 and heater 2 have been considered as different materials because they have slightly different properties.

The parameters used in the simulations have been obtained from the information provided in the guidelines for the modelling work from 2003 and from 2004 (Hökmark and Fälth, 2003; Hökmark, Fälth and Åkesson, 2004). Some of the data have been transformed into mathematical expressions according to CODE_BRIGHT requirements.

The analyses included in this report are TH simulations, and thus only thermal and hydraulic parameters are described in this section. Additionally, as the gas balance equation is taken into account, the gas permeability has been required. Because of the lack of information on that parameter, some assumptions based on the experience of Febex project (FEBEX, 2000; Villar, 2002) have been used.

The boundary conditions refer to the 2D axisymmetric geometry (sometimes referred to as “Quasi3D”). Figure 8 shows a simplified scheme of that geometry and the boundary conditions considered. A summary of the main parameters required for the analyses follow.

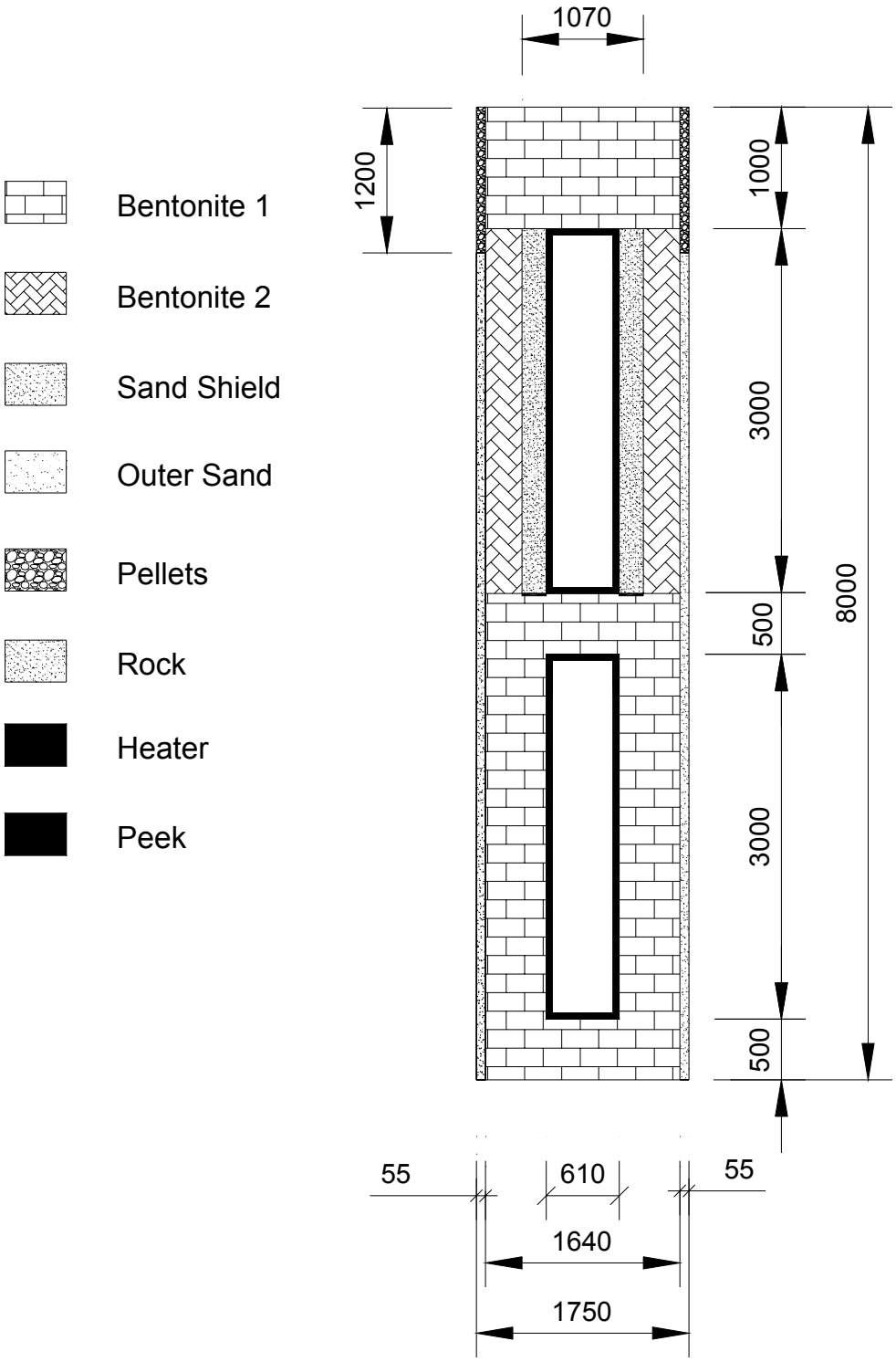

Figure 7. *Basic geometry of the TBT experiment including the materials involved in the modelling work (dimensions in mm).*

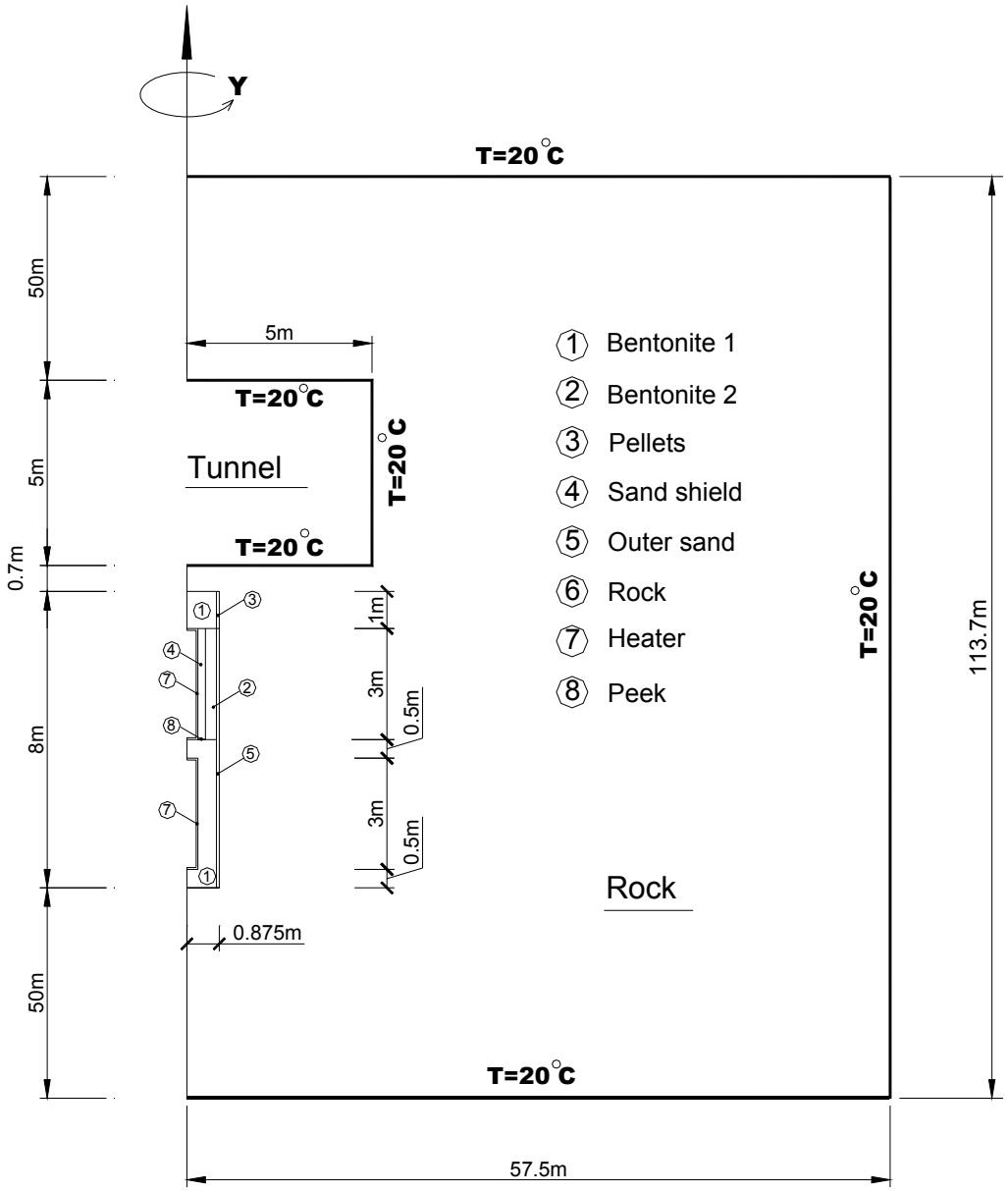

Figure 8. *Scheme of the geometry used in the analyses: Quasi 3D (2D Axisymmetric)*

Basic Parameters

Thermal Problem

Thermal conductivity $\lambda(W/mK)$

Material	Law	λ_{dry}	λ_{sat}
Bentonite 1	$\lambda = \lambda_{sat} \cdot S_r + \lambda_{dry} \cdot (1 - S_r)$	0.3	1.25
Bentonite 2		0.3	1.25
Rock		2.6	2.6
Pellets		0.6	0.8
Sand shield		0.6	1.7
Outer sand		0.6	1.7
Steel		50.16	50.16
Peek		0.25	0.25

Specific Heat $c(J/kgK)$

Material	Bentonite 1 & 2	Rock	Pellets	Sand shield	Outer sand	Steel	Peek
$c(J/kgK)$	1091	800	1091	900	900	460	1091

Hydraulic Problem

Retention Curve

Material	Law (Van Genuchten)	P_0 (MPa)	β	S_m (MPa)	m
Bentonite 1	$S_e = \frac{S_l - S_{rl}}{S_{ls} - S_{rl}} = \left[1 + \left(\frac{P_g - P_l}{P_0}\right)^{\frac{1}{1-\beta}}\right]^{-\beta} \left(1 - \frac{P_g - P_l}{S_m}\right)^m$	60	0.3	800	1.1
Bentonite 2		60	0.3	800	1.1
Sand		0.1	0.3	800	1.1
Pellets	$S_e = \frac{S_l - S_{rl}}{S_{ls} - S_{rl}} = \left[1 + \left(\frac{P_g - P_l}{P_0}\right)^{\frac{1}{1-\beta}}\right]^{-\beta}$	0.2	0.4		
Rock		1000	0.3		
Heater					
Peek					

Intrinsic Permeability $k(m^2)$

Material	Law (Kozeny's Model)	$k_0\,(m^2)$	ϕ_0
Bentonite 1	$k_i = k_0 \frac{\phi^3}{(1-\phi)^2} \frac{(1-\phi_0)^2}{\phi_0^3}$	0.45×10^{-20}	0.389
Bentonite 2		0.35×10^{-20}	0.368
Pellets		2.0×10^{-19}	0.5684
Inner sand		10^{-16}	0.30
Outer sand		10^{-30}	0.36
Rock		10^{-30}	0.003
Heater		10^{-30}	0.001
Peek		10^{-30}	0.001

Liquid Relative Permeability: $k_{rl} = S_e^3$

Gas permeability:

Material	Law (Kozeny's Model)	A
Bentonite 1	$k_g = \frac{\rho g}{\mu_g} \times A \times k_i \times (1 - S_r)^n$	0.1260×10^9
Bentonite 2		0.1105×10^9
Pellets		1
Inner sand		10^7
Outer sand		1
Rock		1
Heater		1
Peek		1

Vapor diffusion

$i_g^w = -\phi \rho_g S_g \tau D_m^{vapor} \nabla \omega_g^w$

where $D_m^{vapor}(m^2/s) = 5.9 \times 10^{-12} \frac{(T + 275.16)^{2.3}}{P_g}$, $\tau = 1$, and P_g is in MPa units.

Diffusivity of dissolved air

$i_l^a = -\phi \rho_l S_l \tau D_m^{air} \nabla \omega_l^a$

where $D_m^{air}(m^2/s) = D \exp\left(\frac{-Q}{R(273.16 + T)}\right)$, $D = 1.1 \times 10^{-4}$, $Q = 24530$ and $\tau = 10^{-5}$

Boundary conditions

(1) Temperature boundary condition:
Outer boundary of rock: $T = 20^\circ C$
Tunnel boundary: $T = 20^\circ C$

(2) Heat flux(Day 0=26/03/03):

a) Overheating within 6 days
Lower heater: 0~8 days, 900W; 8~15 days, 1200W; 15~1000days, 1500W.
Upper heater: 0~8 days, 900W; 8~15 days, 1200W; 15~433days, 1500W;
433~439, 1500-2250W; 439~1000, 2250W.

b) Overheating within 30 days
Lower heater: 0~8 days, 900W; 8~15 days, 1200W; 15~1000days, 1500W.
Upper heater: 0~8 days, 900W; 8~15 days, 1200W; 15~433days, 1500W;
433~463, 1500-2250W; 463~1000, 2250W.

(3) Pore water pressure of outer sand:
From 1~81th day, water level moves from the bottom of the outer sand (0m) to the top of the pellets (8m).
Under water level, $P_w = P_g = 0.1MPa$.

(4) Pore water and gas pressure in rock:
$P_w = P_g = 0.1MPa$

Initial conditions

Materials	Temperature $(^{\circ}C)$	Pore water pressure (MPa)	Porosity	Saturation degree
Bentonite 1	20	-47.5	0.389	0.798
Bentonite 2		-47.5	0.368	0.798
Sand shield		-62.5	0.3	0.058
Outer sand		-62.5	0.36	0.058
Rock		0.1	0.003	1.0
Pellets		-2.03	0.5684	0.211
Heater		0.1	0.001	1.0
Peek		0.1	0.001	1.0

4 Comparison between measured and computed variables

Using the parameters and the geometry and boundary conditions described above, a TH simulation of the test from day 0 (26 March 2003) has been attempted. The objective was to improve previous predictions that were performed before measurements were available, last May 2003. The comparison between computed and measured variables may give an indication of the quality of the models developed.

The comparison is presented as temperature or relative humidity against time, for different sections. The list of figure captions of this section follows:

Figure 9. Level Z = 0.25 m, Cylinder 1. Temperature and relative humidity evolution.

Figure 10. Level Z = 2.25 m, Ring 4. Temperature and relative humidity evolution.

Figure 11. Level Z = 3.75 m, Cylinder 2. Temperature and relative humidity evolution.

Figure 12. Level Z = 5.75 m, Ring 10. Temperature and relative humidity evolution.

Figure 13. Level Z = 7.25 m, Cylinder 3. Temperature and relative humidity evolution.

It can be observed that the general trends of the measured variables are well reproduced. The event described in section 2 is not relevant here because the mechanical problem has not been analyzed.

Differences in temperature that in some cases reach several degrees centigrade may be directly related to the uncertainties in the initial conditions due to the CRT experiment that takes place nearby. Computed relative humidity values exhibit smoother trends that measured ones. In this case heterogeneities of the material and in the installation in contrast with the strict symmetry of the model may explain those discrepancies. Nevertheless, future evaluation modeling work will be required in order to check the predictions of next section and to explain the unexpected mechanical behavior described in section 2.

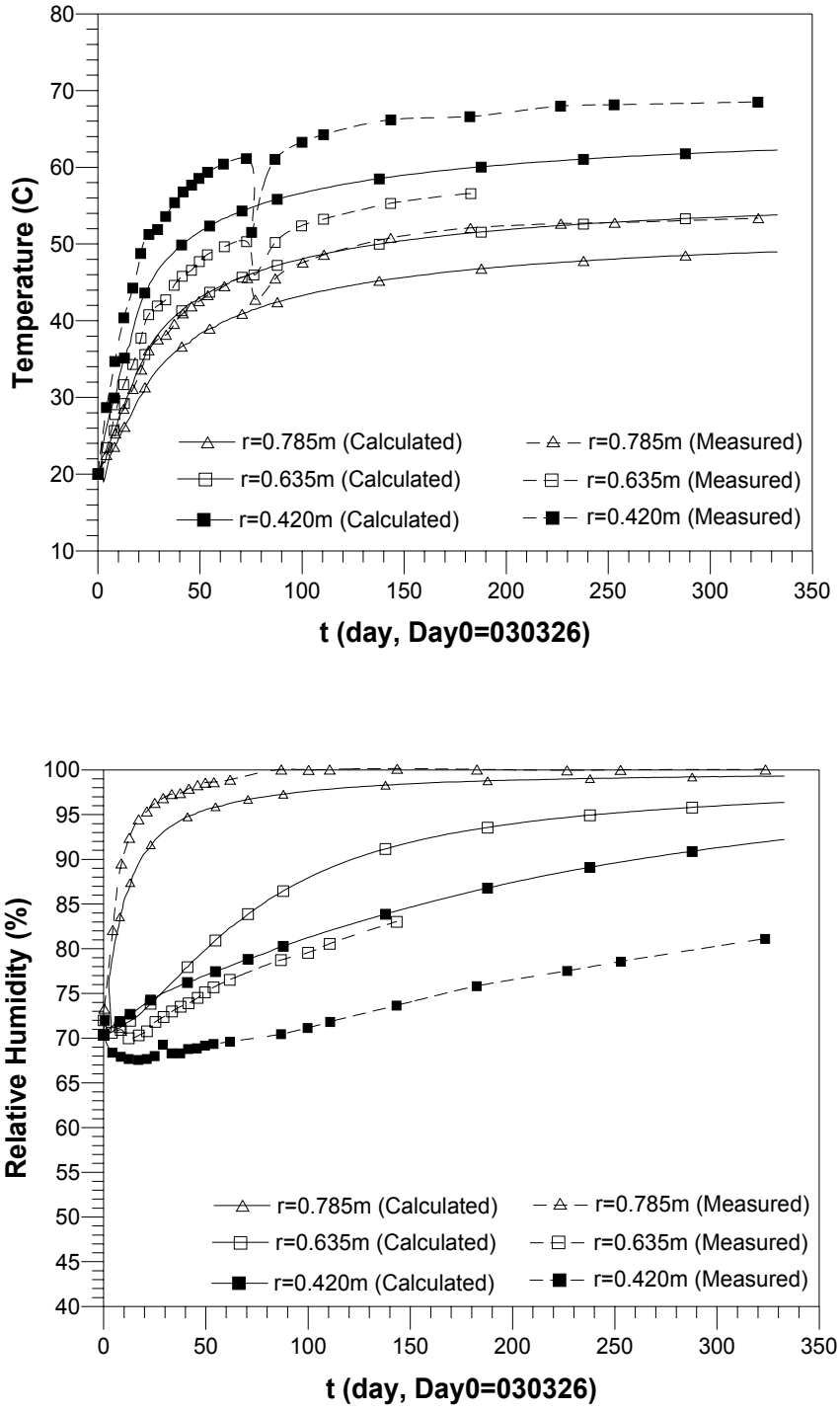

Figure 9. *Level Z = 0.25 m, Cylinder 1. Temperature and relative humidity evolution.*

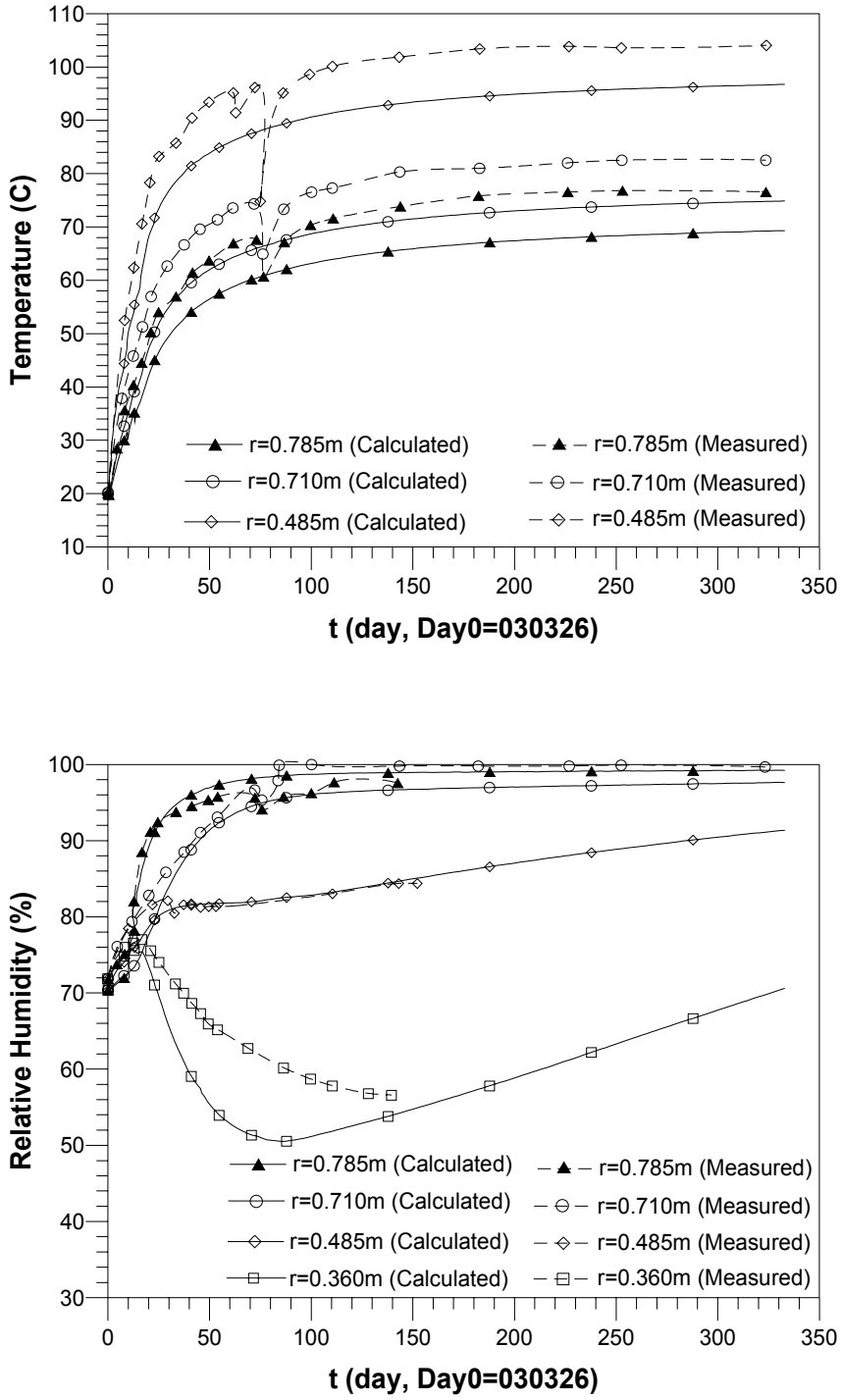

Figure 10. *Level Z = 2.25 m, Ring 4. Temperature and relative humidity evolution.*

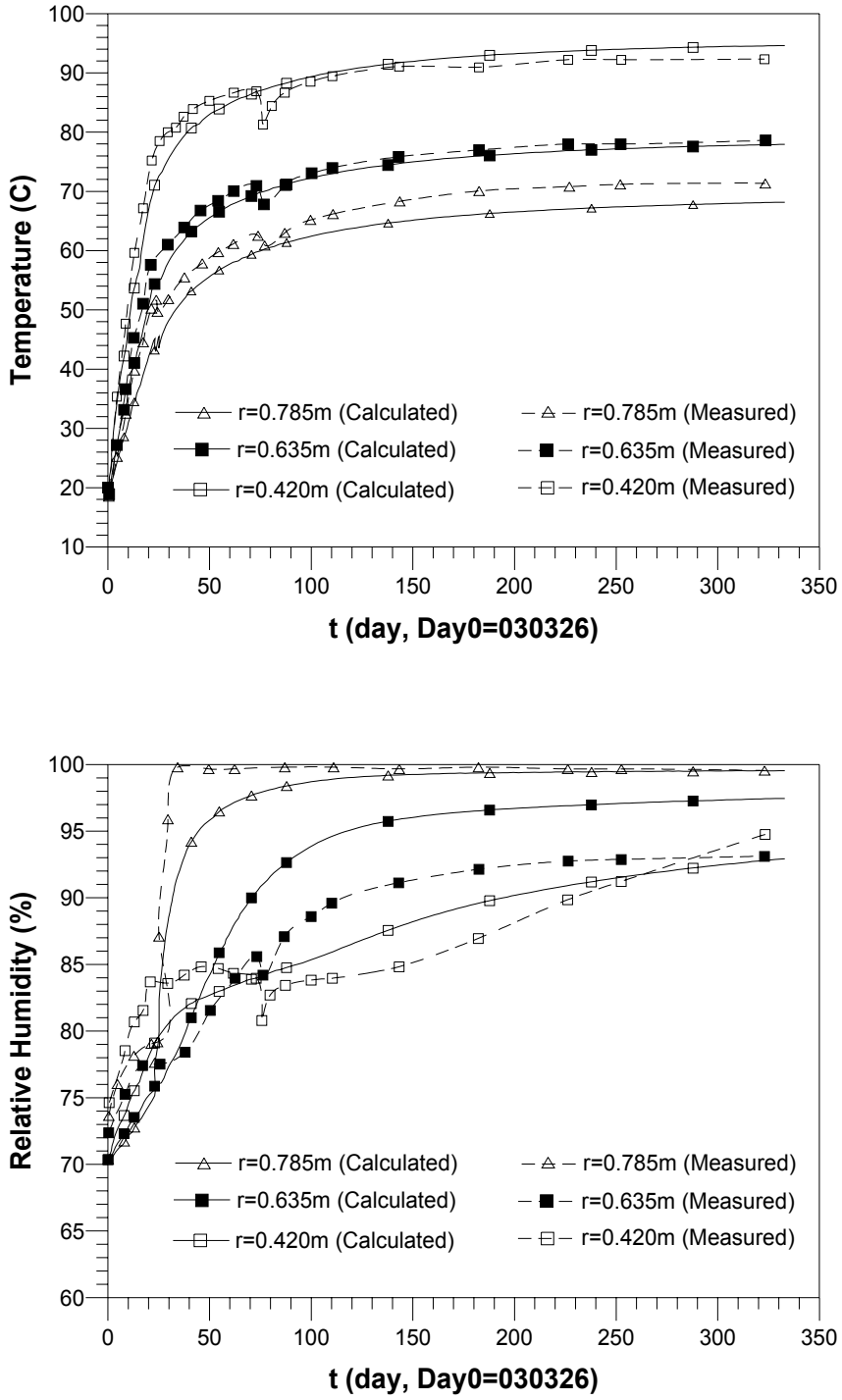

Figure 11. *Level Z = 3.75 m, Cylinder 2. Temperature and relative humidity evolution.*

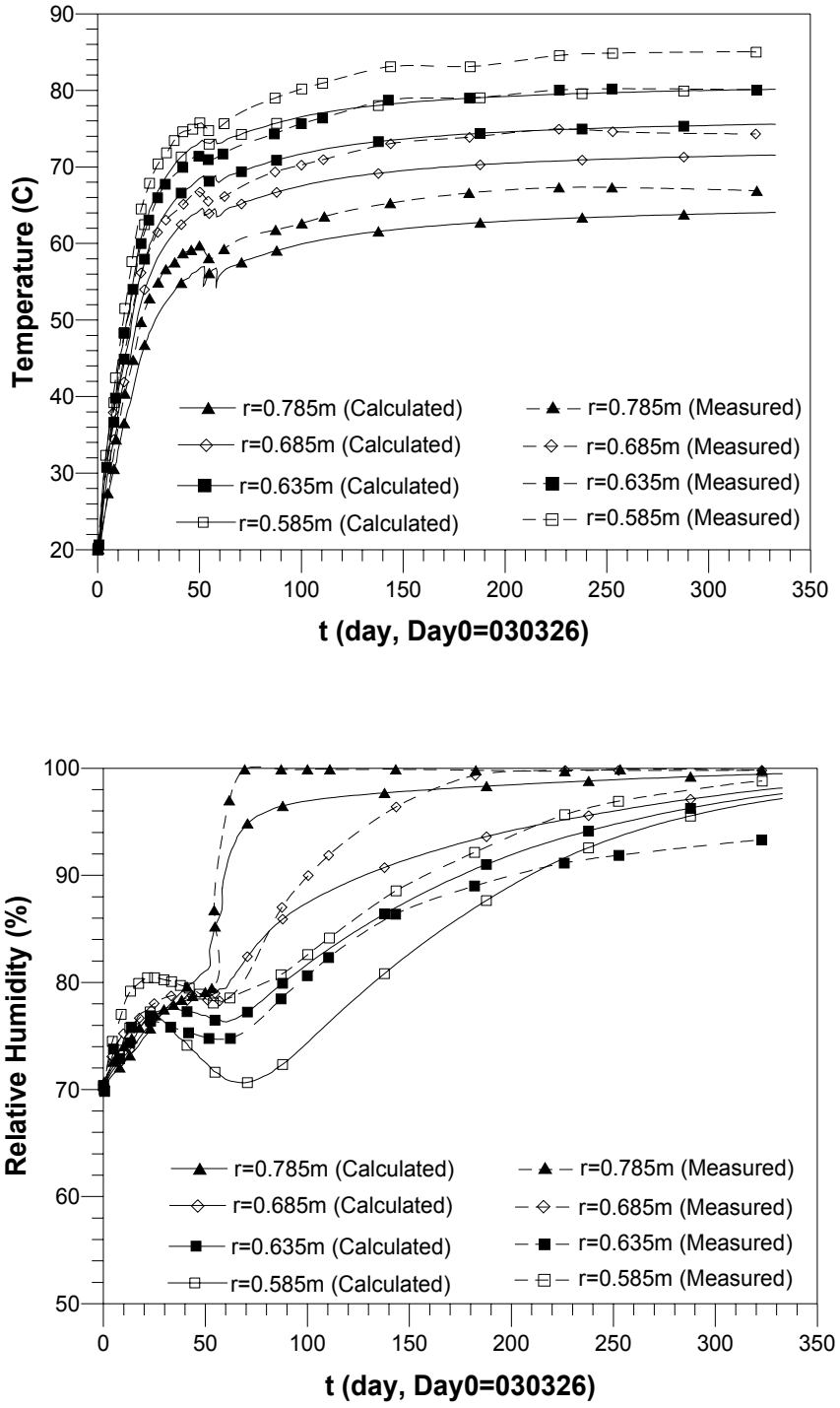

Figure 12. *Level Z = 5.75 m, Ring 10. Temperature and relative humidity evolution.*

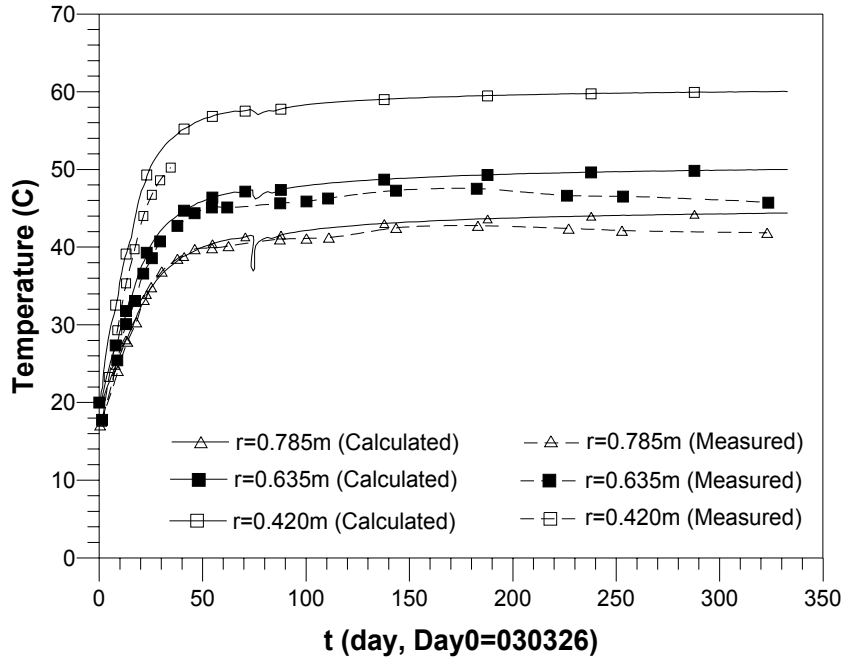

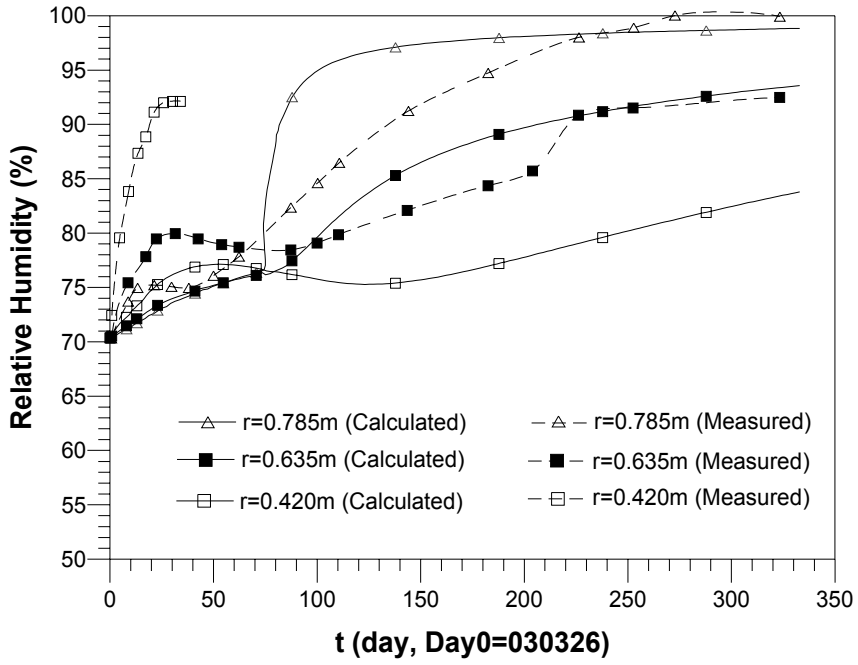

Figure 13. *Level Z = 7.25 m, Cylinder 3. Temperature and relative humidity evolution.*

5 Predictions for the overheating action

The results of the simulation presented as "predictions" of the group for the overheating action are included in this section. A full analysis of this problem including the mechanical behaviour will be developed by November 2004, as indicated in the guidelines.

The parameters, geometry and boundary conditions are the same as the ones indicated in section 3. Although the geometry considered is 2D axisymmetric, the hydraulic problem has been concentrated on the zones close to the heaters. That is, rock has not been taken into account in the hydraulic problem, avoiding water flow from the outer rock boundaries to the deposition hole. In fact this flow will be small because of the rock hydraulic permeability, and additionally, water pressure in the outer sand is fixed. Rock, however, has been taken into account in the heat conduction problem.

The points and scan-lines considered in these analyses are shown in figure 14, obtained from the guidelines of the predictive modeling program (Hökmark and Fälth, 2003).

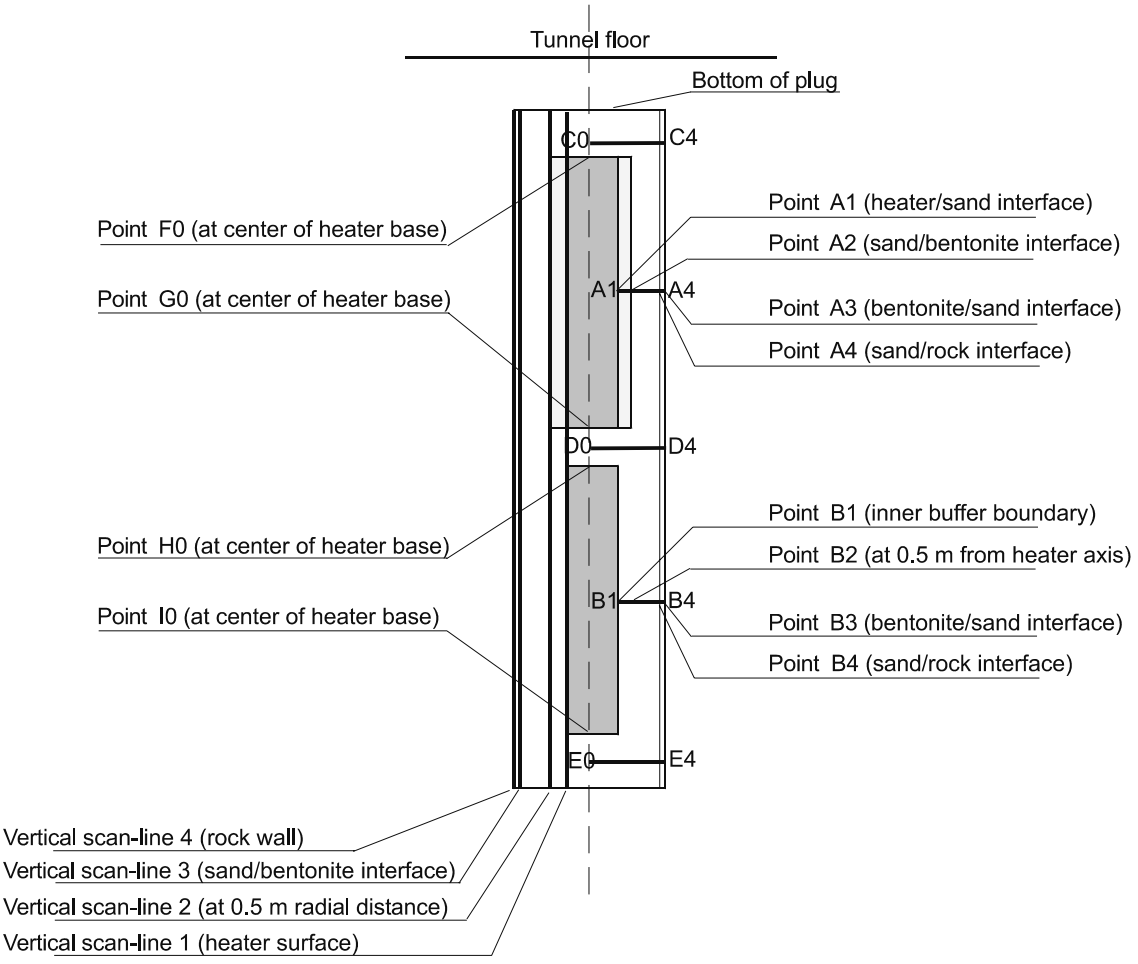

Figure 14. *Scheme of the experiment with proposed scan-lines (Hökmark & Fälth, 2003)*

A list of the figure captions is included here:

Overheating within 6 days

- Figure 15. Overheating within 6 days. Temperature in scan-line A1 to A4
- Figure 16. Overheating within 6 days. Saturation degree in scan-line A1 to A4
- Figure 17. Overheating within 6 days. Relative humidity in scan-line A1 to A4

- Figure 18. Overheating within 6 days. Temperature in scan-line B1 to B4
- Figure 19. Overheating within 6 days. Saturation degree in scan-line B1 to B4
- Figure 20. Overheating within 6 days. Relative humidity in scan-line B1 to B4

- Figure 21. Overheating within 6 days. Temperature in scan-line 1
- Figure 22. Overheating within 6 days. Temperature in scan-line 2
- Figure 23. Overheating within 6 days. Temperature in scan-line 3

Overheating within 30 days

- Figure 24. Overheating within 30 days. Temperature in scan-line A1 to A4
- Figure 25. Overheating within 30 days. Saturation degree in scan-line A1 to A4
- Figure 26. Overheating within 30 days. Relative humidity in scan-line A1 to A4

- Figure 27. Overheating within 30 days. Temperature in scan-line B1 to B4
- Figure 28. Overheating within 30 days. Saturation degree in scan-line B1 to B4
- Figure 29. Overheating within 30 days. Relative humidity in scan-line B1 to B4

- Figure 30. Overheating within 30 days. Temperature in scan-line 1
- Figure 31. Overheating within 30 days. Temperature in scan-line 2
- Figure 32. Overheating within 30 days. Temperature in scan-line 3

These figures correspond to the requirements indicated in the guidelines of the evaluation program. In addition to that, some figures including the time evolution of the basic variables have been included as well. In particular, Temperature evolution and Relative Humidity evolution for Rings number 4 (close to mid lower canister) and 10 (close to mid upper canister) have been included. The list of those figure captions follow:

- Figure 33. Overheating within 6 days. Ring 4. Temperature evolution.
- Figure 34. Overheating within 6 days. Ring 4. Relative Humidity evolution.
- Figure 35. Overheating within 6 days. Ring 10. Temperature evolution.
- Figure 36. Overheating within 6 days. Ring 10. Relative Humidity evolution.

- Figure 37. Overheating within 30 days. Ring 4. Temperature evolution.
- Figure 38. Overheating within 30 days. Ring 4. Relative Humidity evolution.
- Figure 39. Overheating within 30 days. Ring 10. Temperature evolution.
- Figure 40. Overheating within 30 days. Ring 10. Relative Humidity evolution.

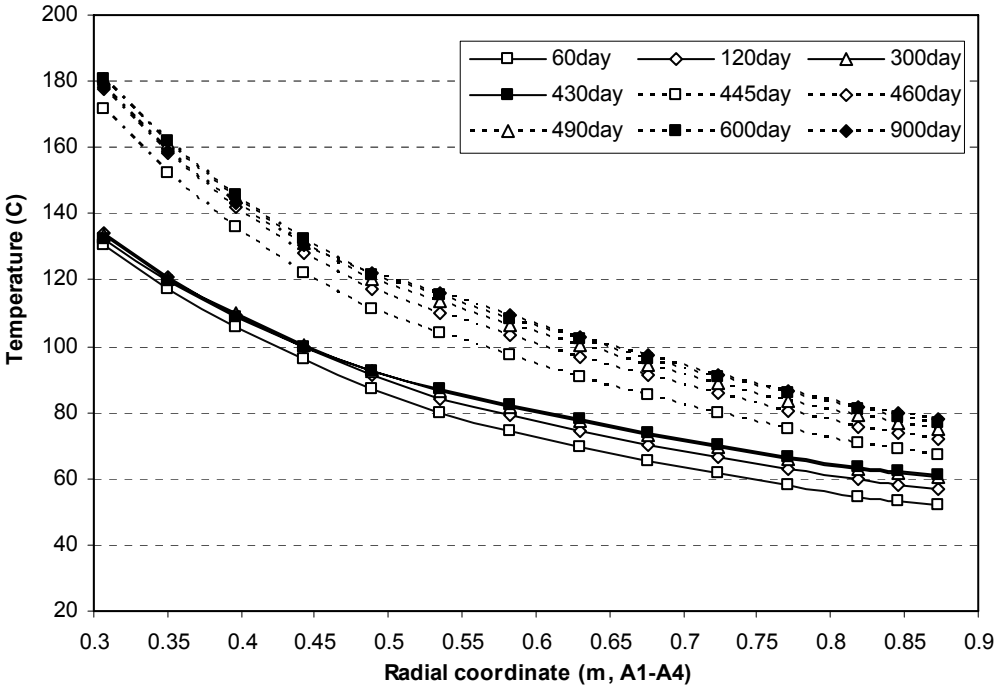

Figure 15. *Overheating within 6 days. Temperature in scan-line A1 to A4*

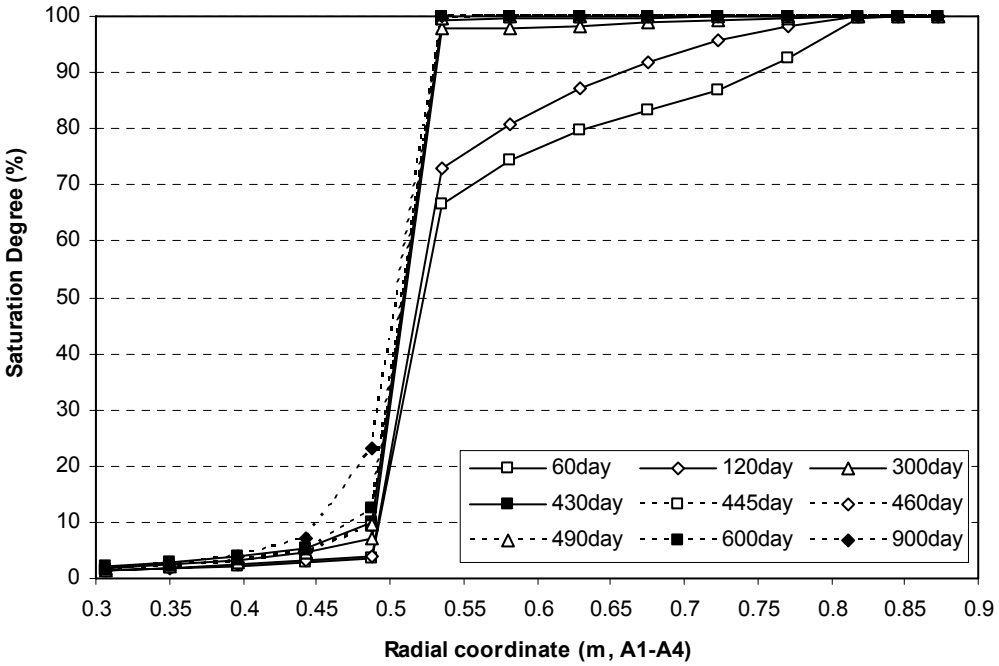

Figure 16. *Overheating within 6 days. Saturation degree in scan-line A1 to A4*

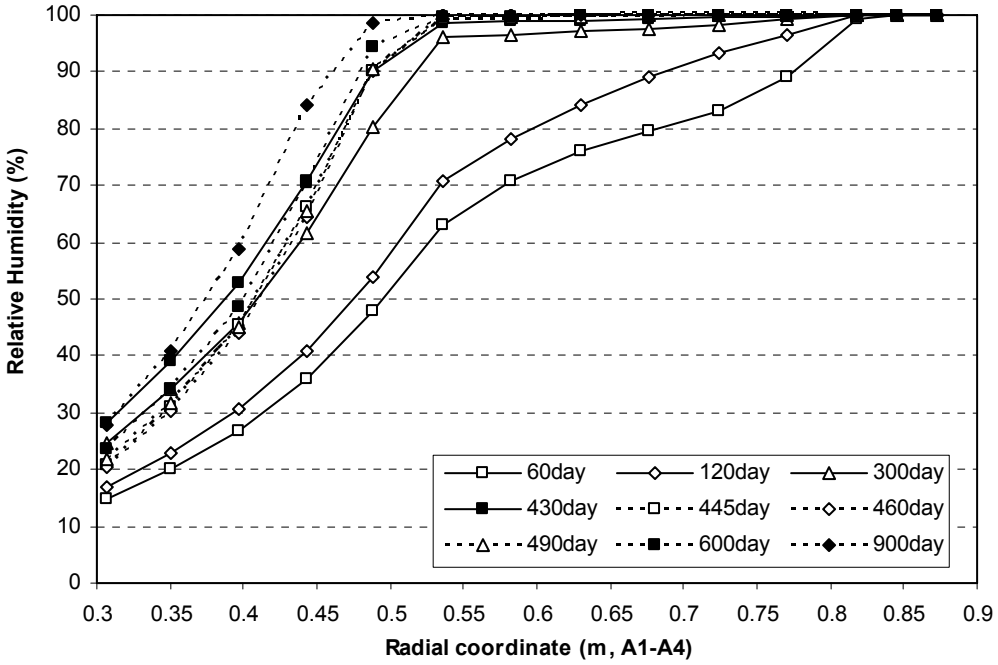

Figure 17. *Overheating within 6 days. Relative humidity in scan-line A1 to A4*

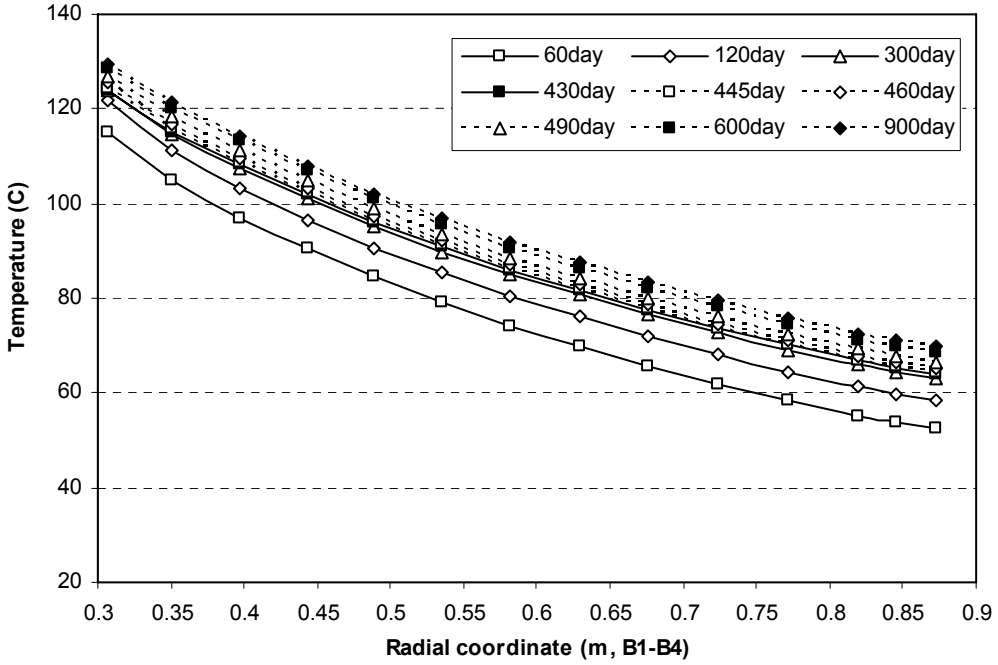

Figure 18. *Overheating within 6 days. Temperature in scan-line B1 to B4*

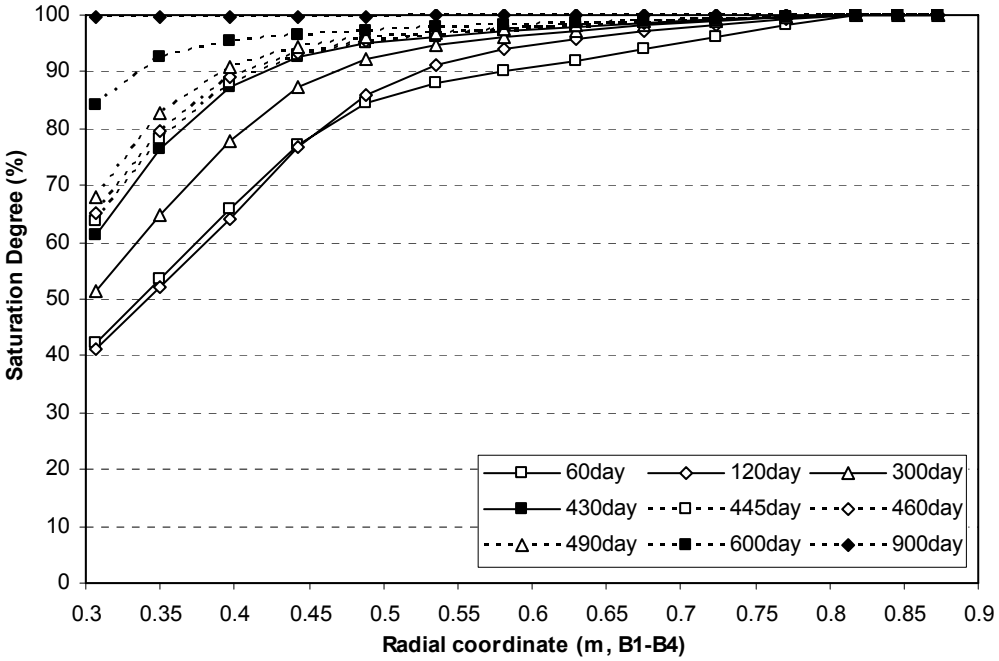

Figure 19. *Overheating within 6 days. Saturation degree in scan-line B1 to B4*

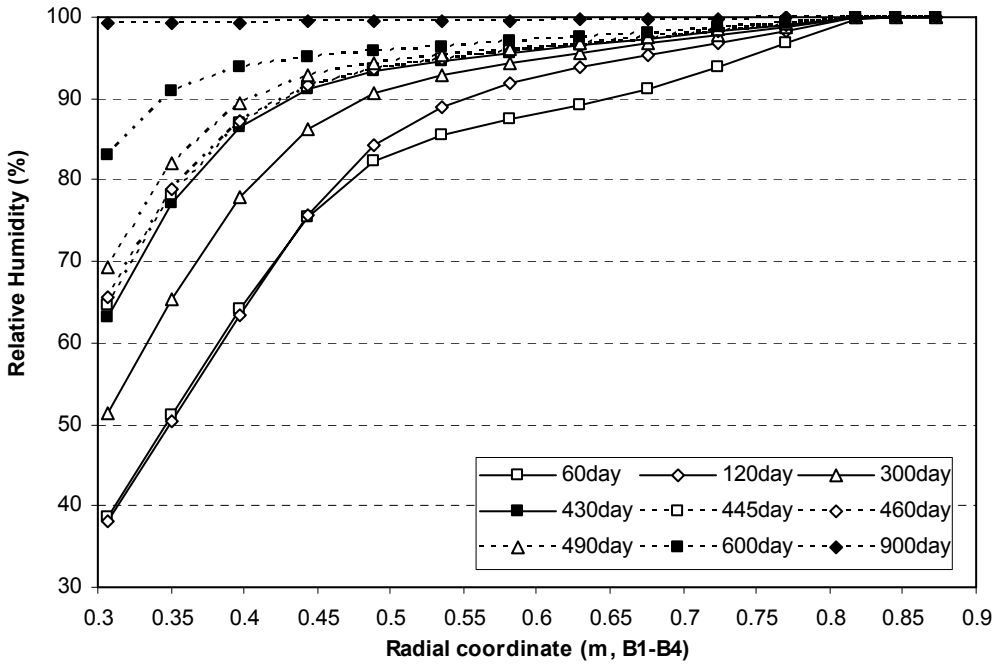

Figure 20. *Overheating within 6 days. Relative humidity in scan-line B1 to B4*

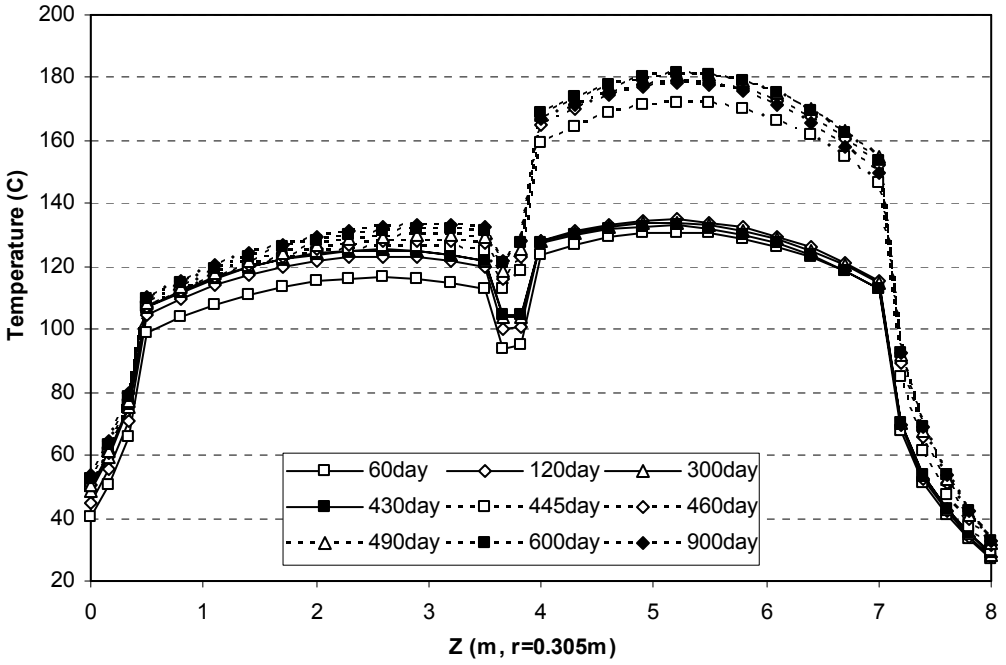

Figure 21. *Overheating within 6 days. Temperature in scan-line 1*

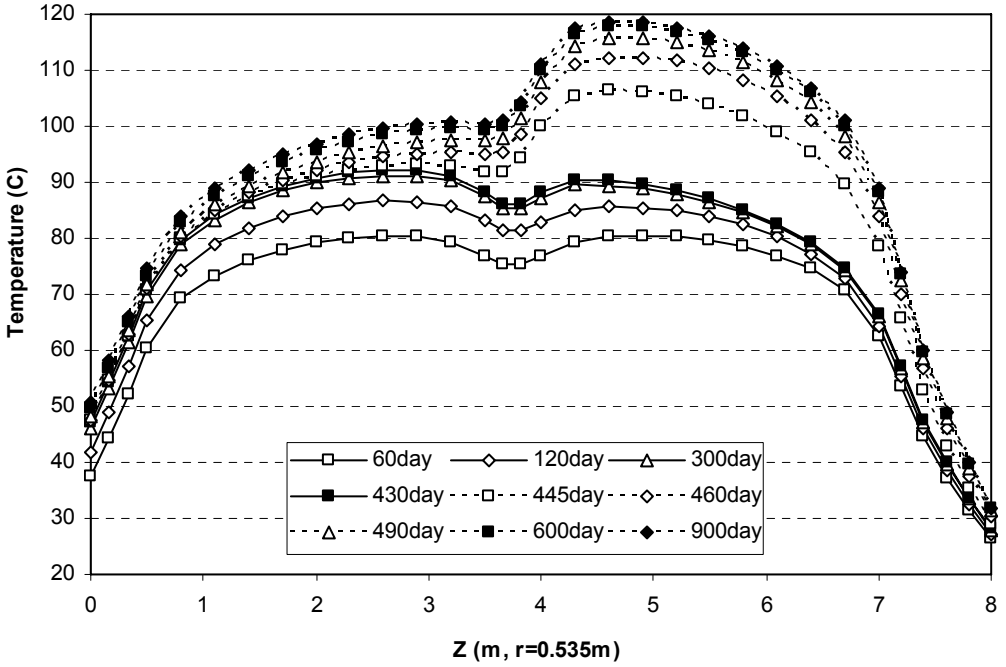

Figure 22. *Overheating within 6 days. Temperature in scan-line 2*

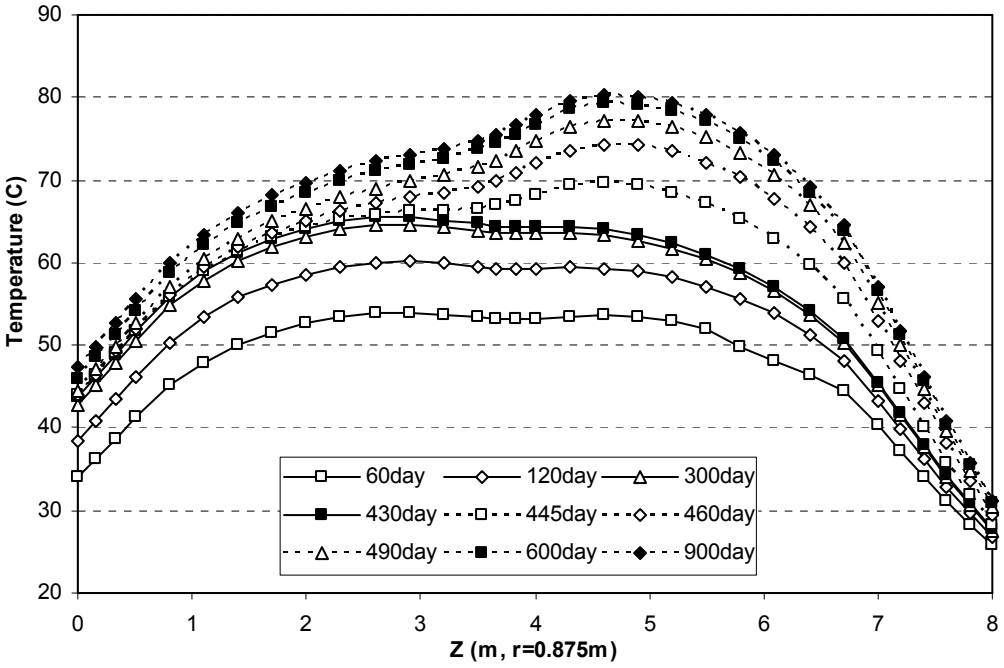

Figure 23. *Overheating within 6 days. Temperature in scan-line 3*

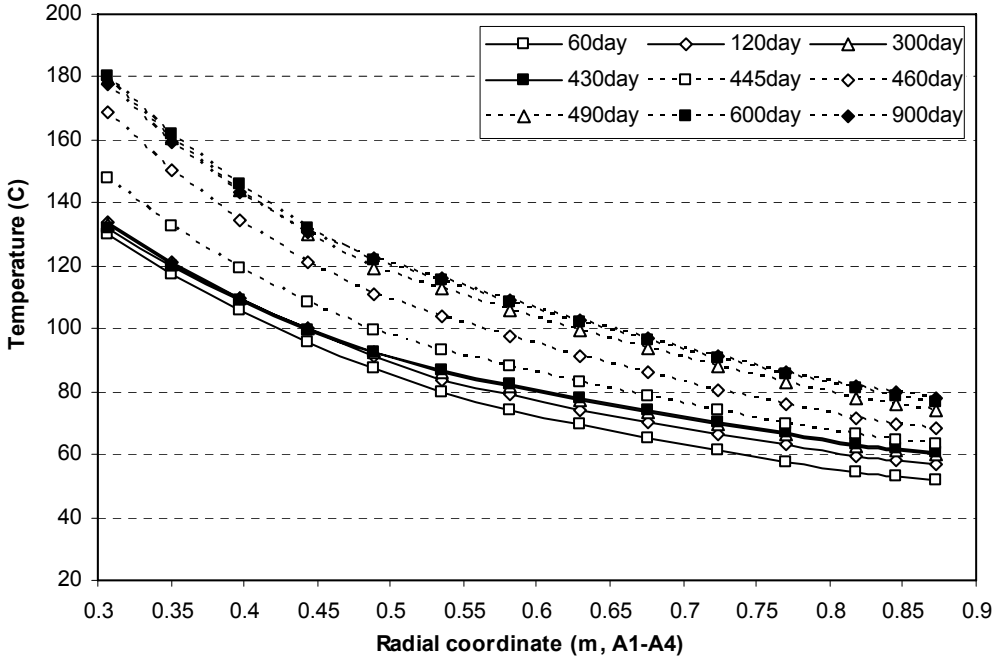

Figure 24. *Overheating within 30 days. Temperature in scan-line A1 to A4*

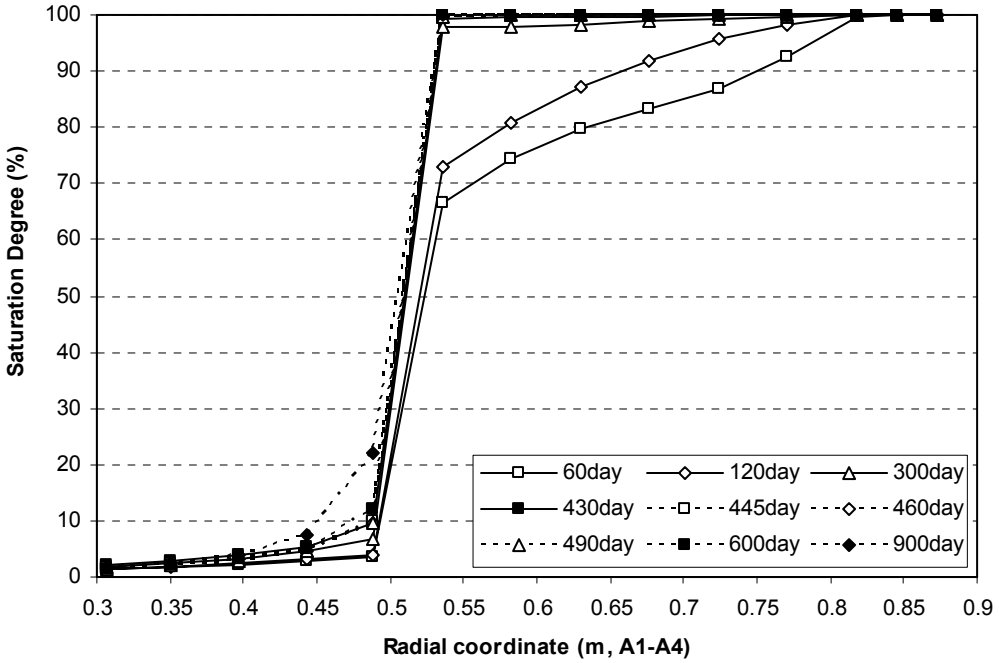

Figure 25. *Overheating within 30 days. Saturation degree in scan-line A1 to A4*

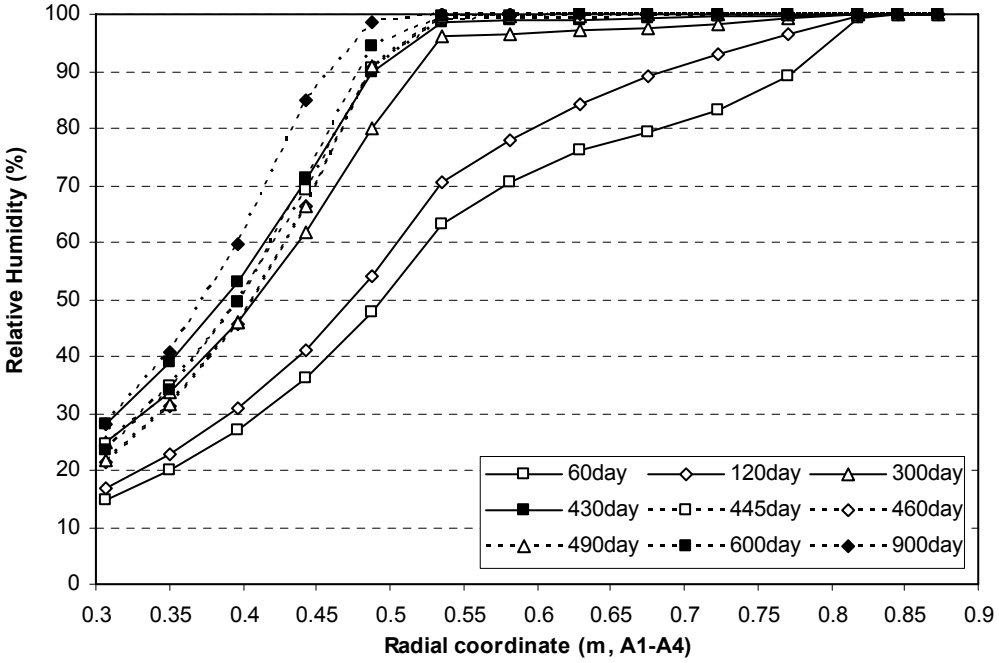

Figure 26. *Overheating within 30 days. Relative humidity in scan-line A1 to A4*

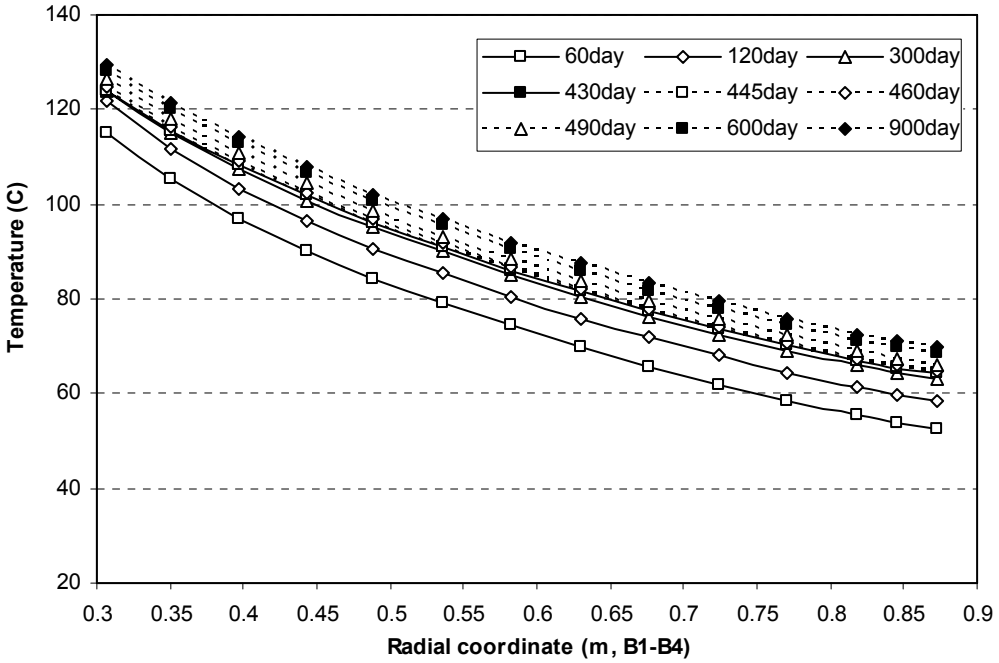

Figure 27. *Overheating within 30 days. Temperature in scan-line B1 to B4*

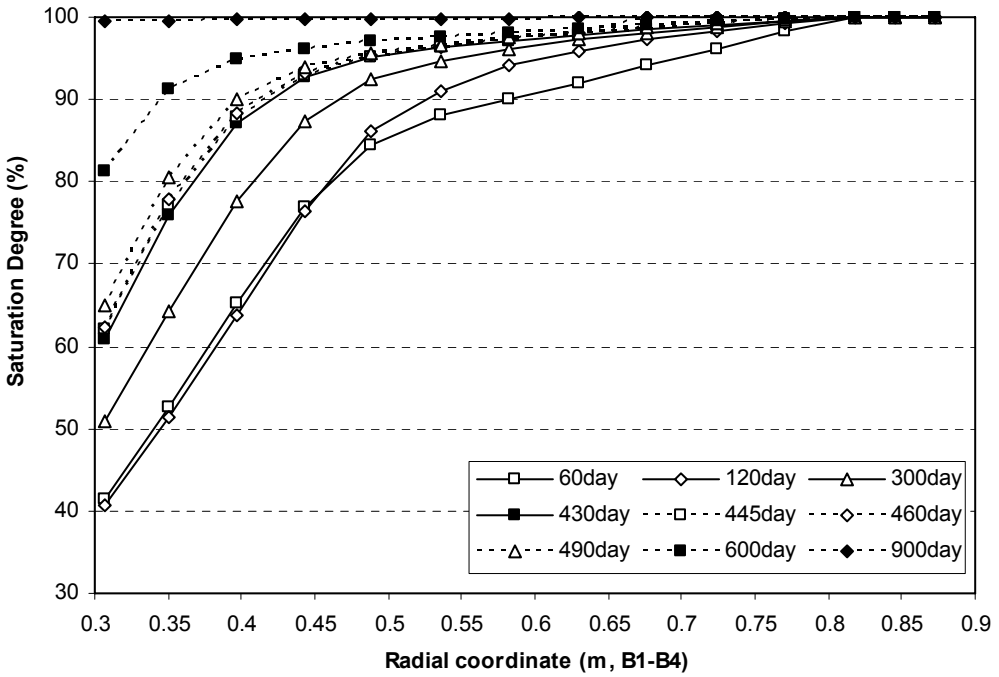

Figure 28. *Overheating within 30 days. Saturation degree in scan-line B1 to B4*

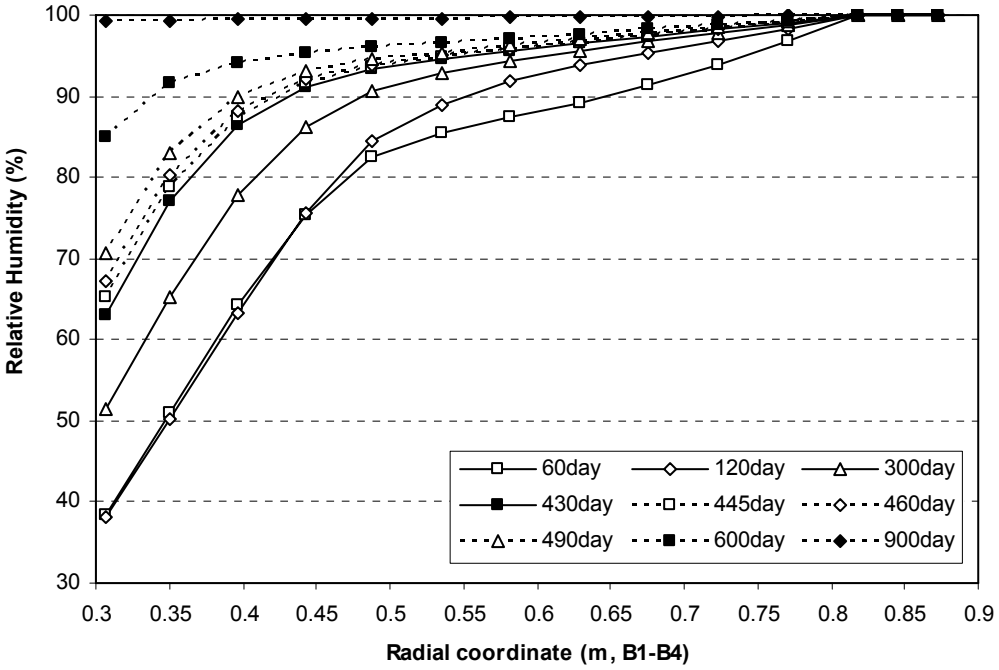

Figure 29. *Overheating within 30 days. Relative humidity in scan-line B1 to B4*

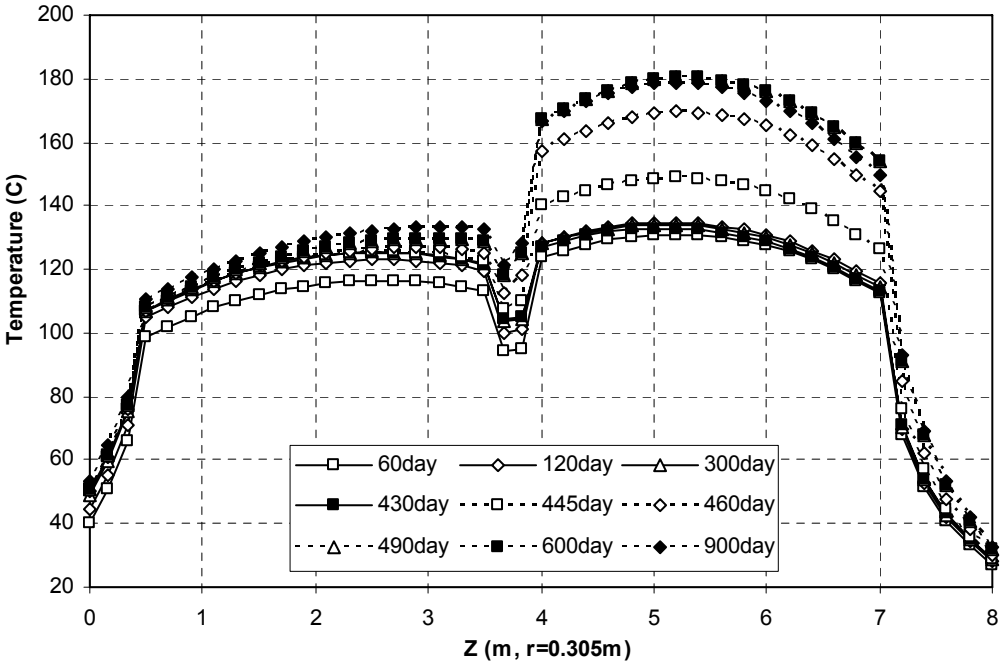

Figure 30. *Overheating within 30 days. Temperature in scan-line 1*

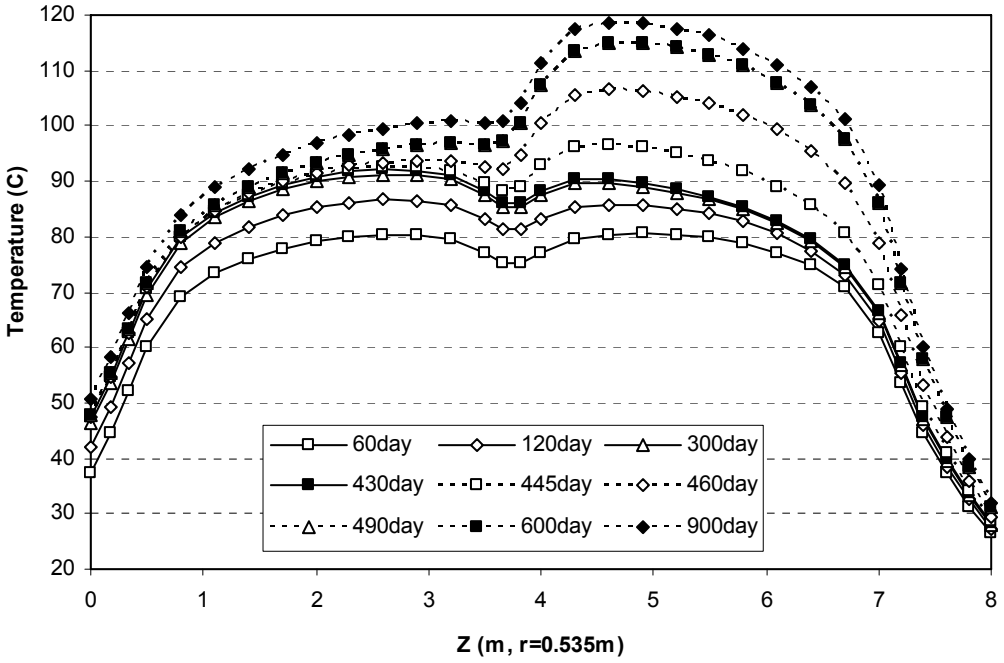

Figure 31. *Overheating within 30 days. Temperature in scan-line 2*

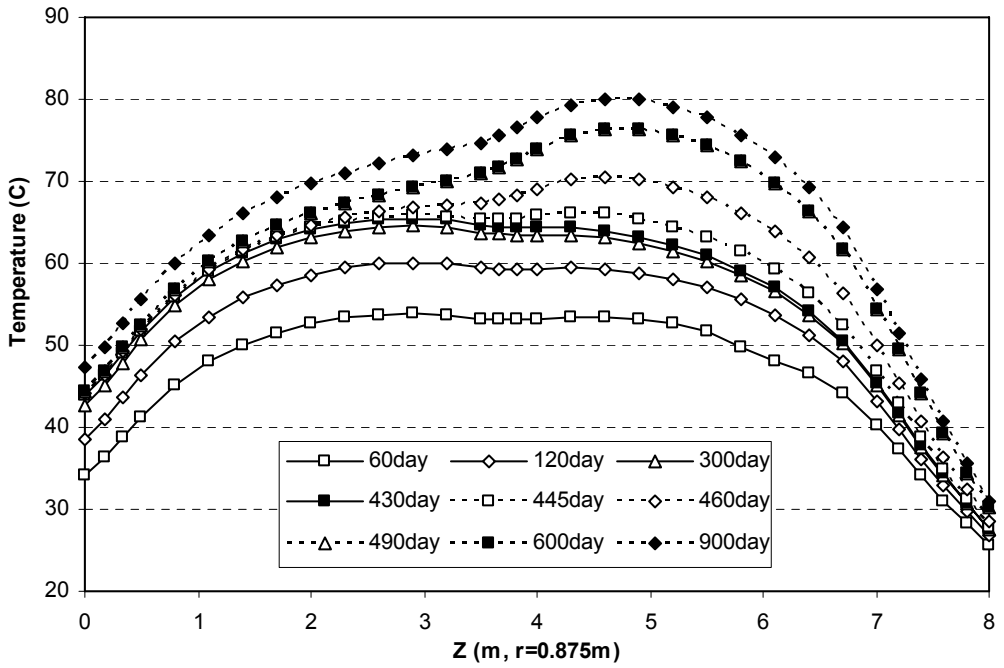

Figure 32. *Overheating within 30 days. Temperature in scan-line 3*

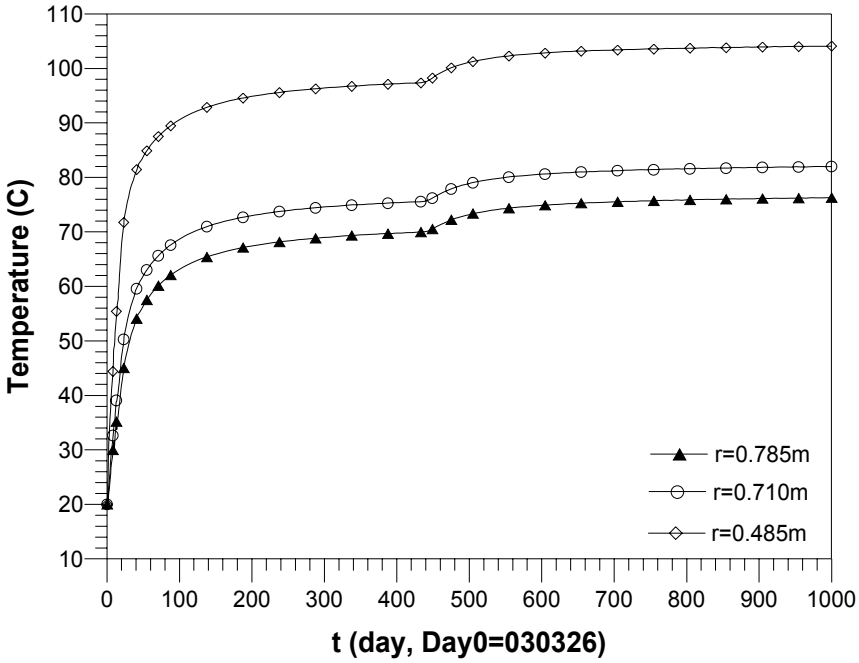

Figure 33. *Overheating within 6 days. Ring 4. Temperature evolution.*

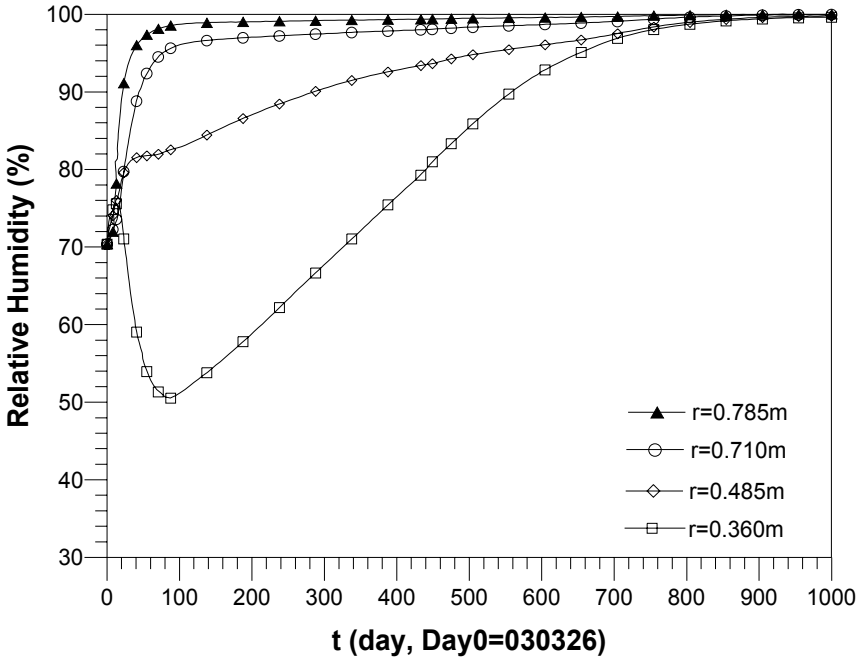

Figure 34. *Overheating within 6 days. Ring 4. Relative Humidity evolution.*

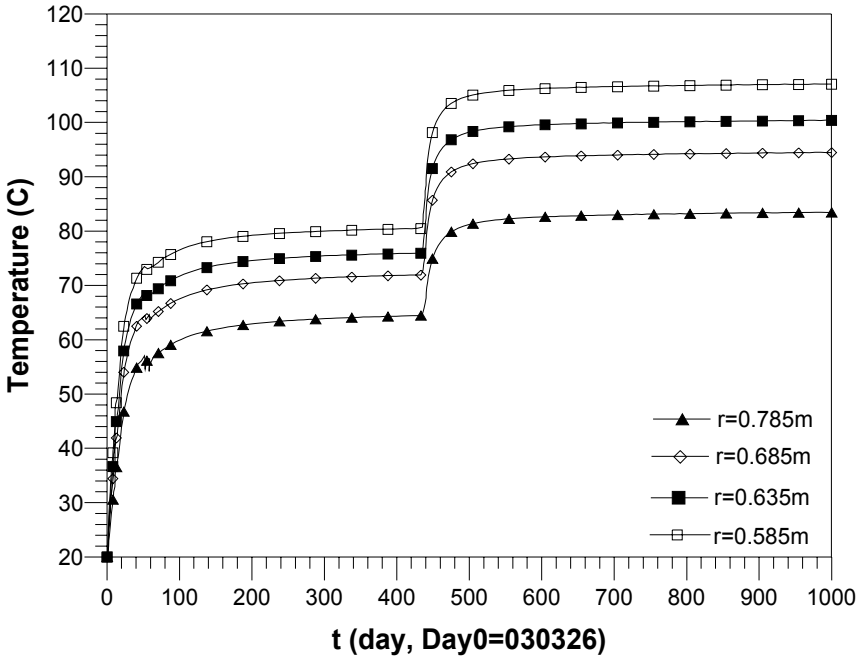

Figure 35. *Overheating within 6 days. Ring 10. Temperature evolution.*

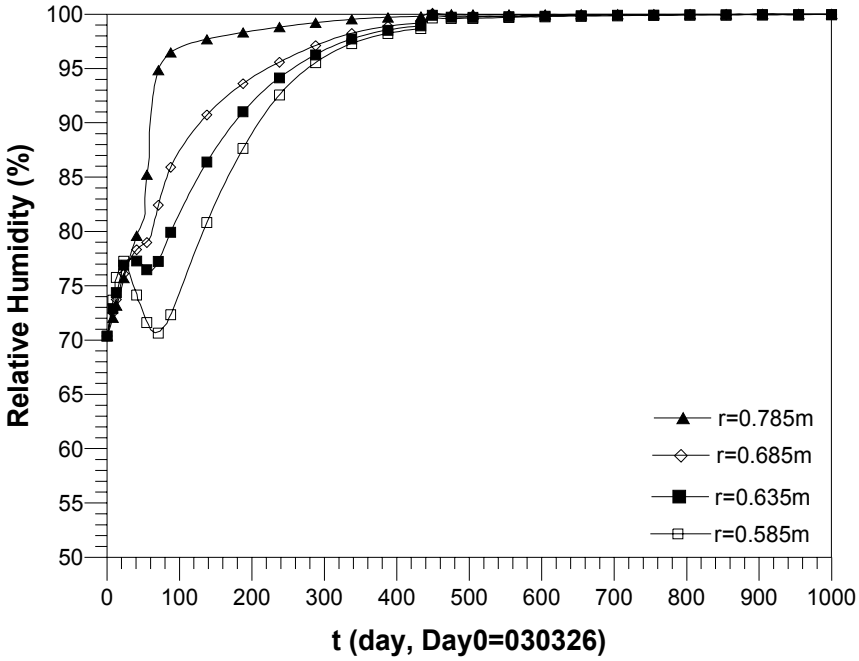

Figure 36. *Overheating within 6 days. Ring 10. Relative Humidity evolution.*

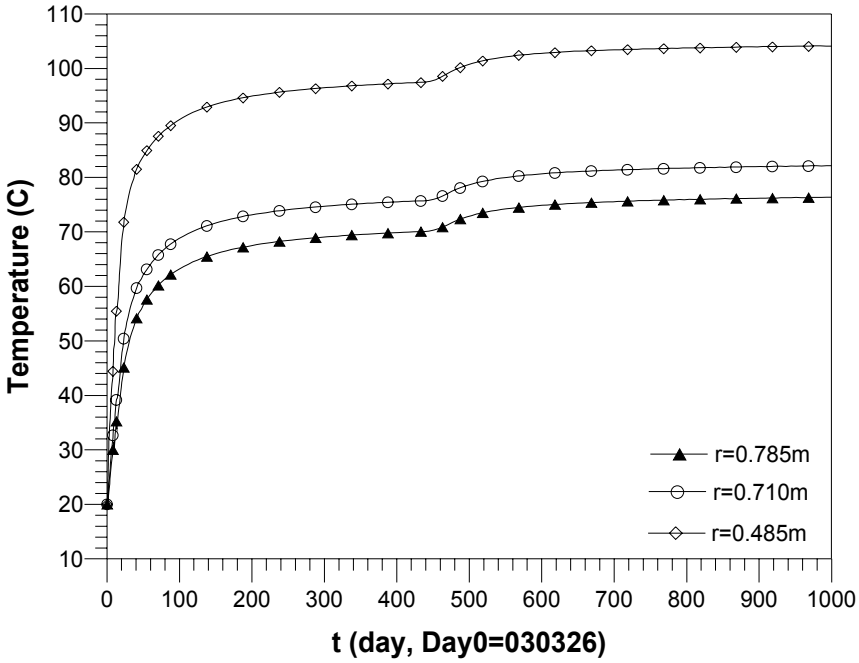

Figure 37. *Overheating within 30 days. Ring 4. Temperature evolution.*

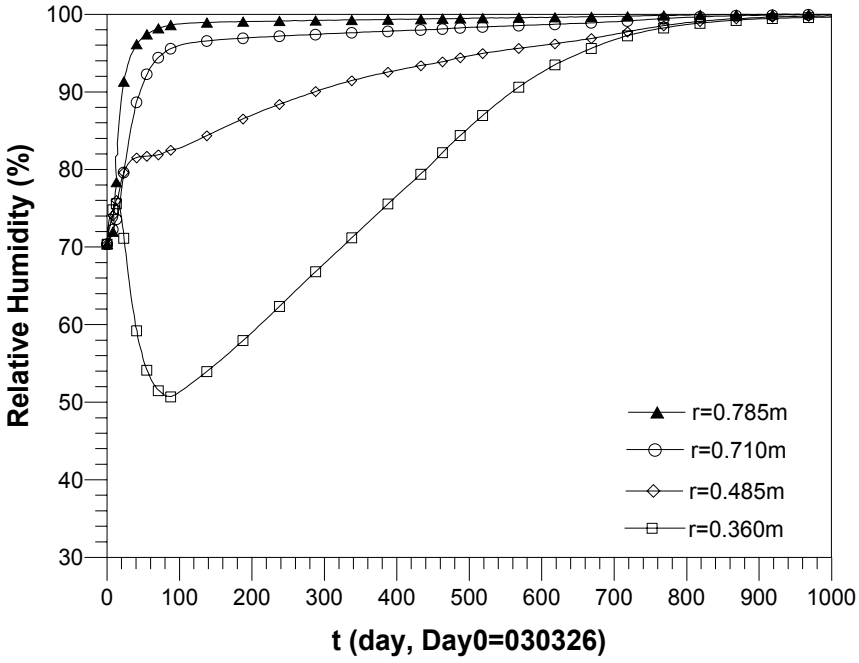

Figure 38. *Overheating within 30 days. Ring 4. Relative Humidity evolution.*

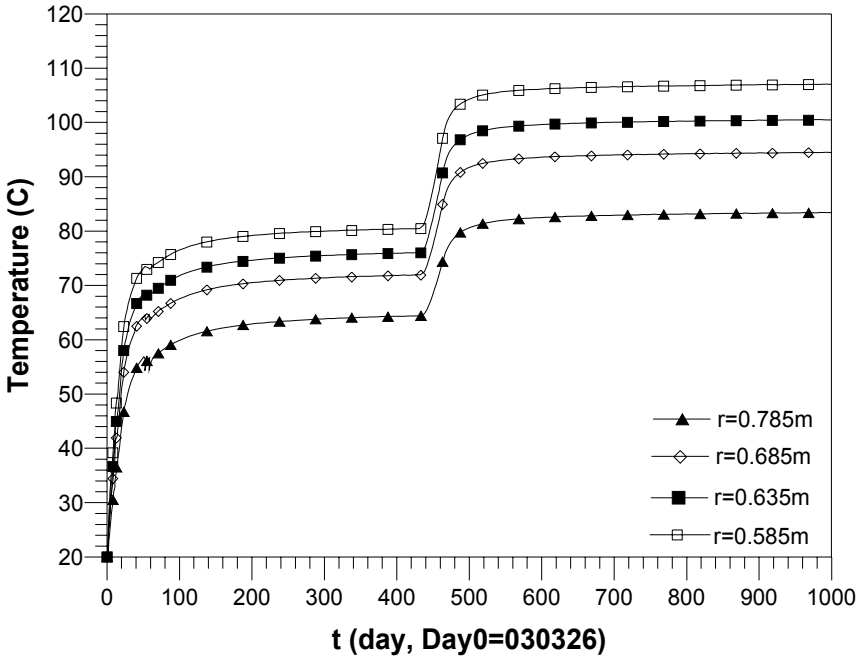

Figure 39. *Overheating within 30 days. Ring 10. Temperature evolution.*

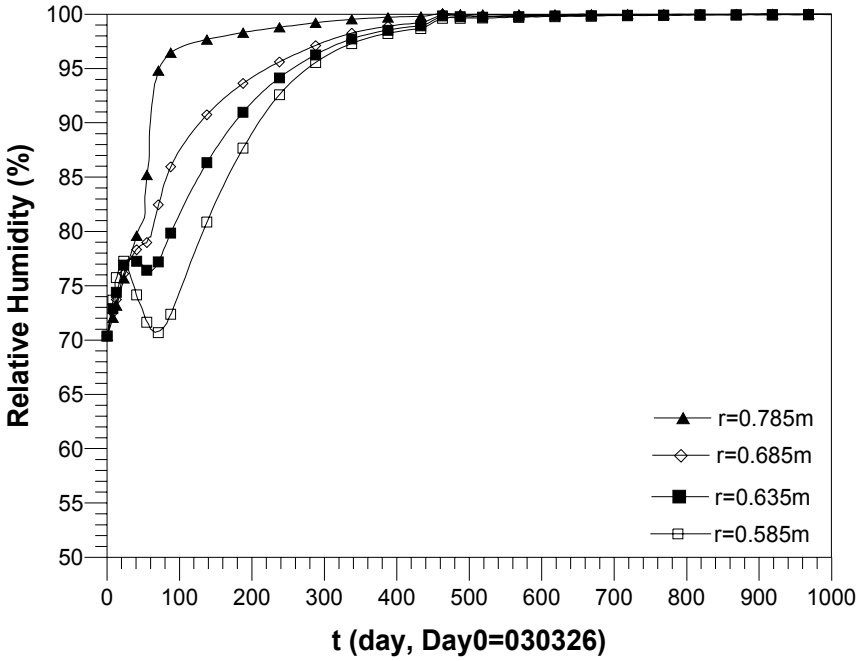

Figure 40. *Overheating within 30 days. Ring 10. Relative Humidity evolution.*

6 Conclusions

This report includes the results of the first evaluation modelling of the TBT experiment performed by the group coordinated by ENRESA. A complete analysis of the current situation of the experiment will be performed by November 2004, according to the guidelines that will be provided by Clay Technology next August. Here, only TH analyses have been carried out, following the suggestions for the mid May 2004 report.

This report also includes some comments about the measurements obtained during the first year of the experiment, focusing in a qualitative analysis of the unexpected stress and suction measurements in the upper canister zone. It also includes a comparison between measurements and computed variables, which required an optimization of some of the parameters involved in the problem using a trial and error procedure. Finally, it presents a prediction of the temperature, relative humidity and degree of saturation at some particular locations due to an overheating action in the upper heater.

The main conclusions that this group have obtained from these analyses are the following:

a) The unexpected trends in the stress and suction measurements in ring 9 may be related to the loose state of the sand shield that allows releasing radial stresses. That creates high deviatoric stresses and seems to produce an apparent "shear failure" of the bentonite. However, further work is required to fully understand this event and its consequences.

b) The comparison between measurements and computed variables is quite reasonable. However, it is believed that some of the processes involved in the experiment are not well defined in the models (i.e. boundary conditions and parameters related to the gas). This is partly due to uncertainties in the field test. A good agreement between measured and computed variables is not a guarantee of future agreements, because the number of parameters involved allow for tuning the response as required.

c) The effect of the overheating seems to be not very relevant from a conceptual point of view. The pattern of temperature or relative humidity against time does not change substantially after that episode (figures 39 and 40).

d) A comprehensive explanation of all the processes that have taken place in the experiment is still very difficult and part of the modeling work in the near future will be devoted to that. When analyzing a field experiment like this, changing the boundary conditions may not be the best strategy. In fact the steady state or long term situation provides with a lot of information in many cases, and for modeling purposes it is better to change as little conditions as possible. Therefore, increasing the power of the upper heater may not be as adequate as expected for the future modeling work. Understanding and simulating the current evolution of the experiment still requires some work, and an overheating episode does not provide any advantage to that work.

e) According to the guidelines, it seems that ANDRA would like to analyze the effect of a significant change in the experimental conditions to check the ability of models to update their approach and to perform blind predictions again. An increase of the power of the upper heater is the action suggested. If that action is finally decided, it would be convenient to check that the main variables of the experiment near the upper heater are as close as possible to steady state conditions. If possible, the event described in section 2 (cycle of suction and decrease of total stresses) should be overcome, and the variables measured at Ring 9 and 10 should be close to the expected values, to assure that this event has already finished.

f) Due to the fact that the test includes some uncertainties, any possibility of obtaining additional information would be welcome. Dismantling the test is one opportunity to measure with reliability the final long term state. This is not an action for the near future, but it is an action that will be eventually performed at the end of the project. It is believed that an important effort of field measurements and modeling work should be carried out when dismantling the experiment.

g) Some experiments are still being performed at Ciemat (Madrid). They involve the measurement of water retention curve at different temperatures and the simulation of a TH cell. Some results are expected by the end of this year and may be included in the November 2004 report.

References

Alonso, E.E., Gens, A., Josa, A. (1990). A constitutive model for partially saturated soils. Géotechnique, 40 (3), 405-430.

FEBEX (2000). FEBEX Project. Full-scale engineered barriers experiment for a deep geological repository for high level radioactive waste in crystalline host rock. Final Report. ENRESA Technical Publication 1/2000. Madrid, Spain.

Fredlund, D.G., Rahardjo, H. (1993). Soil Mechanics for Unsaturated Soils. Wiley. New York.

Hökmark, H., Fälth, B. (2003). Temperature Buffer Test. Predictive Modelling Programme. SKB document F12.1G-1012125. Sweden.

Hökmark, H., Fälth, B., Åkesson, M. (2004). TBT. Evaluation Modeling Program. Clay Technology. Sweden.

Villar, M.V. (2002). Thermo-hydro-mechanical characterization of a bentonite from Cabo de Gata. A study applied to the use of bentonite as sealing material in high radioactive waste repositories. ENRESA Technical Publication 04/2002. Madrid, Spain.

Clay Technology AB

Ideon Research Center

Lund, Sweden

TBT - Evaluation Modelling

May 2004

Billy Fälth

Harald Hökmark

Contents

1 Introduction and background

1.1 TBT experiment

ANDRA is performing a Temperature Buffer Test in granitic rock at Äspö Hard Rock Laboratory, Sweden. The overall objective of the experiment is to investigate how well the bentonite buffer can endure the high temperatures expected to be found around Vitrified Waste canisters of about 0.6 m diameter, deposited in pits of about 1.8 m diameter and with bentonite buffer material in the annular space between canister and pit walls. For the Vitrified Waste concept, two possibilities are considered by ANDRA:

- to surround the canisters with a 0.2 m sand shield
- to have only bentonite between canister and rock wall.

The sand shield will reduce the temperature to which the bentonite will be exposed. Without sand shield, the bentonite will be exposed to temperatures well over 100°C. Both options are tried in the TBT experiment. A drawing of the experiment set-up is provided in Figure 1.1. The experiment includes an extensive instrumentation to monitor temperatures, total pressures, pore pressures, relative humidities, etc. /Goudarzi et al., 2003/.

1.2 Evaluation modelling phase

The experiment (heat generation) started in March 2003 and has been producing data for about 1 year up to the present day. Prior to test start, a Predictive Modelling Program was specified /Hökmark and Fälth, 2002/. Clay Technology and other modelling teams made blind predictions based on the specifications in that program.

In April 2004 an *evaluation* modelling phase was initiated and an evaluation modelling program has been specified /Hökmark, Fälth, Åkesson, 2004/. For this evaluation modelling phase the objectives are to

- "Improve the fit between calculations and measurements by considering the present-day experiment status, new or updated information regarding material properties, boundary conditions etc.
- Apply the updated, or improved, modelling approach to a case in which a significant change is done to the experimental conditions. This means that a new set of blind predictions shall be made. The change done to the test is suggested to be an increase of the power of the upper heater.
- Based on the outcome of the improved simulations and blind predictions, evaluate relevance and discuss the relevance and validity of the conceptual models used in the numerical representation." /Hökmark, Fälth, Åkesson, 2004/

The evaluation modelling work is divided into two parts: Part one, which should be reported in mid-May 2004 and part two, which is to be reported late November 2004.

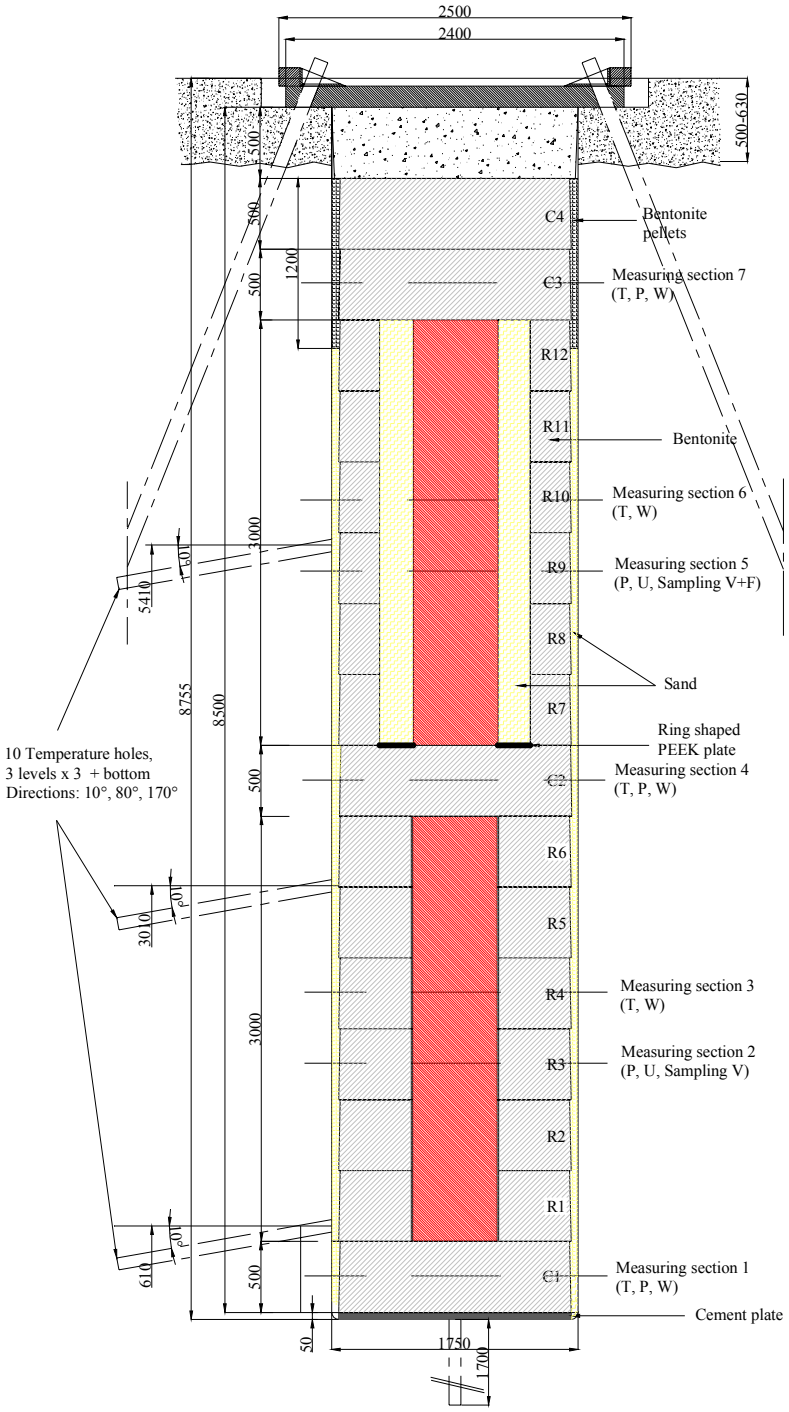

Figure 1.1. *TBT experiment setup*

As mentioned above, it is suggested that the heating power of the upper heater shall be increased. The power increase is planned to be implemented in the beginning of June 2004 (day 430) and part one of the modelling work includes a prediction of the effects of that power increase. The present work is Clay Technology's contribution to part one of the evaluation modelling phase.

2 Objectives

The objectives of this work:

- To consider the updated information regarding material properties, boundary conditions etc. in the experiment
- By taking the new information into account, perform modelling of the experiment from test start up to 900 days. The modelling includes a prediction of the thermal and hydraulic effects of a power increase of 750 W in the upper heater starting at day 430. Two different protocols of increasing the power from 1500 W up to 2250 W should be considered:
  - A ‘sudden increase’ lasting 6 days, with 125 W power increase each day.
  - A ‘step by step’ increase lasting 30 days, with 25 W power increase each day.

Especially, the temperatures in the sand shield/bentonite interface and at the upper heater surface should be considered. The target temperature at the sand/bentonite interface is 100 ºC, which should be reached without exceeding the maximum allowed heater surface temperature, which is specified to 225 ºC.

3 Model geometry and data

3.1 General

The modelling work was performed with the finite element program Code_Bright, version 2.2, which is a 3D finite element code for thermo-hydro-mechanical analyses in geological media /CIMNE 2002/. Three quasi-3D (axi-symmetric 2D) TH-analyses were run. To get a better fit between calculation and measurements, data from the measurements in the experiment as well as laboratory data of MX 80 retention properties have been considered /Hökmark, Fälth, Åkesson, 2004/. A number of items, which are important for the TH processes in the system, have been considered during the work. The main ones are the following:

- An assumption in the predictive modeling work was that the sand filter between the bentonite blocks and the rock wall was water saturated at test start. However, the sand filter was supplied with water through four tubes ending in the bottom of the sand filter and the time for filling up the sand filter completely was approximately 80 days. The measurements indicate that this has an impact on the experiment both hydraulically and thermally. The RH measurements for the outer parts of the bentonite blocks show a delay in saturation which is larger the higher level of the blocks. The heat conductivity increase in the sand slot as it gets saturated can also be seen in the temperature measurements. The temperatures in block 10 have a clear drop which coincides in time with the saturation of the outermost parts of the same block. In an attempt to capture these phenomena, the sand filter saturation process has been simulated in a schematic way.

- The heat conductivities in the sand and bentonite have been considered and adjusted according to measured/calculated data.

- The interface between the sand filter and the pellets filling is 0.2 m below the level first intended.

- The retention properties of the bentonite blocks and the pellets have been updated according to new laboratory data for MX 80.

- The rock thermal conductivity is adjusted to a value that is more consistent with the thermal conditions in the vicinity of the test hole.

3.2 Geometry

The quasi-3D (2D axi-symmetric) model geometry used is shown in Figure 2. Two different bentonite materials where defined. They have different porosities and thus different hydraulic properties.

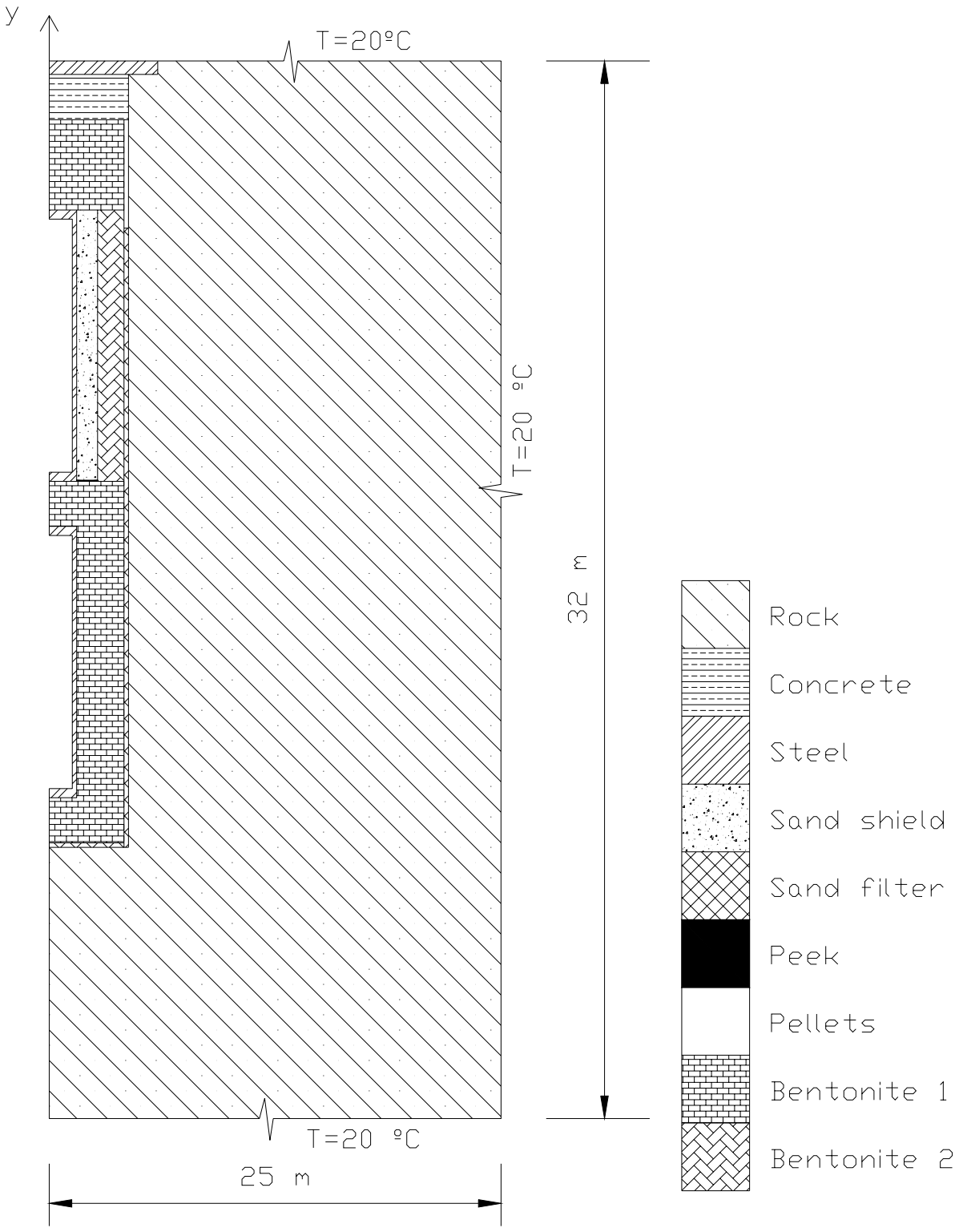

Figure 2. *Model geometry, outer dimensions and thermal boundary conditions.*

3.3 Initial and boundary conditions

In Table 1, the initial conditions for the different materials are presented. The bentonite pellets initial saturation is based on the assumption of a water ratio of 10 %. The sand filter was assumed initially dry except for the bottom part, which was set to be saturated from start. The wetting of the sand filter was modeled in a schematic way according to Figure 3. The white parts of the filter are dry whereas the black parts are water saturated (P_l = 0.1 MPa). At day 370, the water pressure in the sand filter and rock was increased to 0.15 MPa. The temperature at the model's outer and upper boundary was set to 20 ºC, cf. Figure 2. At the upper boundary, the temperature condition was of Cauchy type i.e.

$$j = \gamma(T_0 - T),$$

where j is heat flux at the boundary, T_0 = 20 ºC is the prescribed temperature and γ = 3 is a leakage coefficient. This allows the boundary temperature to rise above the prescribed temperature.

Table 1. Initial conditions

Material	Temperature [ºC]	Gas pressure [Mpa]	Saturation [%]	Porosity
Bentonite 1	20	0.1	78	0.389
Bentonite 2			85	0.368
Pellets			18	0.6
Sand filter			0*, 100*	0.36
Sand shield			0	0.3
Concrete			50	
Steel			100	0.001
Peek			50	
Rock			1	0.005

* The lowest part was initially saturated, cf. Figure 3 below.

The heating power in the upper heater was following the schemes proposed in the Evaluation Modeling Program. /Hökmark, Fälth, Åkesson, 2004/ The power was kept at 1500 W day 0-430. From this point, two different protocols where used for the power increase:

- Fast: 750 W increase during day 430 - 436, i.e. 125 W/day.
- Gentle: 750W increase during day 430 - 460, i.e. 25 W/day.

The heating power in the lower heater was kept constant at 1500 W.

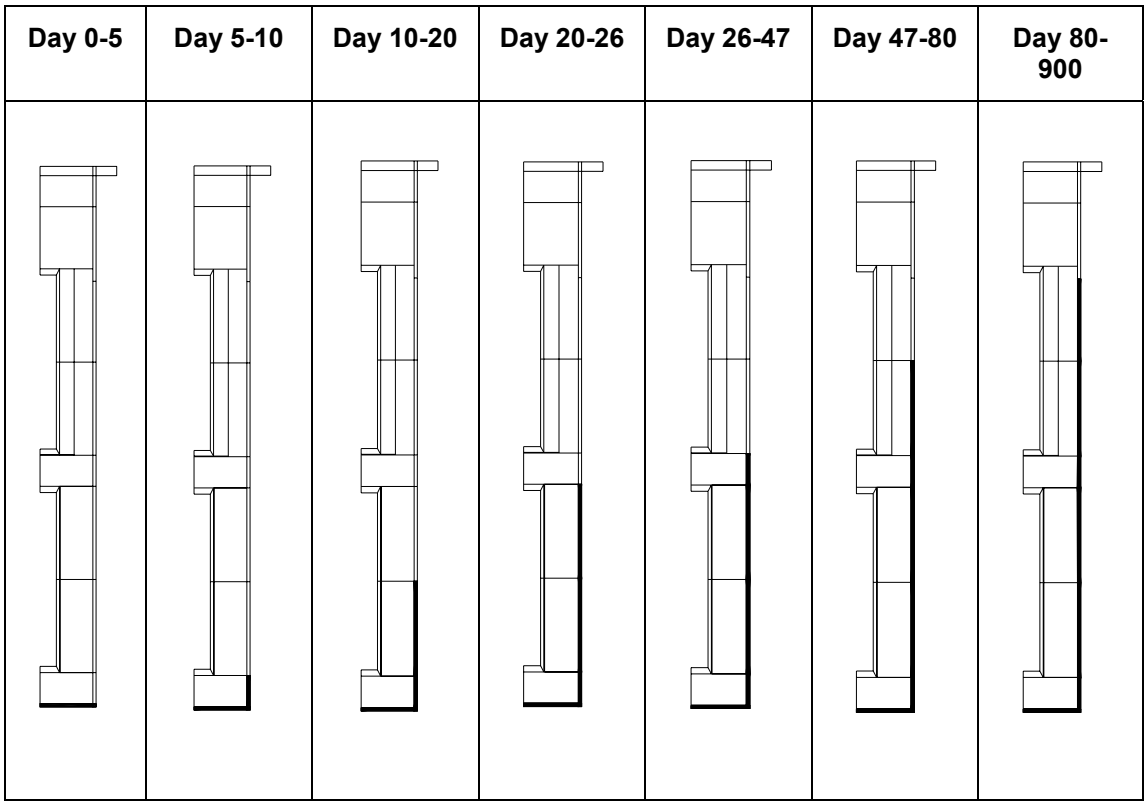

Figure 3. *Scheme for the sand filter water filling. Black parts are saturated.*

3.4 Constitutive laws and materials data

In Table 2 and Table 3, the hydraulic and thermal material properties are presented. The dry state thermal conductivity for the sand where varied during the first 200 days according to the measured-calculated data. /Hökmark, Fälth, Åkesson, 2004/. To enhance numerical performance, the sand intrinsic permeability was set to a low value. This could be done without loosing consistency since k_r for the sand shield is by definition zero from start due to zero initial saturation. The low intrinsic permeability value was of very little importance for the sand filter too since the hydraulic behaviour in this part was controlled by the water pressure boundary condition.

Table 2. Retention properties.

Material	Law	P_0	λ	P_m	λ_m
Bentonite 1	$S_r = \left\{1+\left(\frac{P_g - P}{P_0 \cdot \left(\frac{\sigma}{\sigma_0}\right)}\right)^{\frac{1}{1-\lambda}}\right\}^{-\lambda} \left\{1-\frac{P_g - P}{P_m}\right\}^{\lambda_m}$	65	0.45	800	1.2
Bentonite 2		100	0.5	800	1.2
Pellets		0.43	0.19	550	1.3
Sand filter		0.005	0.6	700	1.1
Sand shield		0.01	0.6	700	1.1
Rock		0.005	0.6	700	1.1
Concrete	$S_r = \left\{1+\left(\frac{P_g - P}{P_0 \cdot \left(\frac{\sigma}{\sigma_0}\right)}\right)^{\frac{1}{1-\lambda}}\right\}^{-\lambda}$	2	0.3	-	-
Steel		500	0.3	-	-
Peek		50	0.3	-	-

Vapour diffusion was modelled according to

$$\mathbf{i} = -(\phi \rho_g (1 - S_r) D_m^{vapour} \mathbf{I}) \nabla \omega_g^{vapour}$$

$$D_m^{vapour} = \tau_v 5.9 \cdot 10^{-6} \frac{(273.15 + T)^{2.3}}{P_g}$$

where P_g is gas pressure and τ_v is coefficient of tortuosity. The diffusion of dissolved gas was modelled as

$$\mathbf{i} = -(\phi \rho_l S_r D_m^g \mathbf{I}) \nabla \omega_l^g$$

$$D_m^g = \tau_g 1.1 \cdot 10^{-4} \exp \frac{-24530}{R(273.15 + T)}$$

where R = 8.314 J/molK. Values of τ_v and τ_g are presented in Table 4.

Table 3. Thermal and hydraulic properties.

Material	**Solid phase density [kg/m^3]**	**Solid phase spec. heat [J/kgK]**	**Intrinsic perm. [m^2]**	**Liq rel. perm.** $k_{rl} = S_r^{\delta_l}$	**Gas rel. perm** $k_{rg} = A(1-S_r)^{\delta_g}$		**Heat cond. [W/mK]** $\lambda = \lambda_{dry}(1-S_r) + \lambda_{sat} S_r$	
				δ_l	A	δ_g	λ_{dry}	λ_{sat}
Bentonite 1	2780	800	$2.8 \cdot 10^{-21}$	3	1e8	4	0.3	1.2
Bentonite 2			$1.6 \cdot 10^{-21}$					
Pellets			10^{-19}				0.2	1.1
Sand filter	2650		10^{-20}				0.45* 0.5** 0.6***	1.7
Sand shield								
Concrete	2800	900	10^{-18}				1.7	1.7
Rock	2600	800	10^{-21}				2.6	2.6
Steel	7800	460	10^{-30}		1	3	45	45
Peek	1300	1000					0.25	0.25

*day 0-60, **day 60-200, ***day 200-900

Table 4. Coefficients of tortuosity

Material	τ_v	τ_g
Bentonite 1	1	10^{-5}
Bentonite 2		
Pellets		
Sand filter		
Sand shield		
Concrete		
Rock		
Steel	10^{-10}	
Peek		

4 Results

In this section, the results from the calculations are presented and commented. The scan-lines used in the results presentation are shown in Figure 4. The results are arranged according to:

- Scan-line A1-A4 and B1-B4: temperature, saturation, RH
- Upper heater mid-height, 570 mm radial distance: Saturation history
- Lower heater mid-height, 410 mm radial distance: Saturation history
- Scan-line 1, 2 and 4: temperature

Results are given for day 60, 120, 300, 430, 445, 460, 490, and 600. A model without the power increase was also run. Results from this model are also presented for comparison.

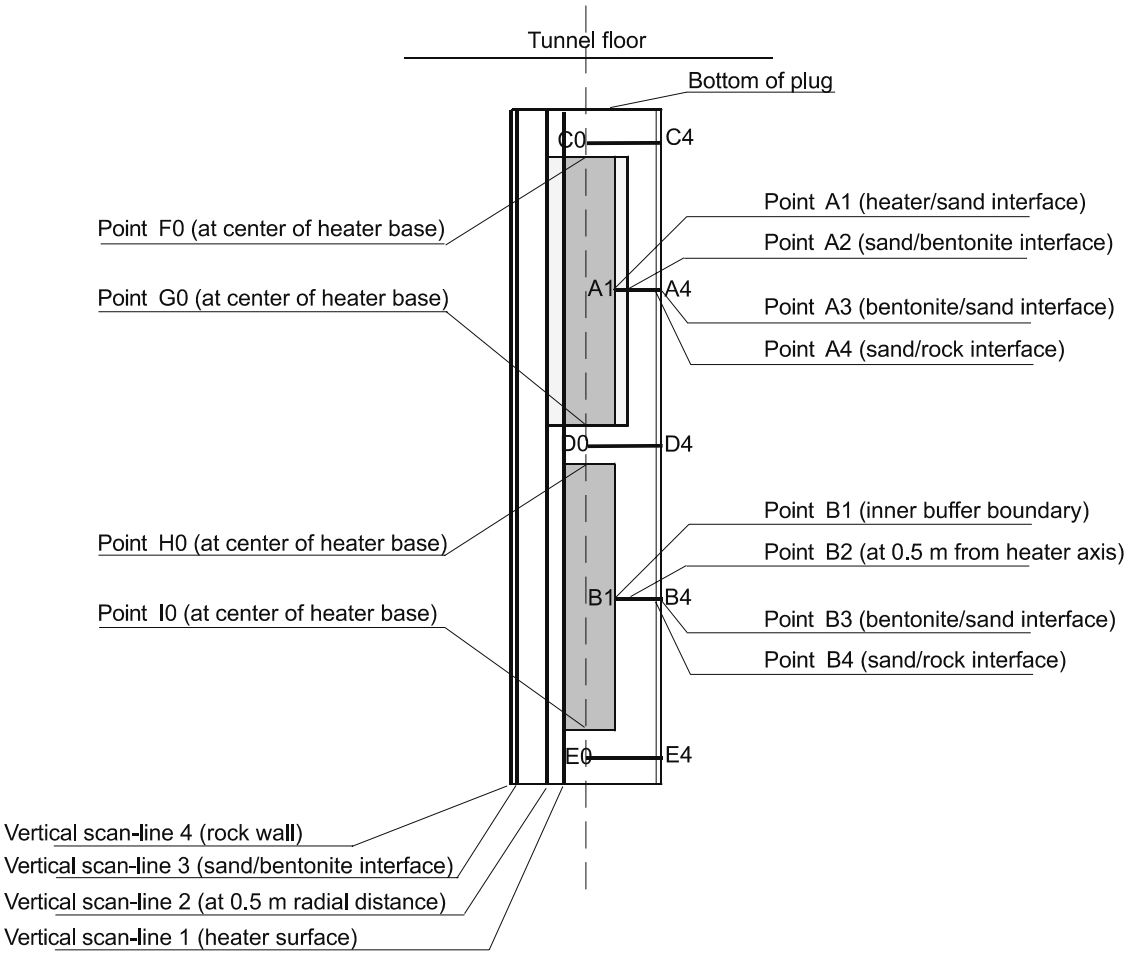

Figure 4. *Output scan-lines.*

Due to numerical problems in the models, there are only results available up to day 600. There are however some observations that can be made. The different power increase protocols give temperature differences only during the first 30 days after power increase start (Figure 5, 13, 14, 15). Eventually, there are only small temperature differences. The power increase applied (750 W) give temperatures at the sand shield/bentonite interface well over 100 ºC (Figure 5, 14). Another observation is that the heater surface temperature will not exceed the limit specified by the heater manufacturer (225 ºC). However, the results indicate that the temperature will reach as high as 220 ºC after 600 days (Figure 5, 13).

The results for scan-line A1-A4 indicate that the power increase in the upper heater will have an impact on the saturation process (Figure 6, 7, 11). In the bentonite near the sand shield/bentonite interface, there is a small decrease in saturation between day 460 and 600. At day 600, the saturation decrease seems to fade out.

Along scan-line B1-B4, the impact on the temperatures from the power increase can be clearly seen after 490 days (Figure 8). An observation that can be done is that the temperature level increases but not the temperature gradients. The raised temperatures may give a decreased water viscosity, which in turn can facilitate the water inflow from outer parts of the bentonite. Since the temperature gradients are constant, the vapour transport may not be facilitated at the same extent. This may be the reason for the increased saturation speed in the inner parts of the bentonite which is shown in Figure 12.

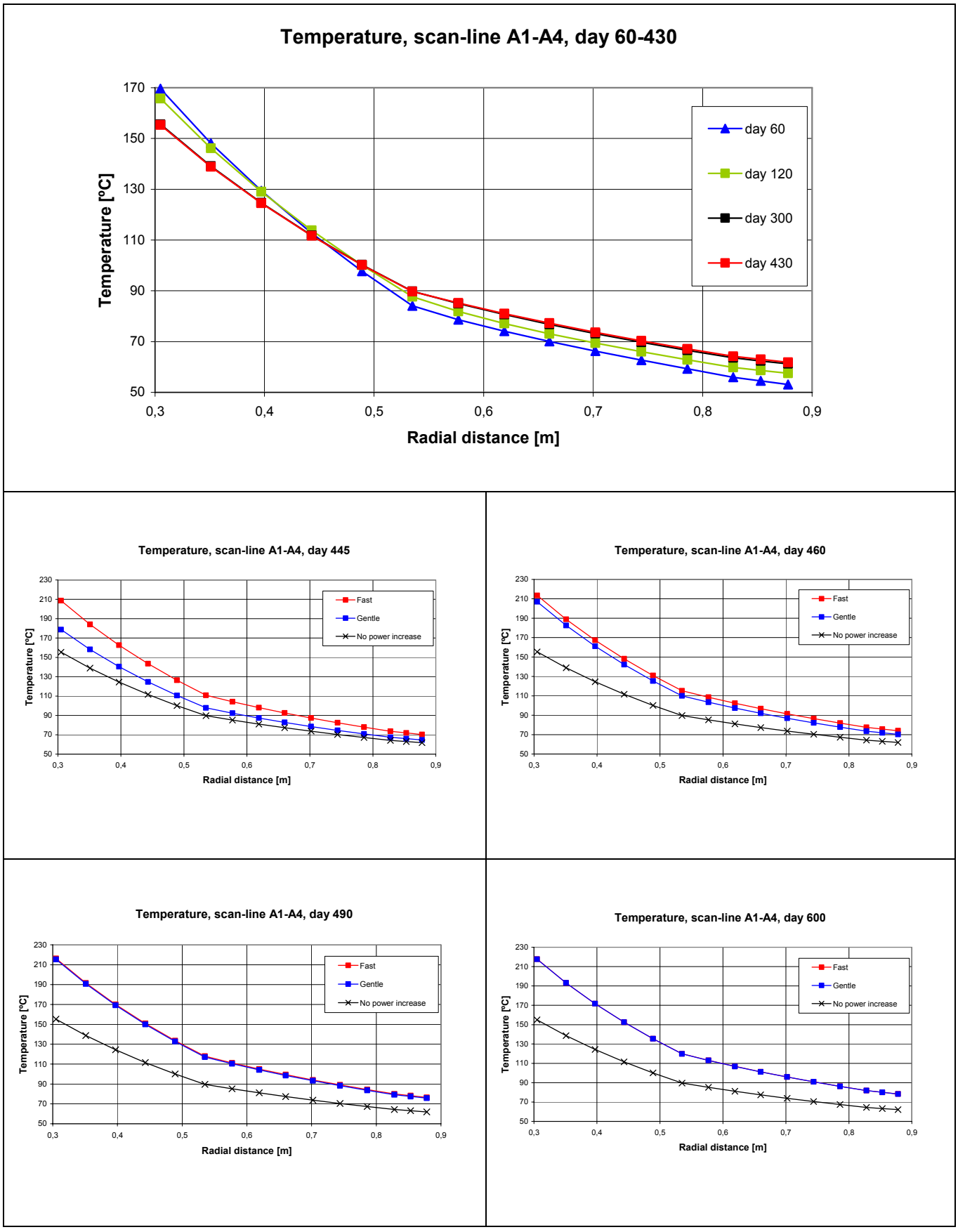

Figure 5. *Temperatures along scan-line A1-A4. The four lower diagrams show the effect of using the different power increase protocols.*

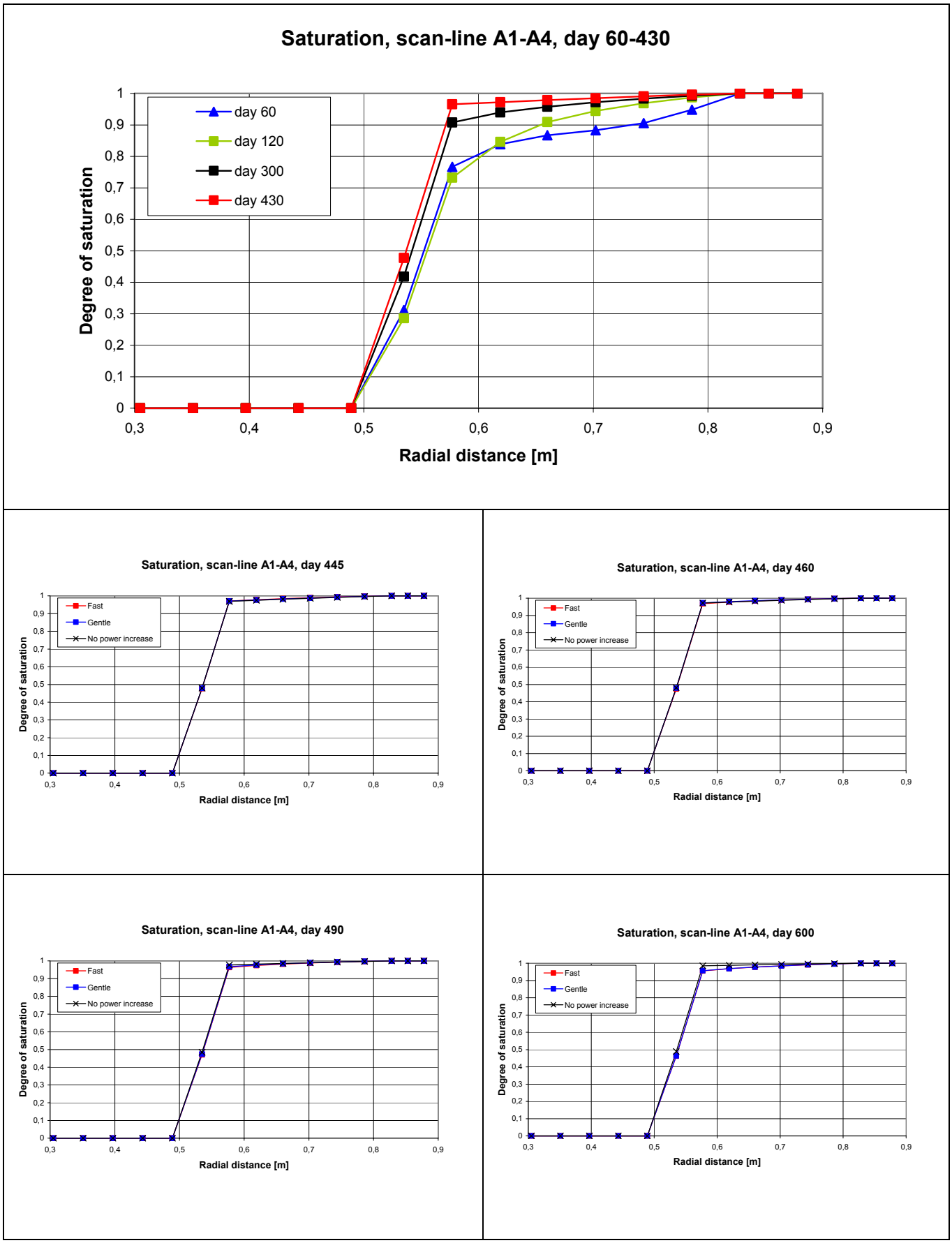

Figure 6. *Degree of saturation along scan-line A1-A4. The four lower diagrams show the effect of using the different power increase protocols.*

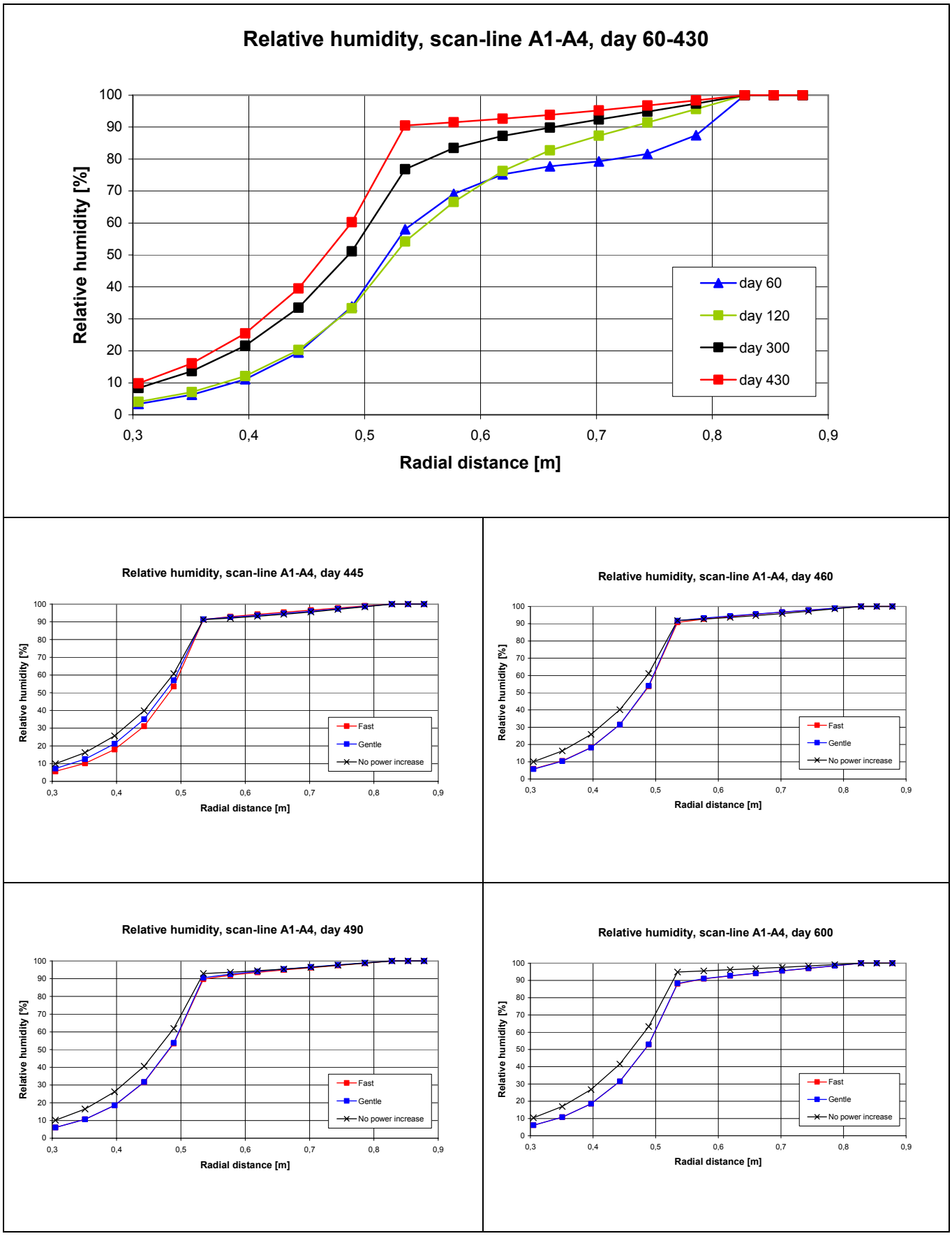

Figure 7. *Relative humidity along scan-line A1-A4. The four lower diagrams show the effect of using the different power increase protocols.*

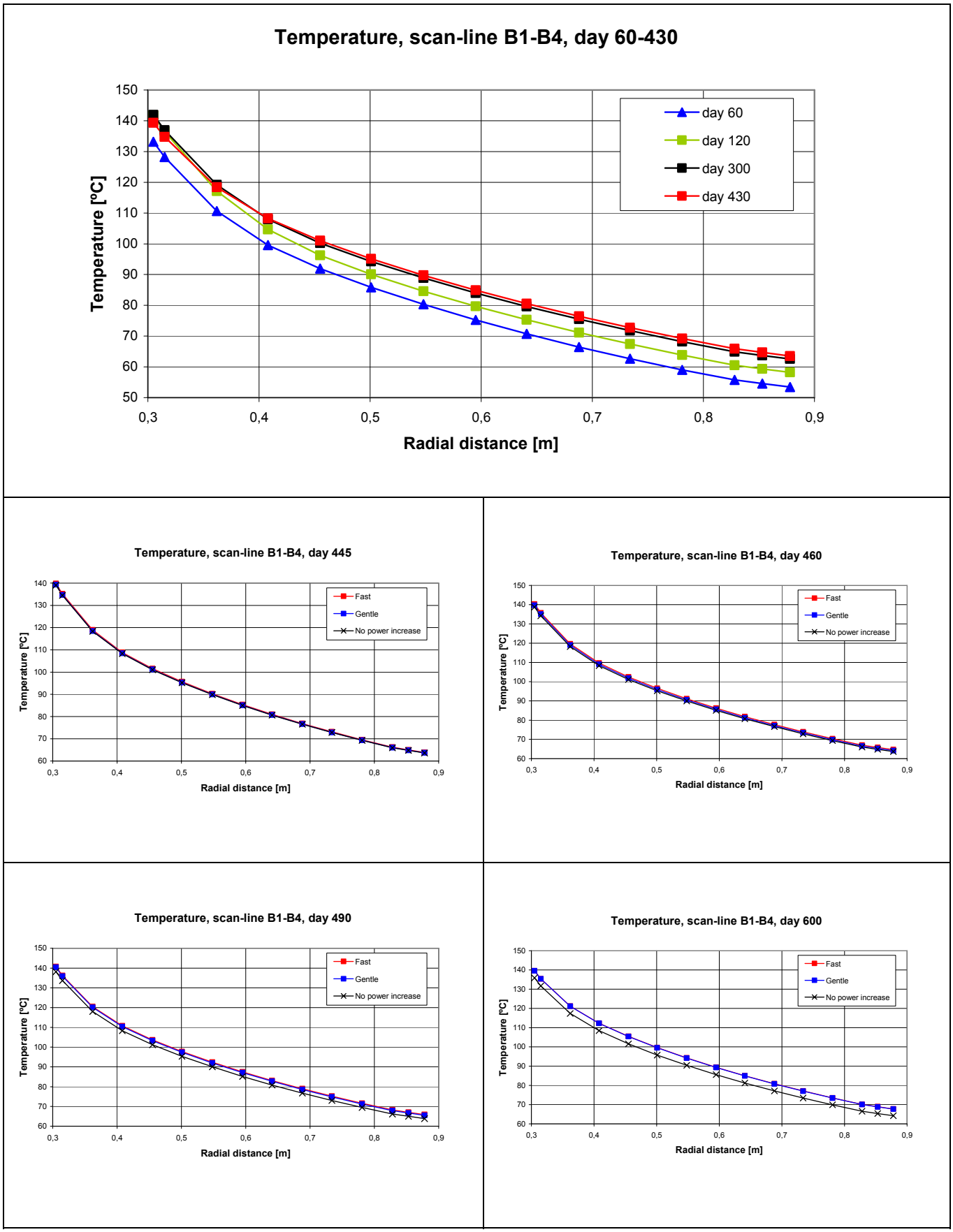

Figure 8. *Temperatures along scan-line B1-B4. The four lower diagrams show the effect of using the different power increase protocols.*

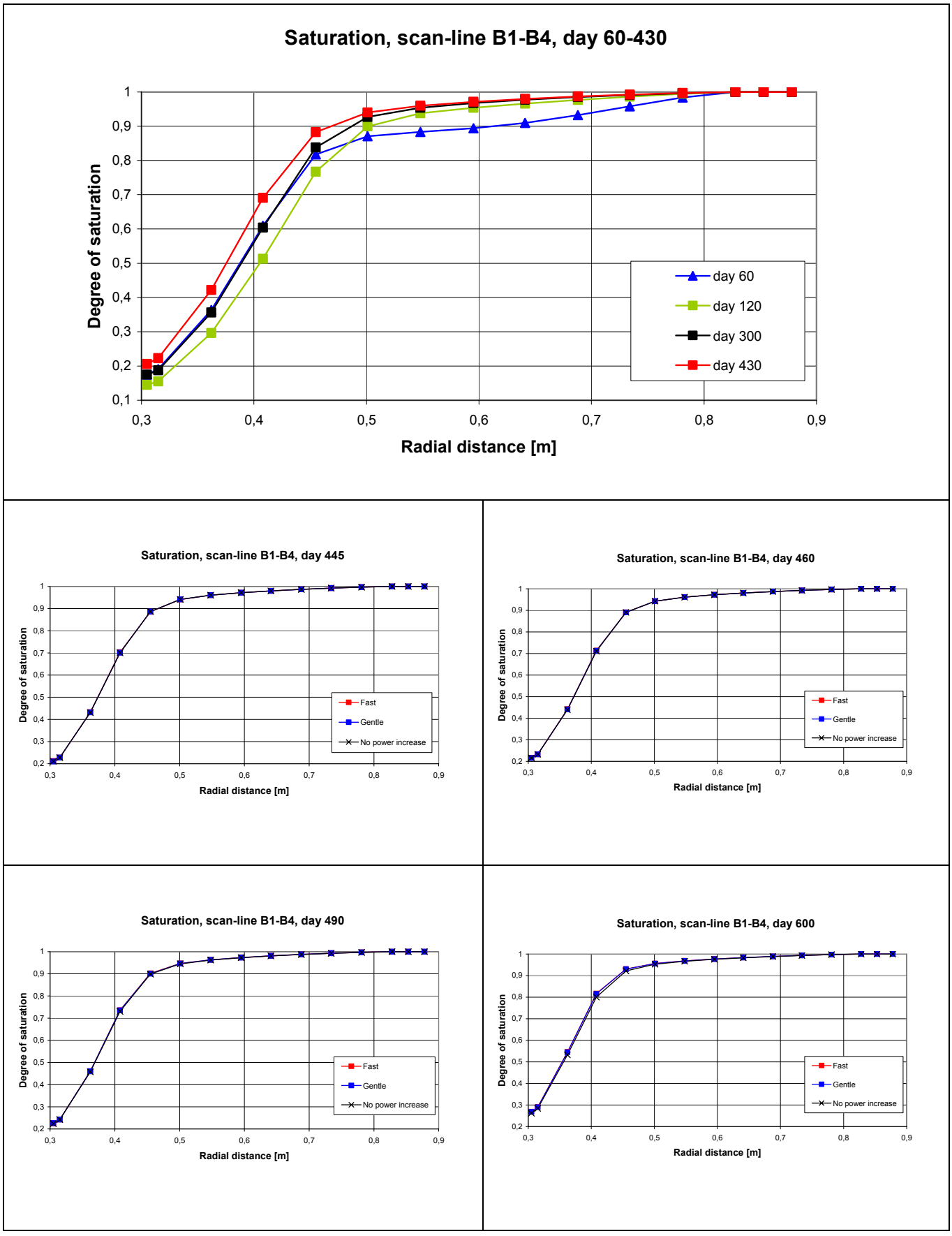

Figure 9. *Degree of saturation along scan-line B1-B4. The four lower diagrams show the effect of using the different power increase protocols.*

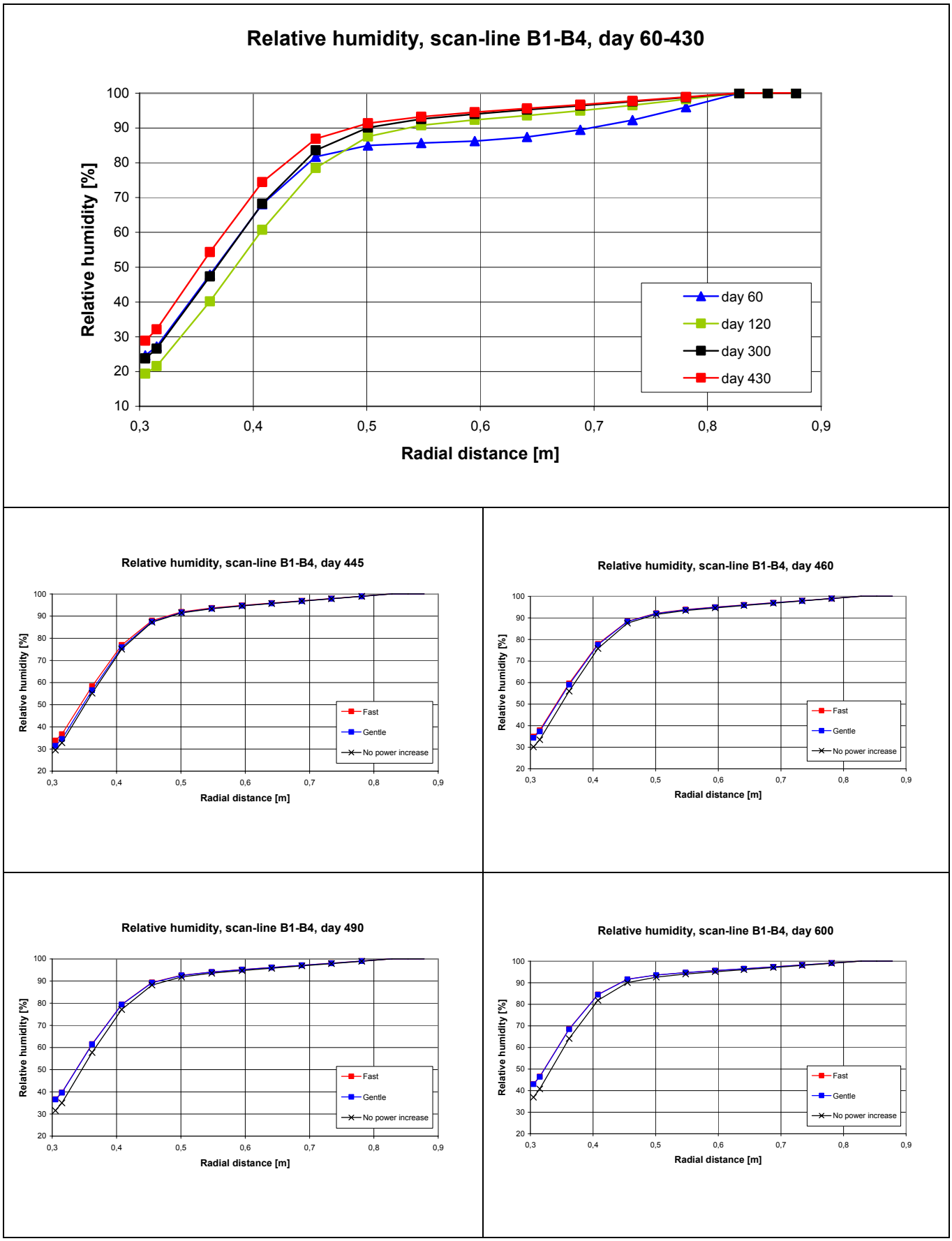

Figure 10. *Relative humidity along scan-line B1-B4. The four lower diagrams show the effect of using the different power increase protocols.*

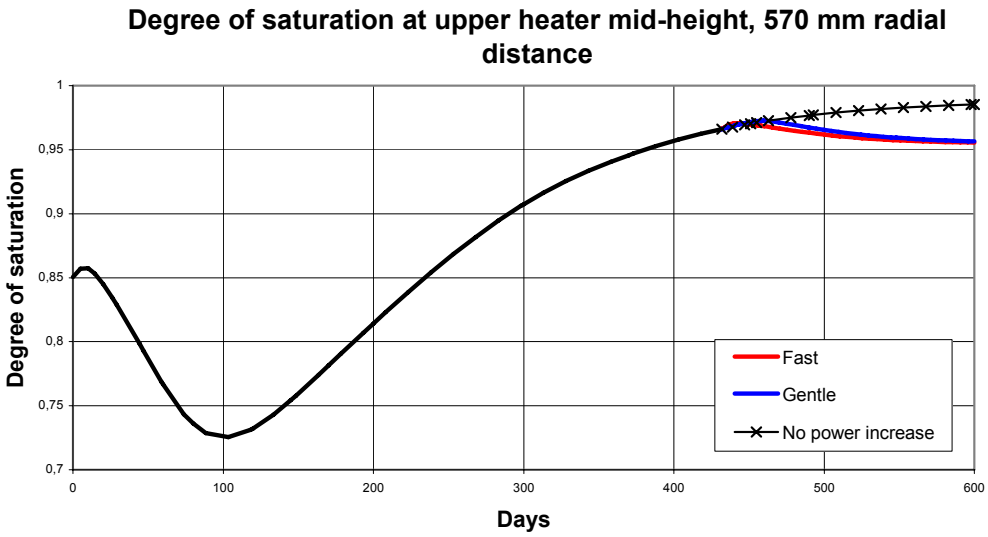

Figure 11. *Degree of saturation at upper heater mid-height at 570 mm radial distance.*

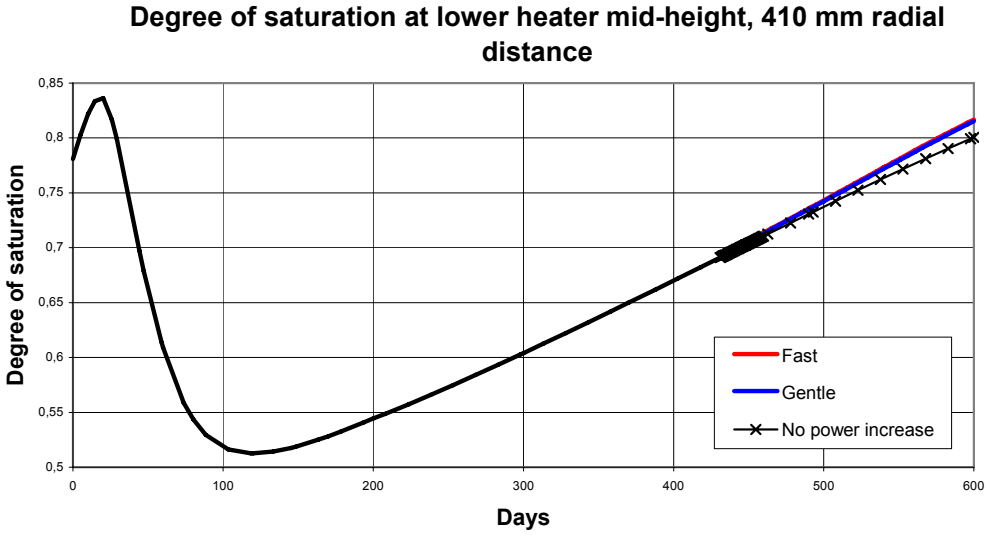

Figure 12. *Degree of saturation at lower heater mid-height at 410 mm radial distance.*

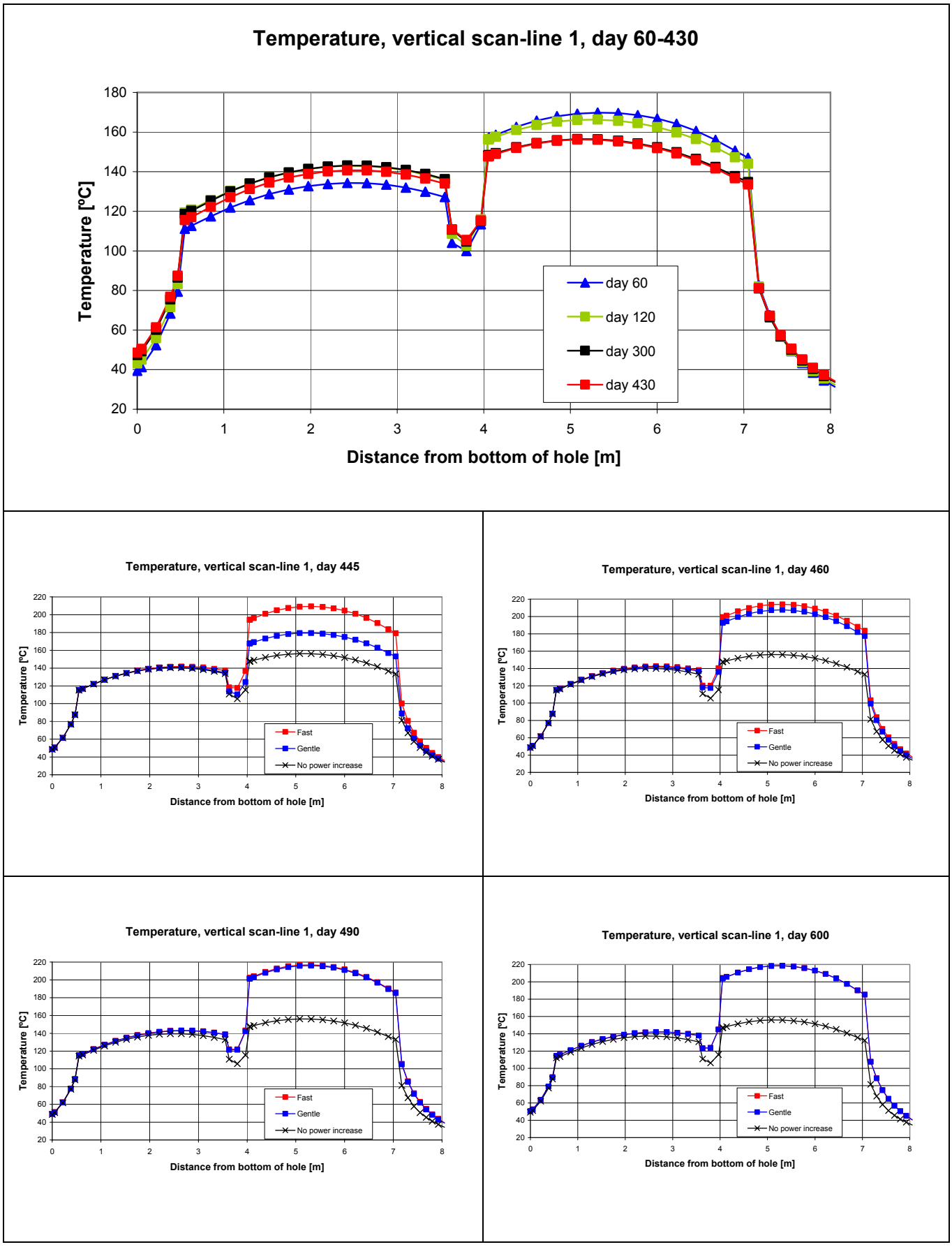

Figure 13. *Temperatures along vertical scan-line 1. The four lower diagrams show the effect of using the different power increase protocols.*

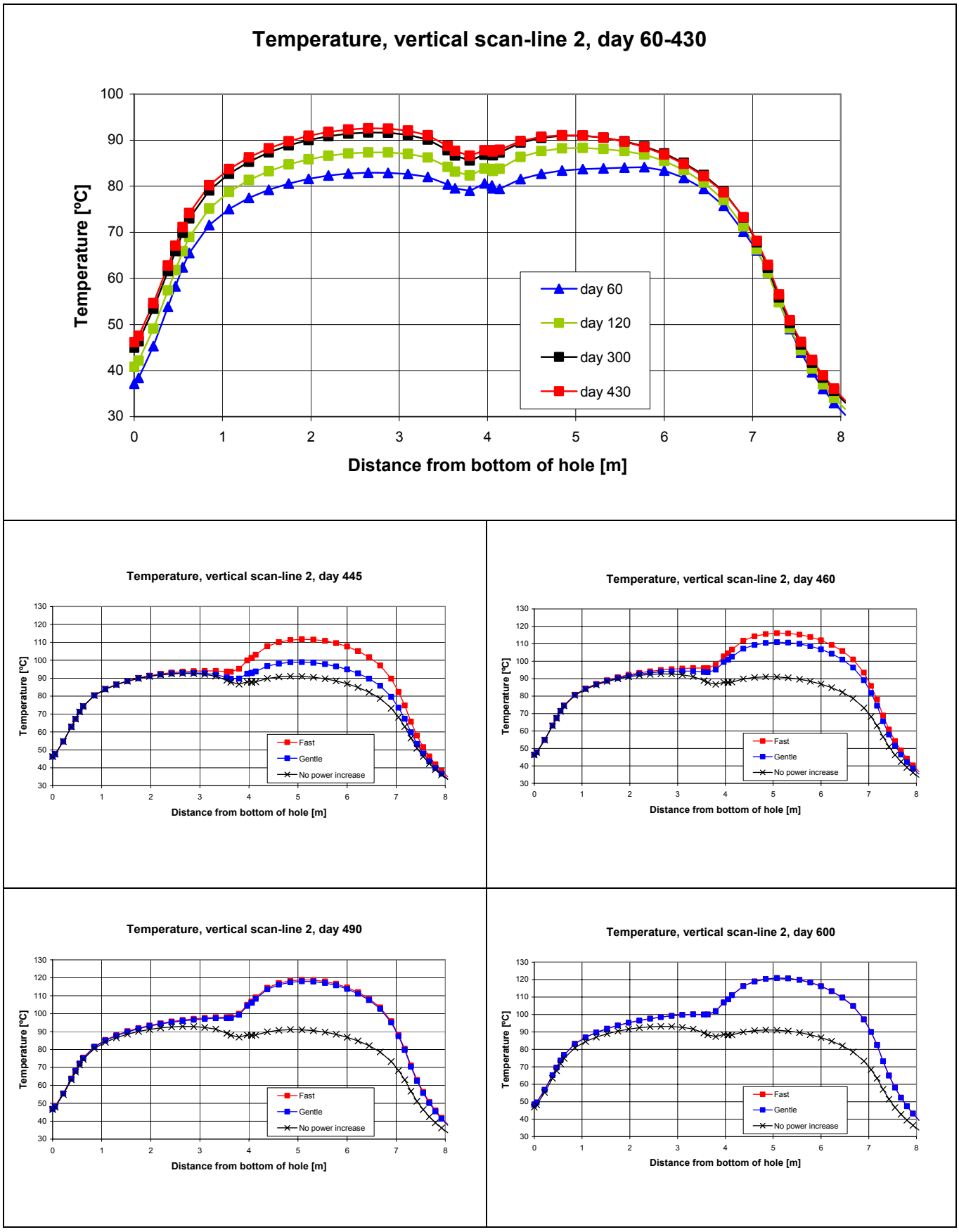

Figure 14. *Temperatures along vertical scan-line 2. The four lower diagrams show the effect of using the different power increase protocols.*

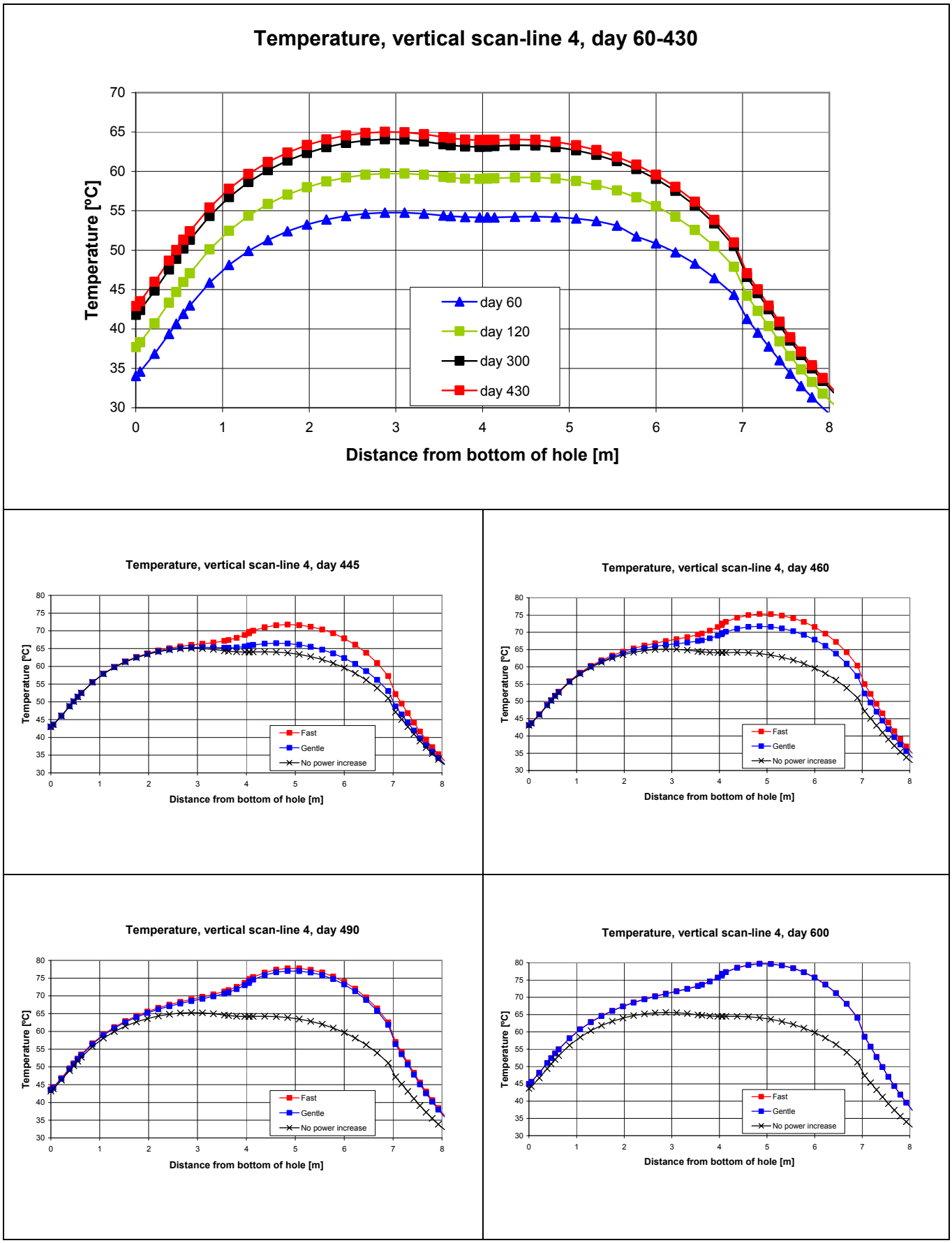

Figure 15. *Temperatures along vertical scan-line 4. The four lower diagrams show the effect of using the different power increase protocols.*

5 Conclusions and discussion

This work contains results from the modelling work performed at Clay Technology within the framework of TBT. According to the results presented, there are some conclusions that can be drawn:

- The innermost parts of the bentonite surrounding the upper heater get slightly desaturated when the heating power in the upper heater is increased. The hydration seems to reach a state with very little changes after some 600 days.
- The saturation in the bentonite surrounding the lower heater seems to be facilitated by the heating power increase. This is probably due to the fact that the temperature level is increased but the temperature gradient is maintained. The increased temperature gives a lower water viscosity, with an accompanying increase in liquid permeability.
- The impact on the experiment's hydraulic behaviour of the power increase is so small that it would be difficult to verify with measurements. Therefore, one may consider how useful a heating power increase would be for testing the conceptual models.
- The two different protocols for increasing the upper heater power give no significant differences in the hydraulic behaviour of the experiment.
- After the power increase, the temperature at the sand shield/bentonite interface exceeds 100 ºC. This is done without exceeding the heater surface temperature limit (225 ºC).

References

Cimne, 2002. Code_Bright. Ver 2.2 Users manual. Departamento de Ingeneria del Terreno, Cartografica y Geofisica, UPC, Barcelona.

Goudarzi R., Börgesson L., Sandén T., Barcena I., 2003, 2004. Temperature Buffer Test. Sensors data report (Period 030326-031001). Report No:1. SKB IPR-04-02

Hökmark H., Fälth B., Åkesson M., 2004. TBT – Evaluation Modeling Program, Clay Technology AB, Lund.

Clay Technology AB

Ideon Research Center

Lund, Sweden

TBT - Evaluation Modeling Program

STEP 2 –proposal for September 2004 - November 2004

August 2004

Harald Hökmark

Billy Fälth

Mattias Åkesson

Contents

1 TBT experiment

TBT (Temperature Buffer Test) is a joint project between SKB/ANDRA, supported by ENRESA and DBE, carried out in granitic rock at Äspö Hard Rock Laboratory, Sweden.

The test aims at understanding and modelling the thermo-hydro-mechanical behaviour of buffers made of swelling clay exposed to high temperatures (over 100°C) during the water saturation process.

Two identical canisters (each 3 m long, 0.6 m diameter) and their bentonite buffer material are stacked in a 8 meters deep and 1.8 m diameter deposition hole, confined by a plug on top.

- The lower canister is directly surrounded by a bentonite buffer.
- Around the upper canister, an annular sand shield is placed between the canister and the bentonite buffer (composite barrier).

The sand shield will reduce the temperature to which the bentonite will be exposed. Without the sand shield, the bentonite will be exposed to temperatures well over 100°C.

Both options are tried in the TBT experiment. A drawing of the experiment set-up is provided in Figure 1-1.

The test started in March 2003, with heating of each canister using internally-located electric heaters set to 1500 W power output and implementing of an artificial wetting of the clay using a pressurized water source.

On completion of the experiment, the bentonite will be sampled and analyzed to determine any mineralogical alterations and changes in hydraulical and rheological properties. To be able to do a fair evaluation of the effects of elevated temperature it is essential that the temperature is sufficiently high during the experiment and that, at the end of the experiment, the bentonite will have reached a high degree of saturation in all parts of the TBT (including the high-temperature regions close to the containers).

To ensure that the temperature condition above will be met, a target temperature of about 100° at 0.5 m radial distance from the heater axis has been specified for the experiment. The power output of the two heaters was dimensioned to meet that condition. To meet the requirement for the TBT to achieve nearly complete water saturation, arrangements for artificial groundwater pressurization were made in the construction of this experiment.

The experiment includes an extensive instrumentation to monitor temperatures, total pressures, pore pressures, relative humidities, etc. /Goudarzi et al., 2003/.

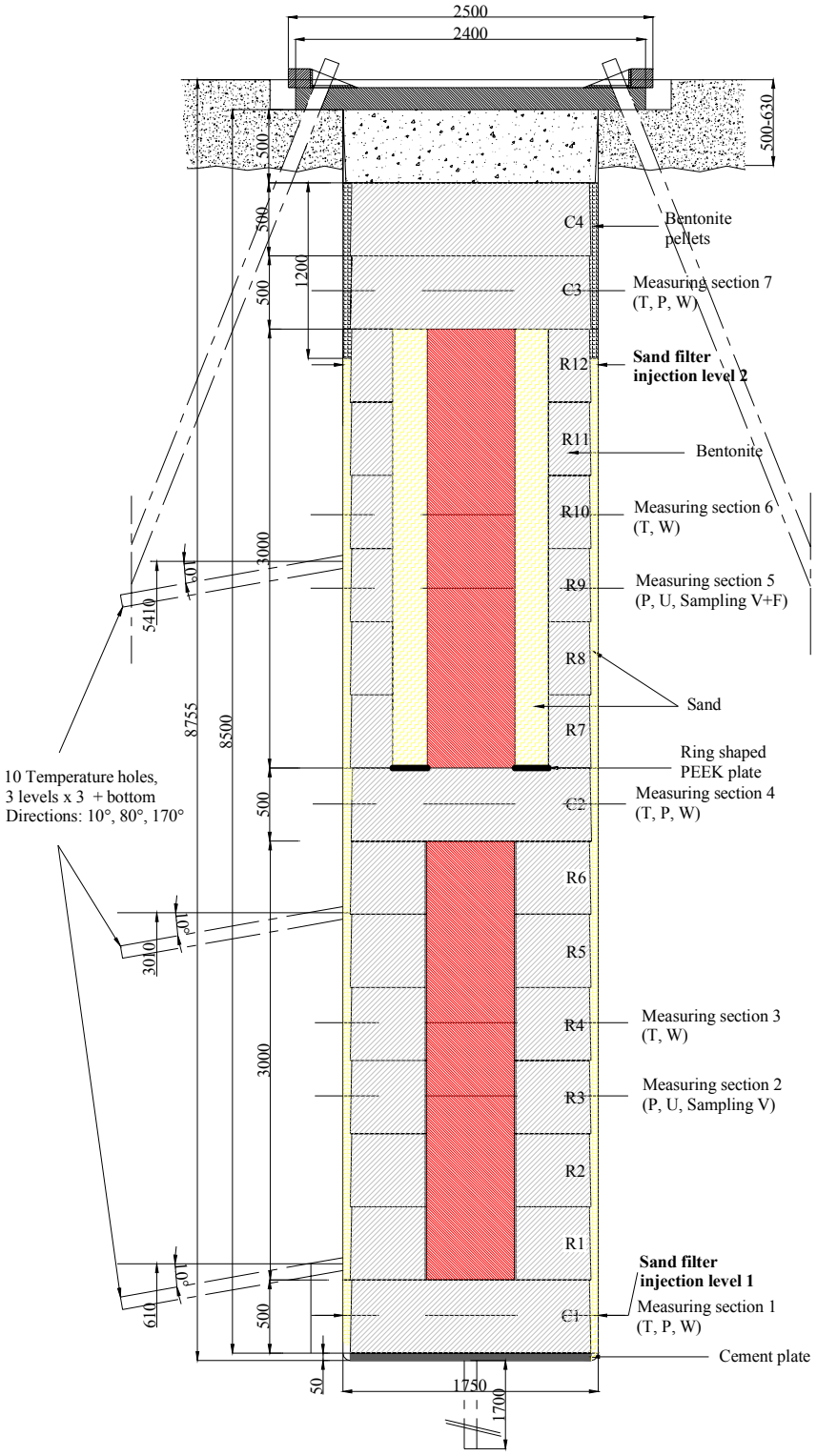

Figure 1-1. *TBT experiment set-up. T= temperature (thermocouples); P = total pressure (radial, tangential and axial stress); W = RH (capacity sensors and psychrometers); U = pore pressure (including option to sample gas or fluid).*

2 Predictive modeling phase

The experiment (heat generation) started in March 2003 and has been producing data for about 500 days up to the present day. Prior to test initiation, a Predictive Modeling Program was specified /Hökmark and Fälth, 2002/. A number of modeling teams made blind predictions based on the specifications in that program. The results are found are in a predictive modeling report.

A preliminary comparison between a selection of predicted results and corresponding measured values was compiled for the Sitges Workshop on large-scale field experiments in granite, November 2003 /Hökmark, 2003/.

Some reflections were:

- There is a systematic dehydration of the inner, hottest part of the bentonite surrounding the lower heater. That dehydration took place soon after test start. During the period of time being covered in the compilation, there were little or no signs of resaturation of that inner part.
- For the bentonite surrounding the sand-shield around the upper heater and for the bentonite at radial distances larger than 0.2 m from the lower heater surface, the state of saturation seemed less clear. The slope of the thermal gradients, which were minutely recorded at mid-height of the two heaters, did not appear to change much after the initial moisture redistribution, which could be interpreted as no or very slow changes in the state of saturation. On the other hand, the RH readings suggested that there were changes, at least around the upper heater.

The comparison of modeling results seemed to point to the possibility that the assumptions made regarding gas escape or gas confinement could be part of the explanation for the differences found regarding the extent of dehydration. The gas escape issue (and the role of gas pressures in general) is consequently an area that needs more attention in the future, in particular for systems where high temperatures are expected.

3 Overview of results

3.1 General

All instrument readings up to February 20 are shown graphically in Appendix 1 in the format used in the sensor data reports (e.g. Goudarzi et al., 2003). Figure numbers with a leading 'A' (Axx) given here refer to that appendix. Figures regard the time up to July 1, except for Fig. A1, which includes also results obtained during August.

3.2 Total inflow of water

The sand filter located in the annular gap between the bentonite buffer and the surrounding rock was filled through four tubes ending at the bottom of the sand filter (injection level 1, c.f. Fig. 1-1). The accumulated water inflow up to day 82 was measured to 1.165 m^3. The pressure in these tubes from day 50 until day 350was measured to about 0.8 MPa (Figure A1). However, that pressure was not effective continuously, but dropped to zero at various times during this period as shown in Figure A-1 . At day 82, water began to flow through tubes connecting the uppermost parts of the sand filter with the atmosphere, indicating that the sand filter was filled after about 80 days. That outflow stopped spontaneously after a few days, indicating that some difficulty had developed in the water supply system or that the flow resistance of the system had increased.

On April 1, i.e. after some 370 days, a major change in the injection system was made. The pressure was reduced to about 0.1 MPa and the four upper injection points (injection level 2, c.f. Fig. 1-1) were connected to that pressure. The intention was to apply a uniform boundary pressure along the height of the sand filter, rather than having a high pressure in the bottom and almost zero pressure in the top region, and with an uncertain pressure/height relation. The change (injection also from the top) gave a significant increase in inflow, indicating that the upper parts of the experiment had not been efficiently supplied with water during the time preceding the change.

At present (day 450, August 2004) approximately 1.75 m^3 has been injected into the system. During the first 75 days the inflow was about $1.7 \cdot 10^{-7}$ m^3/s. After 100 days the inflow had dropped to about $1.5 \cdot 10^{-8}$ m^3/s, while it increased to about $4.4 \cdot 10^{-8}$ m^3/s when the change (engaging all 8 injection points, lowering the pressure) was done to the injection system. Table 3-1 shows the inflow data and the average hydraulic conductivity of the sand filter, calculated assuming the pressure drop to be uniformly distributed over the height of the column during the time before April 1. Table 3-2 shows the pore space available at the beginning of the test and the space remaining now (August 2004).

Table 3-1: Total inflow rate and estimated average sand filter conductivity

Time period	Total inflow [m^3/s] (from Fig A1)		Apparent sand filter conductivity [m/s]
Day 0- 75	$1.7 \cdot 10^{-7}$	(average)	$1 \cdot 10^{-7}$ (at the end of the period)
Day 100 -370	$1.5 \cdot 10^{-8}$	(when pressure was effective)	$5 \cdot 10^{-9}$
	0	(when pressure was zero)	
Day 370 -	$4.4 \cdot 10^{-8}$	(average)	
Lab data, compressed filter sand			$5 \cdot 10^{-7}$

Table 3-2: TBT Pore space

	Available at test start [m^3]		Injected water [m^3]	Remaining [m^3]
Sand filter	0.77		0.77	0.00
Pellets filling	0.24	1.38	0.98	0.40
Bentonite	1.08			
Heater/bentonite clearance	0.06			
Sand shield	0.55		0.00	0.55
Total	2.70		1.75	0.95

3.2.1 Sand filter behavior

The apparent sand filter conductivity at test start was only 20 % of the lab value (Table 3-1), probably because of flow restrictions around the filter tips. In the period between 75 and 100 days, the apparent hydraulic conductivity decreased by a factor of about 20.

The reason for the gradually increased flow resistance may be sand filter compression combined with bentonite intrusion and/or clogging of the filter tips. In addition to increasing the inflow, the change done to the injection system in early April resulted in significant changes in suction and stress evolution. This supported the notion that the upper part of the experiment had not been supplied with sufficient volumes of water in the time period preceding the change in water supply technique. In order to understand the behavior of the sand filter, a preliminary hydraulic test program was performed in mid June. The test confirmed that the flow capacity of the four lower injection points was 10 to 100 times lower than the four upper injection points.

3.3 Temperatures

Temperatures are monitored by use of thermocouples in three cylinders (C1, C2 and C3) and two rings (R4 and R10), cf. Fig. 1-1. In addition, temperature readings are provided by the capacitance-type relative humidity (RH) sensors (Figure A21-A26). In general, the temperature results exhibit consistent trends up to maximum values after about 200 days (Figure A2 – A10). A few exceptions have occurred for inner parts in Cyl 2 and the inner sand shield at Ring 10, where the maximum temperatures were reached after only about 40 and 60 days, respectively (Figure A6 – A7).

A minor temperature decrease has also been recorded at the innermost points in these sections. Similar trends are found on the heater surfaces and in the interior of the heaters (Figure A17 – A20) and can be summarized as follows:

- For the upper heater the trend is very clear and can be explained by the delayed wetting of the upper parts of the sand filter (not completed until after 80 days). The gentle decrease in heater temperature after completion of the sand filter saturation may be due to compression of the sand shield and following increase in sand shield thermal conductivity. Details in these trends may be due to successive and slow changes in the heat flow organization around the heaters.

The temperature readings are compiled in Table 3-3 below. It can be noted that the highest temperatures in the bentonite blocks are found in Ring 4, whereas the lowest can be found in cylinder C3. It should also be noted that the 120° isotherm appears to narrow in the region between the heaters (Cylinder C2).

Table 3-3: Temperature distribution (°C) at day 463.

	Radius (mm):											
	150	200	250	300	350	400	450	500	550	600	650	700
Cyl 3					49	48	48	47	46	45	43	42
Ring10					135	120	**108**	**95**	**89**	**84**	79	74
Cyl 2	127				**109**	**105**	**97**	**92**	**87**	**83**	80	76
Ring 4					125	**117**	**110**	**104**	**97**	**93**	**87**	**82**
Cyl 1	**112**				**92**	**87**	**82**	77	72	69	67	62

Legend: < 80° | 80 - 100° | 100-120° | >120°

The TBT experiment is located 6 m from the CRT experiment. The latter was initiated approximately 850 days before the start of the TBT experiment and has therefore affected the surrounding rock temperature. In general, recorded temperatures in the rock follow the same trend as in the bentonite blocks, but on a lower level (Figure A11 – A14). A compilation of the initial and the recently measured temperatures at different levels, depths and azimuths is presented in Table 3-4 below. It can be noted that the current rock surface temperatures towards the CRT (Az 10°) are up to 5°C higher than the corresponding temperatures on the opposite side (Az 170°). The initial difference was not more than 3°C. This is consistent with the overlapping thermal fields of the CRT and the TBT.

Table 3-4: Rock temperatures at the walls of the experiment hole

Time (d)	Level (m)	Temp.(°C) - rock surface Az:10°	Az:170°	Temp.(°C) - 1,5 m in rock Az:10°	Az:170°
0	5,41	21	19	24	17
	3,01	22	19	26	18
	0,61	22	19	25	18
295	5,41	64	63	44	38
	3,01	71	66	47	40
	0,61	61	57	41	35
463	5,41	66	66	44	39
	3,01	72	67	47	39
	0,61	61	58	41	36

Azimuth 0° is towards the CRT experiment.

Sporadic irregularities in the temperature trends, especially around the lower heater, can be attributed to a number of brief heater power failures (Figure A15 – A16).

Figure 3-1 shows Azimuth 90° temperatures measured in Ring 4 and 10. The effect of the wetting of the sand filter outside Ring 10 is obvious: Within the first 60 days of heating, the temperature drop across the filter had discernibly decreased, as would be expected in a system that had become water saturated and had potentially undergone some swelling pressure – induced compression.

Figure 3-2 and 3-3 below illustrate changes in apparent thermal conductivity. The results are based on the slopes of temperature-distance curves derived from thermocouple readings in rings 10 and 4 (Fig. 3-1), and on the assumption of constant radial heat output at heater mid-height. There are systematic increases that indicate that saturation may be proceeding at a reasonably high rate (as opposed to the findings from the preliminary evaluation). This is consistent with Table 3-2, i.e. that the bentonite (blocks, canister/block clearance and pellet filling) has taken up about 70% of the amount required for full saturation (August, 2004). There is also an apparent increase in the sand shield conductivity, in particular in the period between 60 and 145 days.

Figure 3-2 and 3-3 should be interpreted with some caution: some of the changes may be due to variation of the mid-height heat flux, and some may be due to dislocation of individual sensors. There is also the likelihood that the sand-filled regions of the two sections of the TBT have undergone some degree of compression due to the swelling pressure generated by the saturated portions of the buffer. Similarly, swelling of the buffer would result in a decrease in density and a corresponding reduction in the thermal conductivity of this material. This is shown most clearly in Figure 3-3 (Ring 10) where volume-strains would be expected to be most substantial, the changes in thermal conductivity observed here are consistent with perimeter strains (compression and expansion) as the buffer hydrates.

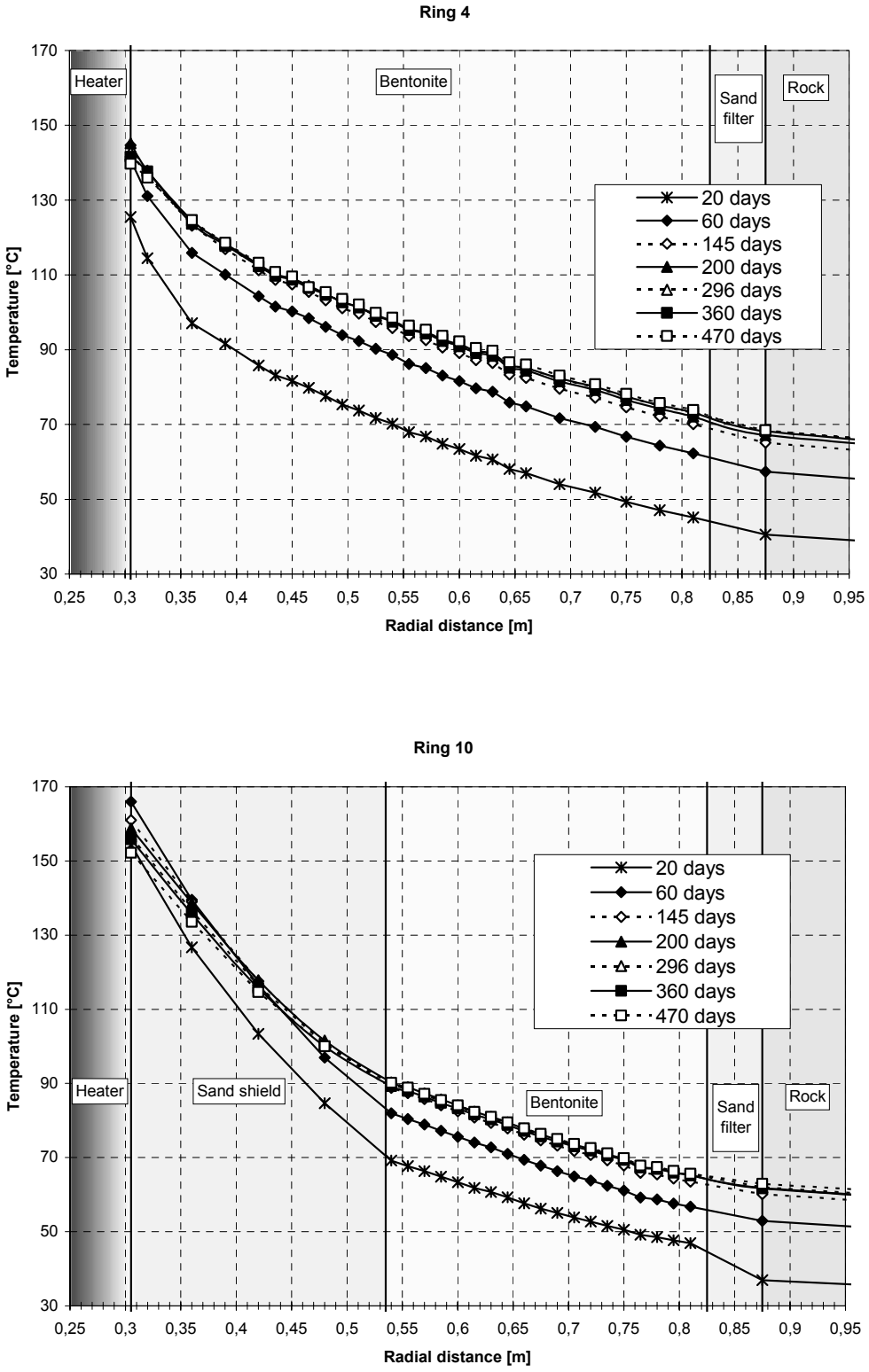

Figure 3-1. *Temperatures measured at mid-height of heater 1 (Ring 4) and heater 2 (Ring 10).*

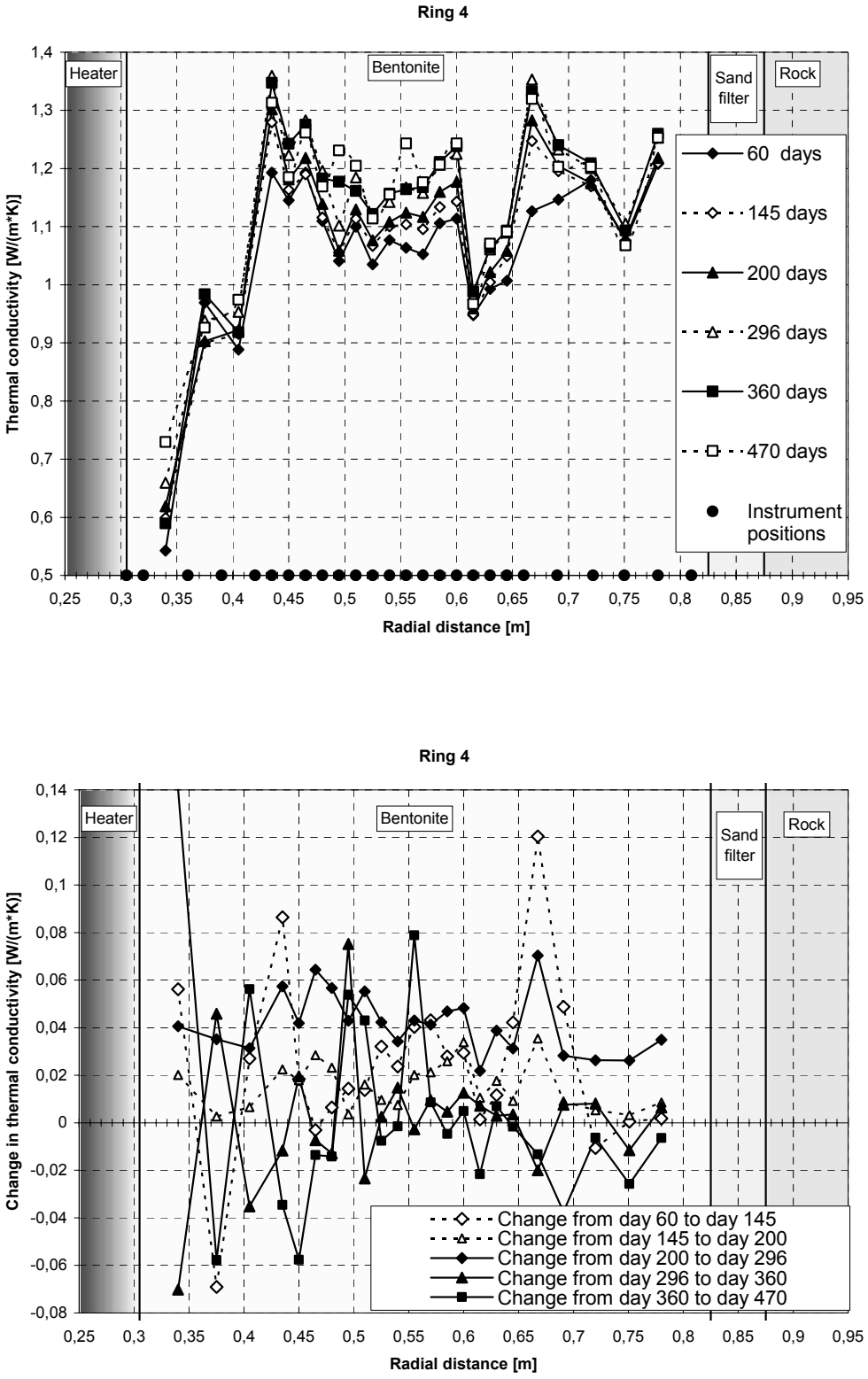

Figure 3-2. *Upper: Thermal conductivity in ring 4 as computed from slopes of distance-temperature relation. Lower: Change in thermal conductivity during four time intervals. Day 60 data are slightly affected by the transient heating effect.*

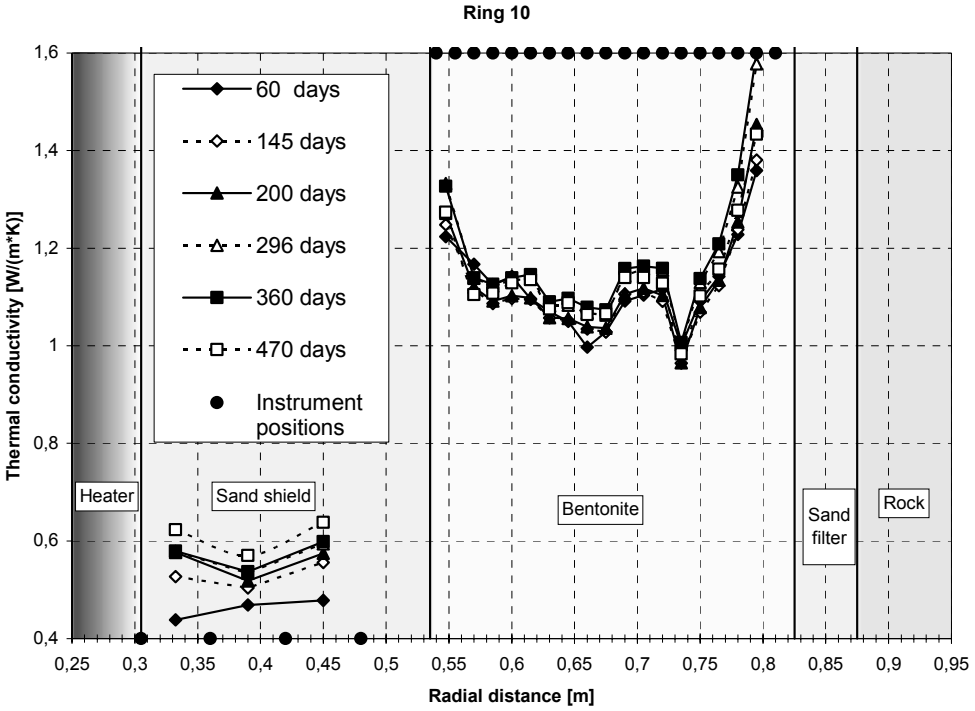

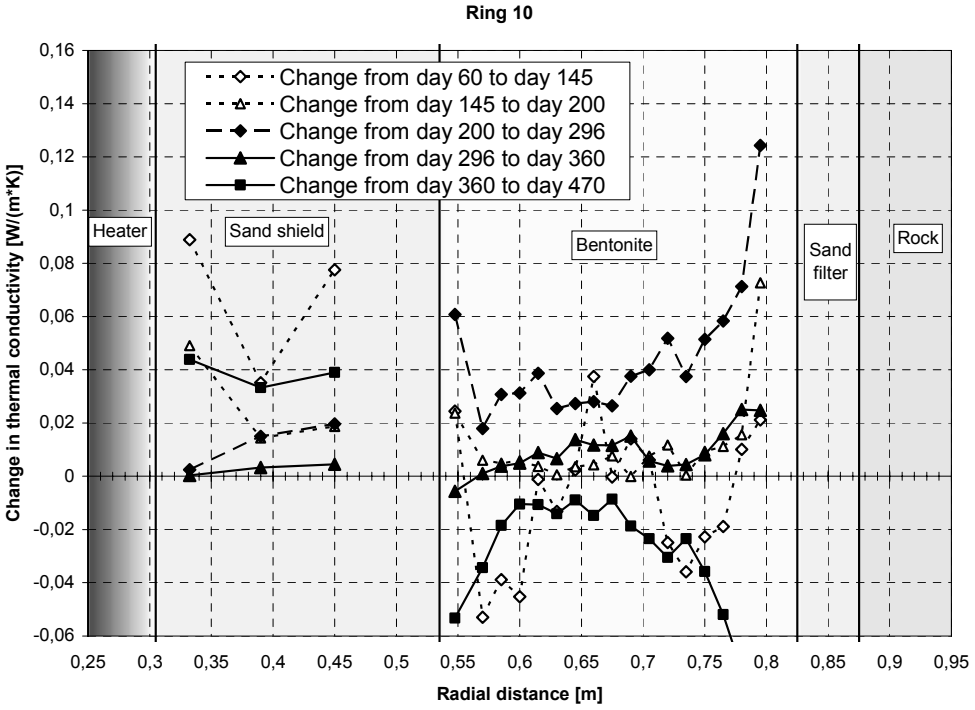

Figure 3-3. *Upper: Thermal conductivity in ring 10 and in sand shield as computed from slopes of distance- temperature relation. Lower: Change in thermal conductivity during four time intervals.*

3.4 Relative humidity/suction

Recorded RH values and suctions indicate that moisture contents generally increase: RH from 72 to maximum 100 % (Figure A21 – A26); suction between 6 and 2 MPa (Figure A27 – A31). A significant exception is the suction increase in Ring 10 at radius 785 and 735 mm after day 225 (Fig. A30).

Although this increase correlated with a general decrease in stresses in parts of Ring 9, it was most likely caused by a shortage in water supply, resulting in a localized desiccation cycle to occur. The trend was also reversed when water injection through the upper tubes was introduced (see Section 3.2), which supports the water supply explanation for these observations.

An indication of drying within 150 mm from the lower heater (Ring 4), measured by a RH sensor at radius 360 which failed around day 140 (Figure A22), has previously been identified through calculation of thermal conductivities (Figure 3-2, upper; /Sandén et al, 2003/).

A compilation of sensors whose output indicate that saturated conditions exist is presented in Table 3-5 below. They are arranged in time intervals. Sensors at radius 785 and 635 mm are indicated with gray and black respectively. As can be noted, the greatest penetration of the saturation front after 480 days of TBT operation is 420 mm in Cylinder 2.

An observation that can be made is that Cylinder 2, closely followed by Ring 4, seems to have gone through a rapid saturation of the outermost parts. The relatively fast saturation here may be an effect of vapor diffusing outwards from the hot, desaturated, parts close to the heater.

Table 3-5: Occurrence of saturation* in different sections.

	Time interval from start (days):											
	0 - 319	40 - 79	80 - 119	120 - 159	160 - 199	200 - 239	240 - 279	280 - 319	320 - 359	360 - 399	400 - 439	440 - 479
Cyl 3						W785	V785					
Ring 10		W785 V785		W735	V685		W685			V585		
Ring 9												
Cyl 2	V785	W785			W635							V420
Ring 4	W785		W710 V710			W635						
Cyl 1		W785	V785									

* W = Wescor sensor generating data, indicating saturation > approx. 95%

V = Vaisala/Rotronic sensor indicating saturation (RH ≈ 100 %)

Number = Radius (mm)

3.5 Total pressure

Results from pressure monitoring are shown in Figures A32 – A40. It is of particular interest to note the stress evolution in Ring 9 (Figs. A37-A39). Some 200 days after test start, the trend towards increasing pressure reversed and total pressures in Ring 9 decreased until early April 2004, when water injection into the upper portion of the TBT was begun. This is consistent with previous indications that this region was not being supplied with sufficient water to drive the saturation front towards the heater at the upper level.

Figure 3-4 below shows the axial stress in different sections. Figure 3-5 shows the vertical buffer force transfer calculated by use of the measured axial stresses, assuming that the forces are transferred within a 0.275 m annular region just inside the sand filter. The total cable force (c.f. Fig. A41) is shown for comparison. The assumed annular force transfer area and the positions of the axial pressure transducers are shown in the right part.

The following can be observed:

- Although the annular transfer cross section area is probably underestimated rather than overestimated, the force transfer in the lower parts is significantly larger than the force taken up by the cables after 330 days. This indicates that the force balance is maintained by considerable shear stresses in the bentonite/sand filter interface.
- The increase in the cable forces was much more rapid than the pressure build-up in the bentonite. This is an effect of thermal volume expansion, in particular that of the two heaters: A 100°C temperature increase will result in about 7 mm increase in total heater length. Some of the axial heater expansion was probably absorbed by low-stiffness interfaces between cylinders and heaters, but some may have contributed to the straining of the cables, see Fig. A42. (The heater temperatures have increased by much more than 100°C, cf. Figs A19 and A20, but the increase relative to the rock is of that magnitude).
- Some 100 or 120 days after test start, the axial stress in Ring 9 did not increase any further (This is true for the tangential stress as well, Fig. A38). This seems to coincide with the appearance of radial stresses in the sand shield (Fig. A37). A possible explanation is that the buffer had gradually taken on sufficient water to begin acting in a more plastic manner and less as a rigid-elastic material and that the volume exhibiting this “plastic” deformation of the was gradually increasing. The plastic deformation of the bentonite block brought about an inward movement and established a supporting lateral pressure on the sand shield. An attempt to model this in a very simplistic way is shown in Appendix 2. (Note that this Appendix is identical to the one issued March 2004 /Hökmark et al, 2004/. The process may have transferred some of the axial forces from the buffer to the sand.
- After about 225 days, most stresses in Ring 9 began to decrease very significantly. This decrease has been found to be a result of insufficient water supply to the upper parts of the experiment. When the four upper injection points were connected in early April, the stresses recovered.
- There was a sudden (local) loss of axial stress in Cylinder 3 after about 80 days. This is probably an effect of brittle block failure. It could also be caused by a temporary malfunctioning of the total pressure sensor, as none of the two other sensors in Cylinder 3 indicated anything at that time.

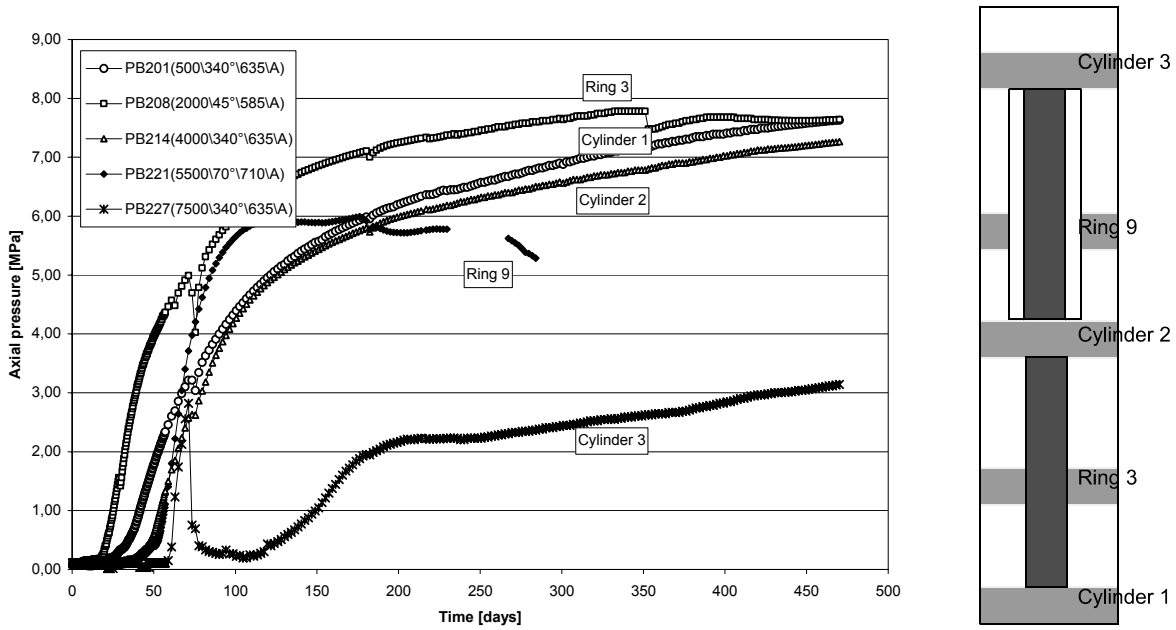

Figure 3-4. *Axial pressure measured in different sections. Sensor in Ring 9 failed after about 300 days.*

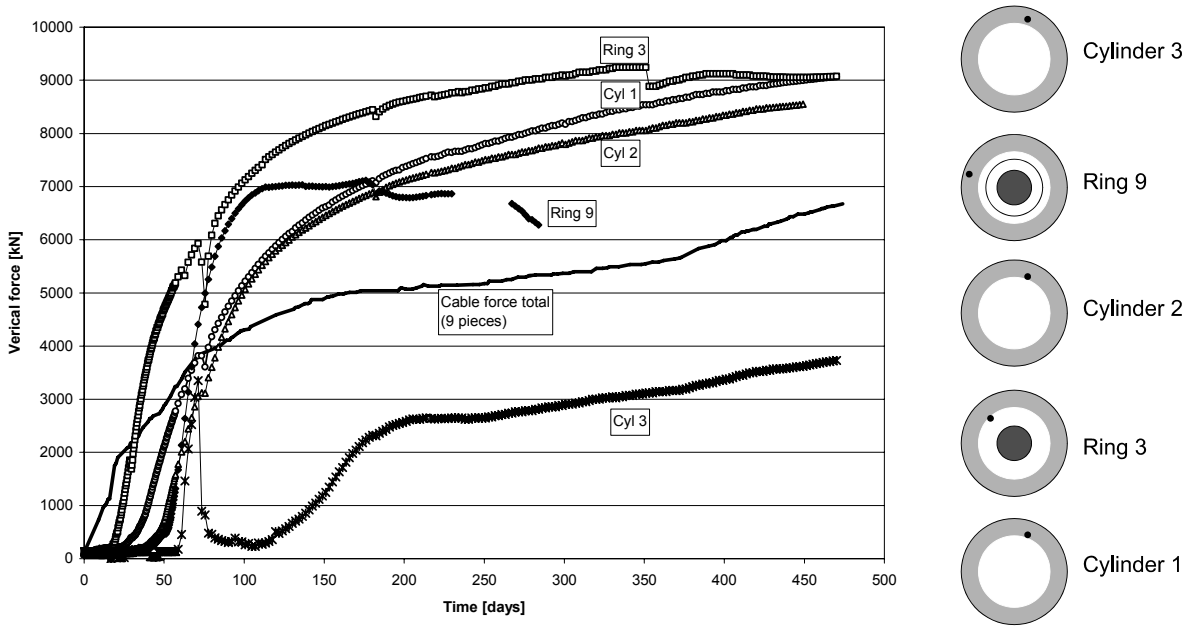

Figure 3-5. *Axial pressure measurement translated into vertical forces, assuming annular region shown to the right (grey-shaded) to be involved in force transfer. The black dots show the stress measurement positions.*

Figure 3-6 shows a schematic of the vertical forces acting on the package. The force balance seems to require that shear stresses in the periphery are significant. The pattern of the internal vertical force transfer is complicated and will vary over time as a result of creep movements in the peripheral parts (leading to reduced shear reactions), swelling, failure of individual blocks and temperature changes. Probably part of the variations in stress and suction readings is due to such changes in the axial force transfer, and not only to differences in wetting rate.

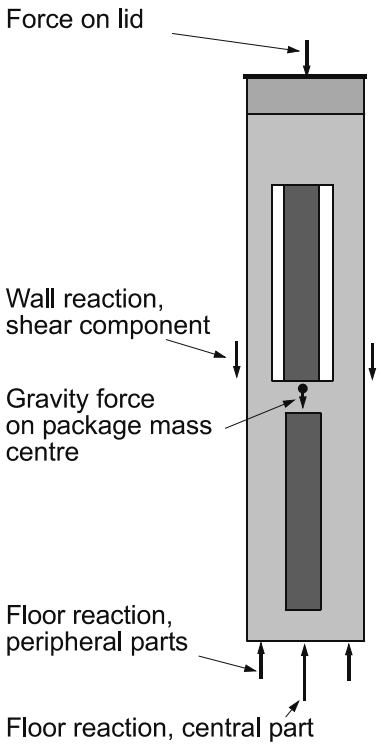

Up		Force [kN]
↑	Floor reaction, peripheral parts (estimated from cylinder 1 axial stress measurement, cf. Fig. 3-5)	9000
	Floor reaction, central part (should be high because of thermal heater expansion)	X
	Total	X+9000
Down		Force [kN]
↓	Force on lid (measured cable forces, cf. Fig. 3-5)	7600
	Gravity force (heaters, bentonite, sand, concrete plug, lid)	500
	Wall shear reaction	X+900
	Total	X+9000

Figure 3-6. *Schematic of vertical forces acting on the package*

3.6 Pore pressure

There was no increase in pore pressure measured within the first 500 days of the experiment (Figure A43 - A44). This could indicate that the system is not gas-tight. However, the bentonite has not yet reached full saturation.

4 Evaluation modeling phase

For ANDRA, the main concern is to improve the understanding of engineered barrier THM behaviour under high temperature conditions. For the evaluation modeling phase there are the following general objectives:

1. Improve the fit between calculations and measurements by considering the present-day experiment status, new or updated information regarding material properties, boundary conditions etc.

2. Apply the updated, or improved, modeling approach to a case in which a significant change is done to the experimental conditions. This means that a new set of blind predictions shall be made. The change done to the test is suggested to be an increase of the power of the upper heater.

3. Based on the outcome of the improved simulations and blind predictions, evaluate relevance and discuss the relevance and validity of the conceptual models used in the numerical representation.

4.1 First set of calculations, May 2004

A first set of simulations has been completed according to the specifications given in the program issued March 2004 /Hökmark et al, 2004/. The simulations were completed by May 2004. The March program addressed mainly objective 2 above: The possible effects of a June 750 W power increase of the upper heater should be explored, in particular whether or not the bentonite surrounding the sand-shield would dehydrate (in a way similar to the bentonite surrounding the lower heater) when subjected to elevated temperatures and heat fluxes. The results of the first set of calculations indicated that the effects of such a power increase would not create any new and useful information.

4.2 Second set of calculations, November 2004

Because of the importance of the hydration phase, the thermo-hydraulic processes have been focused in the TBT modeling work up to the present day. Now (August 2004), the majority of the water needed to saturate the buffer material has been injected and the temperature and the temperature gradients appear to be stable. The saturation rate seems to be possible to predict with the material laws and the parameter values that are available now. Although there are still no definite answers to all questions regarding the relevance and validity of the conceptual models used in the T-H work, it has been decided that more detailed T-H modeling and improvement of fit between experiment an data should wait. Instead, for the time being, the focus should shift to hydro-mechanical issues and in particular to the evolution of suction and stress in the bentonite surrounding the sand-shield in the upper part of the experiment (c.f. Fig. A30; Figs. A37-A39). The modeling guidelines found in Chapter 5 regard the tasks that should be addressed for the second set of evaluation numerical calculations.

4.3 Present-day experiment status

The data obtained so far from the TBT experiment has given much information such that trends of the experiment now are visible, as shown in the previous chapter. However, the result and the trends are not easily interpreted. Some aspects of the development may be related to experimental conditions that result from unintended and/or stochastic processes or events.

4.4 New or updated information

4.4.1 Hydraulic boundary

4.4.1.1 From test start to the end of March 2004

The sand filter between bentonite cylinders/rings and rock was not filled completely with water until some 80 days after test start. Water injection was made only in the bottom part of the sand filter, while the upper injection points were kept at atmospheric pressure. It was necessary to apply a considerable pressure to inject water into the filter, while it was expected (initially) that the permeable sand should get saturated at a low (atmospheric) pressure and that it would be necessary to restrict the water supply in order to control the filling rate. It is not clear if the flow resistance is due to:

- clogging of the filters at the tips of the inflow pipes just above the bottom of the sand filter, or
- increase of flow resistance because of sand filter compression and/or bentonite intrusion.

Both processes could be responsible. The hydraulic conductivity of the sand filter can be approximated to $5 \cdot 10^{-7}$ m/s (lab value, c.f. Table 3-1) after compression from 1700 to 1870 kg/m^3 dry density. The left part of Fig. 4-1 shows results from an oedometer test of the sand filter material. It is not likely that the pressure exerted by the swelling bentonite blocks can have compressed the sand filter to much higher densities than that. Given the high fraction of fines in the sand (right part of Fig. 4-1), it does not seem likely that bentonite intrusion is the only important process. Therefore the hypothesis of clogging around the filter tips or the sand immediately adjacent to them is proposed as the main reason for the high flow resistance.

The pressure history in the sand filter is uncertain. The decrease in bentonite stresses in the upper part of the experiment 225 days after test start (Figs A37-A39) as well as the disturbance of the suction evolution (Fig. A30) indicate that the sand filter may have desaturated (pressure may have dropped below atmospheric).

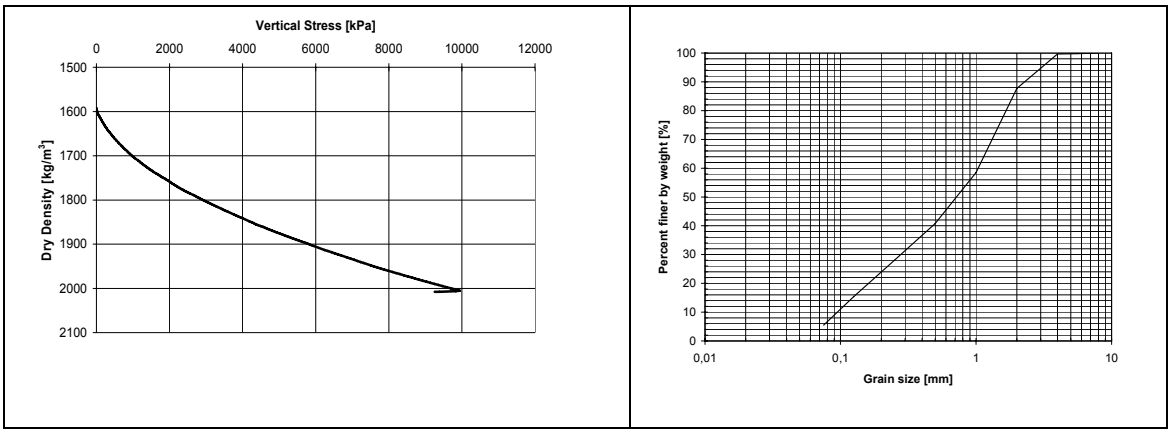

Figure 4-1. *Sand used in filter and shield. Left: compression test result. Right: grain size distribution.*

4.4.1.2 From April 2004 and onwards

From April 2004, water was supplied also from the upper points. From mid June 2004 and onwards the water pressure has been kept at about 0.15 MPa over atmospheric. The hydraulic test program implemented in June showed that the upper filter tips had a much higher flow capacity than the lower ones (c.f. section 3.2.1). It is reasonable to assume that the pressure in the sand filter is uniform at present (August 2004). However it is not impossible that there will be a general increase in flow resistance later and that the injection pressure will have to be increased in order to complete the saturation.

4.4.2 Pellets/sand filter

The sand/pellets interface is 200 mm below the top of Ring 12 (cf. Fig. 1-1). In the original design shown in the predictive modeling program, the pellet filling extended just to the top of Ring 12.

4.4.3 Rock heat conductivity

The rock heat conductivity specified in the predictive modeling program was 2.7 W/(m·K). That value should be reduced because of temperature dependence. Most crystalline rocks will loose about 0.1% of heat conductivity per °C /Kukkonen and Lindberg, 1995/. Therefore a more relevant value would be 2.6 W/(m·K) (cf. calculation example in next section).

4.4.4 Rock initial temperature

The initial temperature at the rock wall should be 20°C (c.f. Table 3-4) rather than the values suggested by the pre-test measurements presented in the predictive modeling program.

4.4.5 MX-80 Thermo-Hydraulic properties

New experiments on MX-80 bentonite have been performed by C. Gatabin, CEA /Gatabin and Robinet, 2003/. Two cylindrical bentonite samples, 200 mm in height and 200 mm in diameter, were confined in steel cells with fixed 20°C temperature at the top and variable temperature (22°C to 150°C) at the base.

The two samples, THM1G_Cell1 and THM1G_Cell2, had initial liquid saturations of 75.5% and 89.7%, respectively. Void ratios were 0.48 and 0.53. The cells were closed hydraulically, but not completely gas-tight. The temperature at the cell bases was increased from 22°C to 150°C in steps.

Figure 4-2 shows the relative humidity as function of distance from the heated base.

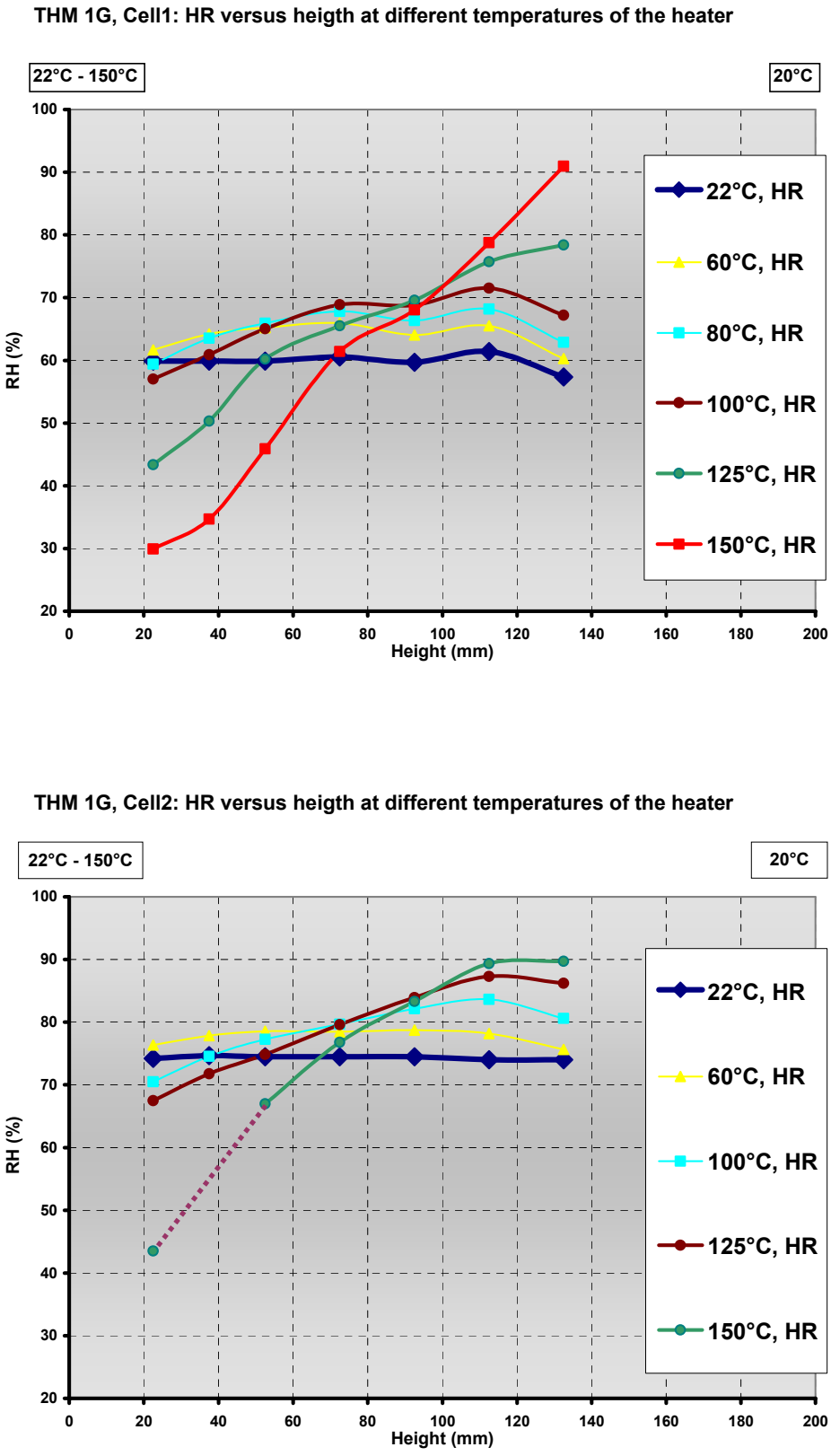

Figure 4-2: *Relative humidity as function of distance from the heated base. From /Gatabin and Robinet, 2003/.*

4.4.6 MX-80 Hydro-Mechanical properties

The figures below give examples of results of hydro-mechanical tests performed on MX-80 bentonite. There is no complete or final set of test results that can be used to define a consistent material model that takes all the nuances of the behaviour of unsaturated MX-80 bentonite into account.

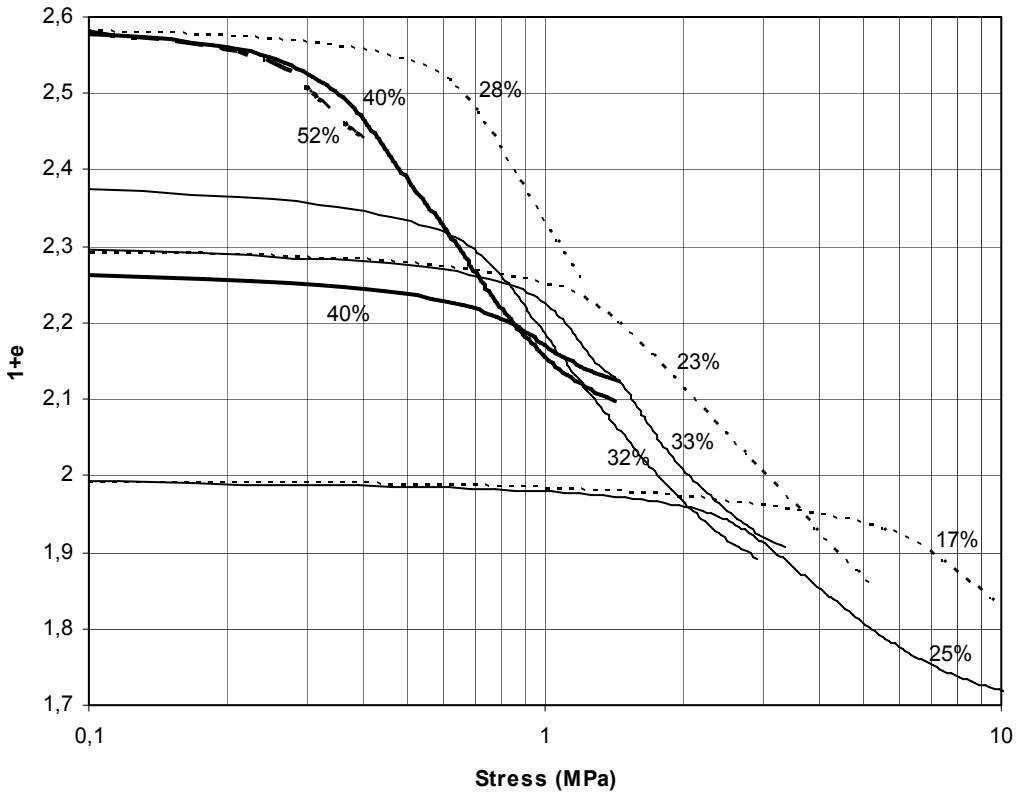

Figure 4-3. *Results from undrained constant (0.7mm/day) strain rate 1-D compression tests on unsaturated MX80. Specific volume (1+e) plotted vs. the stress. The labels give the initial water contents. Derived from /Börgesson, 2001/.*

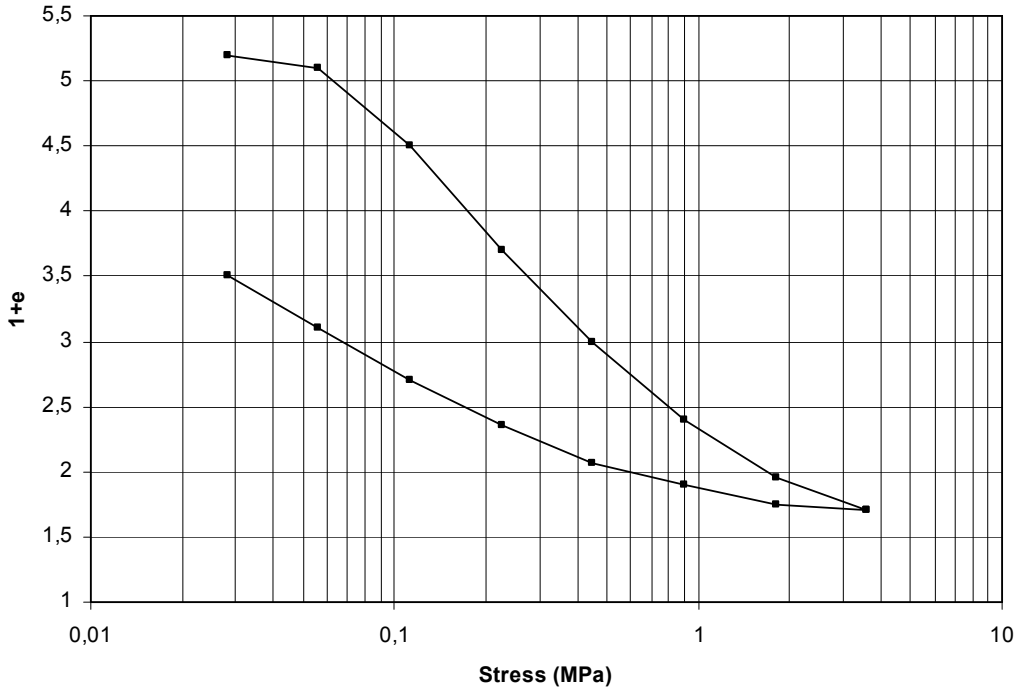

Figure 4-4. *Results from drained oedometer test with saturated MX80. Specific volume (1+e) plotted vs. the stress. From /Börgesson et al., 1988/.*

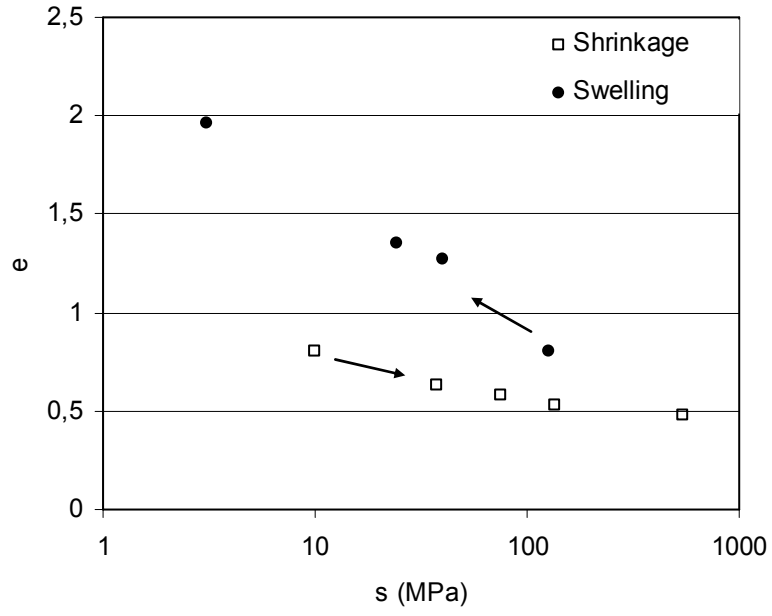

Figure 4-5. *Results from shrinkage and free swelling of MX80. Void ratio (e) plotted vs. suction (s). From /Börgesson, 2001/.*

4.4.7 MX-80 retention

Fig. 4-6 shows suction values based on work being conducted presently at Clay Technology. The new experimental data indicate that the suction is considerably higher than the values proposed in the predictive modeling program.

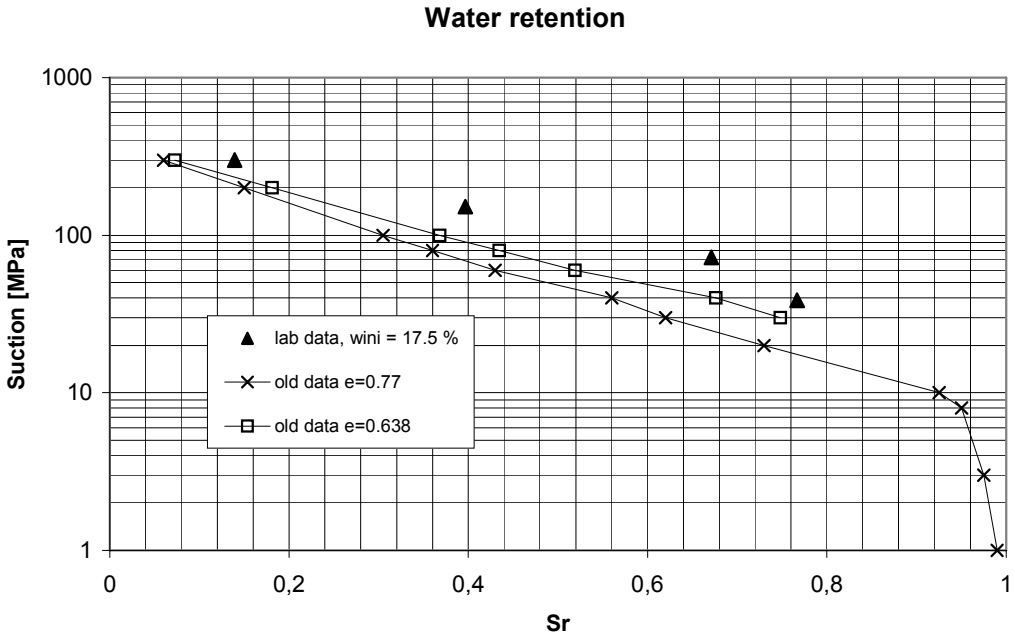

Figure 4-6: *Suction curves. "Old data e = 0.77" is the information given in the predictive modeling program for a void ratio of 0.77. "Old data e = 0.638" are these values translated to a relevant void ratio. Note that the translation is made only in saturation ranges where effects of swelling and confinement are small. The "lab data" are derived from measurements of suction as function of water ratio under unconfined conditions and have been converted here to apply for a void ratio of 0.638.*

4.4.8 Sand shield

In the predictive modeling program, the sand shield thermal conductivity was estimated to be 0.4 W/(m·K). The results obtained so far suggest that the conductivity is a higher: about 0.6 W/(m·K) (cf. Fig. 3-3).

In the predictive modeling program, the initial sand shield saturation was set at 3%. In reality, the sand was dried below that value. The resulting saturation was close to 0%.

5 Modeling guidelines for November 2004

5.1 General

Fig. 5-1 shows the essence of the problem that should be addressed for November. The problem domain consists of the sand shield, the bentonite and the sand filter.

The main issue is to reproduce the behavior of the hydro-mechanical behavior of the bentonite in rings 9 and 10. Hydro-thermally, the problem domain is subject to a temperature boundary condition at the rock/filter interface, a pressure BC in the sand filter and heat flux BC at the heater/shield interface. A very simplistic attempt to model the first episodes of radial stress evolution qualitatively was presented in a previous version of the program.

The thermal boundary conditions can be derived from the experimental results and the power specifications. The sand filter is not instrumented, which means that there are no records of the pressure history. The pressure history P(t) must be defined using estimates/calibrations based on the description of the injection pressure control (c.f. section 3.2).

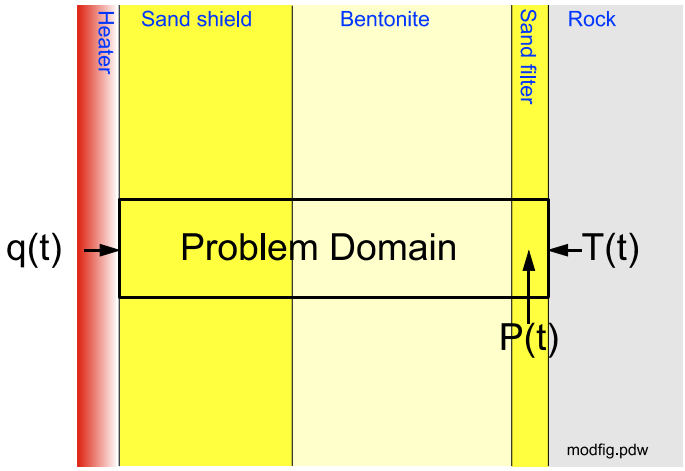

Figure. 5-1*. Problem domain at mid-height of heater 2.*

The time constraints does not allow for extensive efforts. The problem domain corresponds to scan-line A1-A4 in previous versions of the program (c.f. Fig. 5-2).

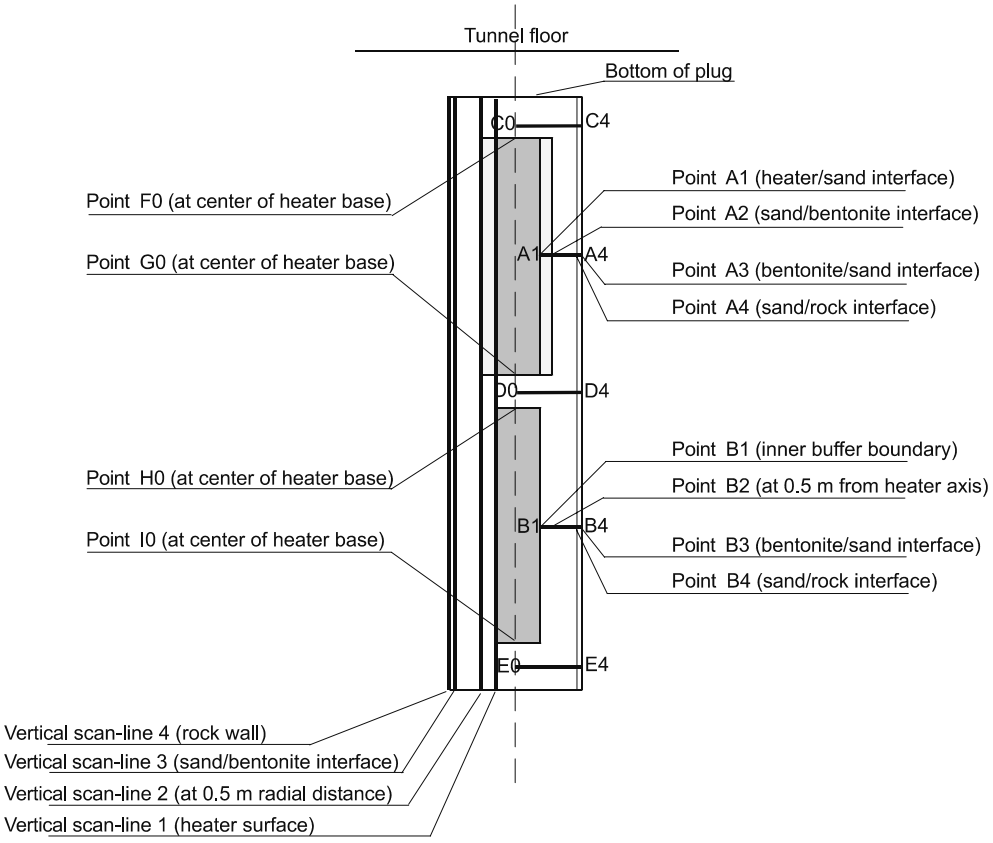

Figure 5-2. *Schematic of TBT with scan-lines.*

5.2 Results proposed for November 2004

For the end of November 2004, the following output is expected to be provided.

1st priority

The main issues are listed below. A model with the features indicated in Fig. 5-1 may be sufficient to accomplish these.

- Analysis of radial stress development in Ring 9. This point should include a suggestion of qualitative description of the hydro-mechanical sand-bentonite interaction as well as actual attempts to reproduce the experimental findings shown in Fig. A30 and Figs. A37-A39.
- Prediction of temperature, saturation, RH, porosity, stresses and displacements on scan-line A1-A4.

Scan-line output should be given for the following days after TBT start:

60, 120, 300, 450, 600, 900

2nd and 3rd priority

The optional items listed below may require full quasi 3D model geometry.

- Prediction of temperature, saturation, RH, porosity, stresses and displacements on scan-lines C0-C4, D0-D4 and E0-E4 (2^{nd} priority)
- Prediction of accumulated total inflow vs. time (2^{nd} priority)
- Prediction of total cable force vs. time (2^{nd} priority)
- Prediction of temperature on vertical scan-lines 1 (heater surface), 2 (at 0.535 m radial distance) and 4 (rock wall) (3^{rd} priority)

Scan-line output should be given for the following days after TBT start:

60, 120, 300, 450, 600, 900

References

Börgesson L., 2001. Äspö Hard Rock Laboratory. Compilation of laboratory data for buffer and backfill materials in the Prototype Repository. SKB IPR-01-34.

Börgesson L., Hökmark H., Karnland O., 1988. Rheological properties of sodium smectite clay. SKB TR 88-30.

Bäck R., 2004. Temperature Buffer Test. Report for retaining plug and anchoring. SKB IPR-02-64

Gatabin C., Robinet J-C, 2003. Mock-up for studying THM behaviour of swelling clay MX80 at temperature > 100°C. CEA/EuroGeomat

Goudarzi R., Börgesson L., Sandén T., Barcena I., 2003., 2004. Temperature Buffer Test. Sensors data report (Period 030326-031001). Report No:1. SKB IPR-04-02

Hökmark H, 2001. Test of vitrified wastes. Study 1 – thermal. One-dimensional radial heat flow in cavity interior. Clay Technology.

Hökmark H, 2003. Temperature Buffer Test – comparison of modeling results and experimental findings: causes of differences. Sitges Workshop on large-scale field experiments in granite. UPC, Barcelona.

Hökmark H., Fälth B., 2002. Predictive modeling Program,. Clay Technology

Hökmark H., Fälth B., Åkesson M., 2004. Evaluation modelling program rev. 3. Clay Technology

Kukkonen I., Lindberg A., 1995. Thermal conductivity of rocks at the TVO investigation sites Olkiluoto, Romuvara and Kievetty. Report YJT-95-08, Nuclear Waste Commission of Finnish Power Companies, Helsinki.

Sandén T., De Combarieu M., Hökmark H., 2003. Description of the instrumentation installed in Temperature Buffer Test. Sitges Workshop on large-scale field experiments in granite. UPC, Barcelona.

Thorsager P., 2002. Temperature Buffer Test. Detailed design materials. Foundation and artificial saturation. SKB IPR-02-62

TBT - Evaluation Modelling Program

STEP 2
(extended version)

ENRESA Contribution

March 2005

A. Ledesma, G. Chen, A. Jacinto
UPC, Barcelona, Spain

Contents

1 Introduction

This report presents the modelling work performed by the team coordinated by ENRESA (Spain) regarding the simulation of the "Temperature Buffer Test" experiment defined by ANDRA (France) and conducted at Äspö Hard Rock Laboratory (Sweden). The work refers to a simulation of the current status of the main variables, as well as a prediction of the THM behaviour of the system for the near future. A first version of this report was presented by December 2004. This report constitutes an "extended version" that was presented at Tours meeting (March 2005), and includes additional simulations of the experiment that improve the previous analyses.

The guidelines to follow in this simulation were defined in a document by Hökmark, Fälth & Åkesson (Clay Technology, 2004), entitled "TBT Evaluation Modeling Program. Step 2 - Proposal for September 2004 – November 2004". That report presented some comments about the current situation of the experiment, including some interpretations of the evolution of the measured variables. Due to the unexpected cycle of suction and stresses measured in the central part of upper heater (rings 9 and 10), the guidelines proposed to concentrate the simulation effort on the analysis of this phenomenon. In addition to that, a prediction of the time evolution for the system THM variables during 2005 was also expected from the computations.

As in previous simulation exercises, we have used the information provided in the Clay Technology Reports to define the parameters and the boundary conditions of the experiment. In that manner, the work from different groups may be compared as they should use similar input data. However, the complexity of this kind of experiment requires quite often the use of additional parameters that have not been defined in advance. In that case we have adopted reasonable values according to our experience, but that may become a source of discrepancy between predictions from other groups, or between predictions and field measurements.

The effect of temperatures well over 100ºC, the composed buffer (sand + bentonite) and the gas related issues constitute the key points that make this experiment unique. Because of that, simulation work requires a continuous innovation and research, and the results presented in this report should be considered only as an intermediate interpretation of the experiment, rather than a final closed analysis of the test. Therefore, the modelling effort should be continued well after dismantling the test, in order to improve the models and parameters and to obtain general conclusions. The parallel work being developed now at a laboratory scale will help also on that direction.

The Spanish participation in this project is coordinated by F. Huertas (ENRESA), and includes groups from UPC and from DM Iberia. In particular, the simulation work described in this report has been developed by the UPC group (A. Ledesma, G. Chen and A. Jacinto). Discussions about the results and the project itself involved F. Huertas (ENRESA) and M. Velasco (DM Iberia) as well.

The code CODE_BRIGHT has been used in all cases, as in the previous simulations performed by the group. Therefore, a comparison between parameters and previous analyses can be performed and that has proven to be very useful when comparing modelling results with measurements.

Section two of this report is devoted to the analysis of the upper heater during the first 500 days of the experiment. Following the indicated guidelines, the idea is to reproduce the cycle of suction and stresses measured there. An important effort has been devoted to that analysis, because it was a sort of check of the capabilities of the code to simulate an actual THM behaviour. The difficulties where linked to the quality of the input data (boundary conditions) and not to the code or to the procedure of analysis itself, but that may be the case in many practical situations.

Section 3 refers to the predictions of the main variables for the scan-lines indicated in the guidelines report. The plots obtained from those simulations are presented and some comments about the results are also included. Three cases have been considered, according to the boundary conditions applied in the simulations. The first two cases were presented in the previous version of this report, and the third case corresponds to the extended work performed between December 2004 and March 2005.

Finally, the report ends up with some concluding remarks about this simulation and the behaviour of the experiment, and includes some proposals for future work.

2 Analysis of the behaviour of Rings 9 & 10

The unexpected behaviour of Rings 9 & 10 in the upper part of the geometry deserves special attention. In fact the guidelines for future analyses suggest concentrating on that behaviour first, even by using a simple 1D geometry if necessary. Then, a prediction of main variables in the rest of the geometry could be presented as well.

The key point of the behaviour of rings 9 and 10 is the cycles of suction and stresses measured between day 150 and day 400, as indicated in the measurements reports (figures 1 and 2). That was not predicted in previous analyses, and it is physically difficult to explain considering that the saturation of the system has been maintained. One of the first tasks was to check if under normal conditions that cycle could be due to the normal behaviour of the bentonite – sand system, or to an anomalous application of the hydraulic boundary condition. The following explanations or "scenarios" were considered at the beginning of the analyses:

a) The cycles of stresses may be due to a mechanical effect of the system sand – bentonite. Bentonite swells and generates compression everywhere, including the sand filter and the sand shield. A sudden deformation of the sand (i.e., a collapse created by wetting an initial unsaturated state under loading), may release stresses in the bentonite for a period of time. The further hydration of the bentonite would increase again the stresses everywhere. Expanding the bentonite due to a stress release, would increase void ratio and suction for a while, and that would explain the measured suction cycle.

b) The cycle of suction may be due to a lack of water available for hydrating the bentonite. The reason could be of a practical nature (i.e. a problem in the water supplying system, etc.). Bentonite stops swelling and even may shrink a bit when water is taken out. That would explain the cycle in stresses as well.

During several weeks, many 1D THM analyses of the geometry sand shield-bentonite-sand filter were performed, in order to simulate the scenario "a)". The conclusion from those calculations is that it is not possible to simulate that cycle of suction/stresses in that manner using the usual range of THM parameters and the assumed boundary conditions. We had to look for other "not natural" reasons (i.e., reasons based on the manipulation of the experiment, rather than on the physics of the problem). Scenario "b)" was then analysed.

The problem with situation "b)" is the simulation of the lack of water. If a 1D geometry is used, that should be imposed directly: a cycle of pore water pressure in the sand filter will eventually generate a cycle of suction in the bentonite. However this procedure would not demonstrate the origin of that cycle, as the boundary condition is "manipulated" accordingly.

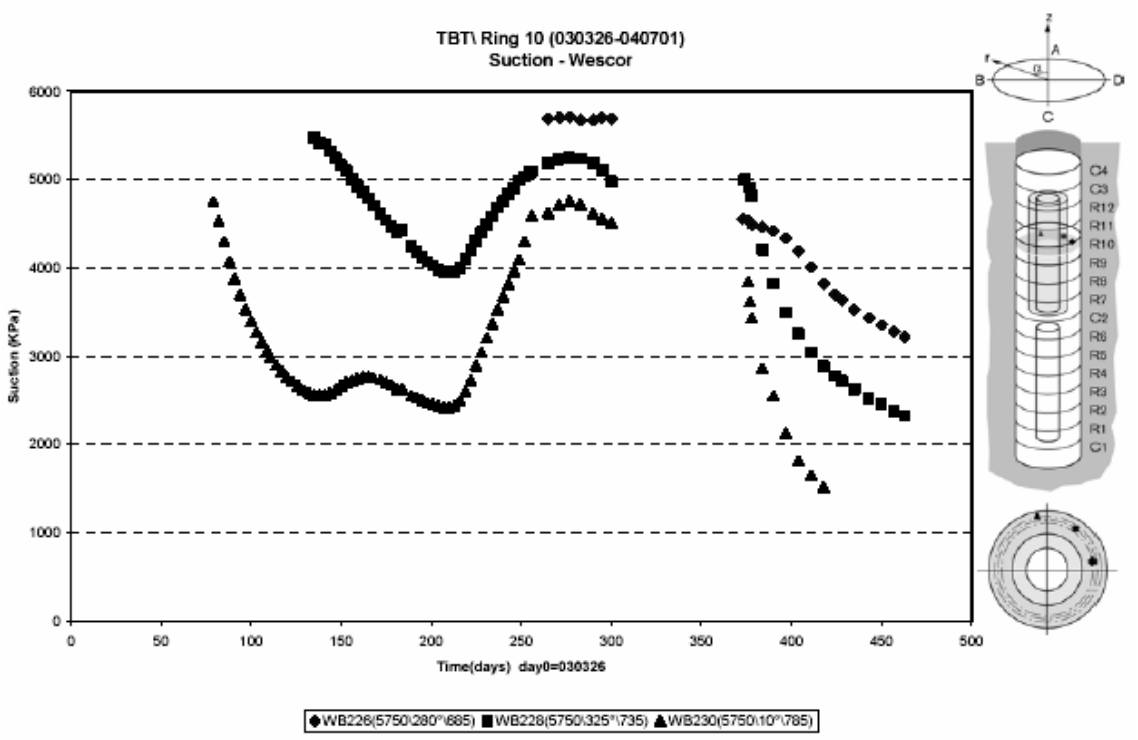

Figure 1. *Cycles of suction measured in ring 10.*

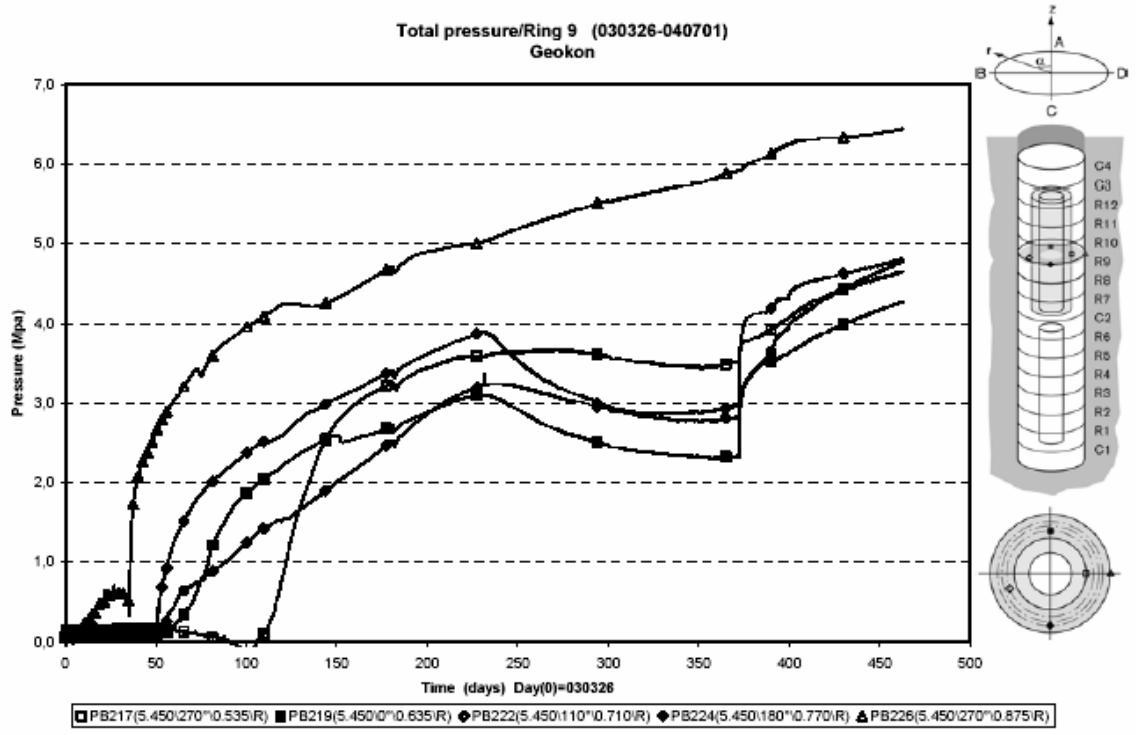

Figure 2. *Cycles of radial stresses measured in ring 9.*

In order to get an insight into the actual evolution of the experiment, a quasi-3D (axi-symmetry) geometry was assumed. When considering the whole geometry, the hydraulic boundary condition can be applied at the bottom of the sand filter, where the water supply pipes are installed. According to the test setup, a water pressure should be imposed at those points.

Figure 3 shows the measured evolution of applied water pressure and inflow & outflow volume of water in the experiment. Note that the curve corresponding to water pressure presents so many changes that it is difficult to use as input data in practice. Indeed, changing in a rapid manner the boundary condition may create numerical instabilities and convergence problems. Smoother changes are, nevertheless, well reproduced by the code. In fact constant water pressure would have been ideal as a boundary condition, but that record with those variations is difficult to use in numerical calculations. On the contrary, the volume inflow of water is a smooth curve, and seems to be a more reliable measurement.

An important effort was therefore devoted to the implementation of total volume of inflow as boundary condition in the simulations. Instead of using a water pressure boundary condition, a flux of water was applied at the bottom nodes of the sand filter. Obviously the hydraulic parameters of the sand filter may have now more importance, but a trial and error procedure can be used in order to obtain a reasonable representation of the amount of water available in the sand filter at different points and times. This analysis will be referred as “Case 1” in this report.

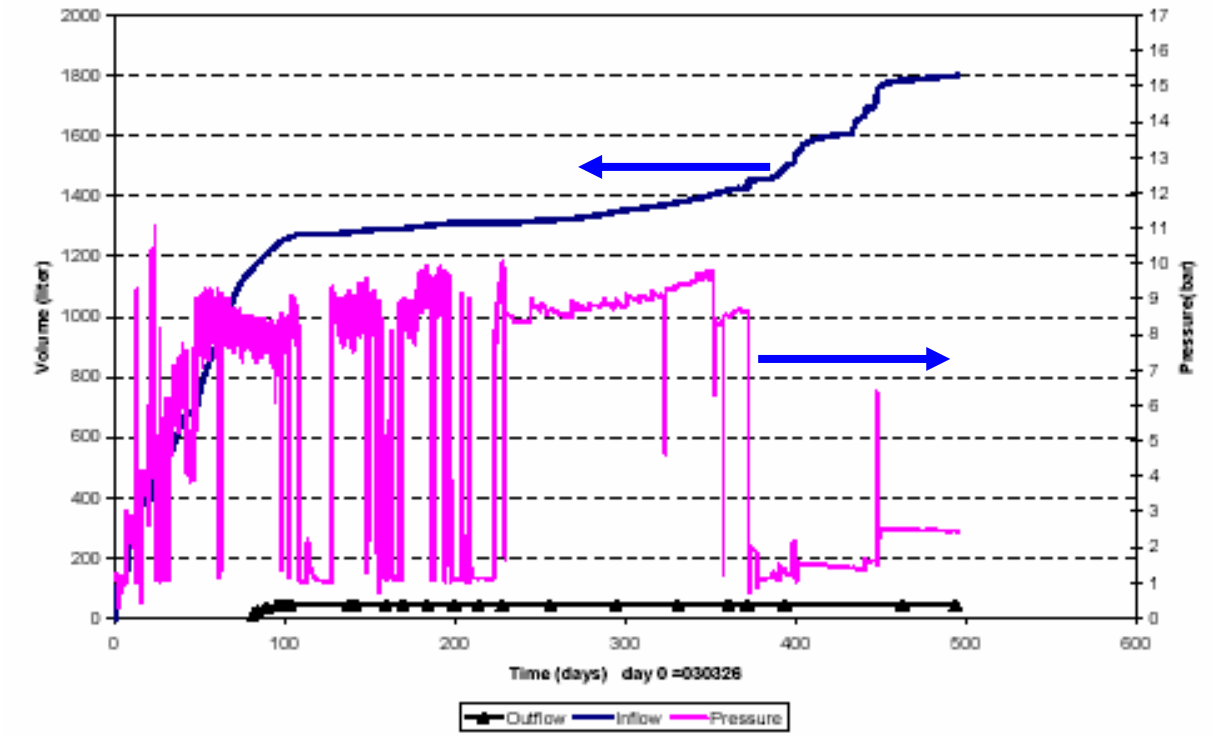

Figure 3. *Hydraulic boundary conditions in the test: Inflow & Outflow of water, and water pressure measured at the injecting pipes.*

For comparison purposes, a classical analysis assuming water pressure as boundary condition was also performed. Not all the cycles of water pressure were represented, but at least some of them were considered in the analysis. This simulation will be referred as "Case 2". An additional "Case 3" was considered later, mixing both boundary conditions along time, according to the field data available. This latter case will be presented in section 3.

Figure 4 presents the basic geometry considered in all cases. Boundaries were defined far enough to consider that they are not influenced by the experiment. For the thermal problem, a constant value of temperature was applied. For the mechanical problem, displacements were set to zero. The external boundaries were considered impervious in the hydraulic problem, although the low value of permeability assigned to the rock makes that material impervious in practice. Additionally, the gas equation was always taken into account, assuming that some nodes at the top of the sand filter were connected to the atmosphere at the beginning, in order to account for the effect of the open pipes. Details on the boundary and initial conditions will be indicated later. Only 500 days of experiment have been simulated for this comparison between Cases 1 & 2, focussing on the cycle of suction and stresses measured in Rings 9 and 10.

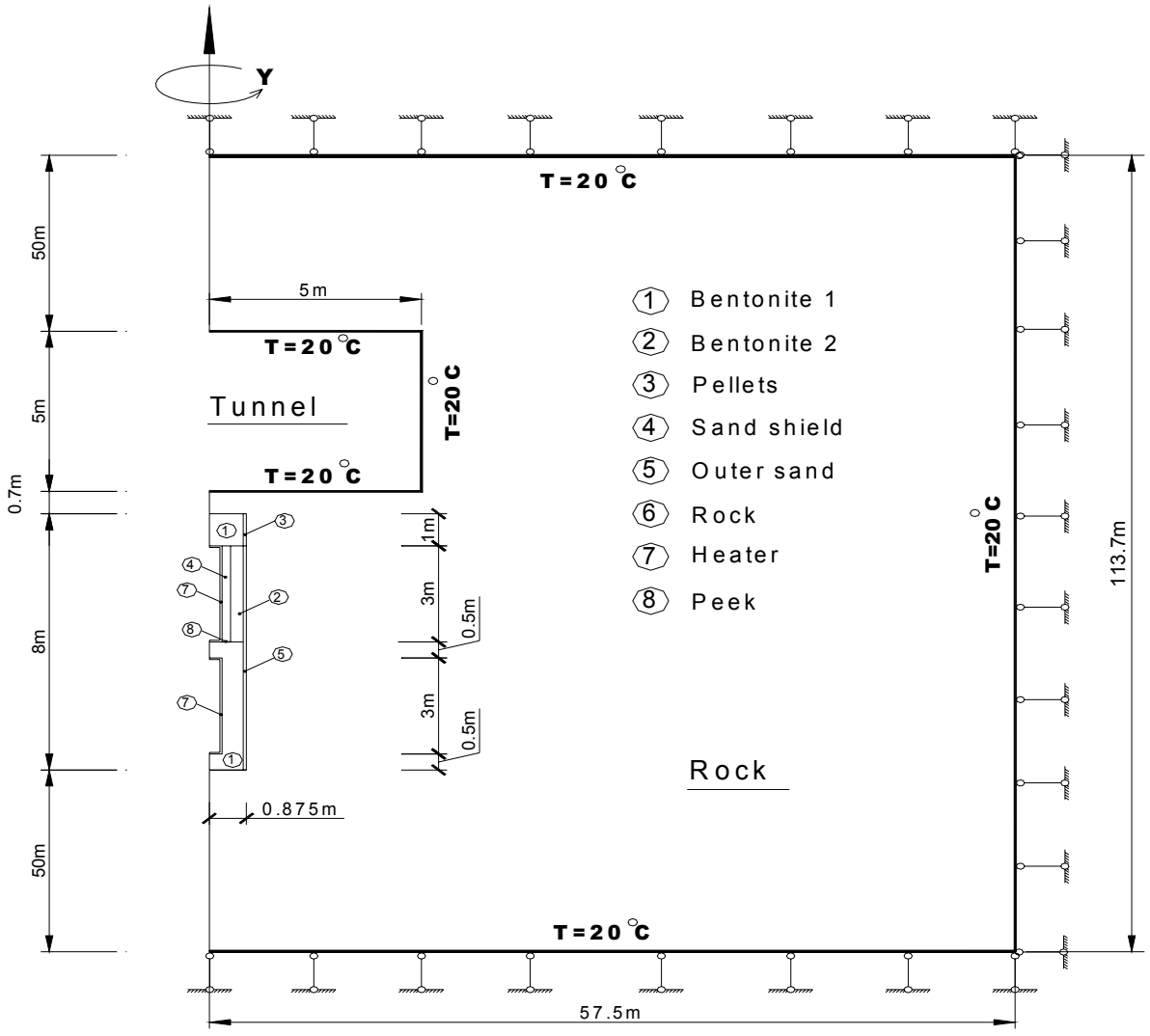

Figure 4. *Geometry considered in all analyses*

2.1 Analysis of Case 1

In this Case, the total inflow of water was used to compute a flux (volume of water/unit time), to be used as input data in the nodes of the bottom of the sand filter. Several trials were performed with the objective of simulating the cycles of suction and stresses indicated in figures 1 and 2. Initially, it was found that the best simulation was obtained when only 85% of the total flux was injected in the sand filter from day 0 till day 72nd. After that day, the total inflow was used to compute the flux in the bottom nodes of the sand filter. Figure 5 presents the curve of the volume of water measured (100%) and the corresponding curve computed in that manner. The outflow of water measured in the upper pipes of the sand filter is also indicated in that figure.

The reason for that value of 85% has not been clear for many weeks. In fact the model took already into account the gas escaped through the open pipes in the top of the sand filter. The model also included the rock although its permeability was very low. Therefore, there was not a clear reason of why we needed only 85% of the water injected to reproduce the measured suction cycles. Only recently it was found out the reason for that: we realized that the initial saturation degree of the sand filter in all those analyses was around 13%, whereas in the test it was probably very small. That was a consequence of specifying an initial suction instead of initial water content or saturation degree in that material. We have used the van Genuchten expression of the water retention curve to relate suction and water content, but that curve was estimated because it was not known for the sand.

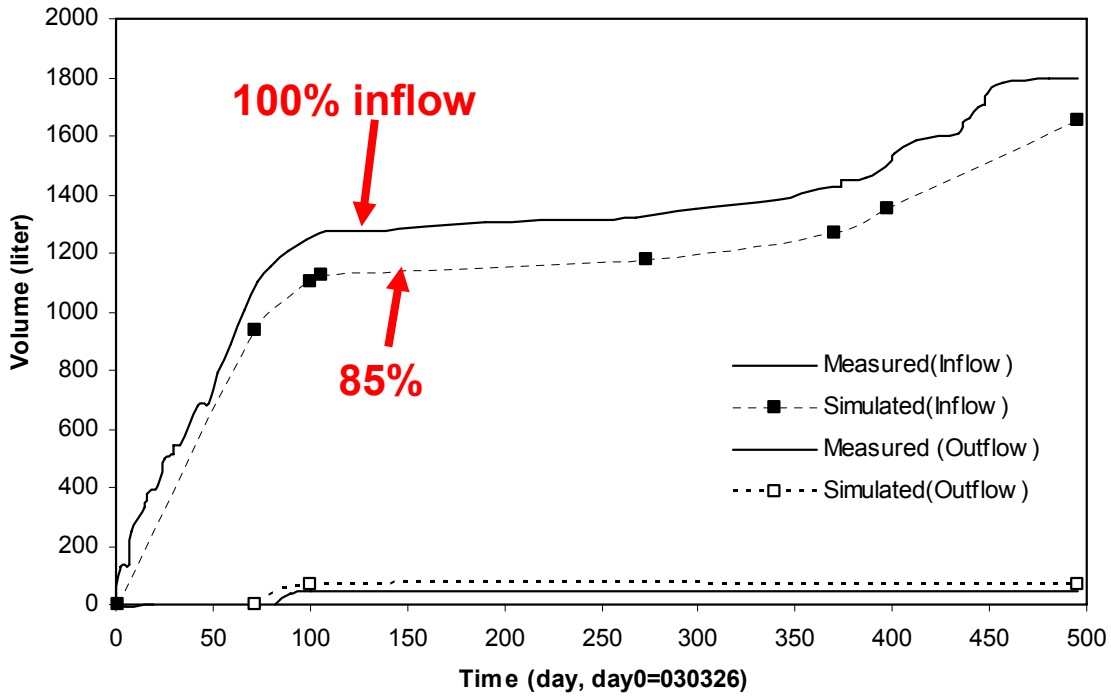

Figure 5. *Measured volume of inflow and outflow in the experiment (continuous lines). Dashed lines represent the values used in the simulation.*

On the other hand it is sometimes difficult, from a numerical point of view, to simulate a dry material, with almost zero degree of saturation. Indeed that condition would imply very high values of suction in the mathematical expression of the retention curve and convergence problems may arise.

In conclusion it can be stated that the cycles of suction and stresses in the bentonite are sensitive to the amount of water available in the system, and therefore, to the initial water content of the sand filter. The effect of that water in the sand filter is not very important from a conceptual point of view, but it explains why in the simulation we need less water to be injected in the experiment. Reducing the initial water content of the sand filter in the simulations (or increasing the initial suction, or changing the water retention curve parameters) would lead to additional numerical difficulties. Thus the example presented here has been computed using that 85% of volume of external water from day 0 till day 72nd. If a dry sand filter were used in the analysis, a 100% of total injected volume would be required in the computations.

Figure 6 shows the distribution of the saturation degree in the sand filter for different times. Rings 9 and 10 correspond to the middle zone of upper heater (z = 5.5 m). Note that saturation increases in those heights up to day 72nd. It is clear that after day 100th, all points in the sand filter de-saturate. It seems that there is a lack of water to continue with the saturation process, and the water taken by the bentonite is greater than the water supplied by the pipes. The fact that outflow of water measured in the experiment (figure 3) stopped close to day 100 would confirm this hypothesis as well.

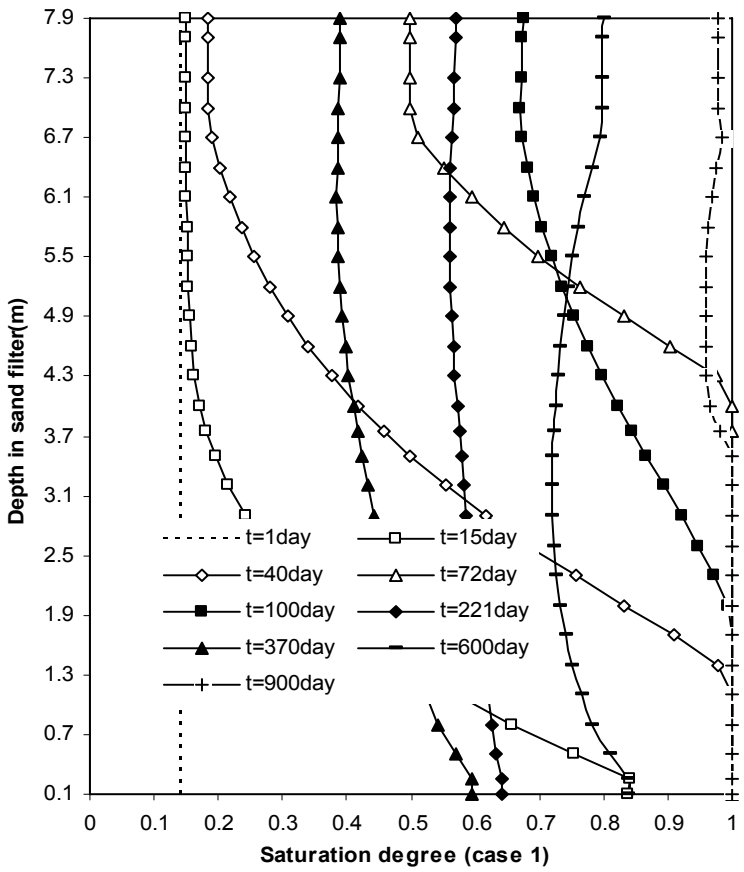

Figure 6. *Profiles of saturation degree in the sand filter for different times.*

Figure 7 presents the computed suction at two particular points of Ring 10, where the cycle has been observed. It must be pointed out that this cycle is obtained in a natural manner as a result of the computations. That is, the cycle is a consequence of the boundary condition applied, in terms of flux of water injected instead of water pressure applied. It becomes evident again that bentonite soaked more water than the supplied by the pipes. The agreement between measured and computed values is very good considering the complexity of the problem.

We have simulated this cycle in many analyses performed by using slightly different parameters. The size of the cycle is sensitive to the values of the parameters, but the cycle itself appears always to be generated by the flux boundary condition and not by a specific combination of the parameters.

Cycles of stresses are more difficult to simulate numerically, but the trend of that cyclic pattern is also obtained as it can be seen in figure 8.

Regarding the gas boundary condition, it was assumed that pipes at the top of the sand filter were open and they allowed the gas to escape. Top nodes of the sand filter had a fixed gas pressure of 0.1 MPa.

As a concluding remark of this case, it can be pointed out that this suction/stress cycle at rings 9 & 10 can be simulated by applying the measured record of volume of injected water in the sand filter as boundary condition. Details of the parameters corresponding to this case are presented in next section.

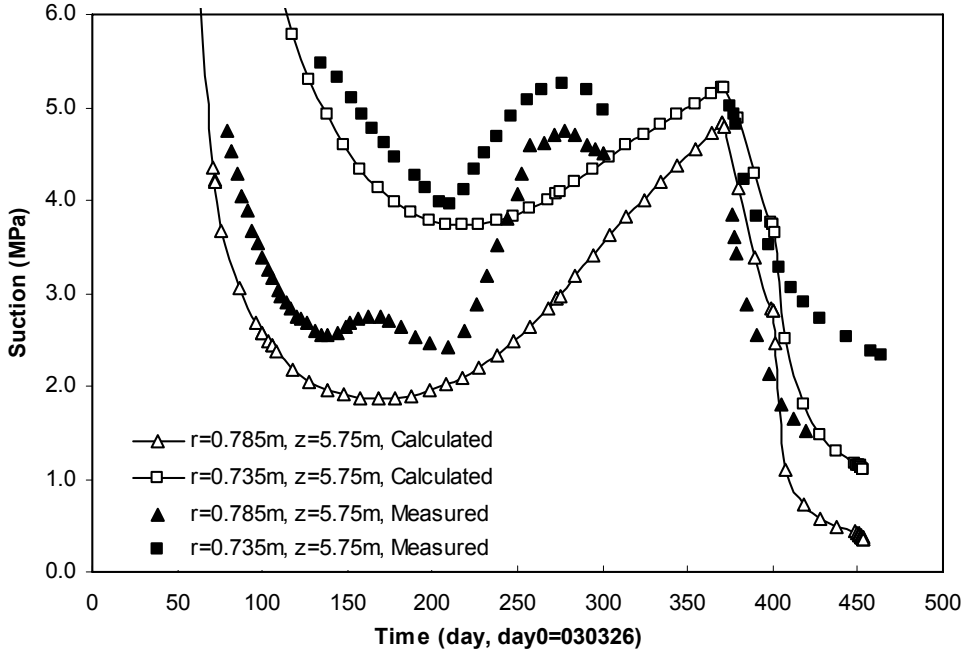

Figure 7. *Comparison between measured and computed suctions at ring 10*

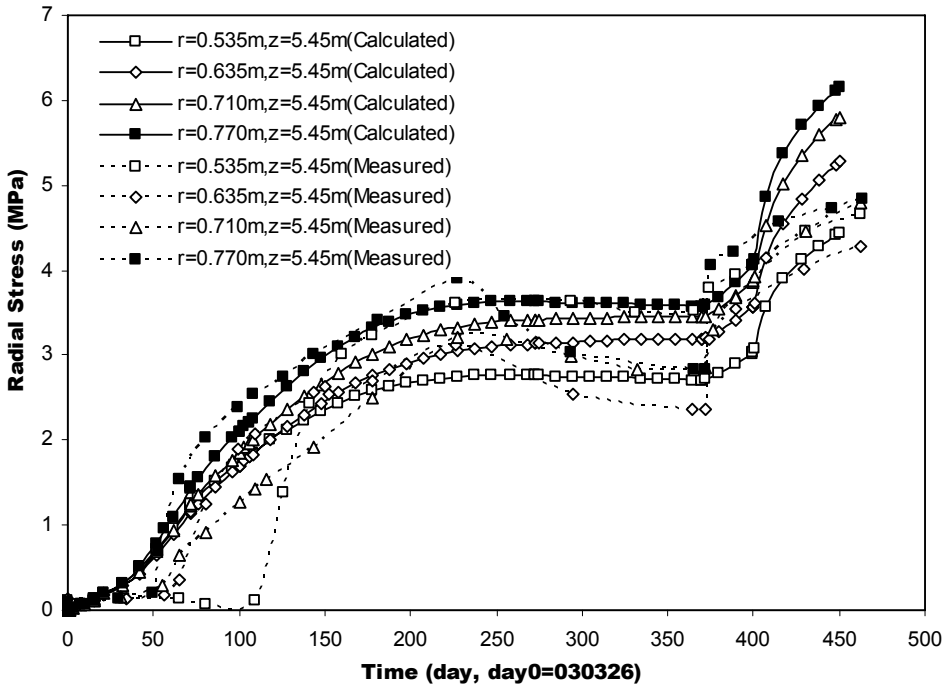

Figure 8. *Comparison between computed and measured radial stresses at ring 9*

2.2 Analysis of Case 2

In case 2, a water pressure boundary condition was applied at the bottom of the sand filter. Figure 9 shows the law of water pressure used, obtained from the measured values. Note that the actual measurements law (figure 3) exhibits many cycles and sudden changes that have not considered in the law presented in this figure. This is for the sake of simplicity. We were interested in conceptual aspects and general trends, rather than trying to reproduce exactly the same numerical values.

Figure 10 shows the evolution of suction along time at two different points of Ring 10. Measurements are also depicted on that figure. Note that cycles of water pressure on the boundary condition in sand filter generate also suction cycles in the zone of Ring 10. The amplitude of those suction cycles is smaller than the extension of the cycles applied at the boundary. That is, the system smoothes that effect from the boundary, but it appears that each cycle of the boundary condition may generate a cycle in the suction response. Due to the fact that measurements exhibit only one important cycle of suction, it could be concluded that this "case 2" does not represent the experiment properly.

According to the information available, water pressure measurements were performed outside the test, and Clay Technology has provided with some explanations for the anomalous behaviour of this pressure boundary condition (i.e., clogging of the pipes). However, even an obstruction of the pipes would difficult explaining all the cycles of water pressure measured.

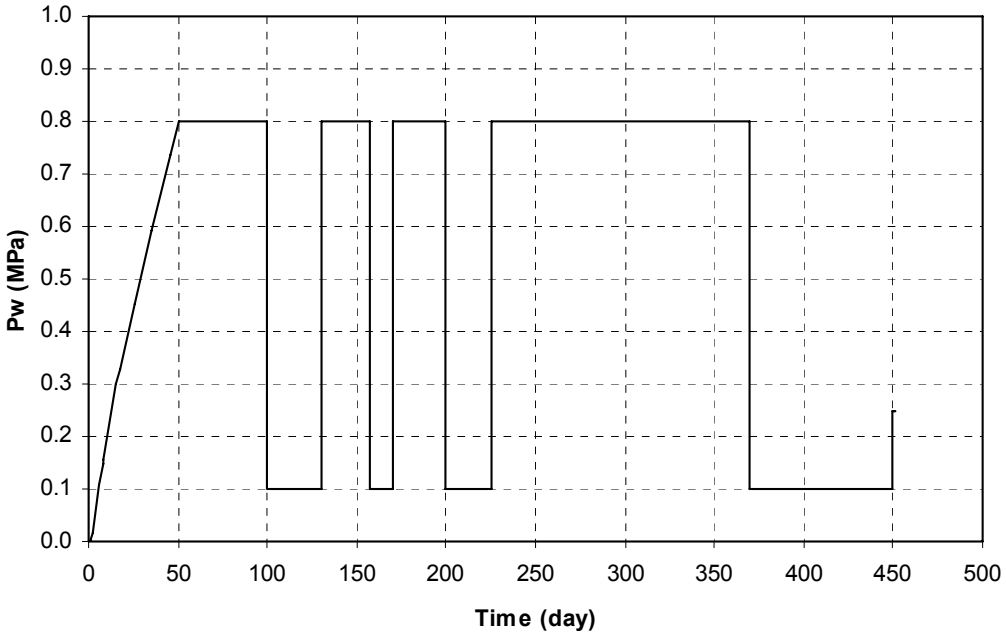

Figure 9. *Water pressure boundary condition in sand filter*

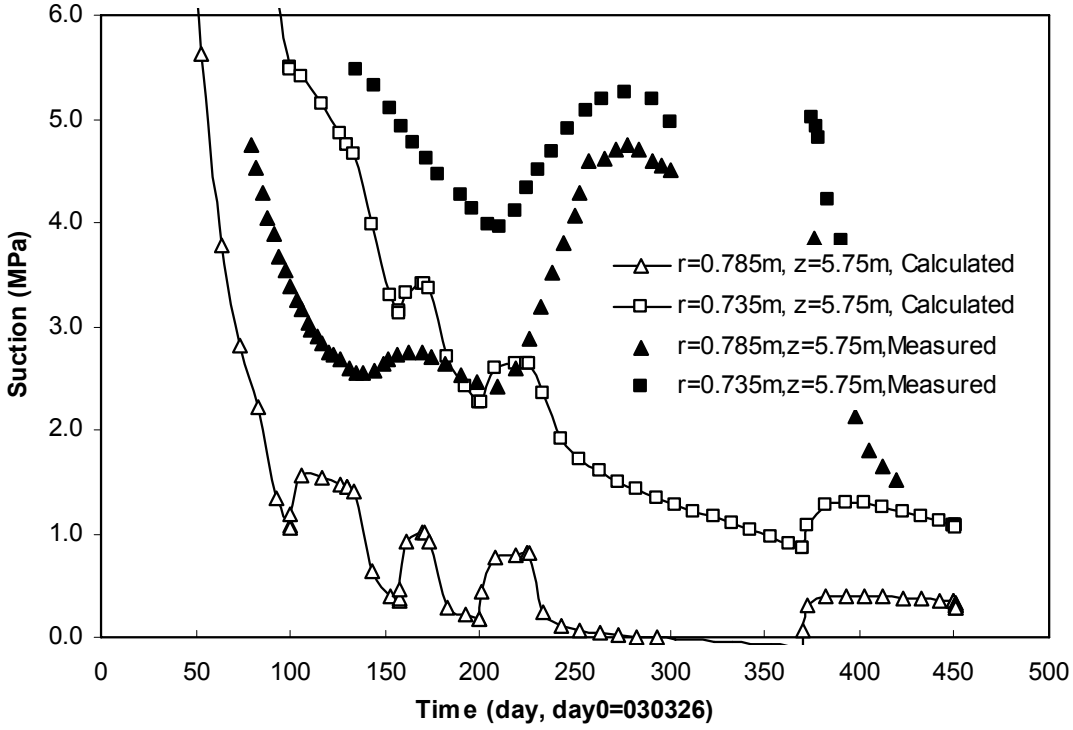

Figure 10. *Suction against time at ring 10. Comparison between measured and computed values.*

Finally, figure 11 shows the measured and computed radial stresses at some particular points of Ring 9. Note that simulations show to some extent the water pressure cycles applied to the boundary. A similar pattern has been found for the rest of the THM variables involved in the problem.

The analyses performed corresponding to this case suggest that those cycles in water pressure at the bottom pipes of the sand filter were not "transferred" to the rest of the geometry (or at least not all of them). Otherwise, most of the sensors in the bentonite would have shown a cyclic pattern as well. Perhaps the measurement is not reliable, or maybe there is another reason related to practical operational aspects. This is an important argument in favour of using Case 1 for the interpretation of the experiment during this period.

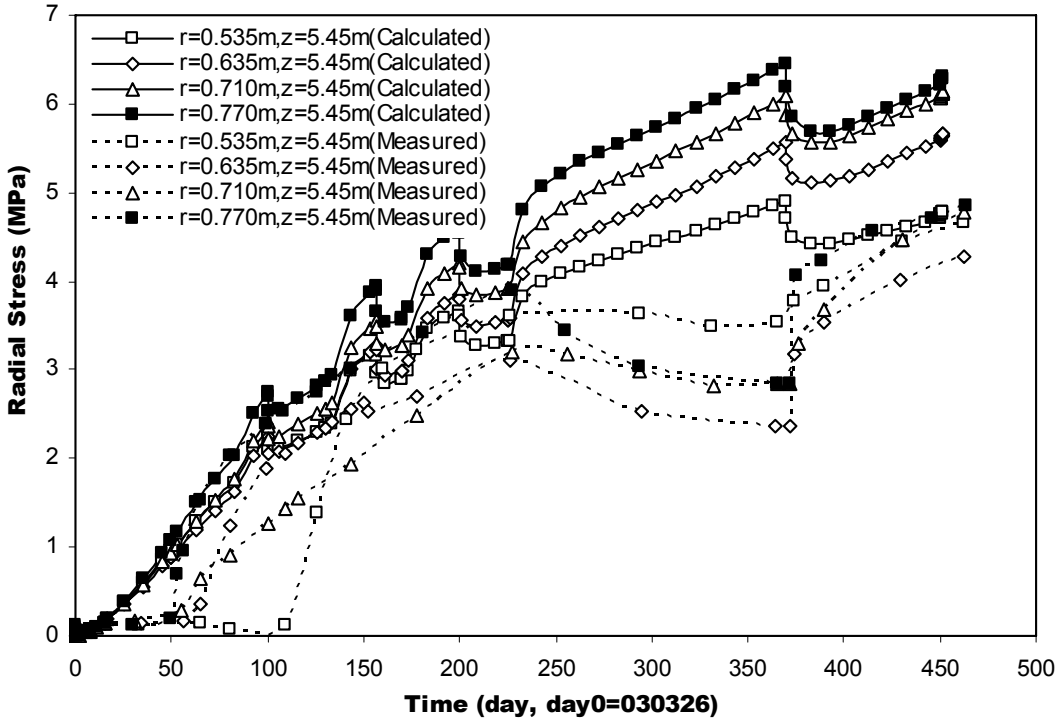

Figure 11. *Measured and computed radial stresses in Ring 9.*

2.3 Conclusions about the behaviour of Rings 9 & 10

Comparing results from Case 1 and Case 2 with actual measurements, it becomes evident that the behaviour of Rings 9 & 10 during this period of the experiment can be explained by a lack of water available in the sand filter (especially after day 100th). The scenario "b)" indicated above seems to be more realistic than the explanation "a)", based on the mechanical response of the system sand-bentonite-sand.

Despite that evidence, it should be pointed out that there is little experience in this combined system including different materials in the context of THM problems. Indeed in most of the "in situ" or mock up experiments the bentonite is confined between a heater and the rock. Stresses usually develop due to swelling of the bentonite, in a quite homogeneous manner, and final state should be mainly isotropic. In TBT, however, deviatoric stresses have been developed according to the measurements available.

From the records of stresses in different directions in Ring 9, it is possible to obtain the stress path followed by some points during the experiment. Figure 12 presents those paths, where it becomes evident that deviatoric stresses develop at the beginning of the experiment. The final trend is a decrease in shear, which may indicate eventually a development of isotropic confinement.

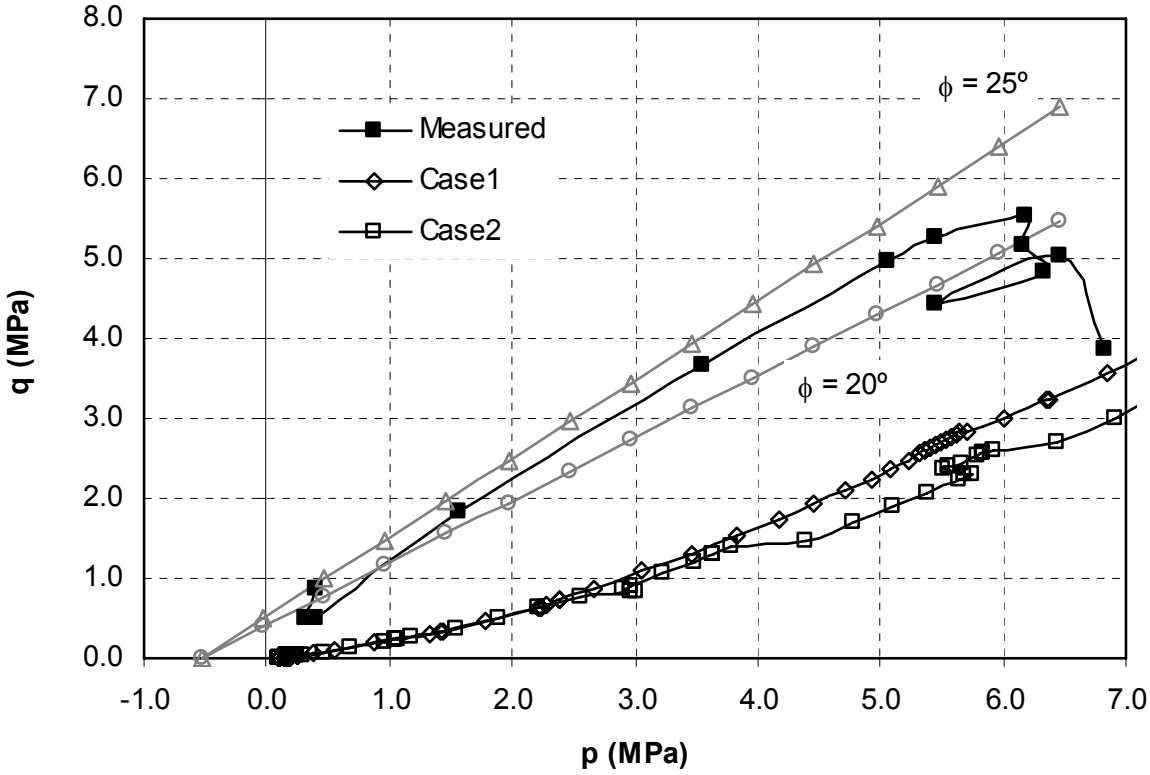

Figure 12. *Total stress paths obtained from measurements and computations (Cases 1 &2). Straight lines correspond to the estimated Mohr-Coulomb envelopes for friction angles of 20º and 25º. Ring 9, r=0.635 m. Mean stress: "p", Deviatoric stress: "q".*

The increase and decrease of deviatoric stresses in the bentonite could be, nevertheless, a typical trend in other experiments if the presence of gaps is taken into account. The stress state at the beginning of the bentonite swelling may be anisotropic because of those gaps in one direction whereas in other directions the confinement is effective. In the TBT experiment at Ring 9, vertical stresses exhibit a high value due to the confinement of other Rings, whereas radial stresses are initially small due to the low confinement provided by the sand shield and sand filter. That may explain the behaviour shown in figure 12.

The deviatoric computed stresses are always below the measured values. A possible explanation to that would be that mechanical parameters are quite uncertain. This is mainly due to the limited laboratory experiments available regarding the mechanical behaviour of MX-80 bentonite and the sand. Also it should be pointed out that stresses are difficult to measure with accuracy, especially for low values. Altogether suggests waiting for the end of the experiment in order to obtain definite conclusions regarding stress behaviour.

As a partial conclusion of this section, it can be stated that the cycle of suction and stress measured in the bentonite surrounding the upper heater was mainly due to a lack of water available for saturating the bentonite. Therefore the reason for that behaviour was mainly hydraulic. An explanation in mechanical terms seems less feasible, although the unexpected high deviatoric stresses may play a certain role which should be investigated when dismantling the experiment.

3 Prediction of main variables

According to the guidelines proposed by Clay Technology, a prediction of the main THM variables of the test has been attempted as well. In the previous section it was shown that case 1 was appropriate for simulating the experiment, at least for the initial period. However, nowadays all pipes are supplying water to the system at the same pressure, and the boundary condition seems to be controlled. Therefore, predictions of future behaviour should be performed by using the applied water pressure boundary condition. It follows from this explanation that an ideal simulation would have to include both boundary conditions, i.e. from day 1st to 400th, a flux of water should be applied at the bottom part of the sand filter, keeping the top pipes open (allowing gas to escape); whereas after day 400th, a water pressure boundary condition should be considered at all pipes.

The problem with that strategy is the difficulty in numerical analysis of changing boundary conditions suddenly. Indeed we have found many convergence problems when changing from one boundary condition to another at day 400th, and finally it was not possible to obtain a reasonable simulation with those characteristics before December 2004. However, between December 2004 and March 2005 there was a success when simulating that change in the boundary conditions. Finally it was possible to smooth the effect of the sudden change of conditions, and convergence of the computation was achieved. This new case will be referred as "Case 3", with mixed boundary conditions, and it is presented in this extended version of the report, in section 3.4.

Convergence problems in THM problems occur quite often due to the complexity of the analyses, and therefore this is not an extraordinary case. In addition to that, the history of the hydraulic boundary condition of TBT has been quite complex and unexpected. Despite that, quite often there are some numerical alternatives that allow obtaining approximate solutions of reasonable quality. In this case, we decided to compute several cases, following the framework used in previous section. First, a "Case 1" with a flux boundary condition and a "Case 2" with water pressure boundary condition were considered. Both cases presented in previous section were continued up to day 900, as required in the guidelines. Some parameters were slightly changed in order to improve the convergence, but we did not have important problems after day 370th, as boundary condition was maintained.

For Case 1, after day 500, a forecast of the flux was used to continue the analysis. In fact, the slope of the curve Volume – Time after day 500th was assumed constant and introduced as input data in the computations. This case is the best for reproducing the suction/stress cycle at Rings 9 & 10, but as a consequence of that assumption, the amount of water entering the system will be probably overestimated for long times (i.e. 900 days).

Case 2, however, applies a water boundary condition after day 370th, as it is actually performed in the experiment. This case is not good when looking at the cycle of suction/stresses of Rings 9 & 10, but it may be a good prediction case for long times (i.e. after 900 days).

Finally, a Case 3, combining both boundary conditions is presented as well. In this analysis, a special attention has been devoted to the external variables that may influence the experiment. From the information available, it was decided to impose a flux boundary condition up to day 456.5, and then, to change to a pore water pressure boundary condition after that date. Some parameters were changed slightly, with respect to previous cases, in order to improve the convergence conditions of the iterative procedures involved in the calculations. This case, developed after the initial deadline of December 2004, has some advantages with respect to the previous ones, as it shows a reasonable agreement between measurements and computed results not only for the short term, but also for longer times.

In the following sections all cases are presented and predictions of the required variables are included, as requested in the guidelines from Clay Technology.

3.1 Case 1: Parameters and initial conditions

The following tables present the parameters, initial conditions and basic assumptions considered in the simulation of the prediction phase of Case 1.

Thermal Problem

Thermal conductivity $\lambda(W/mK)$

Material	Law	λ_{dry}	λ_{sat}
Bentonite 1	$\lambda = \lambda_{sat}^{S_l} \cdot \lambda_{dry}^{1-S_l}$	0.3	1.3
Bentonite 2		0.3	1.3
Rock		2.6	2.6
Pellets		0.1	1.0
Sand shield		0.6	1.7
Outer sand		0.6	1.7
Steel		50.16	50.16
Peek		0.25	0.25

Specific Heat $c(J/kgK)$

Material	Bentonite 1 & 2	Rock	Pellets	Sand shield	Outer sand	Steel	Peek
$c(J/kgK)$	1091	800	1091	900	900	460	1091

Hydraulic Problem

Retention Curve

Material	Law (Van Genuchten)	P_0 (MPa)	β	S_m (MPa)	m
Bentonite 1	$S_e = \frac{S_l - S_{rl}}{S_{ls} - S_{rl}} = \left[1 + \left(\frac{P_g - P_l}{P_0}\right)^{\frac{1}{1-\beta}}\right]^{-\beta} \left(1 - \frac{P_g - P_l}{S_m}\right)^m$	60	0.3	800	1.1
Bentonite 2		60	0.3	800	1.1
Outer/Inner Sand		0.2/0.1	0.25/0.3	800	1.1
Pellets	$S_e = \frac{S_l - S_{rl}}{S_{ls} - S_{rl}} = \left[1 + \left(\frac{P_g - P_l}{P_0}\right)^{\frac{1}{1-\beta}}\right]^{-\beta}$	0.2	0.4		
Rock		100	0.56		
Heater		10^{-5}	0.45		
Peek					

Intrinsic Permeability $k(m^2)$

Material	Law (Kozeny's Model)	$k_0\,(m^2)$	ϕ_0
Bentonite 1	$k_i = k_0 \frac{\phi^3}{(1-\phi)^2} \frac{(1-\phi_0)^2}{\phi_0^3}$	0.32×10^{-20}	0.389
Bentonite 2		0.32×10^{-20}	0.368
Pellets		2.0×10^{-19}	0.5684
Inner sand		1×10^{-15}	0.30
Outer sand		2×10^{-15}	0.36
Rock		10^{-30}	0.003
Heater		10^{-30}	0.001
Peek		10^{-30}	0.001

Liquid Relative Permeability: $k_{rl} = S_e^3$

Gas permeability:

Material	Law (Kozeny's Model)	A
Bentonite 1	$k_g = \frac{\rho g}{\mu_g} \times A \times k_i \times (1 - S_r)^n$	0.2181×10^9
Bentonite 2		0.2274×10^9
Pellets		1
Inner sand		1
Outer sand		10^{-29}
Rock		1
Heater		1
Peek		1

Mechanical Problem

Thermal Elasticity

Material	Law (Linear Elasticity)	$b_s\left(^{\circ}C^{-1}\right)$
Bentonita 1 & 2	$\Delta\varepsilon_v = 3b_s\Delta T$	1.0×10^{-5}
Rock		7.8×10^{-6}
Outer sand		10^{-5}
Inner sand		10^{-5}
Pellets		10^{-5}
Steel		10^{-5}
Peek		10^{-5}

Stress-strain Mechanical Model

Material	Model	Parameters
Bentonite 1 & 2	Barcelona Basic Model (BBM)	$\kappa_{i0} = 0.207, \kappa_{s0} = 0.1563,$ $K_{\min} = 13.33MPa, \nu = 0.2,$ $\lambda(0) = 0.621, r = 0.75, \beta = 0.05,$ $p^c = 0.1MPa, p_0^* = 9.542MPa$ $M = 0.78, \alpha = 0.395, k = 0.1$
Rock	Linear Elasticity	$E = 5.0 \times 10^4 MPa, \nu = 0.25$
Steel		$E = 2.1 \times 10^5 MPa, \nu = 0.2$
Outer sand		$E = 24.93MPa, \nu = 0.25$
Inner sand		$E = 55.37MPa, \nu = 0.25$
Pellets		$E = 20MPa, \nu = 0.25$
Peek		$E = 20MPa, \nu = 0.25$

Boundary conditions

(1) Temperature boundary condition:
Outer boundary of rock: $T = 20^{\circ}C$
Tunnel boundary: $T = 20^{\circ}C$

(2) Heat flux(Day 0=26/03/03):
Two heaters: 0~8 days, 900W; 8~15 days, 1200W; 15~1000days, 1500W.

(3) Pore water and gas pressure in rock:
$P_w = P_g = 0.1MPa$

(4) Gas and liquid boundary conditions
Before 370th day, at $z = 6.75m$, $P_g = 0.1MPa$; after 370th, the system is closed for gas.

Case 1: liquid boundary condition

Time interval (day)	0~1th	1~72th $J_l(kg/s)$	72~100th $J_l(kg/s)$	100~105.6th $J_l(kg/s)$	105.6~273th $J_l(kg/s)$	273~370th $J_l(kg/s)$
B. C. sand filter at Z=0.25m	0	0.8966×10^{-4} $\times 85\%$	0.2098×10^{-4}	0.2377×10^{-4}	0.1763×10^{-5}	0.5668×10^{-5}

Time interval (day)	370~400th $J_l(kg/s)$	400~450th $J_l(kg/s)$	450~500th $J_l(kg/s)$	500~1000th $P_w(MPa)$
B. C. sand filter at Z=0.25m	0.2834×10^{-5}	0.2834×10^{-5}	0.2310×10^{-5}	0.2310×10^{-5}
B. C. sand filter at Z=6.75m	0.1607×10^{-4}	0.2228×10^{-4}	0.2310×10^{-5}	0.2310×10^{-5}

(5) Mechanical boundary conditions
(See Figure 4)

Initial conditions

Materials	Temperature $(^{\circ}C)$	Pore water pressure (MPa)	Porosity	Saturation degree
Bentonite 1	20	-47.5	0.389	0.798
Bentonite 2		-47.5	0.368	0.798
Sand shield		-62.5	0.300	0.0579
Outer sand		-62.5	0.360	0.135
Rock		0.1	0.003	1.0
Pellets		-2.03	0.568	0.211
Heater		0.1	0.001	0.0
Peek		0.1	0.001	0.0

Basic Assumptions

1. Liquid pressures in rock, heater and peak are fixed, and their permeability is set to be very low, so there is no liquid exchange with them.

2. Gas pressure in rock is fixed and the gas permeability of rock is also set to be very low, so there is no gas exchange with rock.

3. Gas pressure in sand filter is fixed (this is not realistic, but is used to solve convergence problem; due to its limited volume this assumption may be practically accepted).

4. In order to simulate the upper pipe which is open to air before 370th day, and is used to inject water after 370th day, gas pressure of the contact line between sand filter and bentonite is fixed before 370th day, and it is under no control after 370th day. Although only points of the upper pipe are open to air, the gas permeability of the sand filter is very high, so it is acceptable assuming all the contact line between bentonite and sand filter is open to air.

5. In this analysis, applied water inflow from lower pipe between 1st and 72nd days is multiplied by 0.85 (which is 165 liter less than measured) in order to include the effect of initial saturation degree 13.5% (104 liter) used in the simulations.

6. After 500th day, the applied total water flux is assumed to be the same as the value between 450th~500th day.

7. After the 370th day, only the total measured water flux from both pipes is known, and the percentage from upper and lower, respectively, is assumed (see Figure 13).

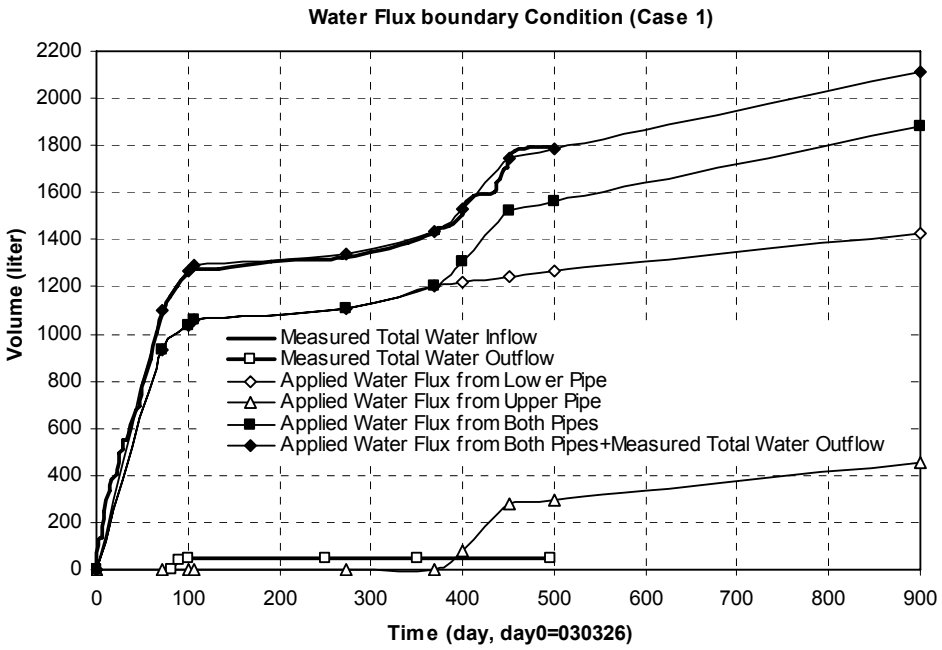

Figure 13. *Water flux used as boundary condition*

3.2 Case 1: Predictions

The required predictions follow:

Scan-line A1-A4 (z=5.5 m)

- Figure 14: Temperature
- Figure 15: Saturation degree
- Figure 16: Relative Humidity
- Figure 17: Porosity
- Figure 18: Radial stress
- Figure 19: Radial displacement

Scan-line C0-C4 (z=7.30 m)

- Figure 20: Temperature
- Figure 21: Saturation degree
- Figure 22: Relative Humidity
- Figure 23: Porosity
- Figure 24: Radial stress
- Figure 25: Radial displacement

Scan-line D0-D4 (z=3.75 m)

- Figure 26: Temperature
- Figure 27: Saturation degree
- Figure 28: Relative Humidity
- Figure 29: Porosity
- Figure 30: Radial stress
- Figure 31: Radial displacement

Scan-line E0-E4 (z=0.25 m)

- Figure 32: Temperature
- Figure 33: Saturation degree
- Figure 34: Relative Humidity
- Figure 35: Porosity
- Figure 36: Radial stress
- Figure 37: Radial displacement

Vertical scan-lines

- Figure 38: Scan-line 1 (r=0.305 m). Temperature
- Figure 39: Scan-line 2 (r=0.535 m). Temperature
- Figure 40: Scan-line 4. (r=0.875 m).Temperature

Other required predictions

- Figure 41: Anchor force
- Figure 42: Suction cycle Ring 10
- Figure 43: Radial stresses. Ring 9
- Figure 44: Axial stresses. Ring 9
- Figure 45: Tangential stresses. Ring 9

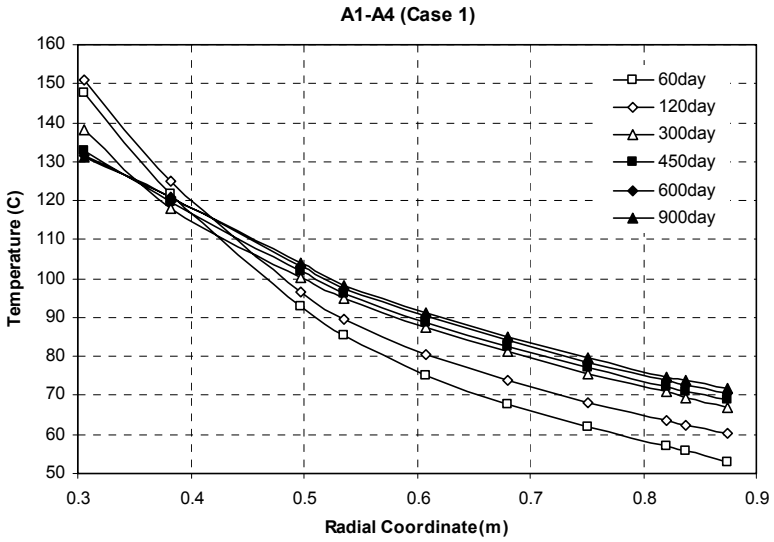

Figure 14

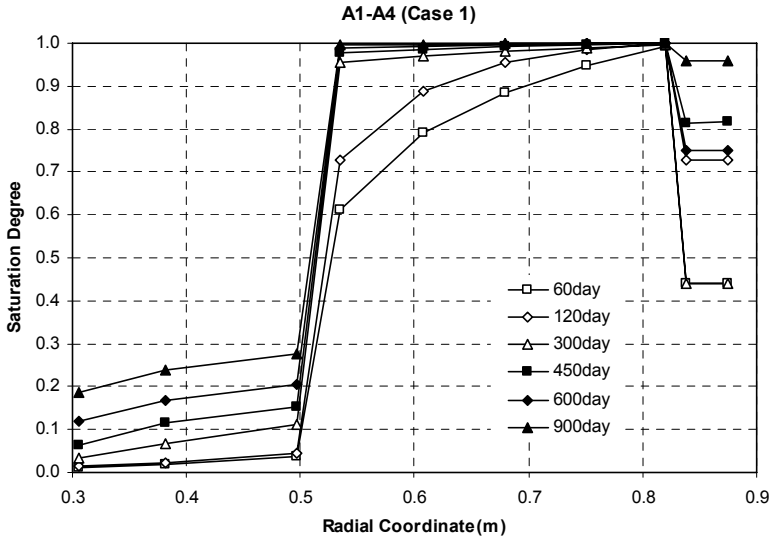

Figure 15

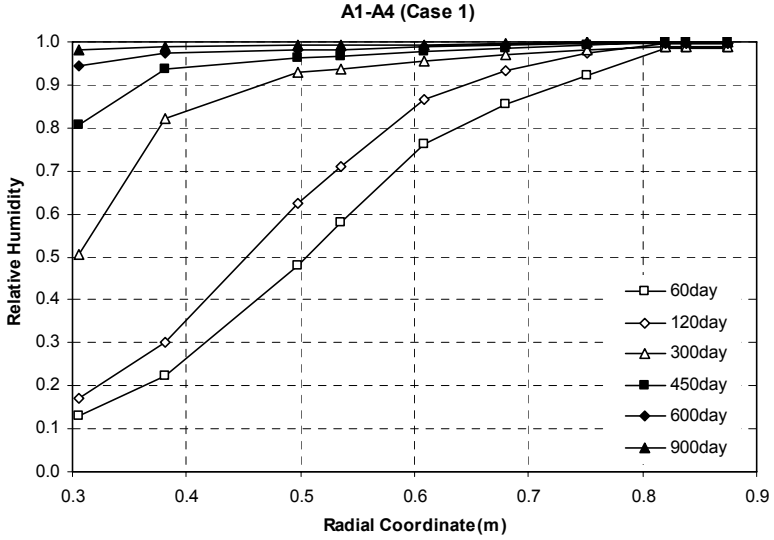

Figure 16

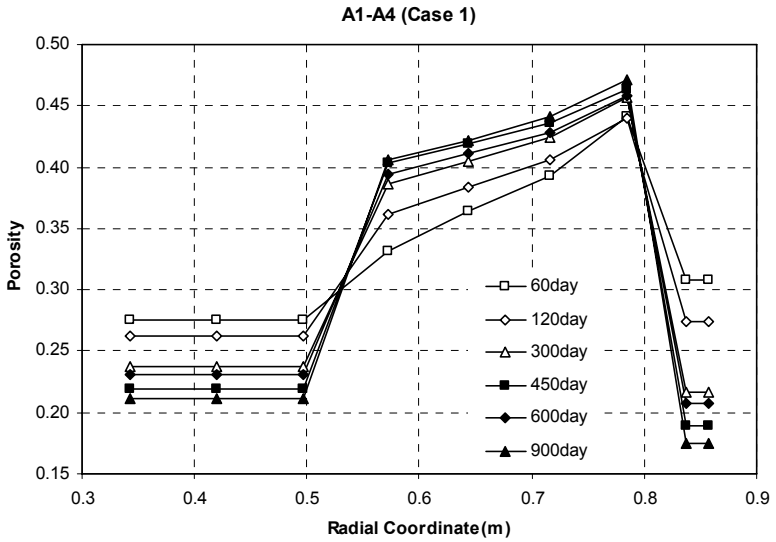

Figure 17

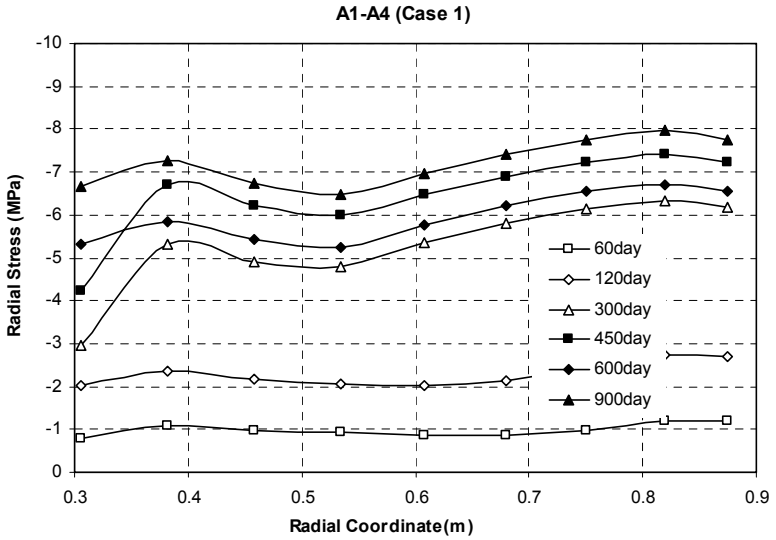

Figure 18

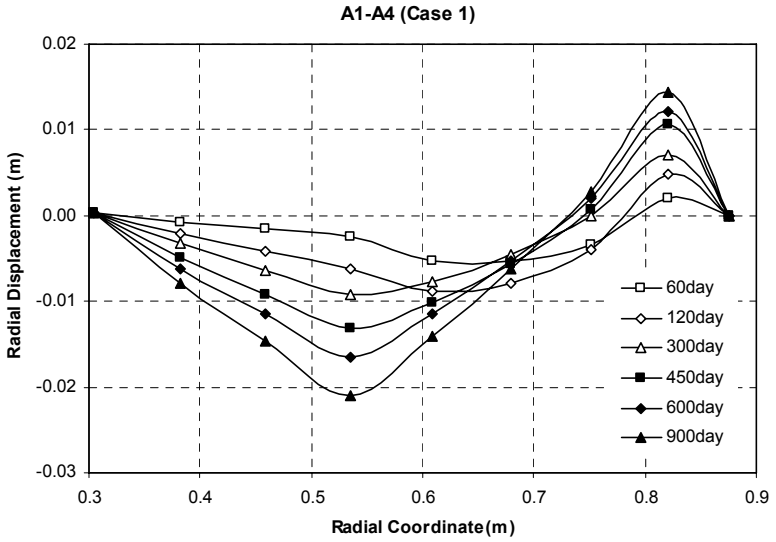

Figure 19

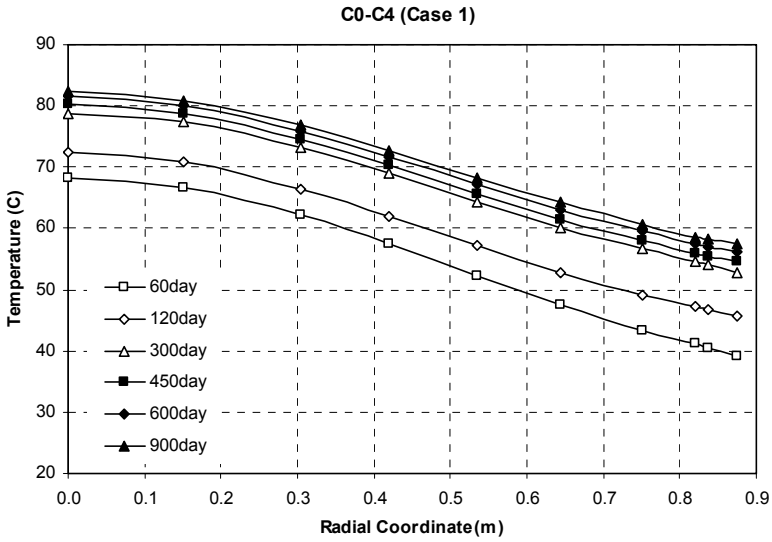

Figure 20

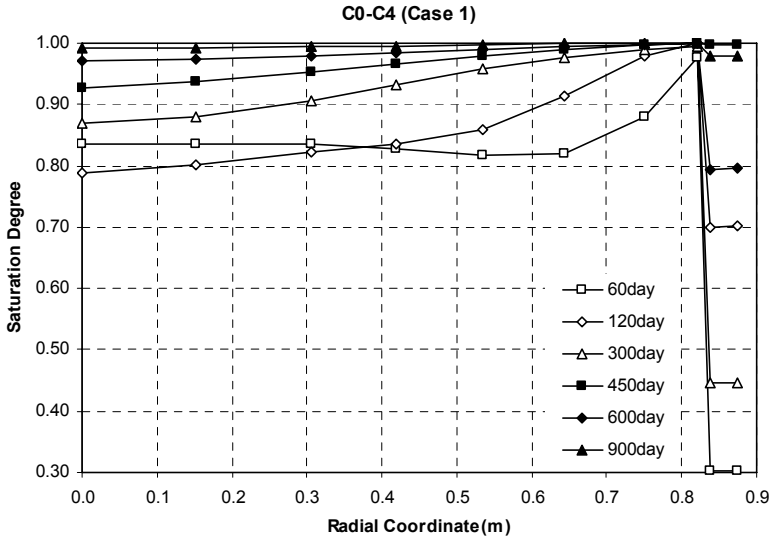

Figure 21

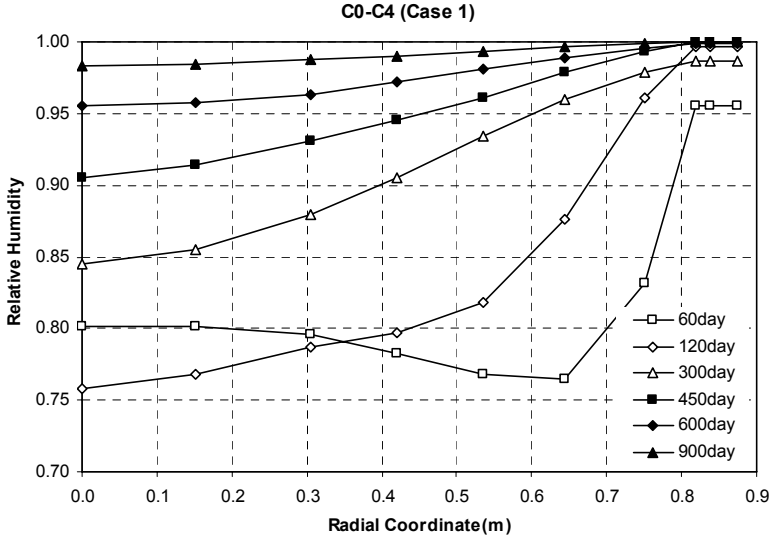

Figure 22

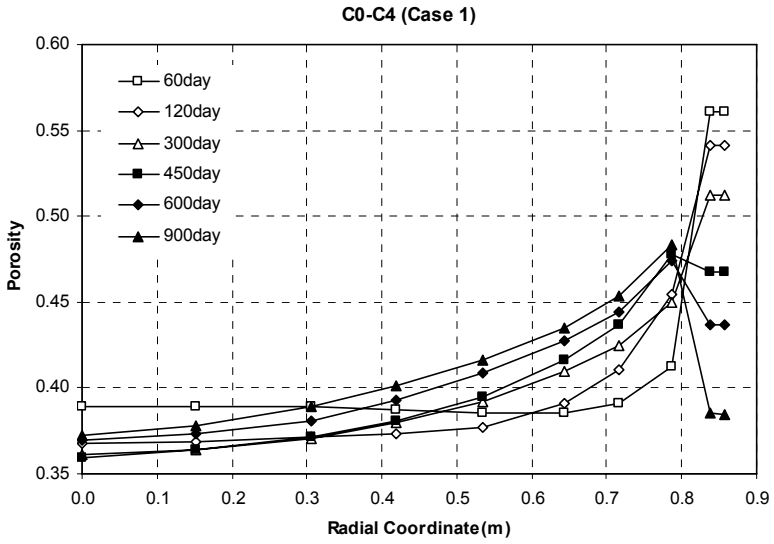

Figure 23

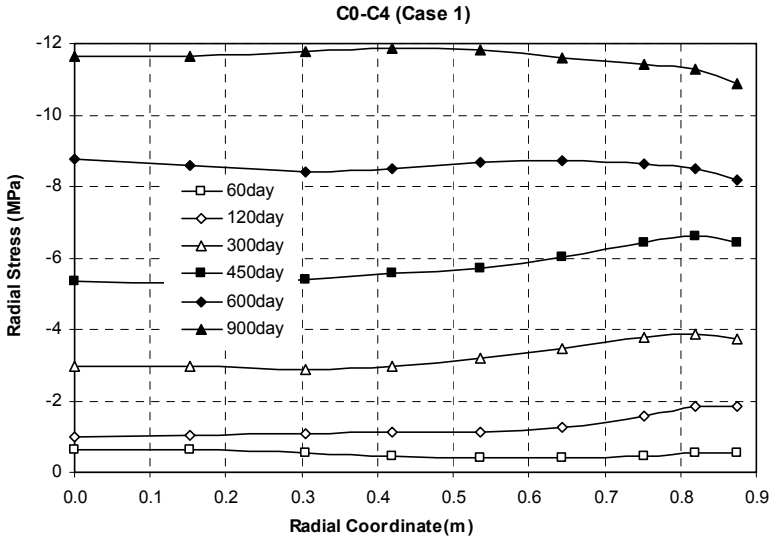

Figure 24

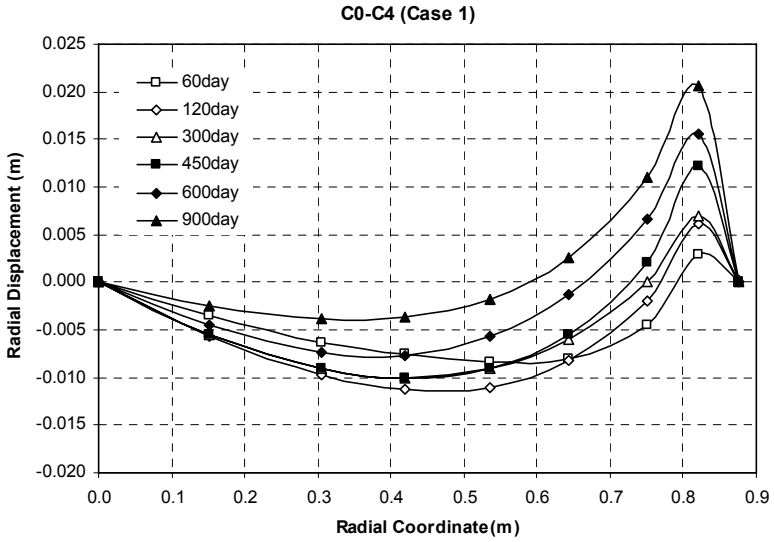

Figure 25

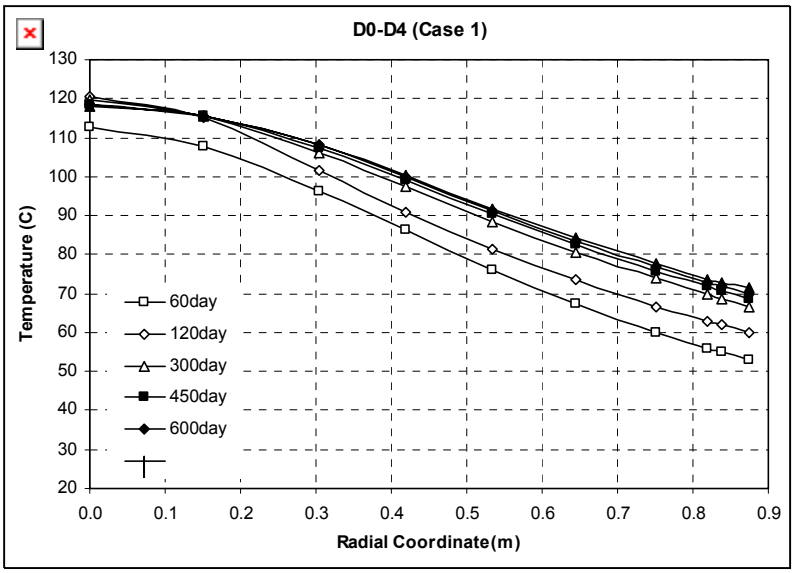

Figure 26

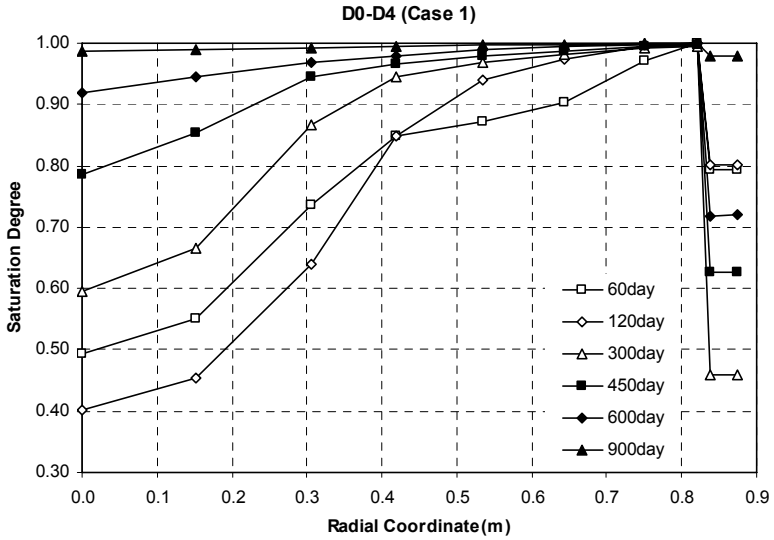

Figure 27

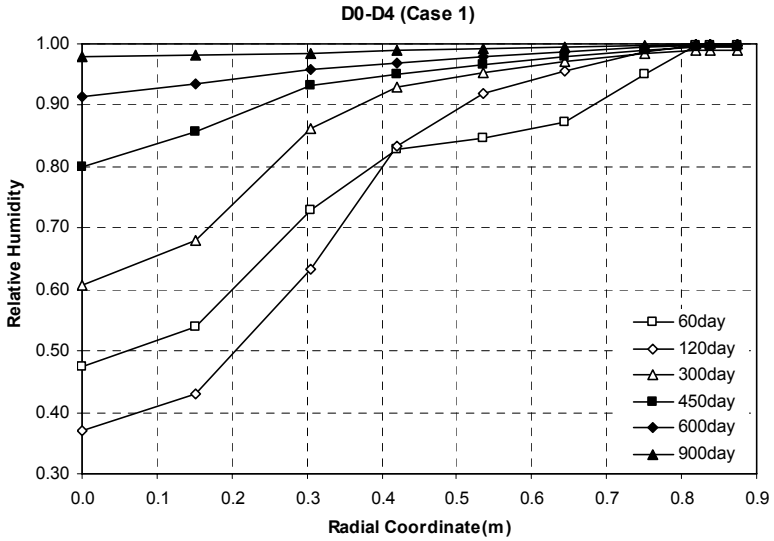

Figure 28

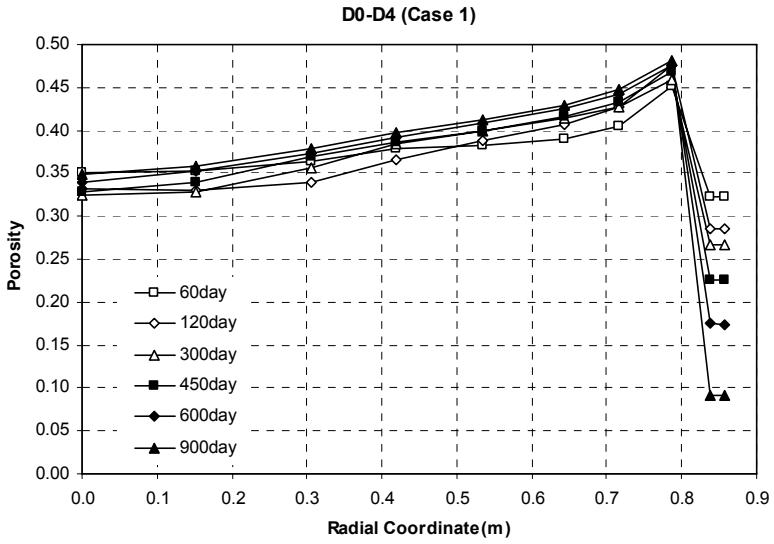

Figure 29

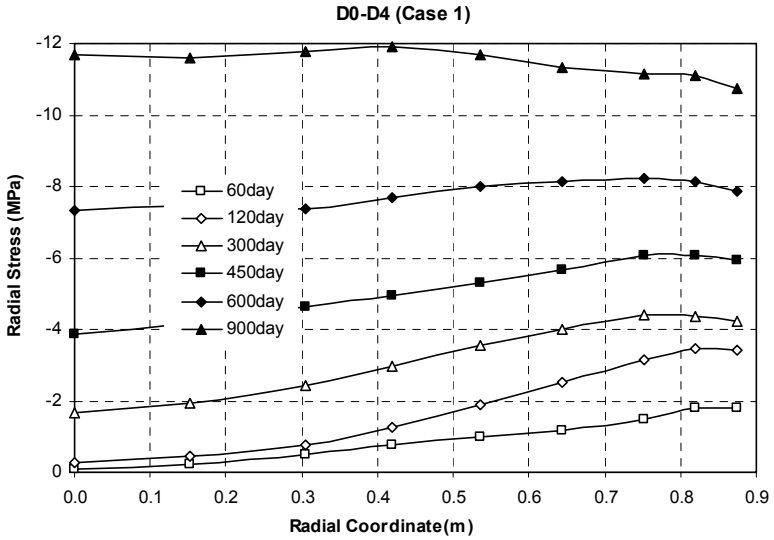

Figure 30

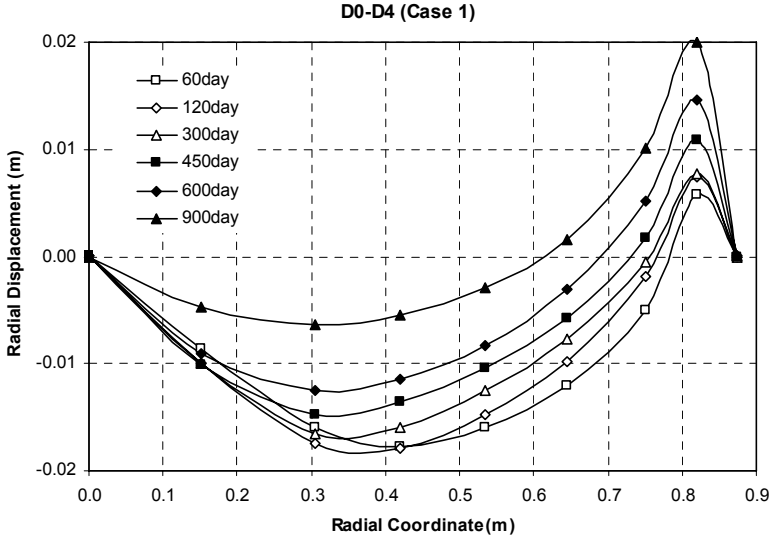

Figure 31

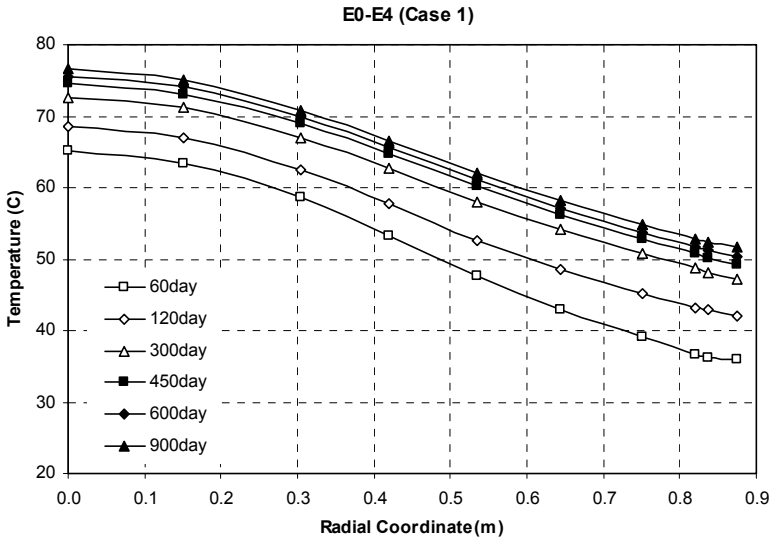

Figure 32

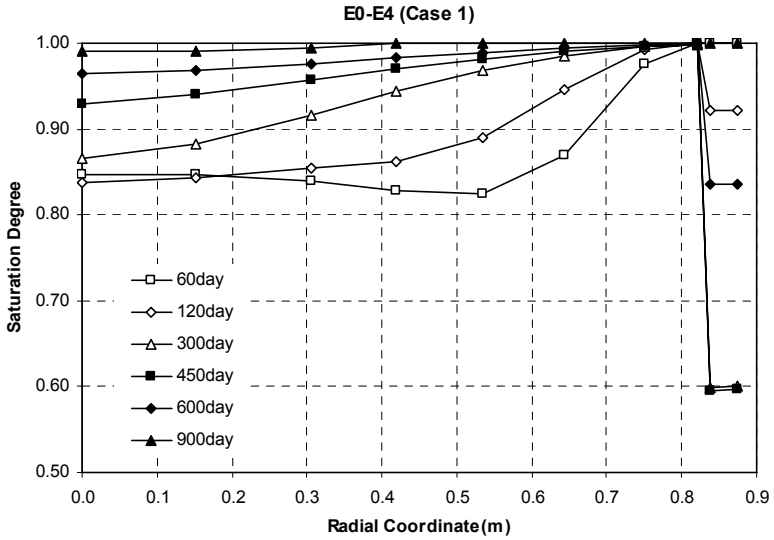

Figure 33

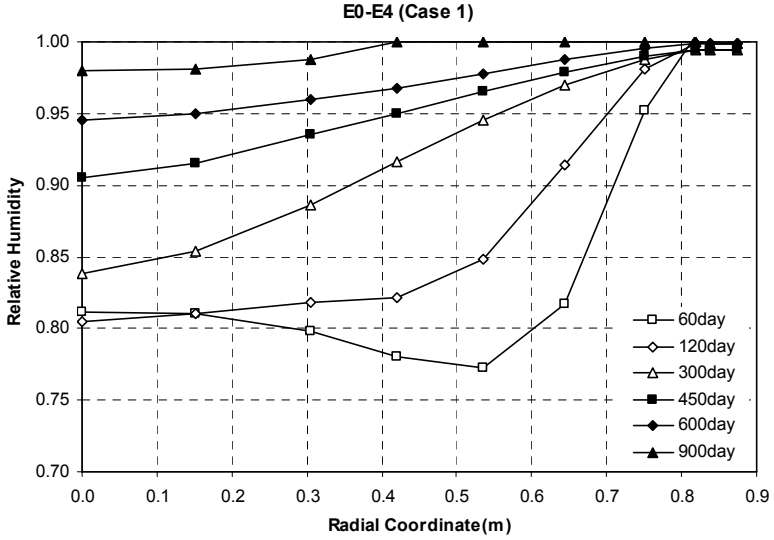

Figure 34

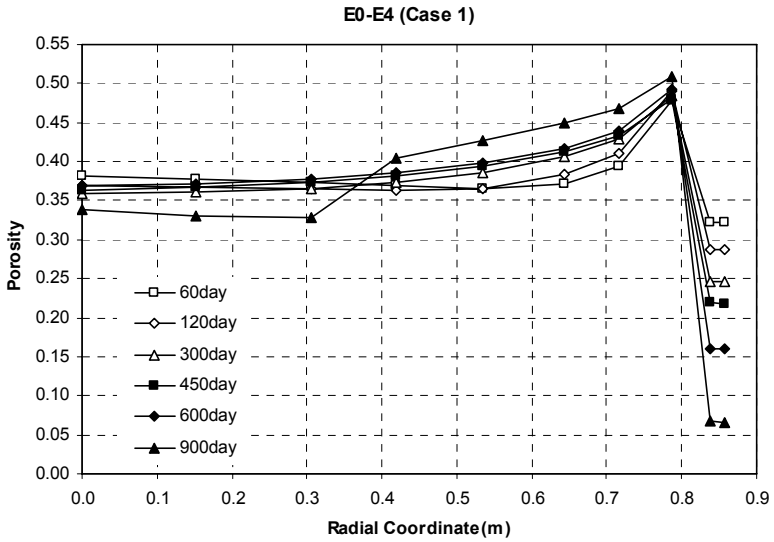

Figure 35

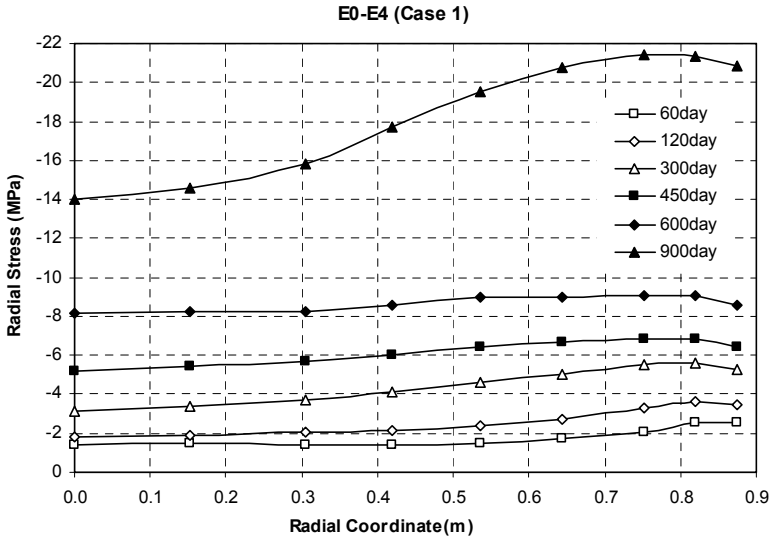

Figure 36

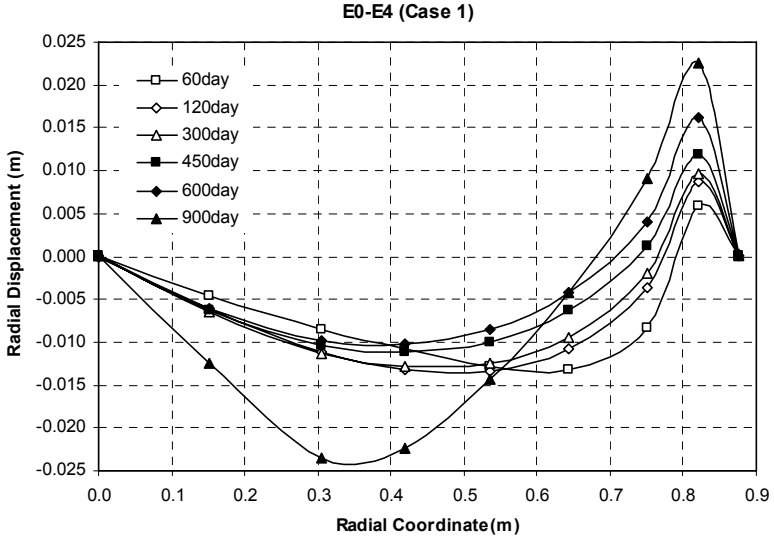

Figure 37

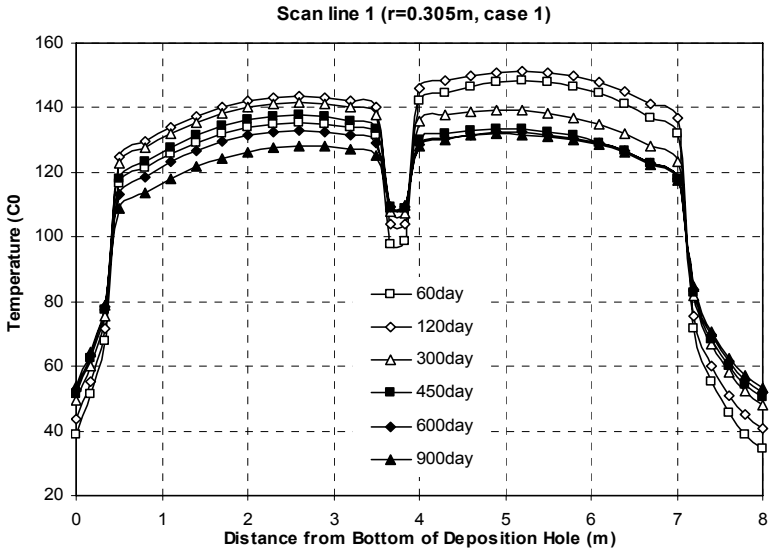

Figure 38

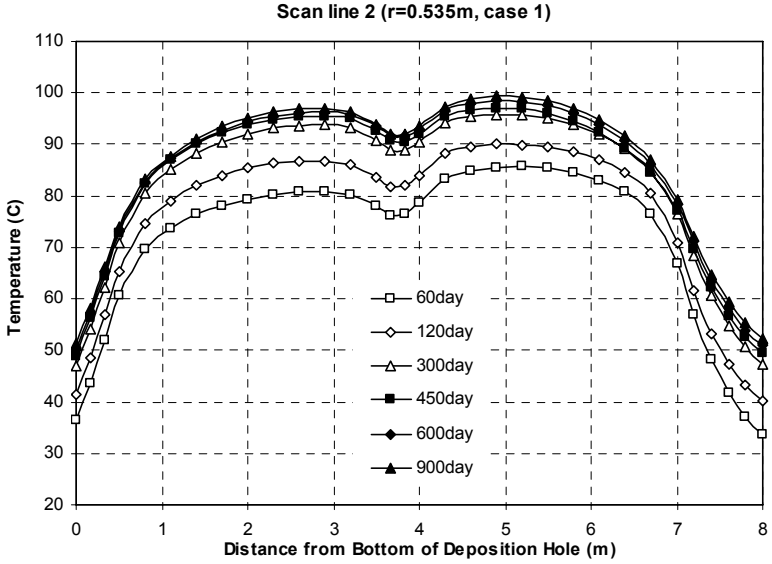

Figure 39

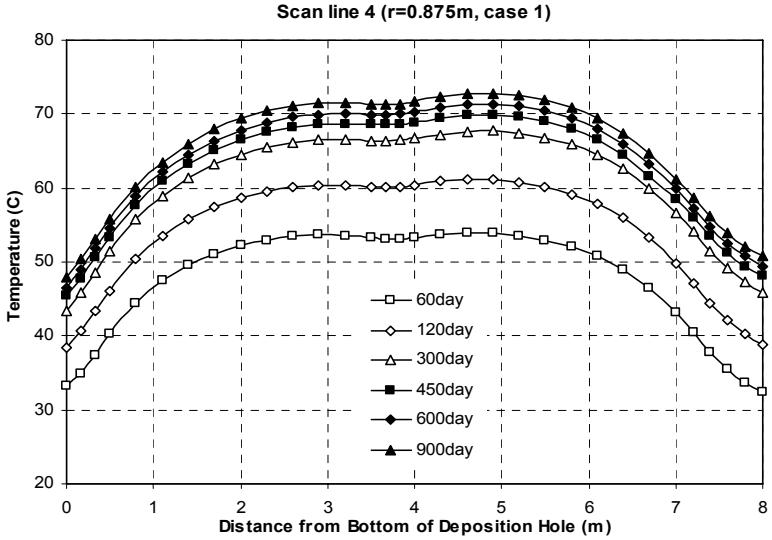

Figure 40

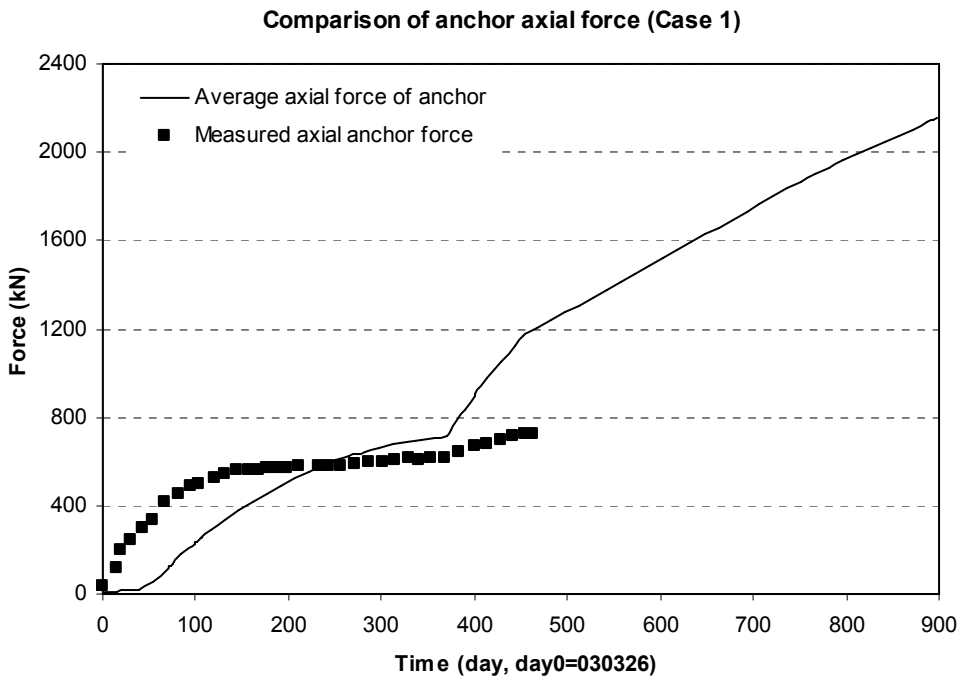

Figure 41

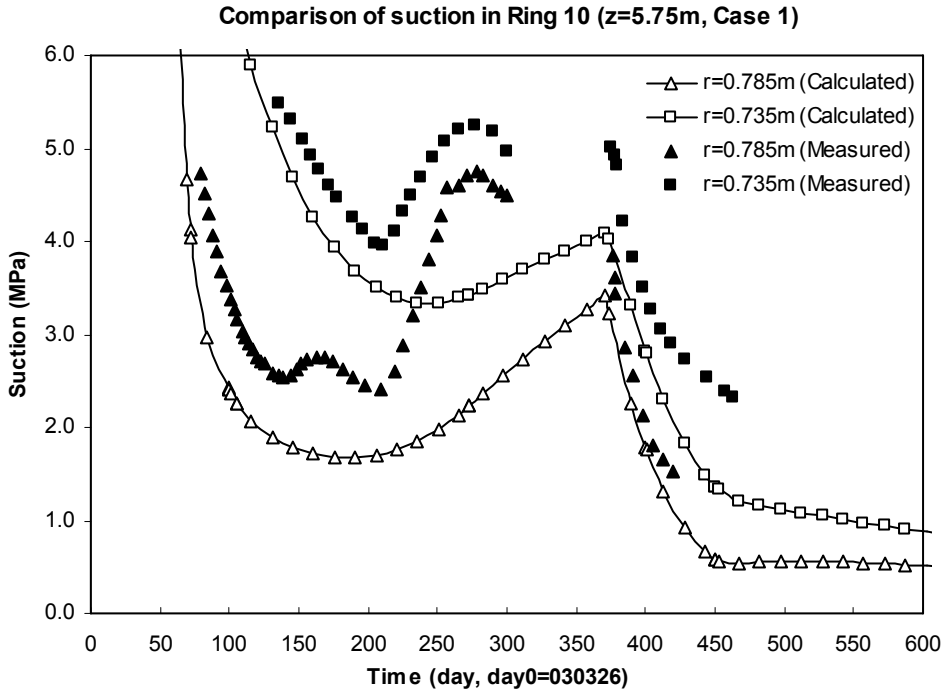

Figure 42

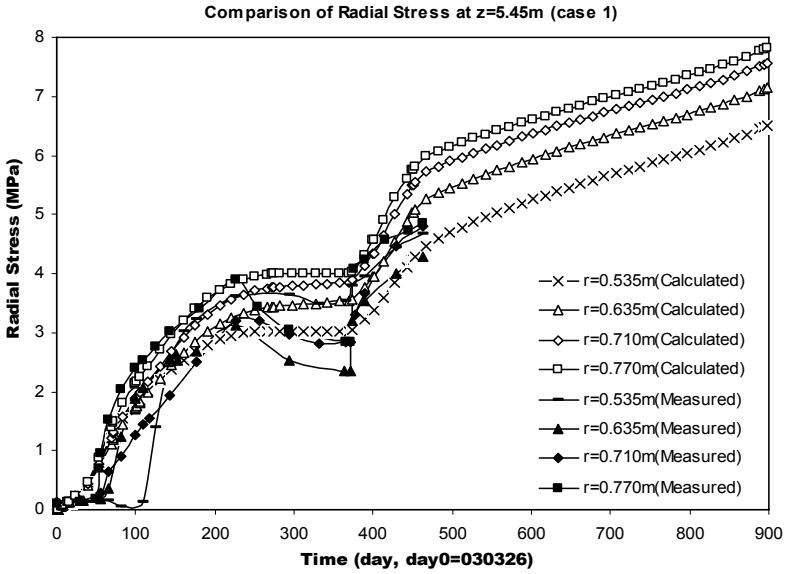

Figure 43

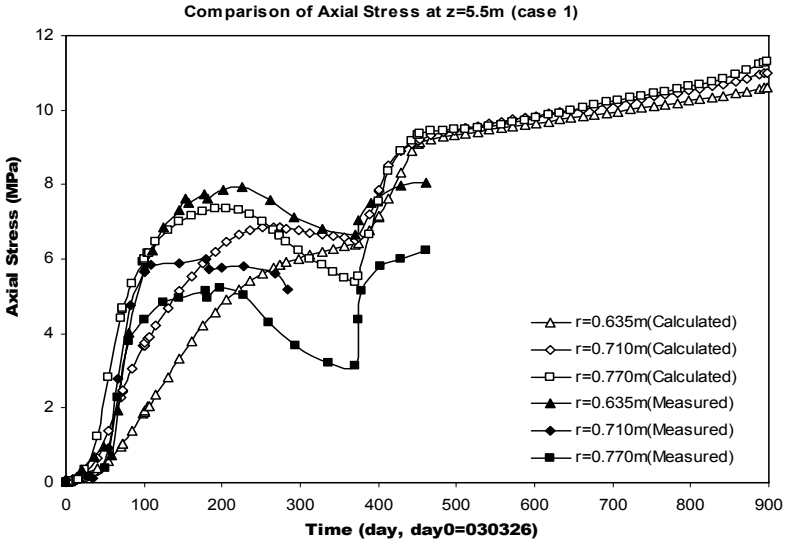

Figure 44

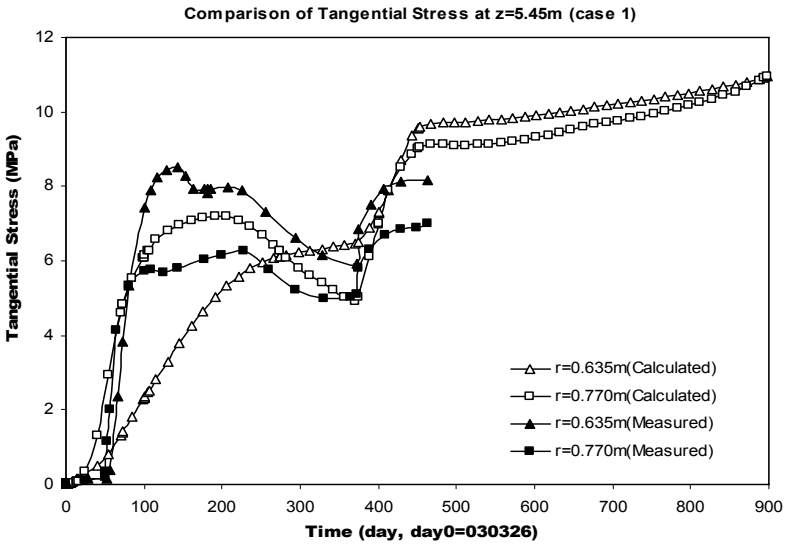

Figure 45

3.3 Case 2: Parameters and initial conditions

The following tables present the parameters, initial conditions and basic assumptions considered in the simulation of the prediction phase of Case 2.

Thermal Problem

Thermal conductivity $\lambda(W/mK)$

Material	Law	λ_{dry}	λ_{sat}
Bentonite 1	$\lambda = \lambda_{sat}^{S_l} \cdot \lambda_{dry}^{1-S_l}$	0.3	1.3
Bentonite 2		0.3	1.3
Rock		2.6	2.6
Pellets		0.1	1.0
Sand shield		0.6	1.7
Outer sand		0.6	1.7
Steel		50.16	50.16
Peek		0.25	0.25

Specific Heat $c(J/kgK)$

Material	Bentonite 1 & 2	Rock	Pellets	Sand shield	Outer sand	Steel	Peek
$c(J/kgK)$	1091	800	1091	900	900	460	1091

Hydraulic Problem

Retention Curve

Material	Law (Van Genuchten)	P_0 (MPa)	β	S_m (MPa)	m
Bentonite 1	$S_e = \frac{S_l - S_{rl}}{S_{ls} - S_{rl}} = \left[1 + \left(\frac{P_g - P_l}{P_0}\right)^{\frac{1}{1-\beta}}\right]^{-\beta} \left(1 - \frac{P_g - P_l}{S_m}\right)^m$	60	0.3	800	1.1
Bentonite 2		60	0.3	800	1.1
Outer/Inner Sand		0.2/0.1	0.25/0.3	800	1.1
Pellets	$S_e = \frac{S_l - S_{rl}}{S_{ls} - S_{rl}} = \left[1 + \left(\frac{P_g - P_l}{P_0}\right)^{\frac{1}{1-\beta}}\right]^{-\beta}$	0.2	0.4		
Rock		100	0.56		
Heater		10^{-5}	0.45		
Peek					

Intrinsic Permeability $k(m^2)$

Material	Law (Kozeny's Model)	$k_0\,(m^2)$	ϕ_0
Bentonite 1	$k_i = k_0 \frac{\phi^3}{(1-\phi)^2} \frac{(1-\phi_0)^2}{\phi_0^3}$	0.32×10^{-20}	0.389
Bentonite 2		0.32×10^{-20}	0.368
Pellets		2.0×10^{-19}	0.5684
Inner sand		2×10^{-15}	0.30
Outer sand		2×10^{-15}	0.36
Rock		10^{-30}	0.003
Heater		10^{-30}	0.001
Peek		10^{-30}	0.001

Liquid Relative Permeability: $k_{rl} = S_e^3$

Gas permeability:

Material	Law (Kozeny's Model)	A
Bentonite 1	$k_g = \frac{\rho g}{\mu_g} \times A \times k_i \times (1 - S_r)^n$	0.2181×10^9
Bentonite 2		0.2274×10^9
Pellets		1
Inner sand		1
Outer sand		10^{-29}
Rock		1
Heater		1
Peek		1

Mechanical Problem

Thermal Elasticity

Material	Law (Linear Elasticity)	$b_s\left(^\circ C^{-1}\right)$
Bentonita 1 & 2	$\Delta\varepsilon_v = 3b_s\Delta T$	1.0×10^{-5}
Rock		7.8×10^{-6}
Outer sand		10^{-5}
Inner sand		10^{-5}
Pellets		10^{-5}
Steel		10^{-5}
Peek		10^{-5}

Stress-strain Mechanical Model

Material	Model	Parameters
Bentonite 1 & 2	Barcelona Basic Model (BBM)	$\kappa_{i0} = 0.207, \kappa_{s0} = 0.1563,$ $K_{\min} = 13.33MPa, \nu = 0.2,$ $\lambda(0) = 0.621, r = 0.75, \beta = 0.05,$ $p^c = 0.1MPa, p_0^* = 9.542MPa$ $M = 0.78, \alpha = 0.395, k = 0.1$
Rock	Linear Elasticity	$E = 5.0 \times 10^4\, MPa, \nu = 0.25$
Steel		$E = 2.1 \times 10^5\, MPa, \nu = 0.2$
Outer sand		$E = 24.93MPa, \nu = 0.25$
Inner sand		$E = 55.37MPa, \nu = 0.25$
Pellets		$E = 20MPa, \nu = 0.25$
Peek		$E = 20MPa, \nu = 0.25$

Boundary conditions

(1) Temperature boundary condition:
Outer boundary of rock: $T = 20^{\circ}C$
Tunnel boundary: $T = 20^{\circ}C$

(2) Heat flux(Day 0=26/03/03):
Two heaters: 0~8 days, 900W; 8~15 days, 1200W; 15~1000days, 1500W.

(3) Pore water and gas pressure in rock:
$P_w = P_g = 0.1MPa$

(4) Gas and liquid boundary conditions
Before 370th day, at $z = 6.75m$, $P_g = 0.1MPa$; after 370th, the system is closed for gas.

Case 2: liquid boundary condition

Time interval (day)	0~1th	1~50th $P_w(MPa)$	50~100th $P_w(MPa)$	100~130th $P_w(MPa)$	130~190th $P_w(MPa)$
B. C. sand filter at Z=0.25m	0	$0.0 \rightarrow 0.8$	0.8	0.1	0.8

Time interval (day)	190~225th $P_w(MPa)$	225~370th $P_w(MPa)$	370~450th $P_w(MPa)$	450~1000th $P_w(MPa)$
B. C. sand filter at Z=0.25m	0.1	0.8	0.1	0.25
B. C. sand filter at Z=6.75m	/	/	0.1	0.25

(5) Mechanical boundary conditions
(See Figure 4)

Initial conditions

Materials	Temperature $(^{\circ}C)$	Pore water pressure (MPa)	Porosity	Saturation degree
Bentonite 1	20	-47.5	0.389	0.798
Bentonite 2		-47.5	0.368	0.798
Sand shield		-62.5	0.300	0.0579
Outer sand		-62.5	0.360	0.135
Rock		0.1	0.003	1.0
Pellets		-2.03	0.568	0.211
Heater		0.1	0.001	0.0
Peek		0.1	0.001	0.0

Basic assumptions

The assumptions described at the end of section 3.1 also apply for this case. Regarding the water pressure boundary condition, figure 46 presents the time evolution of this variable used in this case 2. Note that before 370 days, a simplified profile of the water pressure has been used.

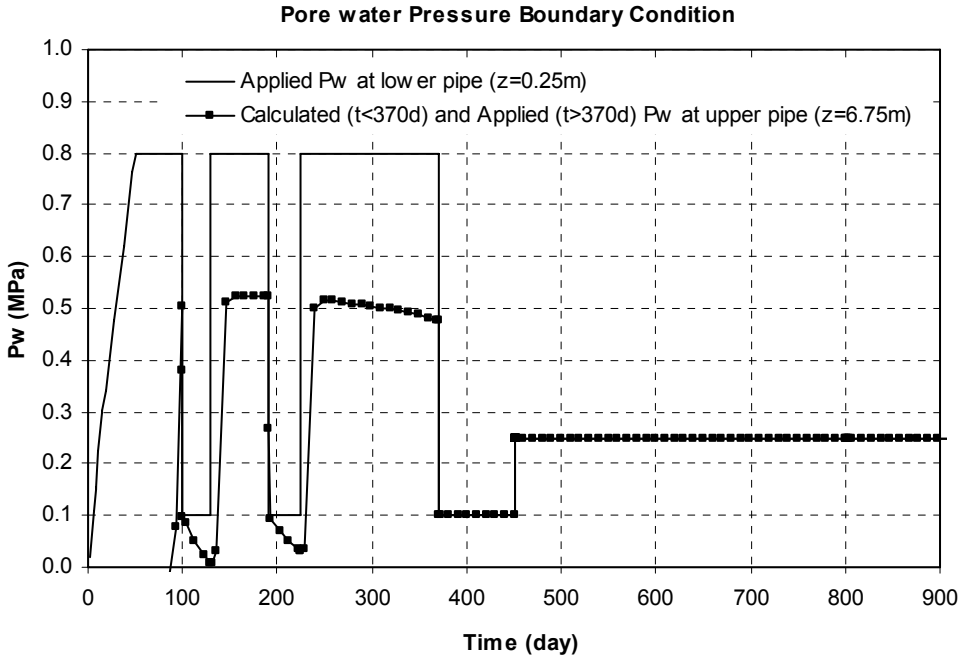

Figure 46. *Temporal evolution of pore water pressure boundary condition at sand filter used in the analyses of case 2.*

3.4 Case 2: Predictions

The required predictions follow:

Scan-line A1-A4 (z=5.5 m)

- Figure 47: Temperature
- Figure 48: Saturation degree
- Figure 49: Relative Humidity
- Figure 50: Porosity
- Figure 51: Radial stress
- Figure 52: Radial displacement

Scan-line C0-C4 (z=7.30 m)

- Figure 53: Temperature
- Figure 54: Saturation degree
- Figure 55: Relative Humidity
- Figure 56: Porosity
- Figure 57: Radial stress
- Figure 58: Radial displacement

Scan-line D0-D4 (z=3.75 m)

- Figure 59: Temperature
- Figure 60: Saturation degree
- Figure 61: Relative Humidity
- Figure 62: Porosity
- Figure 63: Radial stress
- Figure 64: Radial displacement

Scan-line E0-E4 (z=0.25 m)

- Figure 65: Temperature
- Figure 66: Saturation degree
- Figure 67: Relative Humidity
- Figure 68: Porosity
- Figure 69: Radial stress
- Figure 70: Radial displacement

Vertical scan-lines

- Figure 71: Scan-line 1 (r=0.305 m). Temperature
- Figure 72: Scan-line 2 (r=0.535 m). Temperature
- Figure 73: Scan-line 4. (r=0.875 m).Temperature

Other required predictions

- Figure 74: Anchor force
- Figure 75: Suction cycle Ring 10
- Figure 76: Radial stresses. Ring 9
- Figure 77: Axial stresses. Ring 9
- Figure 78: Tangential stresses. Ring 9

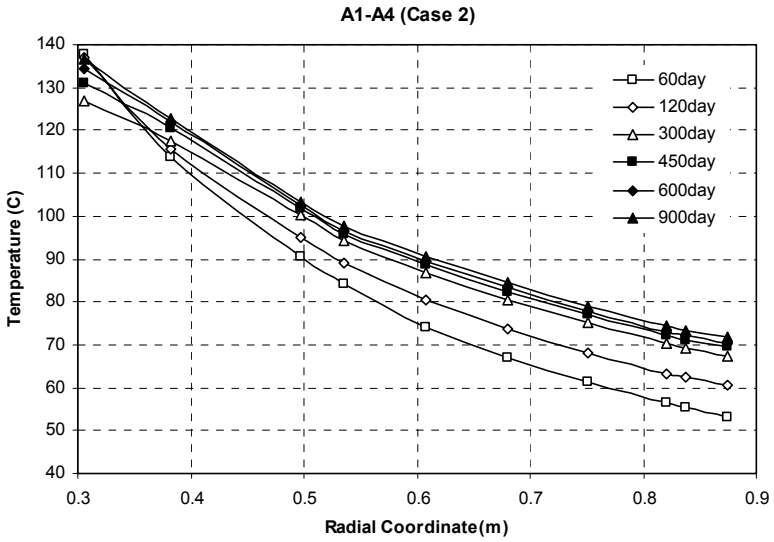

Figure 47

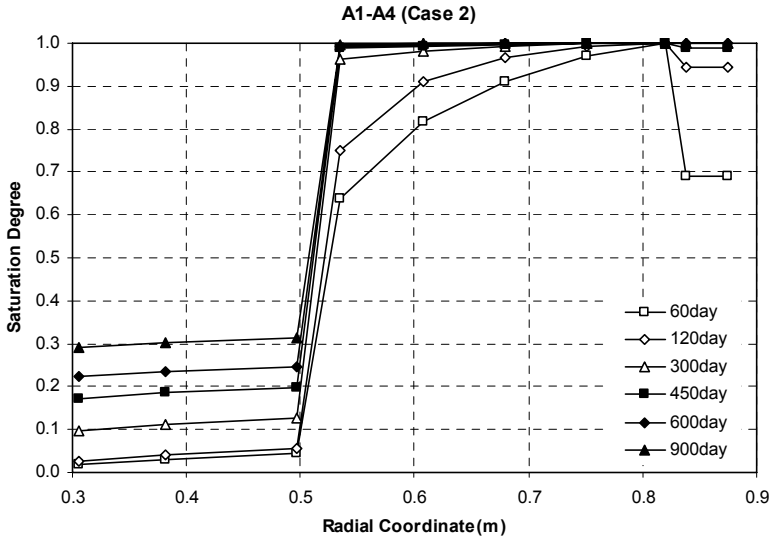

Figure 48

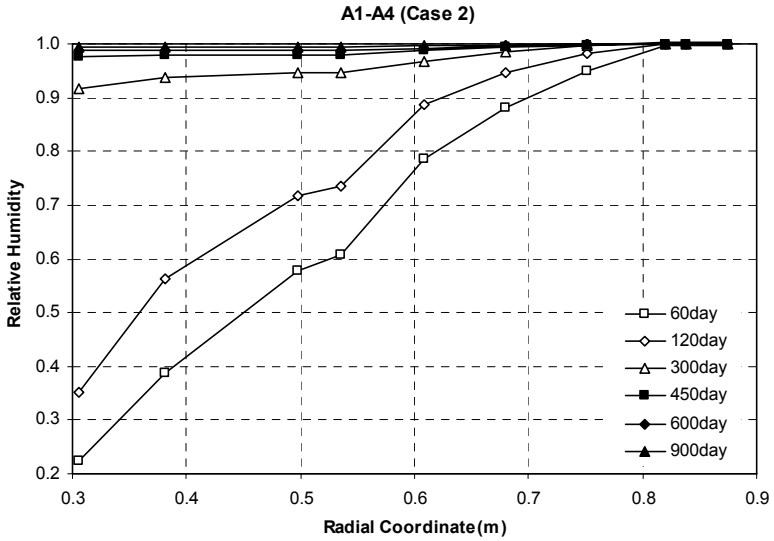

Figure 49

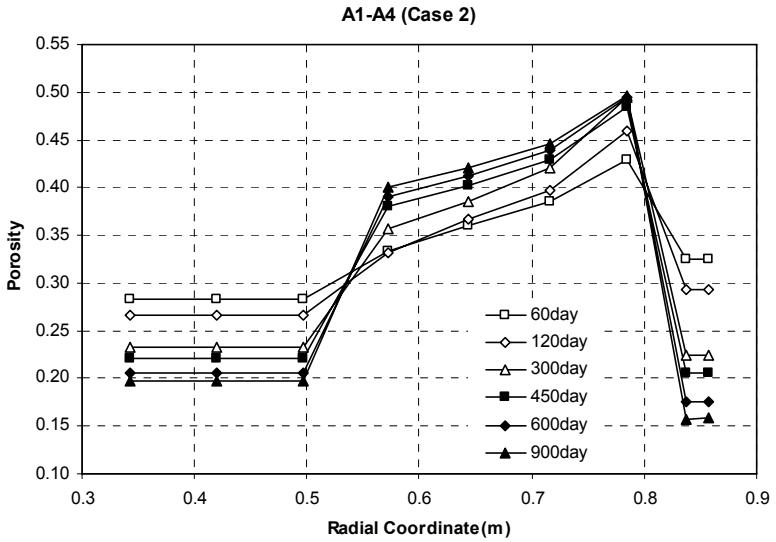

Figure 50

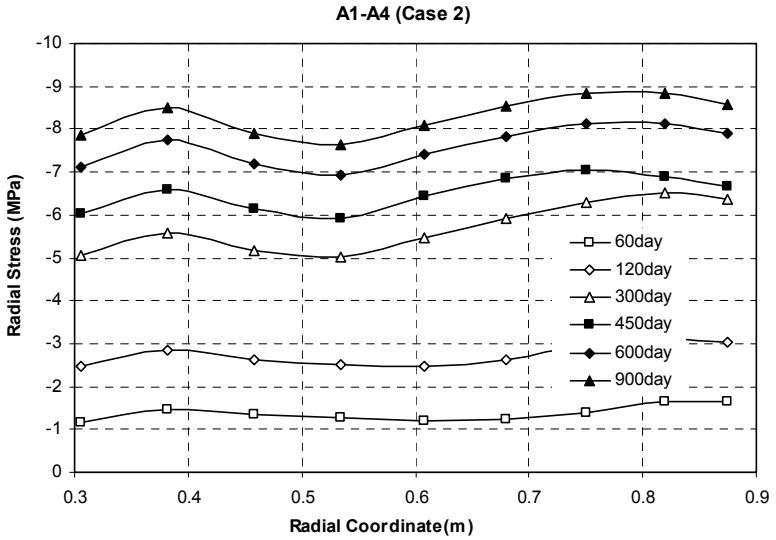

Figure 51

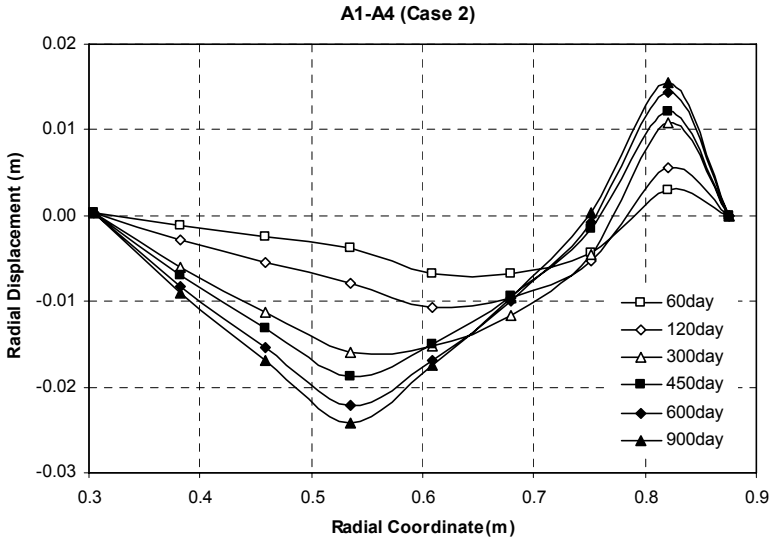

Figure 52

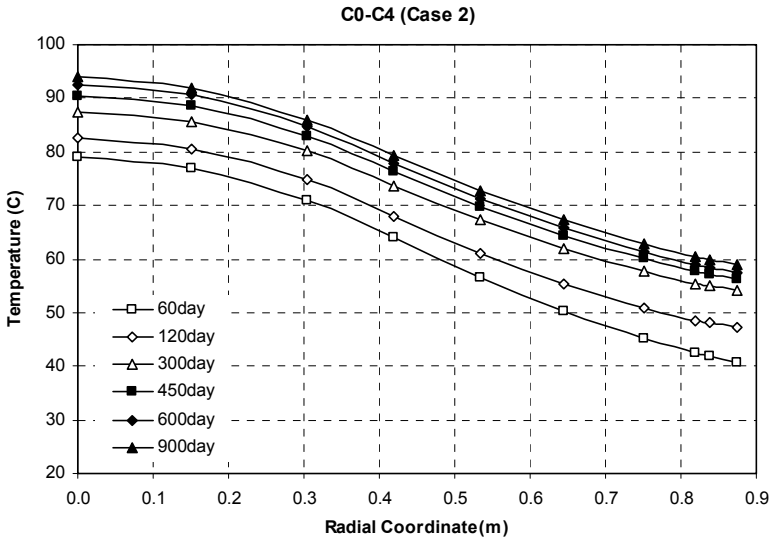

Figure 53

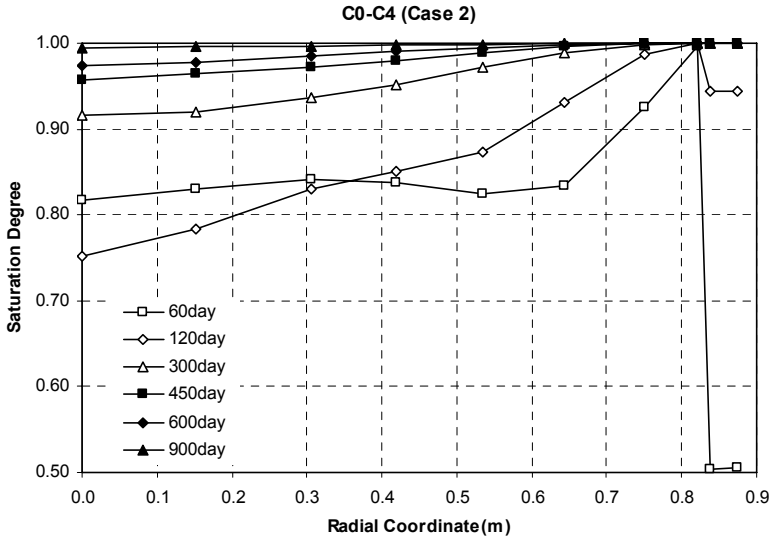

Figure 54

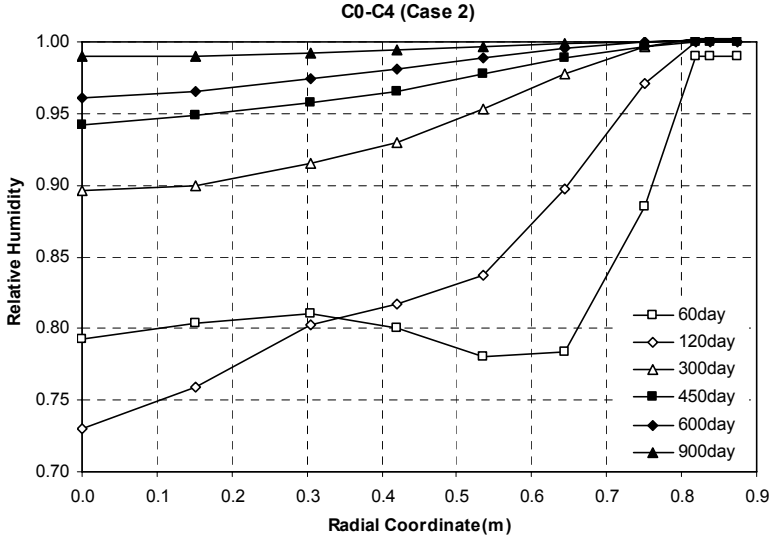

Figure 55

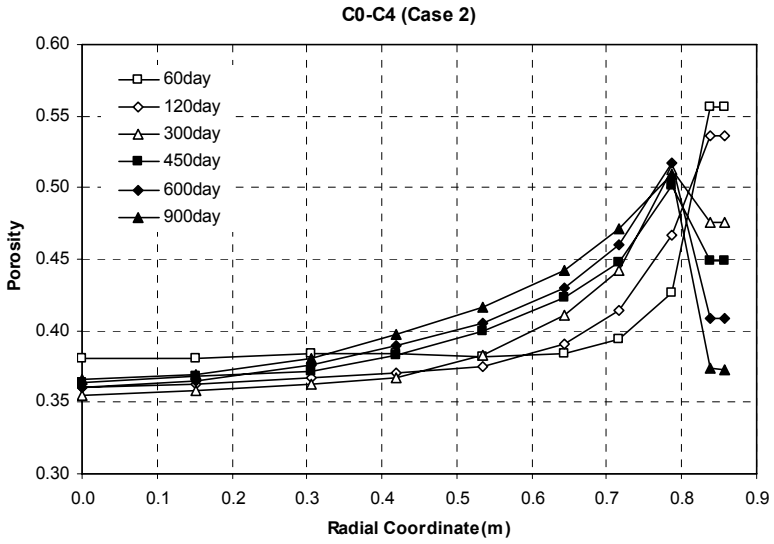

Figure 56

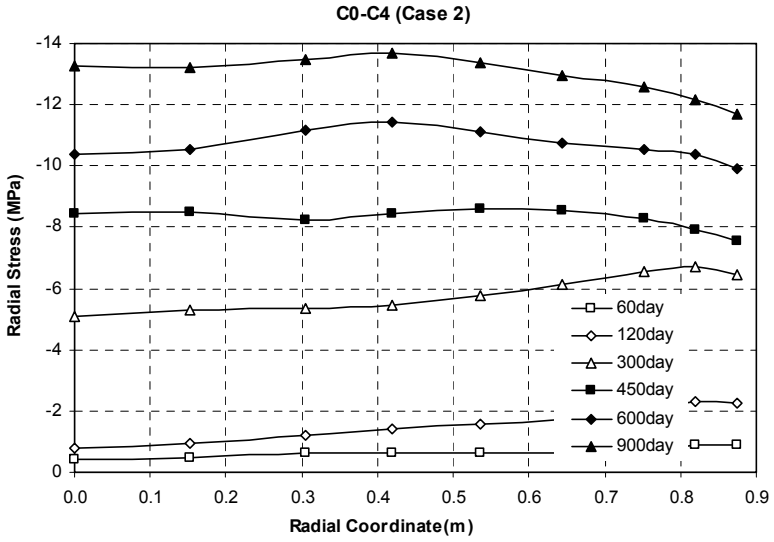

Figure 57

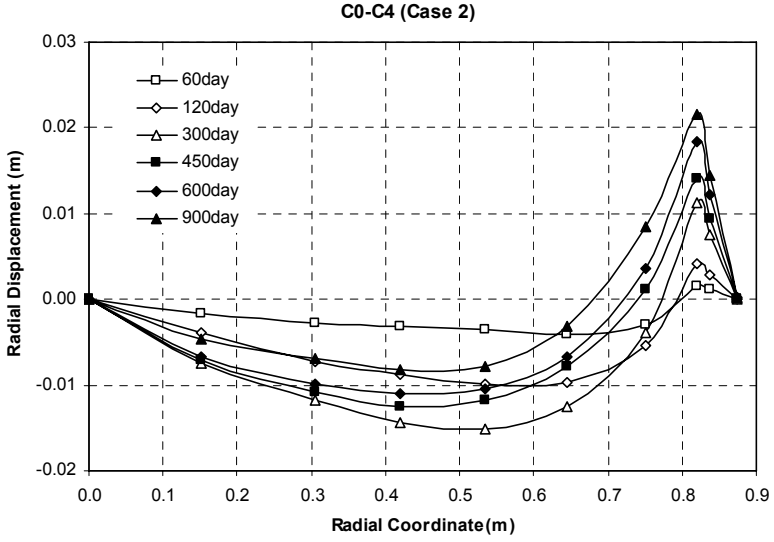

Figure 58

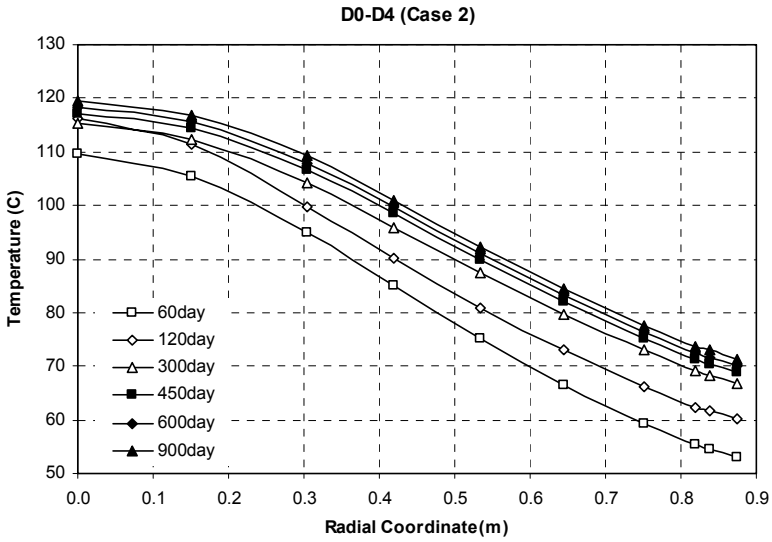

Figure 59

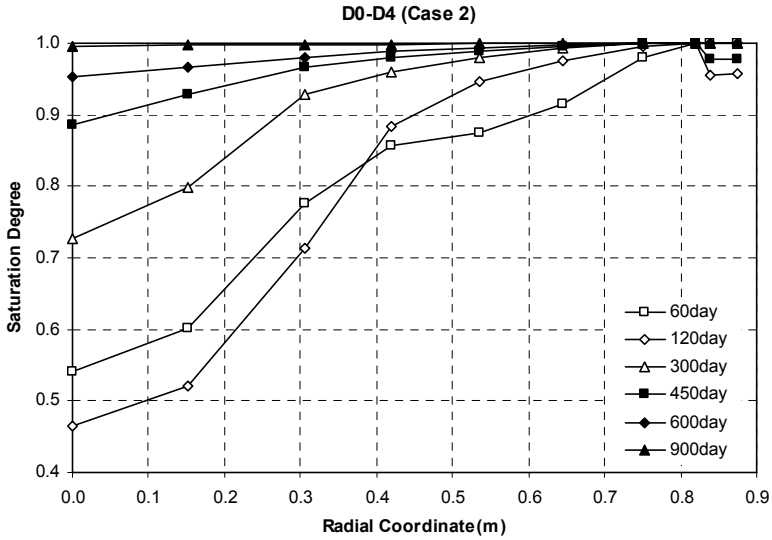

Figure 60

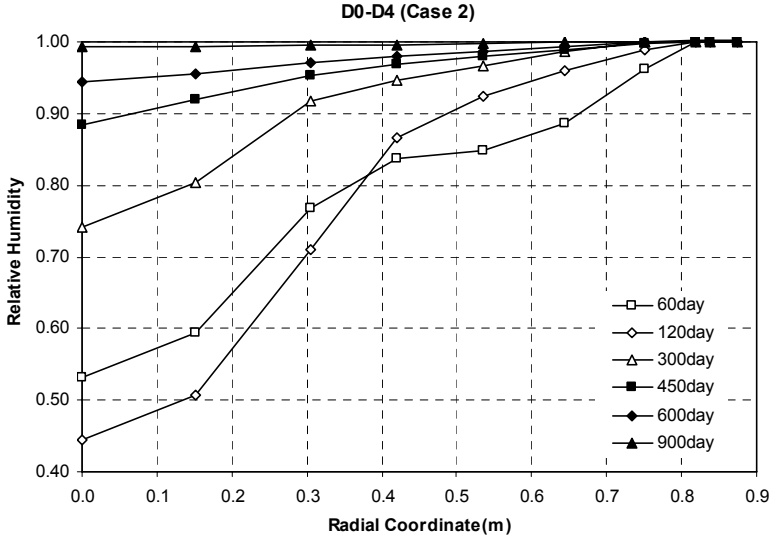

Figure 61

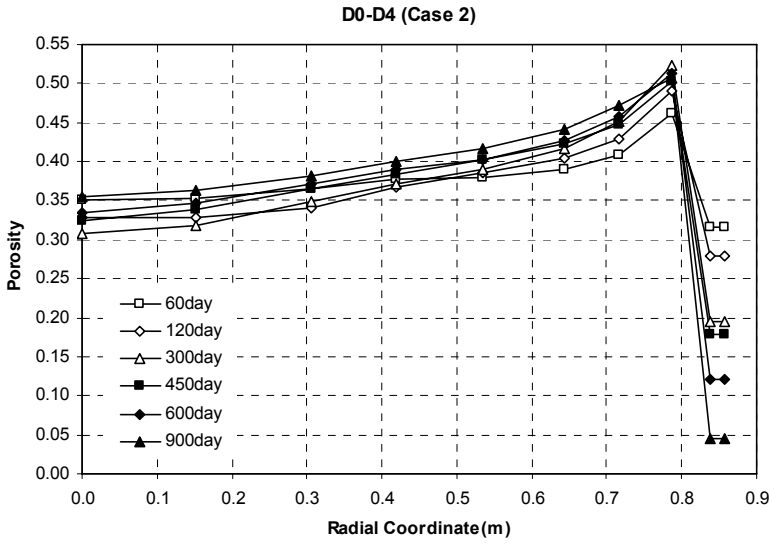

Figure 62

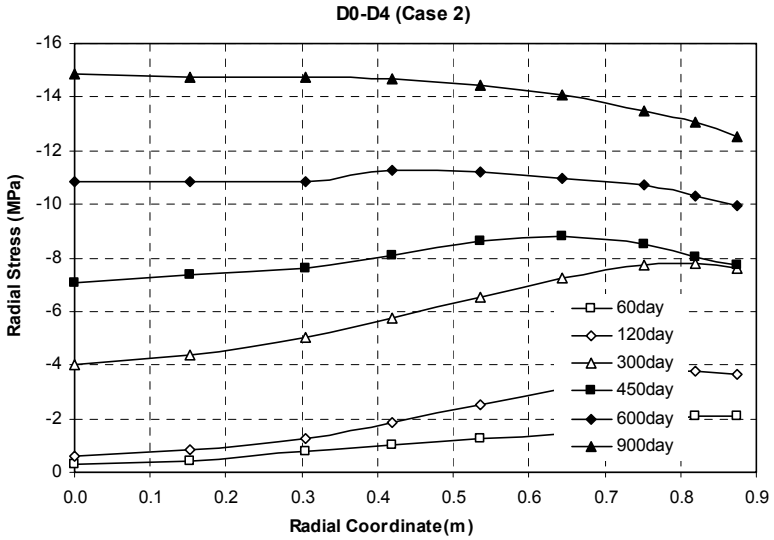

Figure 63

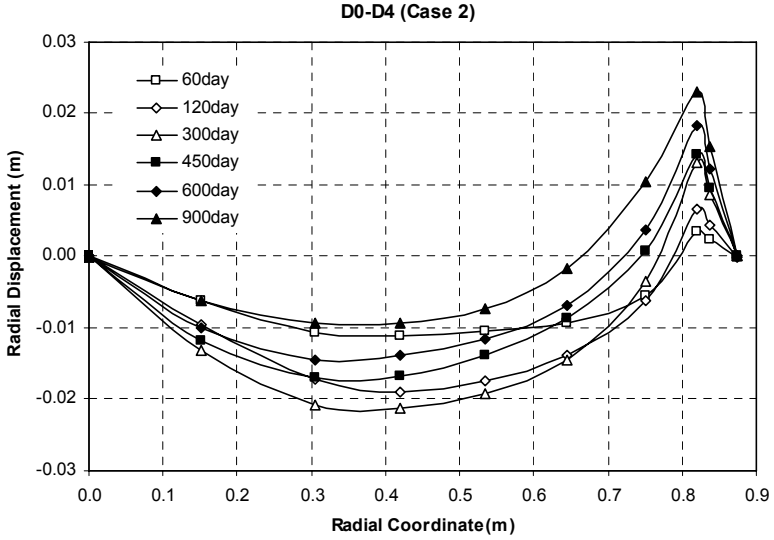

Figure 64

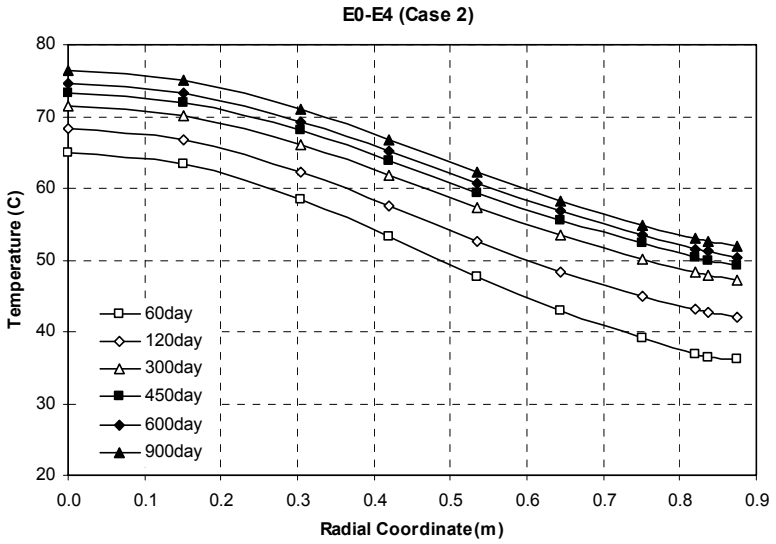

Figure 65

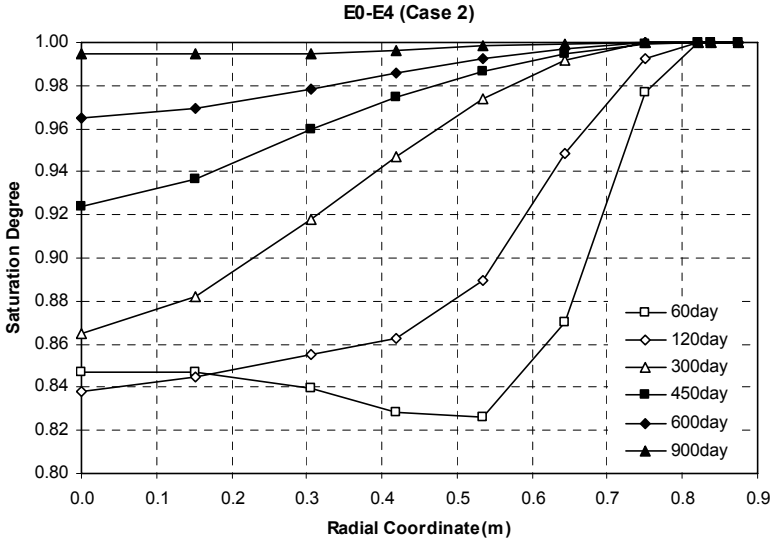

Figure 66

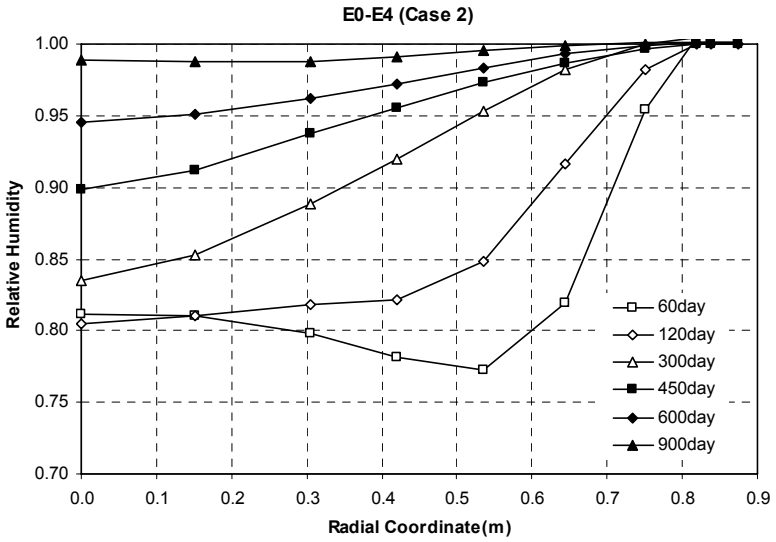

Figure 67

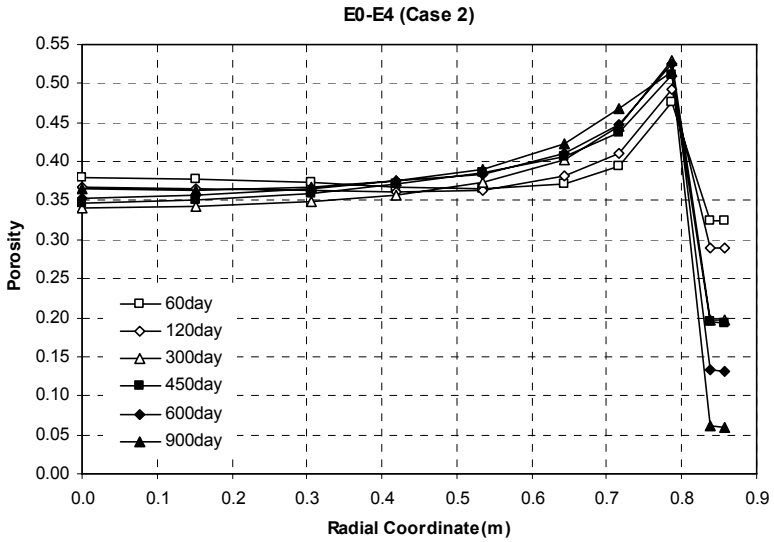

Figure 68

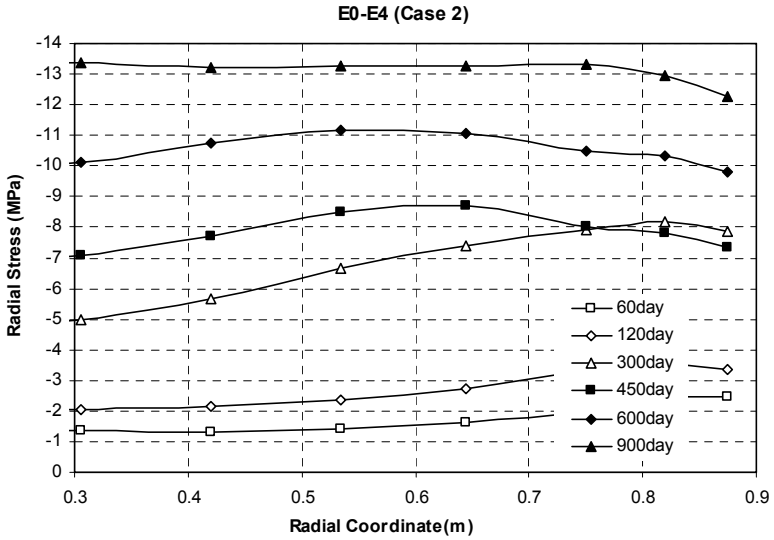

Figure 69

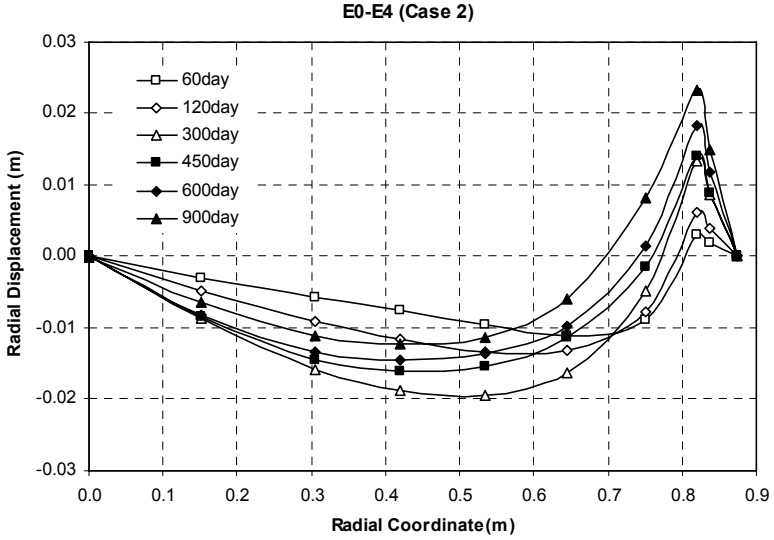

Figure 70

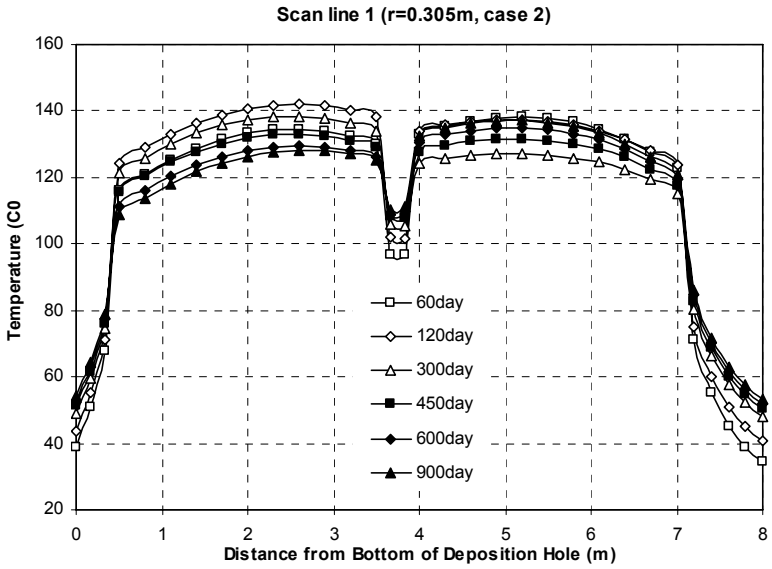

Figure 71

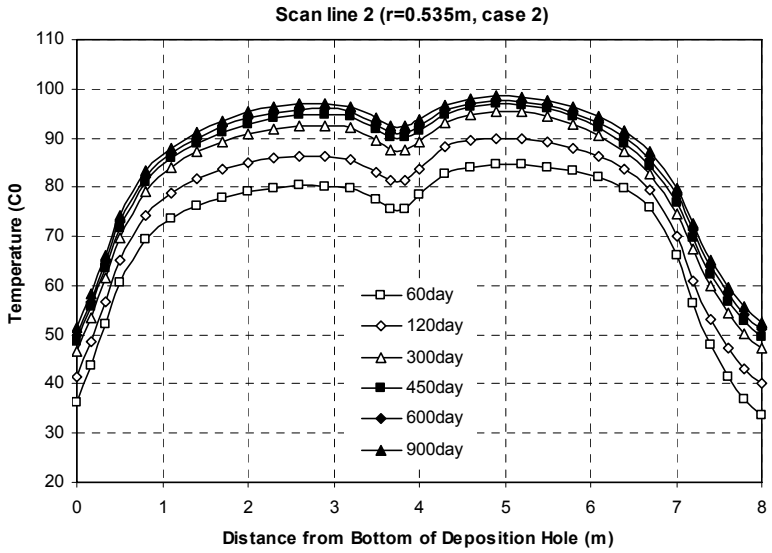

Figure 72

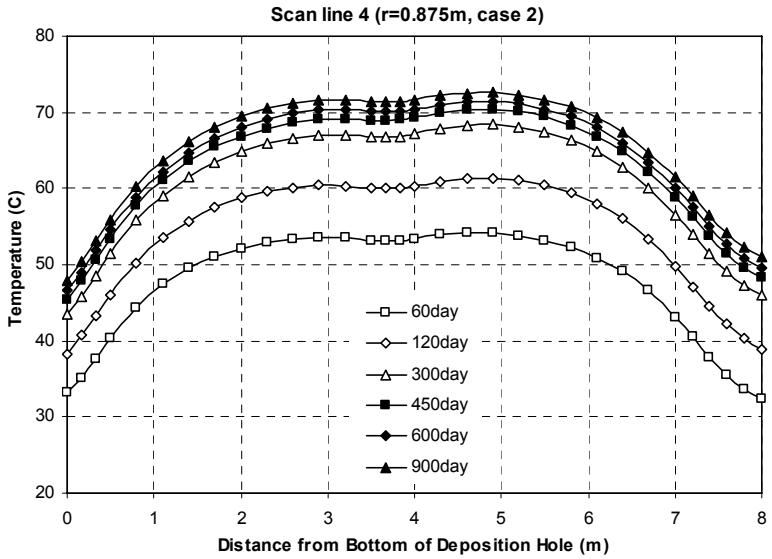

Figure 73

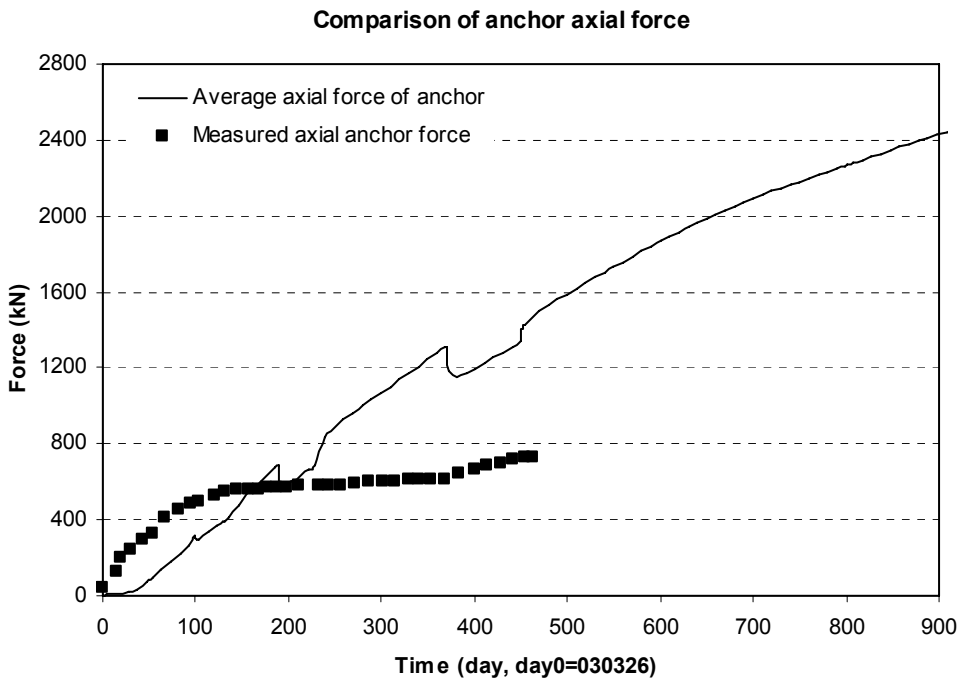

Figure 74

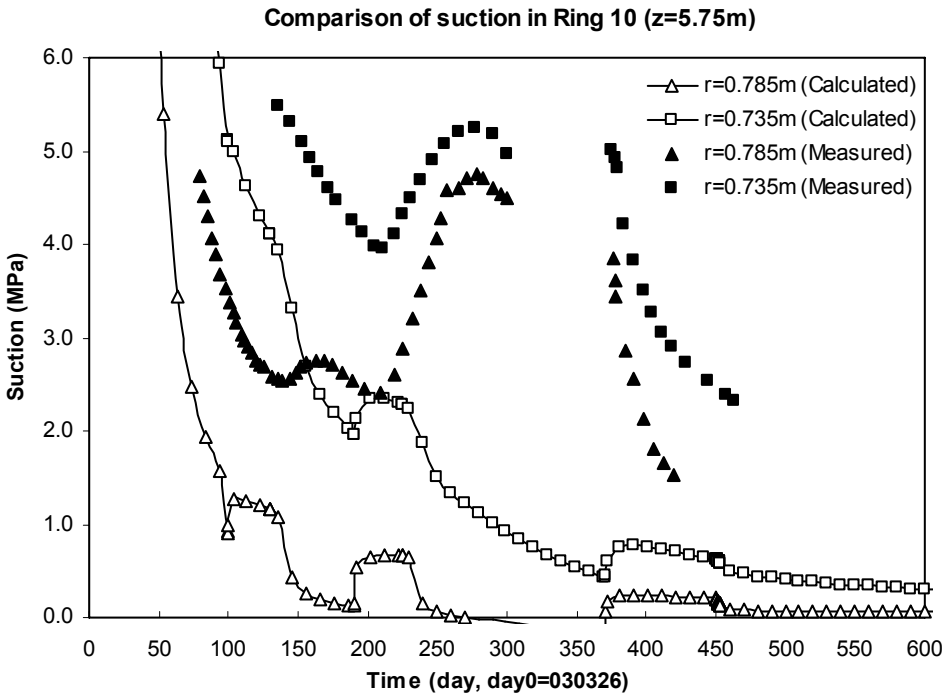

Figure 75

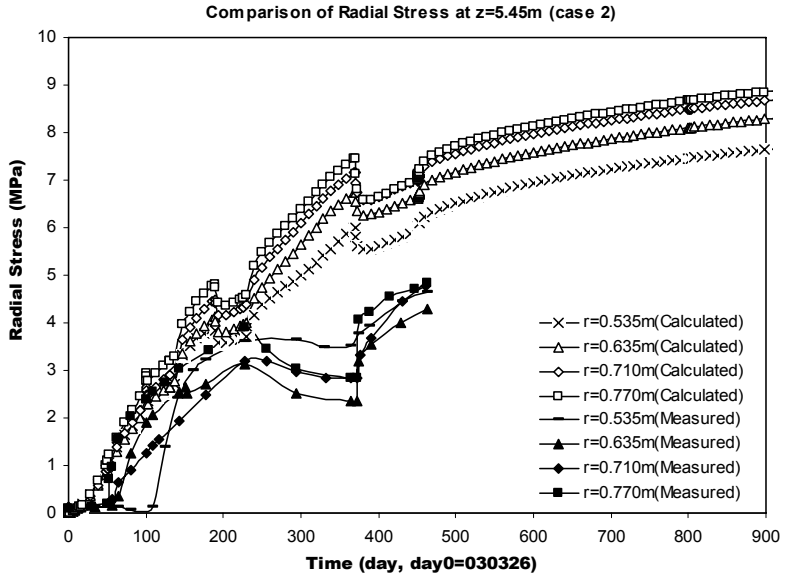

Figure 76

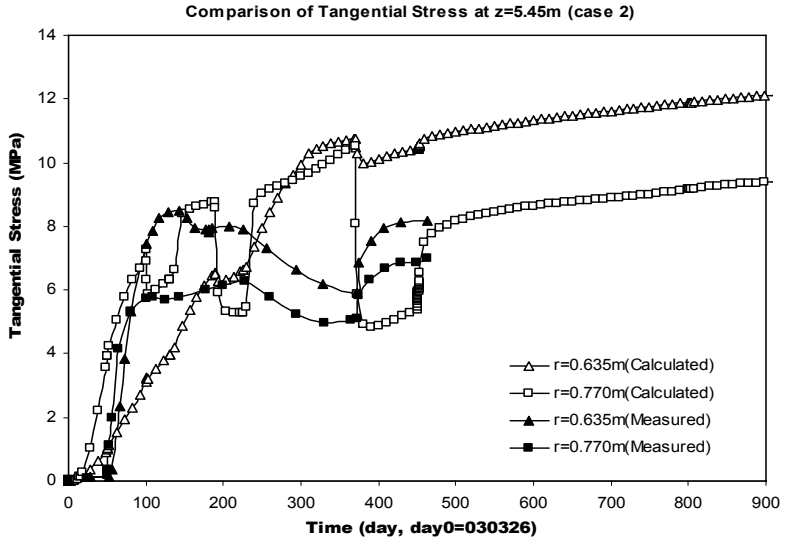

Figure 77

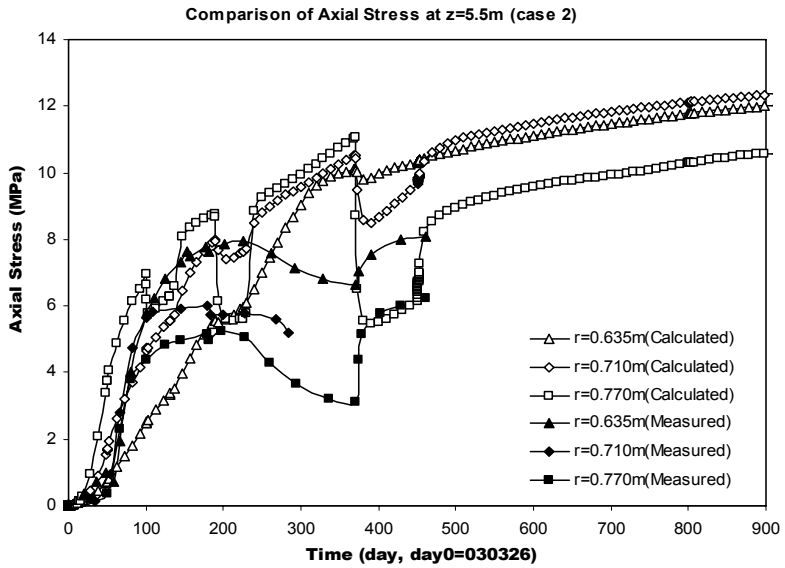

Figure 78

3.5 Case 3: Parameters and initial conditions

The following tables present the parameters, initial conditions and basic assumptions considered in the simulation of the prediction phase of Case 2.

Thermal Problem

Thermal conductivity $\lambda(W/mK)$

Material	Law	λ_{dry}	λ_{sat}
Bentonite 1	$\lambda = \lambda_{sat}^{S_l} \cdot \lambda_{dry}^{1-S_l}$	0.3	1.3
Bentonite 2		0.3	1.3
Rock		2.6	2.6
Pellets		0.1	1.0
Sand shield		0.6	1.7
Outer sand		0.6	1.7
Steel		50.16	50.16
Peek		0.25	0.25

Specific Heat $c(J/kgK)$

Material	Bentonite 1 & 2	Rock	Pellets	Sand shield	Outer sand	Steel	Peek
$c(J/kgK)$	1091	800	1091	900	900	460	1091

Hydraulic Problem

Retention Curve

Material	Law (Van Genuchten)	P_0 (MPa)	β	S_m (MPa)	m
Bentonite 1	$S_e = \frac{S_l - S_{rl}}{S_{ls} - S_{rl}} = \left[1 + \left(\frac{P_g - P_l}{P_0}\right)^{\frac{1}{1-\beta}}\right]^{-\beta} \left(1 - \frac{P_g - P_l}{S_m}\right)^m$	60	0.3	800	1.1
Bentonite 2		60	0.3	800	1.1
Outer/Inner Sand		0.2/0.1	0.25/0.3	110/600	1.1
Pellets	$S_e = \frac{S_l - S_{rl}}{S_{ls} - S_{rl}} = \left[1 + \left(\frac{P_g - P_l}{P_0}\right)^{\frac{1}{1-\beta}}\right]^{-\beta}$	0.2	0.4		
Rock		100	0.56		
Heater		10^{-5}	0.45		
Peek					

Intrinsic Permeability $k(m^2)$

Material	Law (Kozeny's Model)	$k_0\ (m^2)$	ϕ_0
Bentonite 1	$k_i = k_0 \frac{\phi^3}{(1-\phi)^2} \frac{(1-\phi_0)^2}{\phi_0^3}$	0.36×10^{-20}	0.389
Bentonite 2		0.36×10^{-20}	0.368
Pellets		2.0×10^{-19}	0.5684
Inner sand		1×10^{-15}	0.30
Outer sand		2×10^{-15}	0.36
Rock		10^{-30}	0.003
Heater		10^{-30}	0.001
Peek		10^{-30}	0.001

Liquid Relative Permeability: $k_{rl} = S_e^3$

Gas permeability:

Material	Law (Kozeny's Model)	A
Bentonite 1	$k_g = \frac{\rho g}{\mu_g} \times A \times k_i \times (1 - S_r)^n$	0.2181×10^9
Bentonite 2		0.2274×10^9
Pellets		1
Inner sand		10
Outer sand		10^{-30}
Rock		1
Heater		1
Peek		1

Mechanical Problem

Thermal Elasticity

Material	Law (Linear Elasticity)	$b_s\left(^{\circ}C^{-1}\right)$
Bentonita 1 & 2	$\Delta\varepsilon_v = 3b_s\Delta T$	1.0×10^{-5}
Rock		7.8×10^{-6}
Outer sand		10^{-5}
Inner sand		10^{-5}
Pellets		10^{-5}
Steel		10^{-5}
Peek		10^{-5}

Stress-strain Mechanical Model

Material	Model	Parameters
Bentonite 1 & 2	Barcelona Basic Model (BBM)	$\kappa_{i0} = 0.207, \kappa_{s0} = 0.1563,$ $K_{\min} = 13.33MPa, \nu = 0.2,$ $\lambda(0) = 0.621, r = 0.75, \beta = 0.05,$ $p^c = 0.1MPa, p_0^* = 9.542MPa$ $M = 0.78, \alpha = 0.395, k = 0.1$
Rock	Linear Elasticity	$E = 5.0 \times 10^4\, MPa, \nu = 0.25$
Steel		$E = 2.1 \times 10^5\, MPa, \nu = 0.2$
Outer sand		$E = 24.93MPa, \nu = 0.25$
Inner sand		$E = 55.37MPa, \nu = 0.25$
Pellets		$E = 20MPa, \nu = 0.25$
Peek		$E = 20MPa, \nu = 0.25$

Boundary conditions

(1) Temperature boundary condition:
Outer boundary of rock: $T = 20^{\circ}C$
Tunnel boundary: $T = 20^{\circ}C$

(2) Heat flux(Day 0=26/03/03):
Two heaters: 0~8 days, 900W; 8~15 days, 1200W; 15~1000days, 1500W.

(3) Pore water and gas pressure in rock:
$P_w = P_g = 0.1MPa$

(4) Gas and liquid boundary conditions
Gas boundary condition: before 372.3th day, for contact line between outer sand and bentonite $P_g = 0.1MPa$; after 372.3th day, this line is closed for gas.

Case 3: Liquid boundary condition

Time interval (day)	0~1th	1~72th $J_l(kg/s)$	72~108.3th $J_l(kg/s)$	108.3~270.4th $J_l(kg/s)$	270.4~372.3th $J_l(kg/s)$
B. C. sand filter at Z=0.25m	0	0.7746×10^{-4}	0.2453×10^{-4}	0.1820×10^{-5}	0.5695×10^{-5}

Time interval (day)	372.3~456.5th $J_l(kg/s)$	456.5~500th $P_w(MPa)$	500~900th $P_w(MPa)$
B. C. sand filter at Z=0.25m	1.215×10^{-5}	$0.082 \rightarrow 0.25$	0.25
B. C. sand filter at Z=6.75m	1.215×10^{-5}	$-0.45 \rightarrow 0.25$	0.25

(5) Mechanical boundary conditions
(See Figure 4)

Initial conditions

Materials	Temperature $(^{\circ}C)$	Pore water pressure (MPa)	Porosity	Saturation degree
Bentonite 1	20	-47.5	0.389	0.798
Bentonite 2		-47.5	0.368	0.798
Sand shield		-62.5	0.300	0.0563
Outer sand		-62.5	0.360	0.0584
Rock		0.1	0.003	1.0
Pellets		-2.03	0.568	0.211
Heater		0.1	0.001	0.0
Peek		0.1	0.001	0.0

Basic assumptions

In order to minimise the problems of convergence in this Case 3, some additional assumptions have been made. It is considered, however, that they do not influence too much the final results. They refer to the following aspects:

1. Liquid pressures in rock, heater and peek are fixed, and their permeability is set to be very low, so there is no liquid exchange with them.

2. Gas pressure in rock is fixed and the gas permeability of rock is also set to be very low, so there is no gas exchange with rock.

3. Gas pressure in sand filter is fixed (this is not realistic, but is used to solve a convergence problem; due to its limited volume this assumption may be practically accepted).

4. In order to simulate the upper pipe which is open to air before 370^{th} day, and is used to inject water after 370^{th} day, gas pressure of the contact line between sand filter and bentonite is fixed before 370^{th} day, and it is under no control after 370^{th} day. Although only points of the upper pipe are open to air, the gas permeability of the sand filter is very high, so it is acceptable to assume that the contact line between bentonite and sand filter is open to air.

5. In this analysis, applied water inflow from lower pipe between 1st and 108.3th days is multiplied by 0.9 (which is 127 liters less than measured) in order to include the effect of initial saturation degree of sand, 5.84% (45 liters), used in the simulations.

6. From the 372.3^{th} day to 456.5^{th} day, water flux boundary conditions are applied to both pipes. Only the total measured water flux from both pipes is known, and the percentages from the upper and the lower, are assumed (see Figure 79) to be 50%, respectively.

7. From 456.5^{th} day to day 900^{th}, pore water pressure boundary condition is applied from both pipes. From 456.5^{th} day to 500^{th} day, pore water pressures at both pipes are assumed to increase up to 0.25MPa linearly; and from 500^{th} day to 900^{th} day, pore water pressures at both pipes are assumed to be at constant value 0.25MPa (see Figure 80).

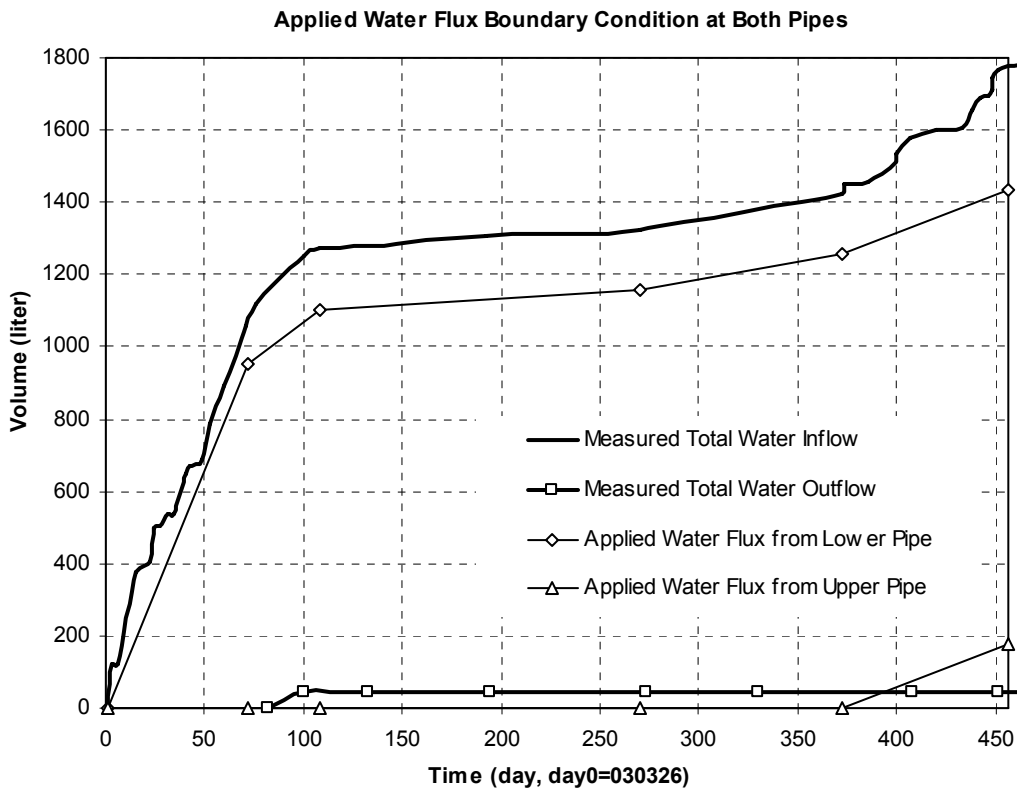

Figure 79. *Applied water flux boundary conditions at both pipes before day 456.5th*

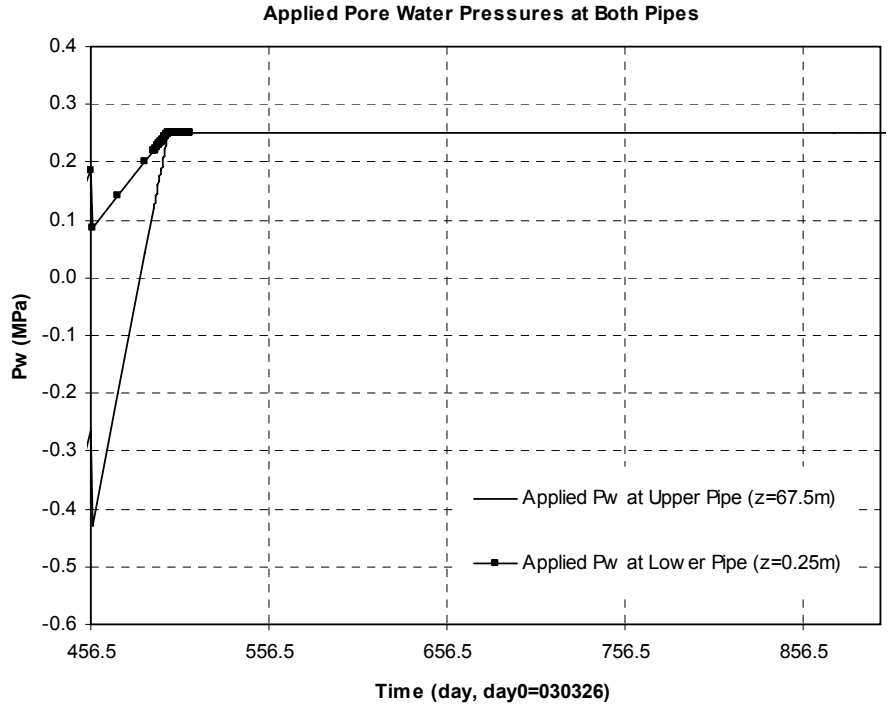

Figure 80. *Applied pore water pressure boundary conditions at both pipes after day 456.5th*

3.6 Case 3: Predictions

The required predictions follow:

Scan-line A1-A4 (z=5.5 m)

- Figure 81: Temperature
- Figure 82: Saturation degree
- Figure 83: Relative Humidity
- Figure 84: Porosity
- Figure 85: Radial stress
- Figure 86: Radial displacement

Scan-line C0-C4 (z=7.30 m)

- Figure 87: Temperature
- Figure 88: Saturation degree
- Figure 89: Relative Humidity
- Figure 90: Porosity
- Figure 91: Radial stress
- Figure 92: Radial displacement

Scan-line D0-D4 (z=3.75 m)

- Figure 93: Temperature
- Figure 94: Saturation degree
- Figure 95: Relative Humidity
- Figure 96: Porosity
- Figure 97: Radial stress
- Figure 98: Radial displacement

Scan-line E0-E4 (z=0.25 m)

- Figure 99: Temperature
- Figure 100: Saturation degree
- Figure 101: Relative Humidity
- Figure 102: Porosity
- Figure 103: Radial stress
- Figure 104: Radial displacement

Vertical scan-lines

- Figure 105: Scan-line 1 (r=0.305 m). Temperature
- Figure 106: Scan-line 2 (r=0.535 m). Temperature
- Figure 107: Scan-line 4. (r=0.875 m).Temperature

Other required predictions

- Figure 108: Anchor force
- Figure 109: Suction cycle Ring 10
- Figure 110: Radial stresses. Ring 9
- Figure 111: Axial stresses. Ring 9
- Figure 112: Tangential stresses. Ring 9

Other predictions for reference:

Comparison between measured and calculated T, RH (figures a & b)

- Figure 113: z=0.25m
- Figure 114: z=2.25m
- Figure 115: z=3.75m
- Figure 116: z=5.75m
- Figure 117: z=7.25m

Profiles of saturation degree in the sand filter for difference times (Figure 118)

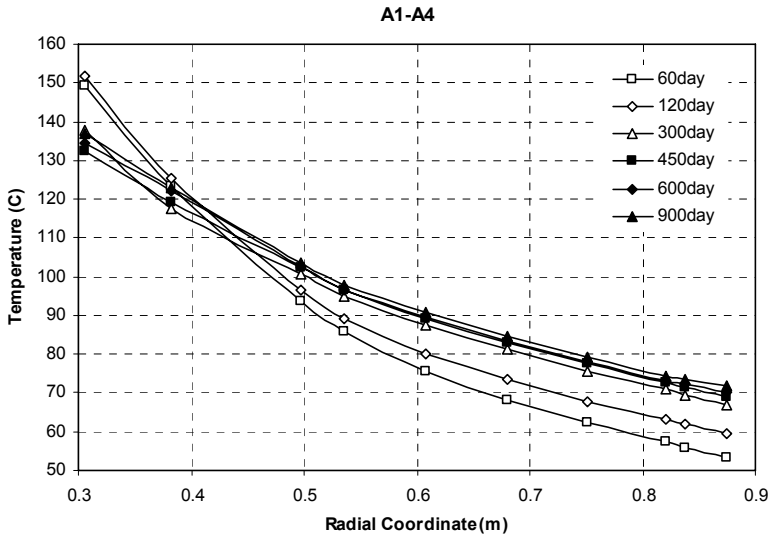

Figure 81

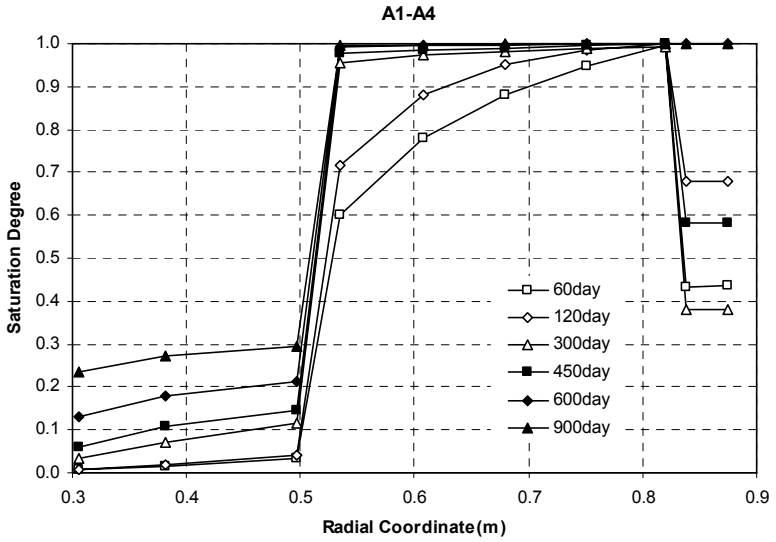

Figure 82

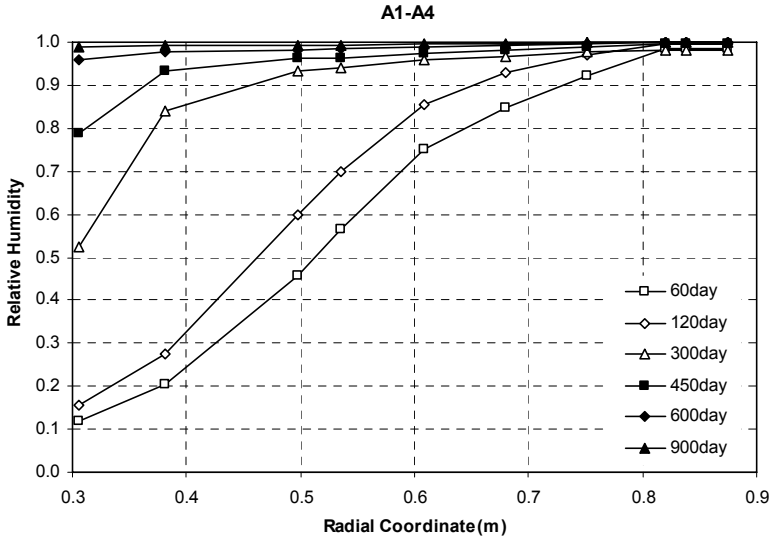

Figure 83

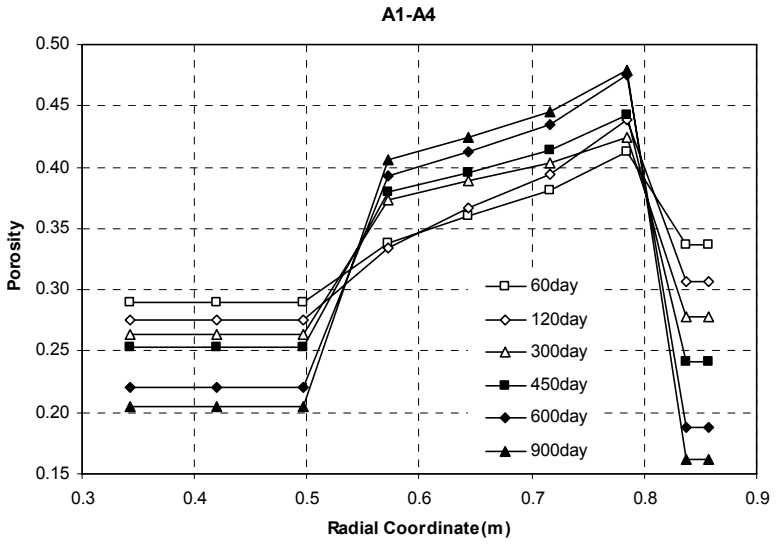

Figure 84

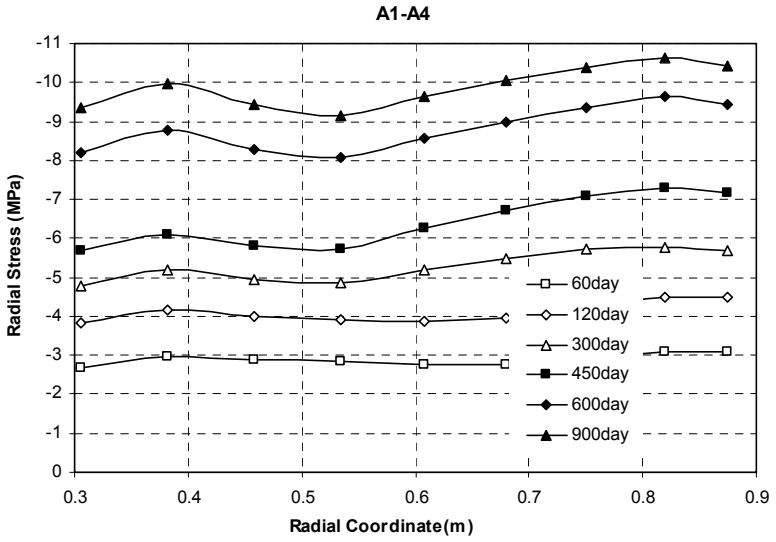

Figure 85

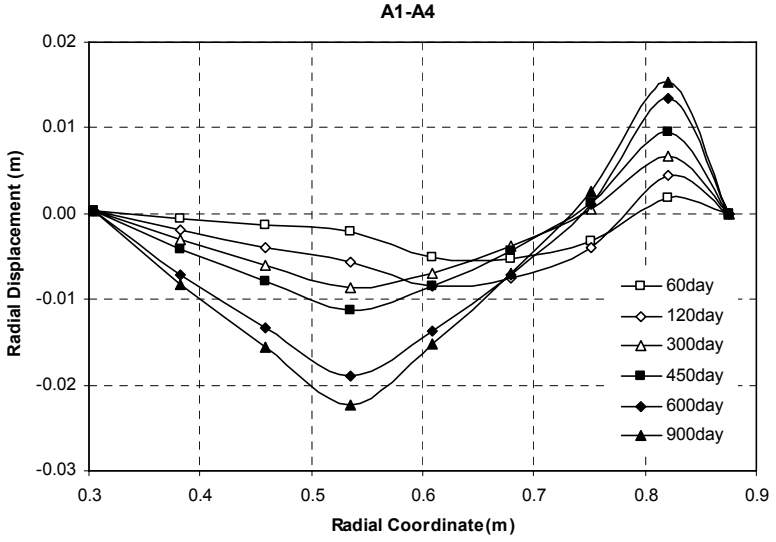

Figure 86

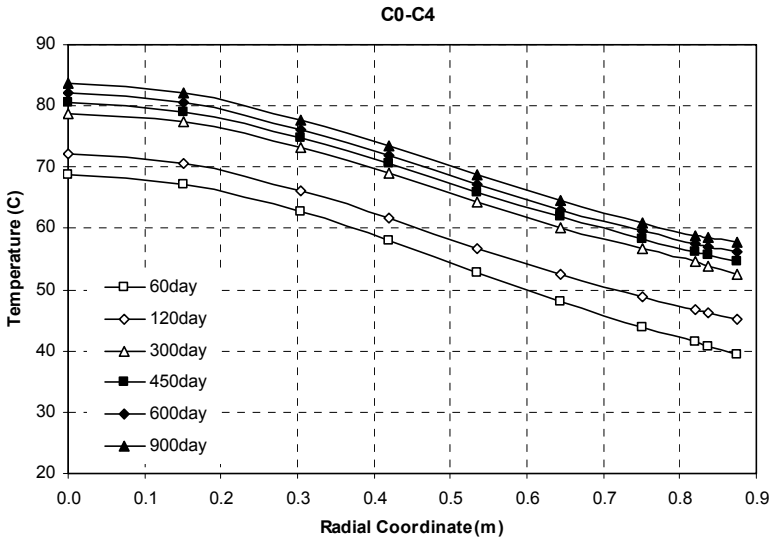

Figure 87

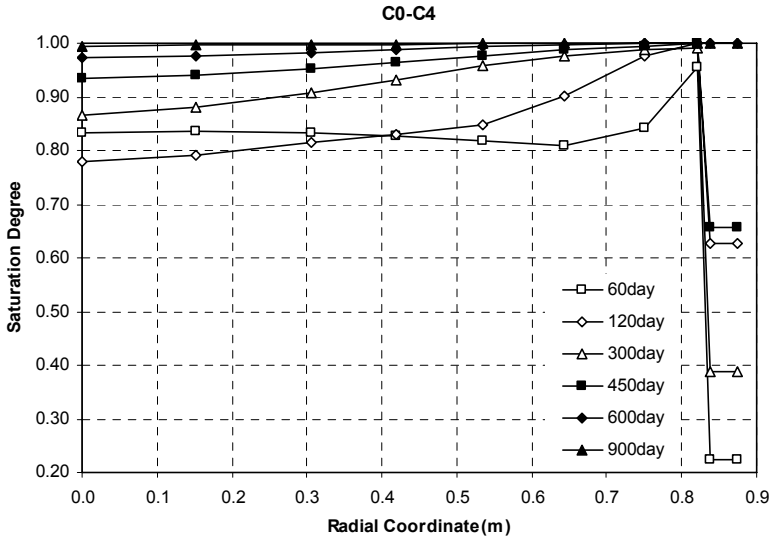

Figure 88

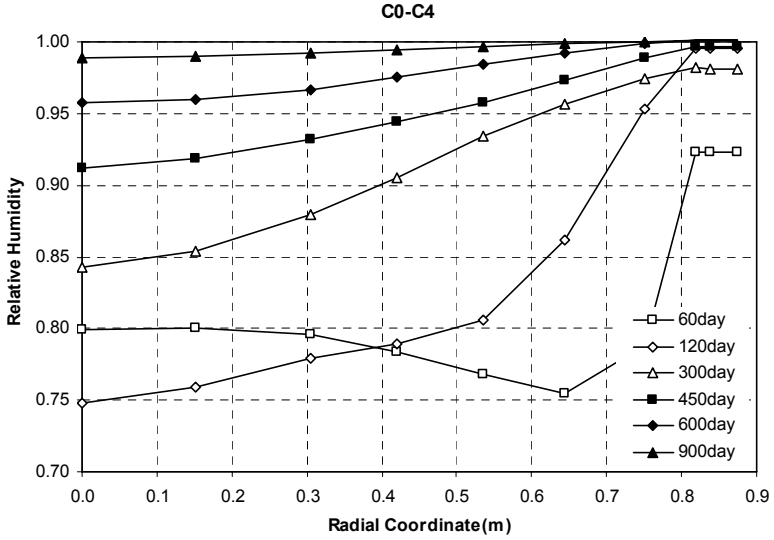

Figure 89

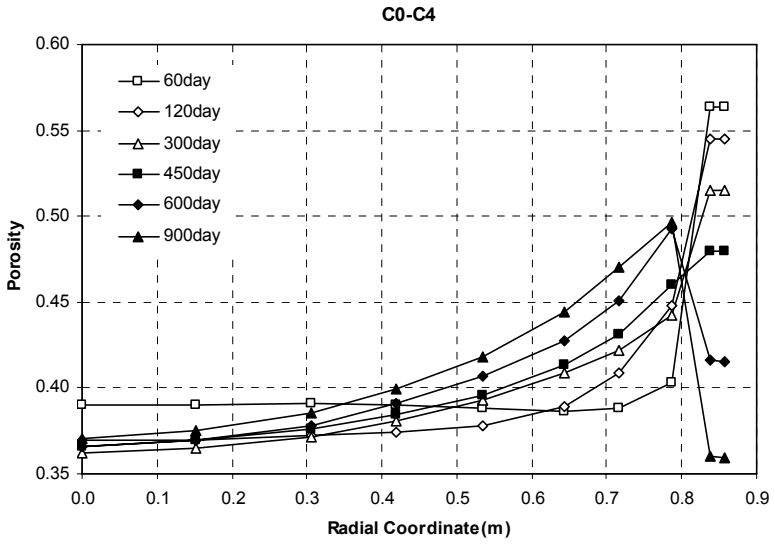

Figure 90

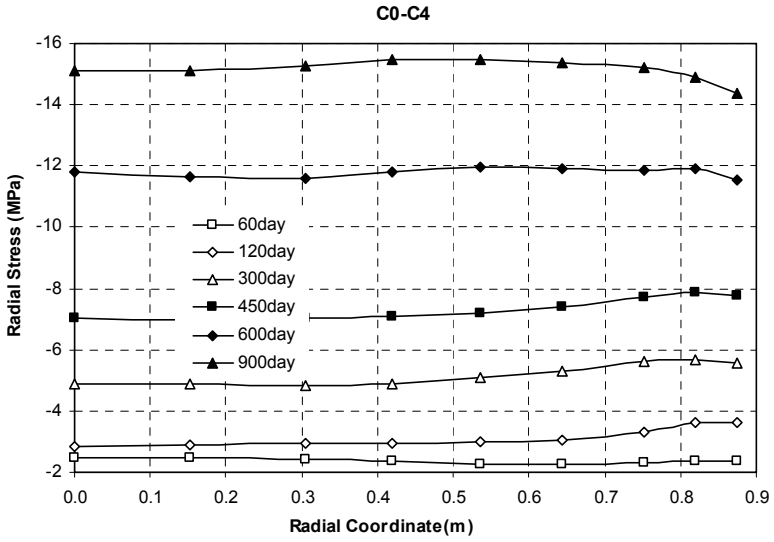

Figure 91

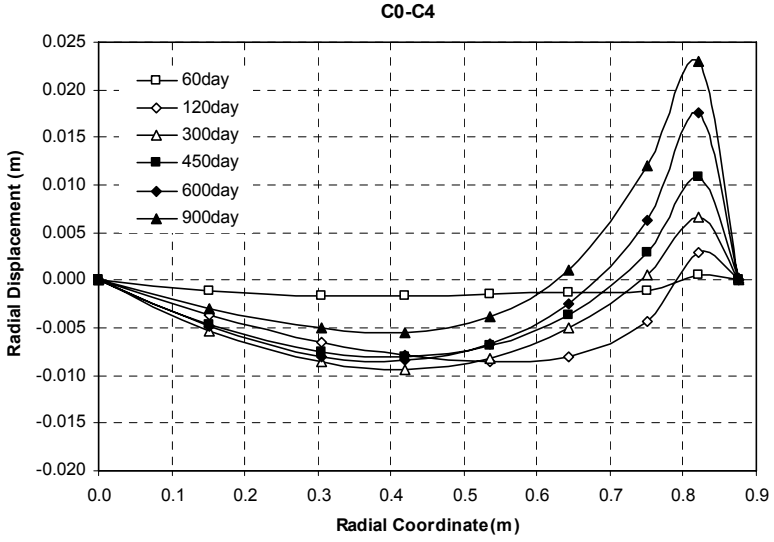

Figure 92

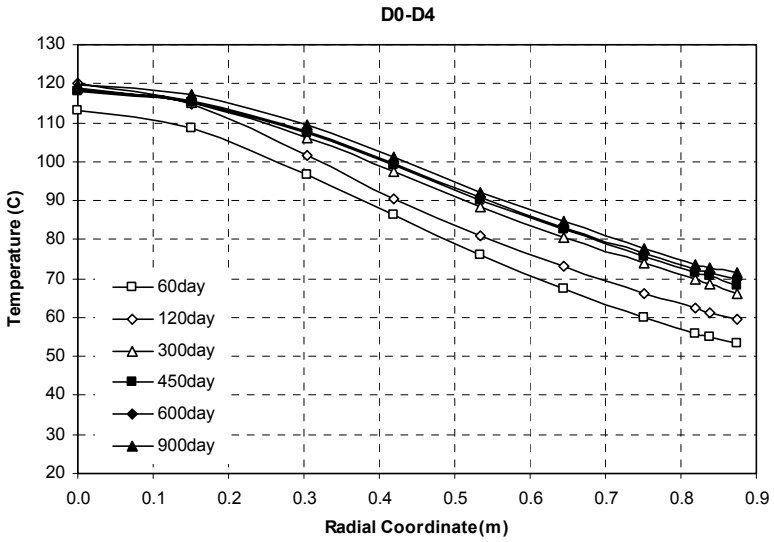

Figure 93

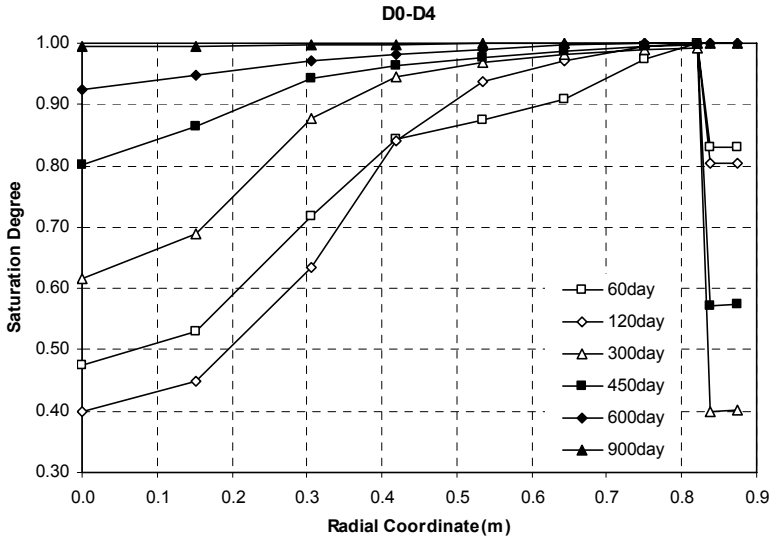

Figure 94

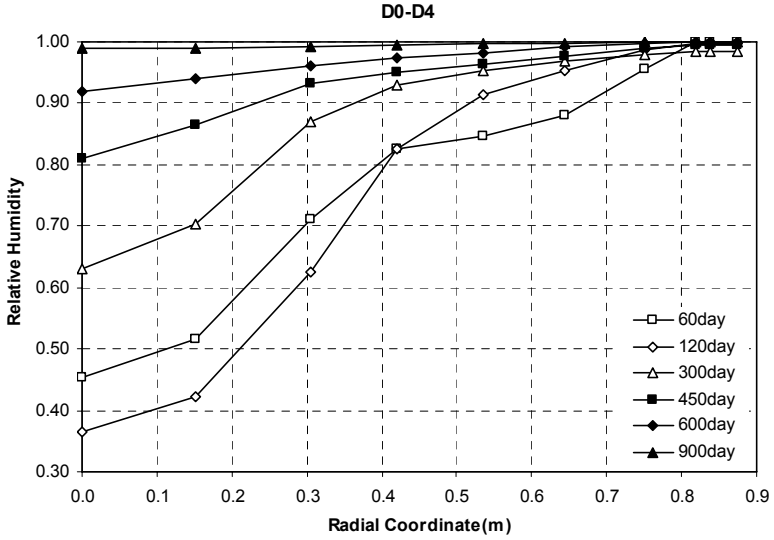

Figure 95

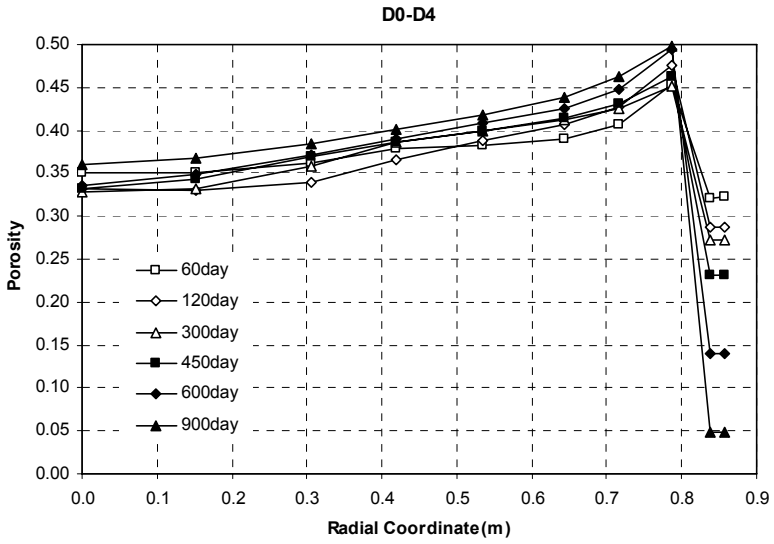

Figure 96

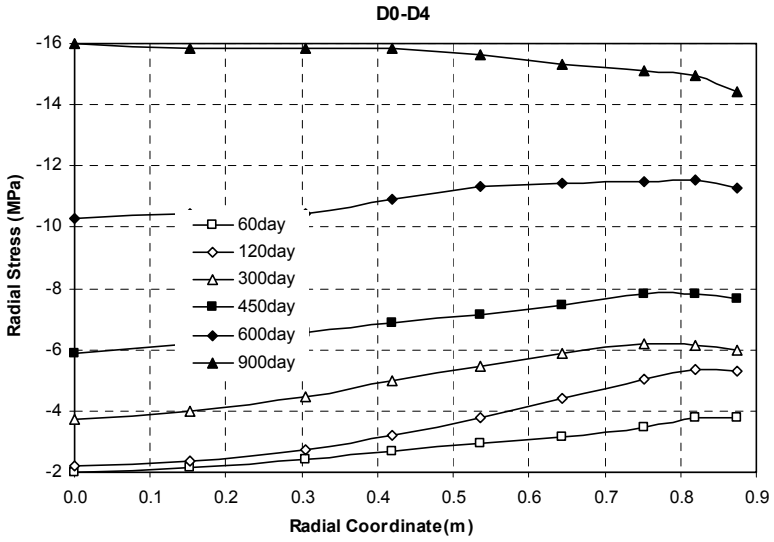

Figure 97

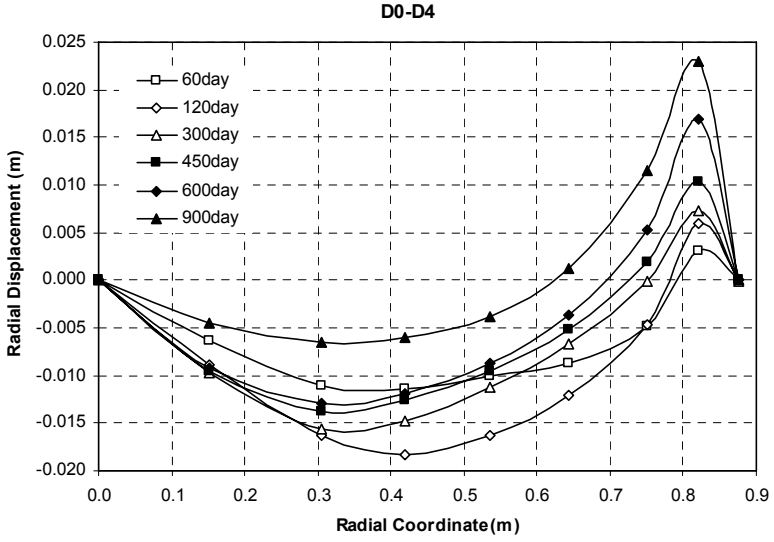

Figure 98

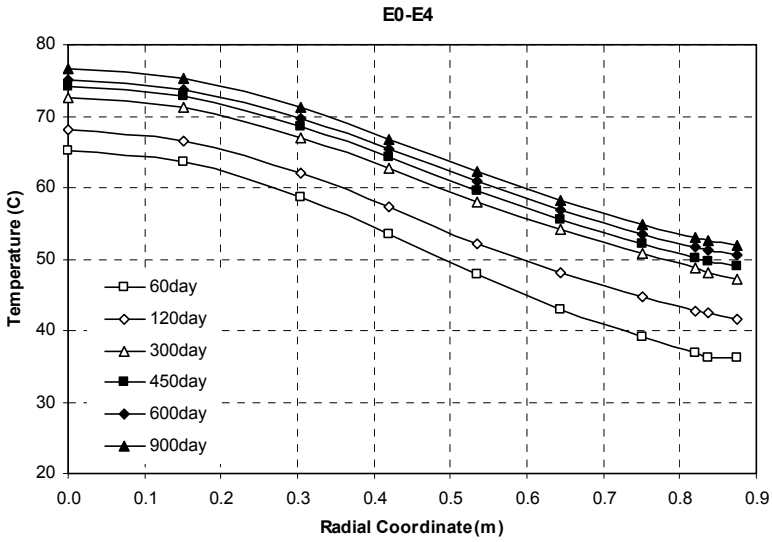

Figure 99

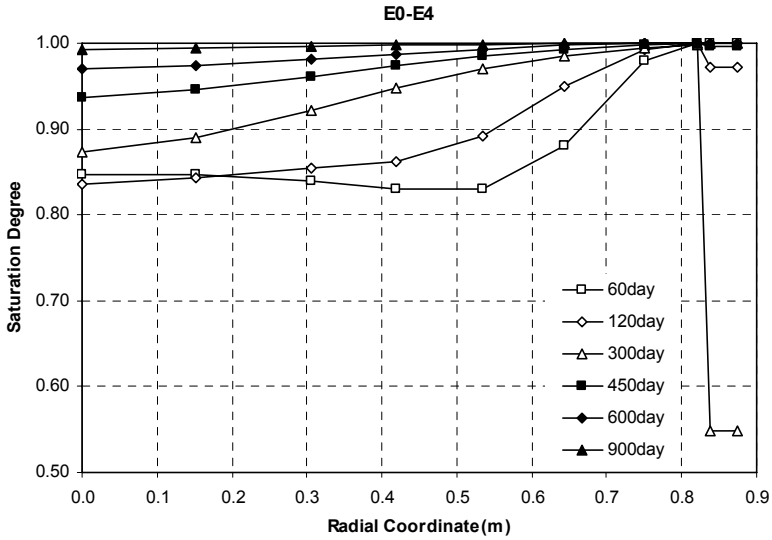

Figure 100

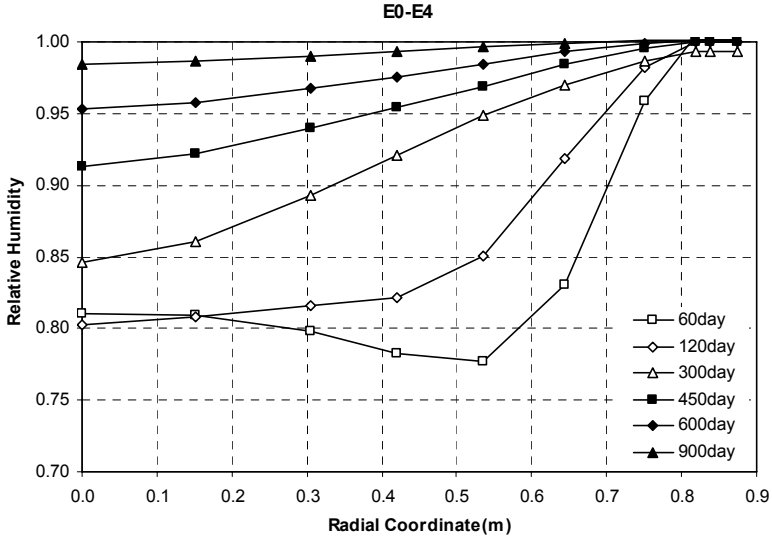

Figure 101

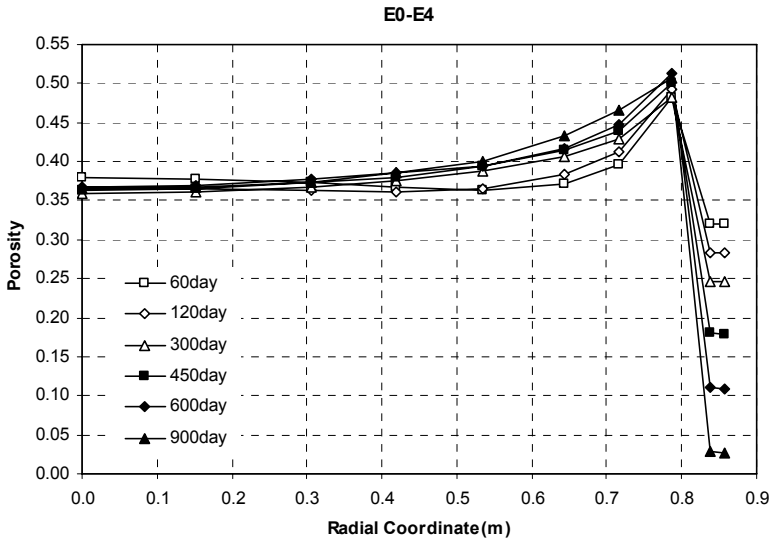

Figure 102

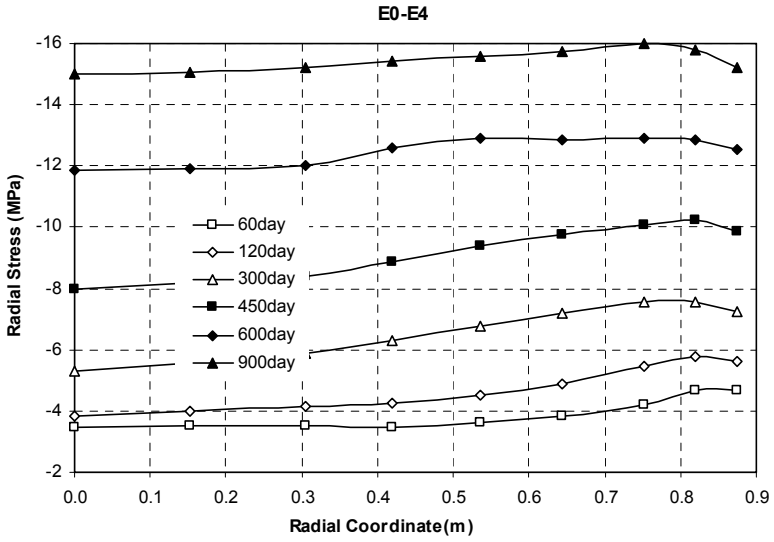

Figure 103

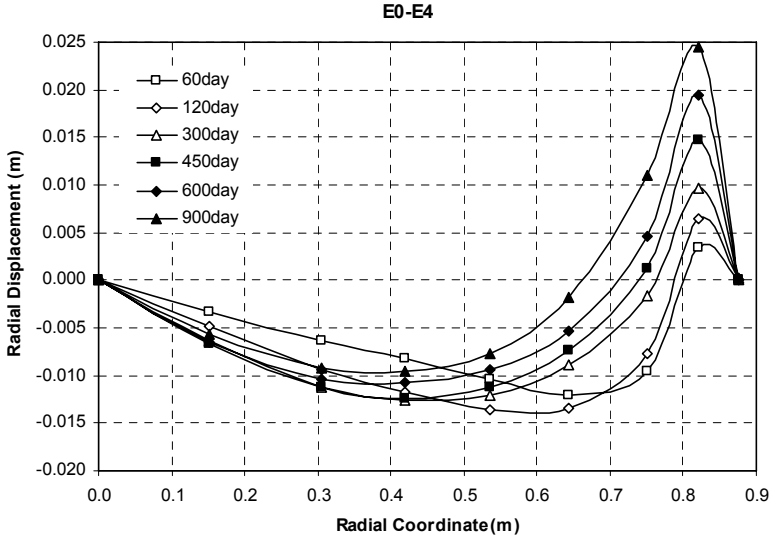

Figure 104

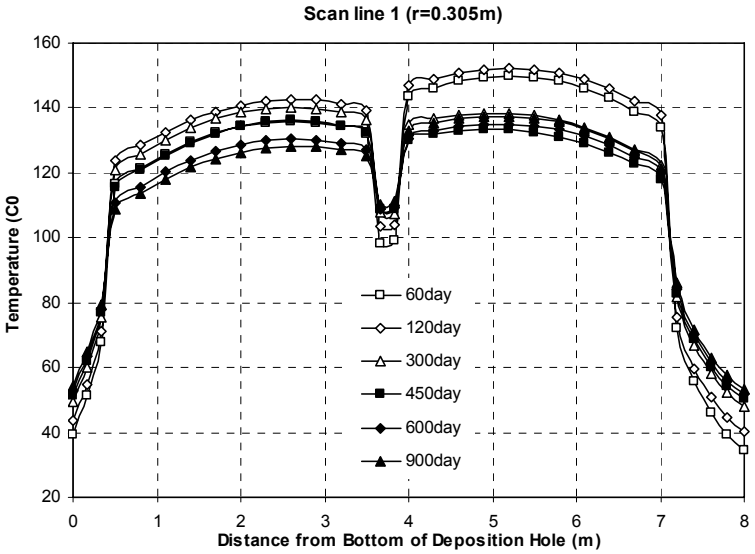

Figure 105

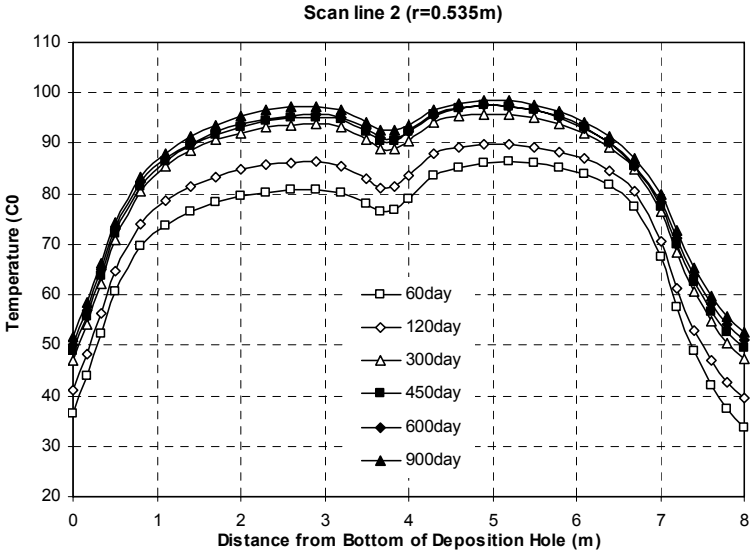

Figure 106

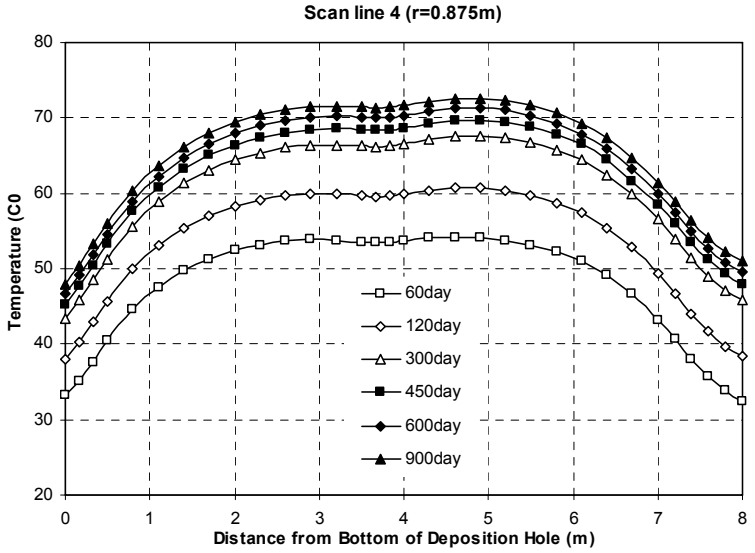

Figure 107

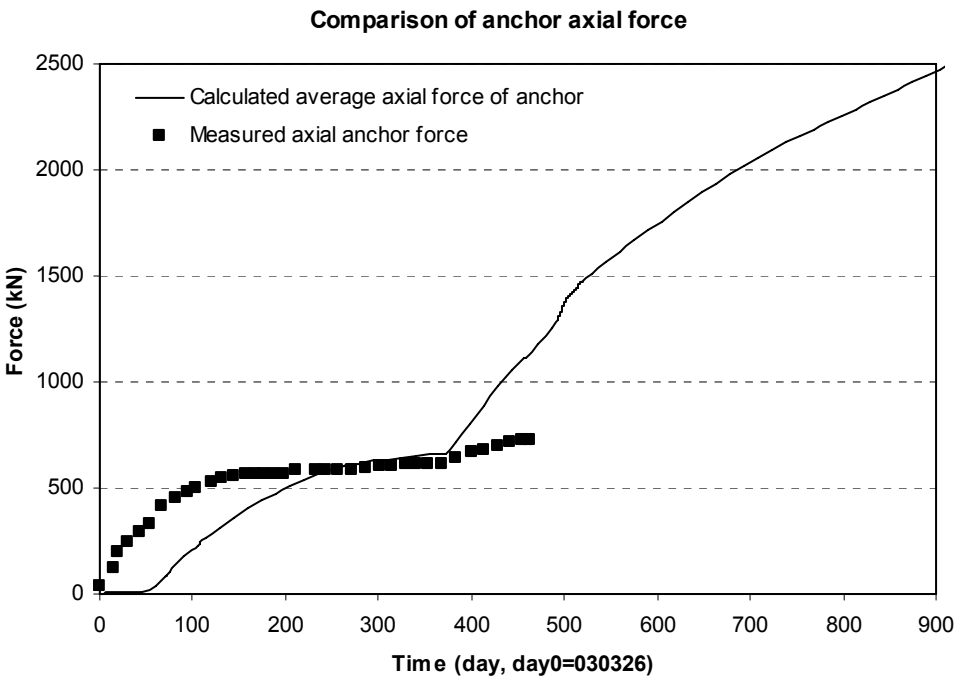

Figure 108

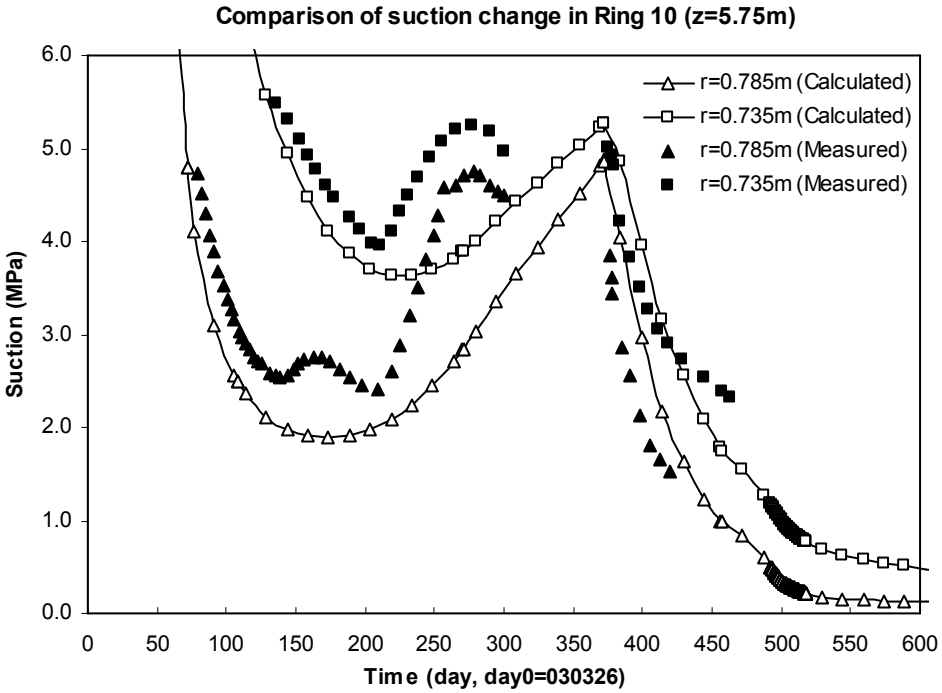

Figure 109

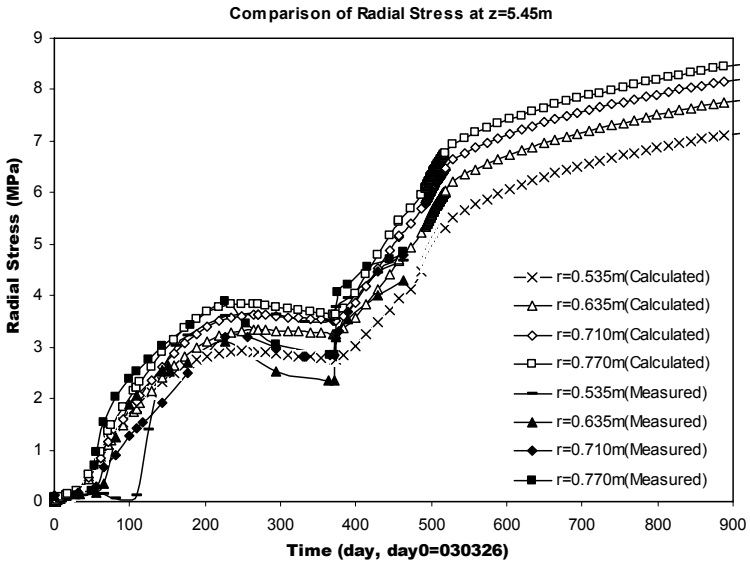

Figure 110

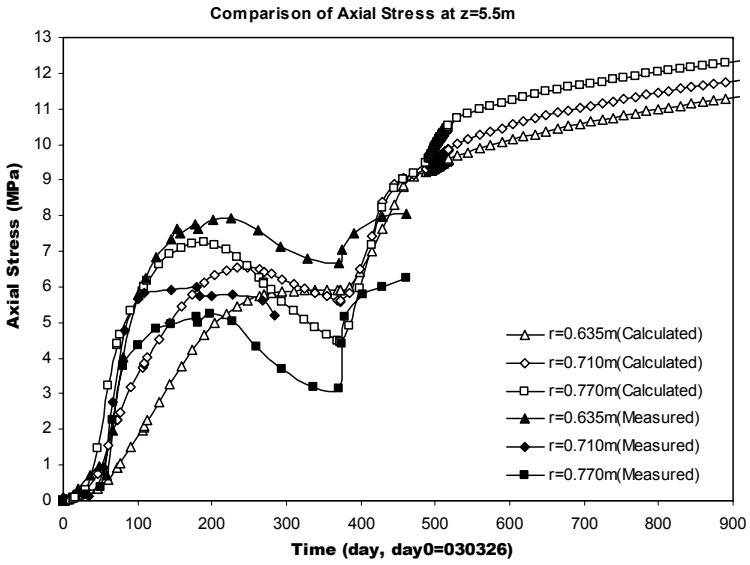

Figure 111

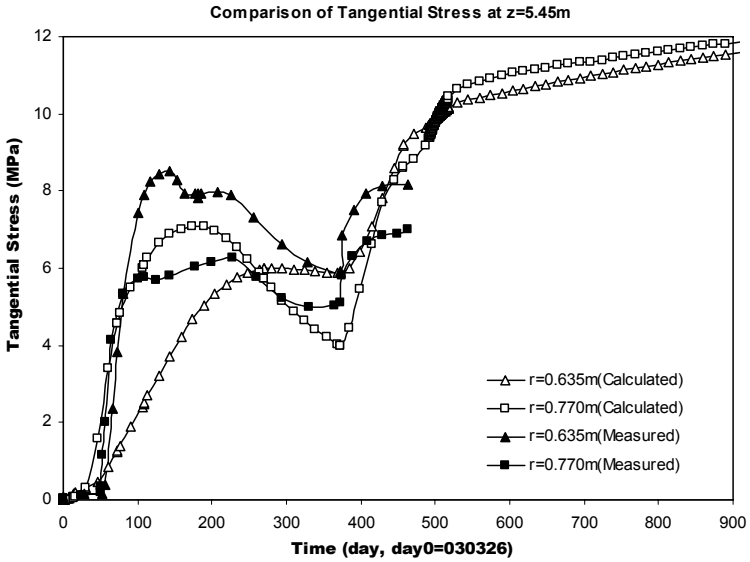

Figure 112

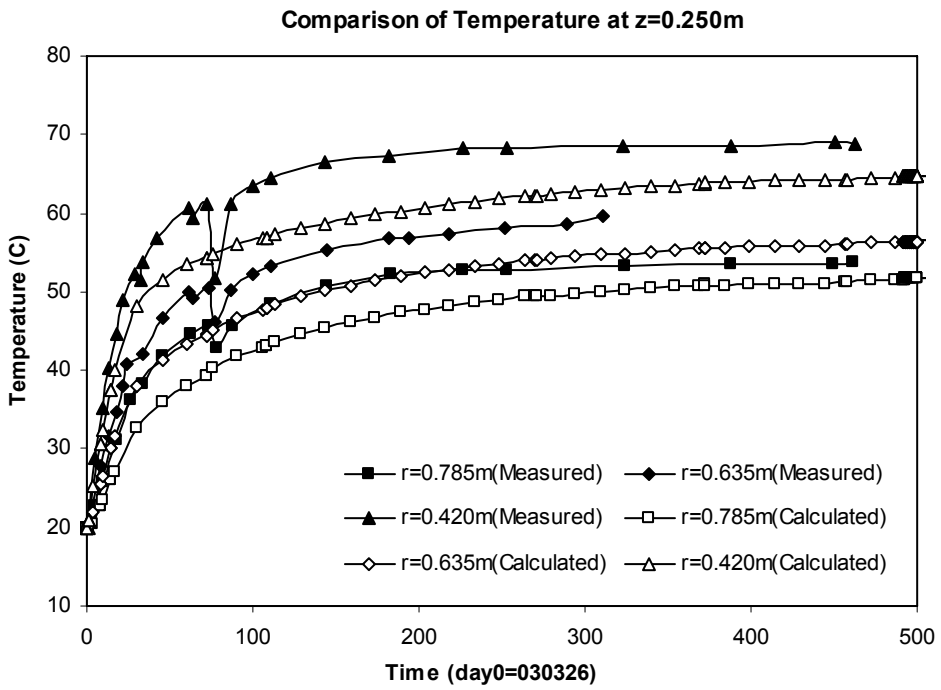

Figure 113a

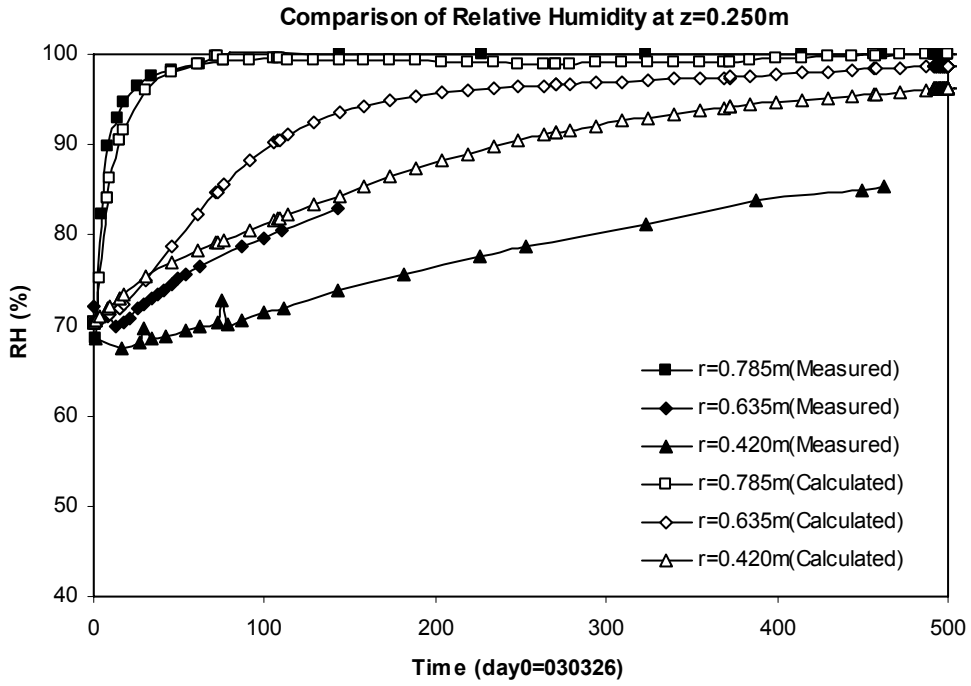

Figure 113b

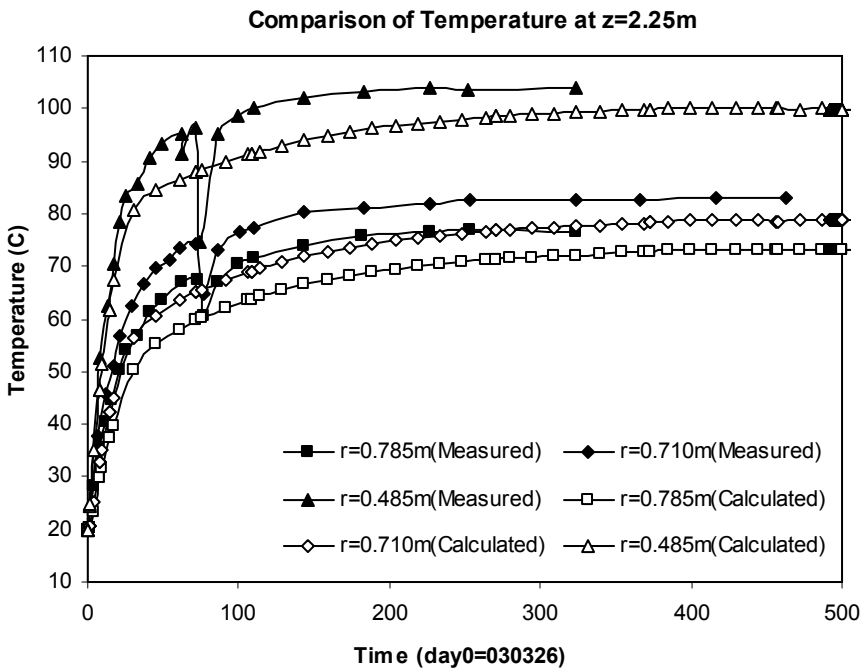

Figure 114a

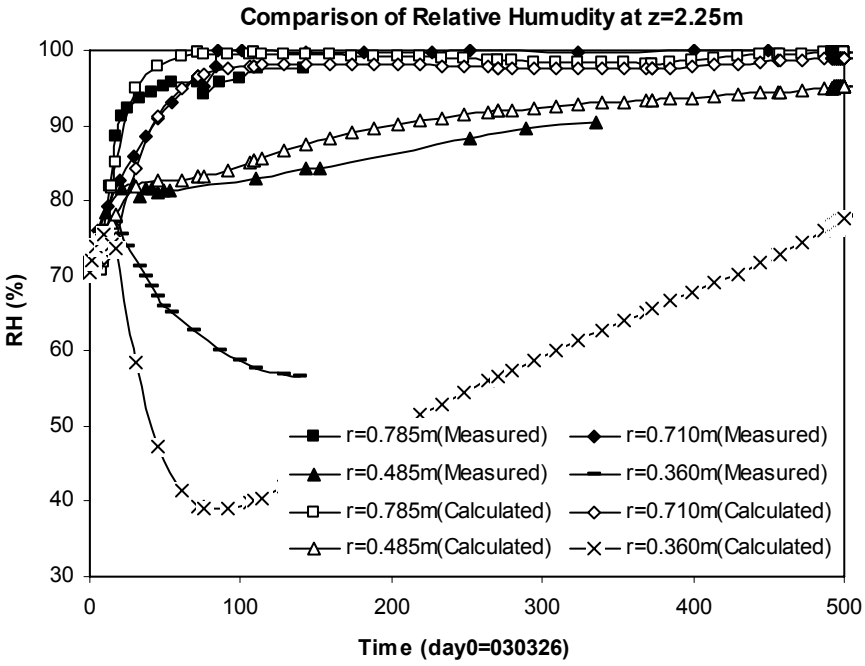

Figure 114b

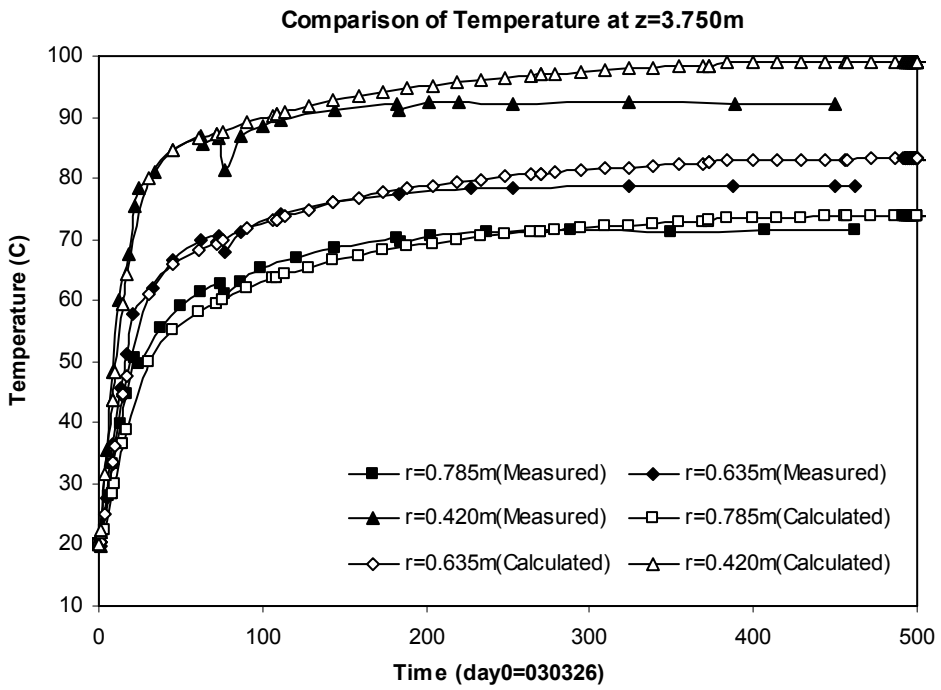

Figure 115a

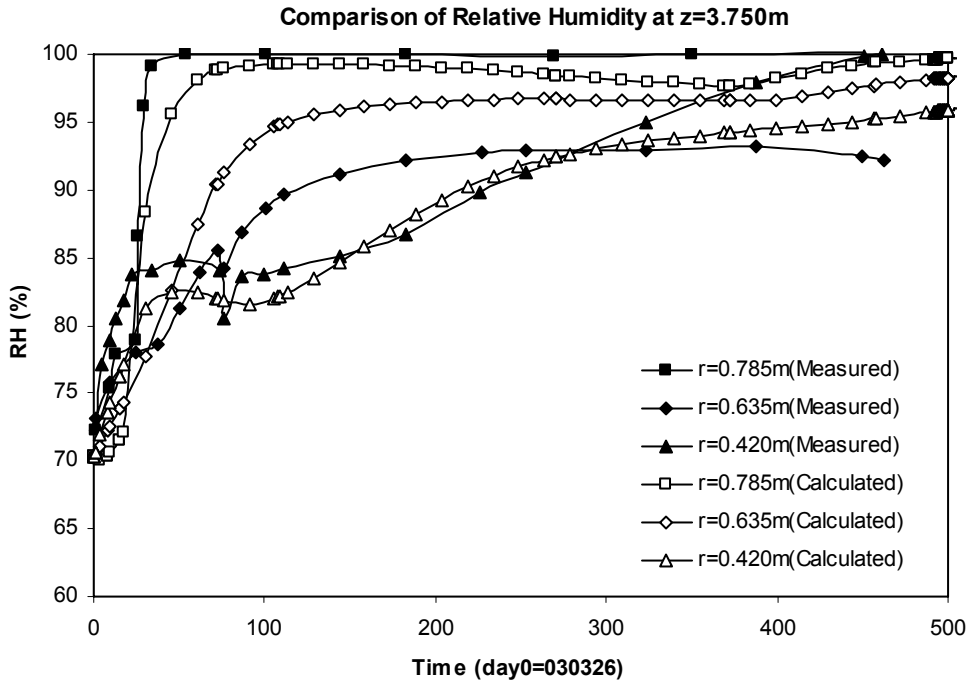

Figure 115b

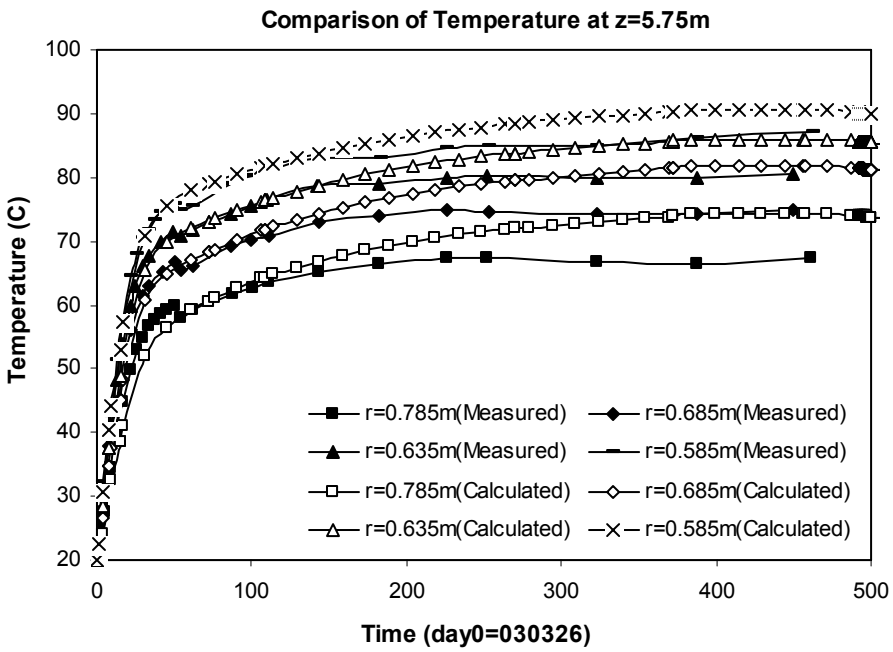

Figure 116a

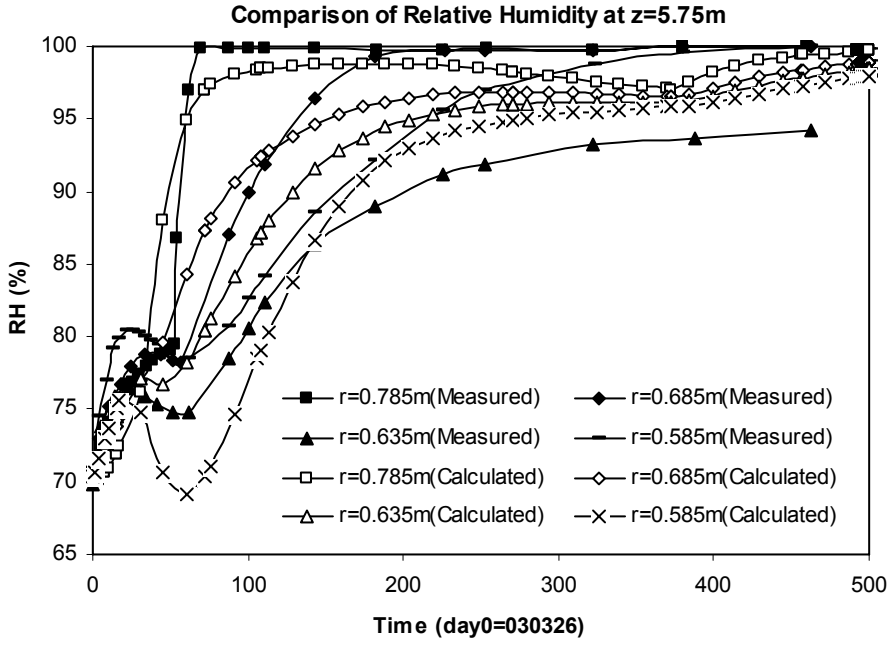

Figure 116b

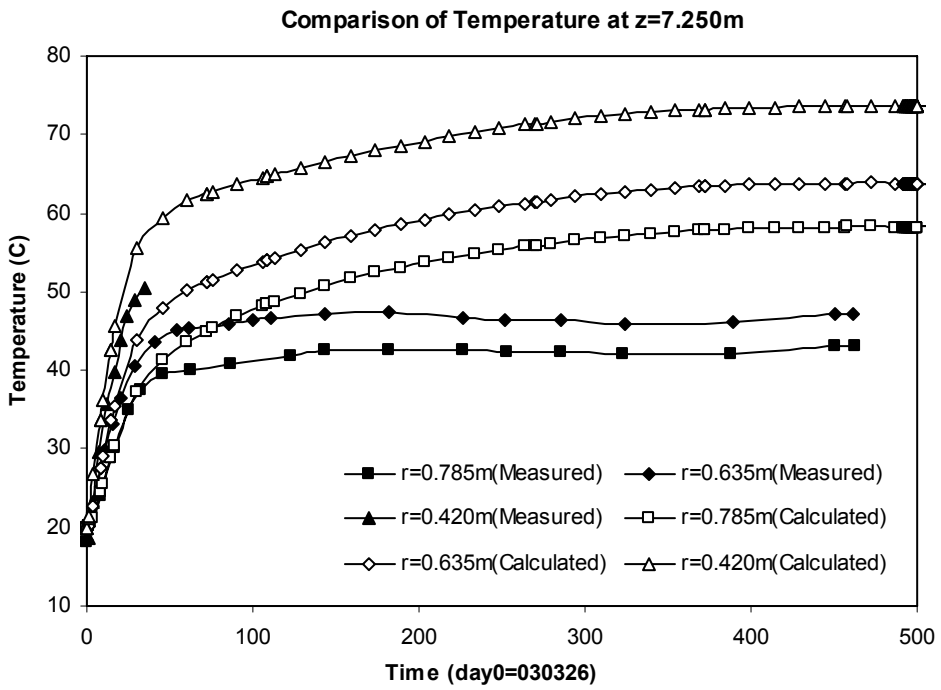

Figure 117a

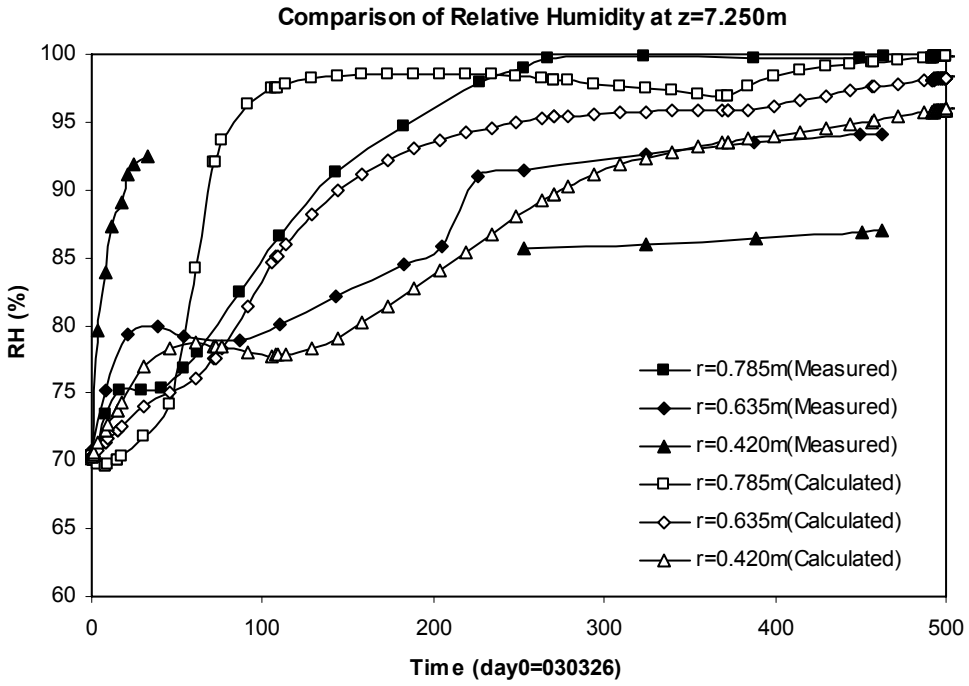

Figure 117b

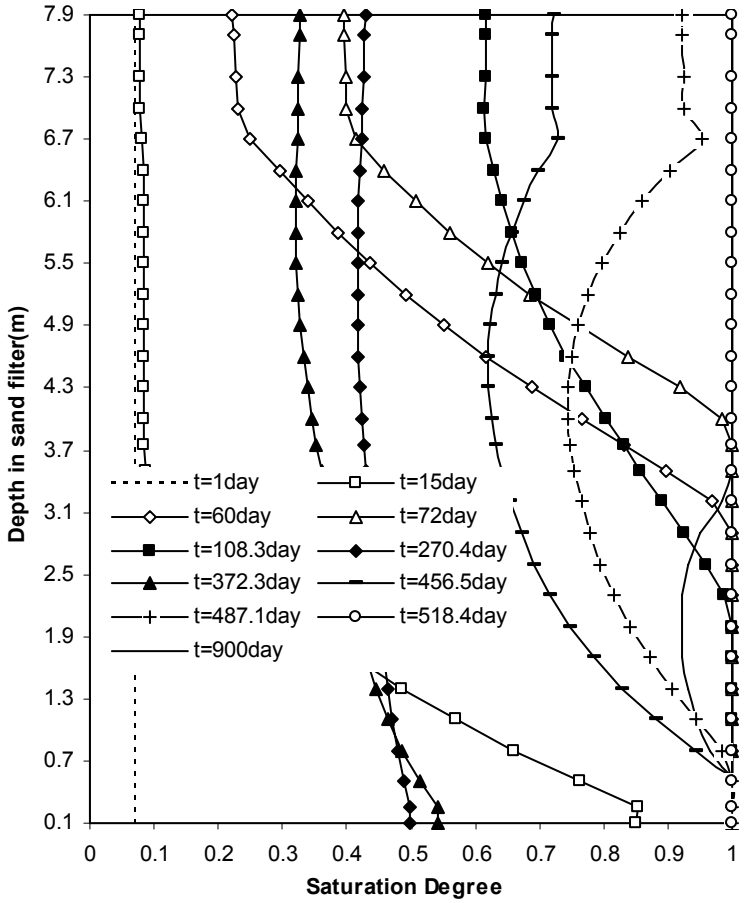
Depth in sand filter(m)
7.9
7.3
6.7
6.1
5.5
4.9
4.3
3.7
3.1
2.5
1.9
1.3
0.7
0.1
0
0.1
0.2
0.3
0.4
0.5
0.6
0.7
0.8
0.9
1
Saturation Degree
t=1day
t=15day
t=60day
t=72day
t=108.3day
t=270.4day
t=372.3day
t=456.5day
t=487.1day
t=518.4day
t=900day

Figure 118

3.7 Conclusions from Case 1 & Case 2 predictions

Two different analyses were initially performed: Case 1, using water flux as boundary condition and Case 2 applying a known water pressure at sand filter. Predictions reached day 900th. In general, both cases gave reasonable results, and the trends of the main variables were similar to the measured ones in both approaches. There are, however, some comparisons with measurements that are better in one Case than in the other.

Note that the parameters used for this Cases 1 & 2 are slightly different than the parameters used in section 2, when analysing Rings 9 & 10. That can be inferred from the comparison of figures 7 and 42 which correspond to the same situation. This is due to the fact that parameters have been changed during the development of the work, in order to improve the convergence conditions of the numerical analysis. Cases presented in section 2 were computed only up to day 500th, whereas cases included in section 3 cover all days, from the 1st till day 900th. Nevertheless, differences are negligible for the purpose of this modelling programme.

In case 1, the detailed comparison between measured and calculated variables for many points is fine, including the suction cycle in Ring 10 and the stress cycle in Ring 9. However, the applied flux between day 500th and 900th may be too high and thus the sand filter becomes saturated probably too fast. As a consequence of that, the stresses and the pore water pressure in the bentonite increase very fast after day 700th.

There are actually some results that do not agree very much with measurements, and they could be improved in future simulations. This is the case of variables in the bentonite in Cylinder 3 (z=7.25 m). Also, the variation of saturation degree in the sand shield seems to be not realistic, and the temperature computed at r=0.305 around upper heater does not match measurements. All those discrepancies are quite local. Finally, the prediction of the anchor force is well above the measured value in the anchors. That could be due to the numerical process used to computed that value (anchors are not simulated in the model, and their force is estimated in an indirect manner); but we also must recognise that mechanical results are of less quality than TH variables, most probably due to the uncertainties of the mechanical models involved.

As a general criterion for selecting the best prediction, due to the definition of each case one could expect that Case 1 would be convenient for simulating the initial period of the test (before day 500th), whereas Case 2 would be appropriate for analysing long term behaviour (i.e. day 900th). All those drawbacks have been overcome in Case 3, where a mixed boundary condition has been considered.

3.8 Conclusions from Case 3 predictions

In Case 3, an attempt to reproduce the actual boundary conditions in the field test has been performed. The assumptions adopted, described in section 3.4, represent quite reasonably the situation of the experiment. A compromise between the representation of field conditions and the corresponding difficulties of the analyses (i.e. convergence problems) has been adopted. Some of the parameters were adopted slightly different to those considered in Cases 1 & 2, in order to improve the convergence conditions of the analysis.

As a result of this compromise, Case 3 gives a good representation of the problem, showing a simulation of the suction cycle at Rings 9 & 10 as well as a reasonable prediction of the variables for long term conditions. That is, Case 3 combines the advantages of Case 1 and Case 2, and it is in fact a more consistent analysis. Therefore, it can be adopted as the final prediction for comparison purposes. It should be pointed out, however, that still some variables are not well reproduced, as in previous cases. That refers to the variables in Cylinder 3 (z=7.25 m), and temperature at r=0.305 around the upper heater. In addition to that, the prediction of the anchor force is still above the current value measured in the test. Those discrepancies suggest that the boundary conditions do not explain the differences between computed and measured values at these points, and most probably they are quite local and due to other causes not considered in the simulations.

4 Concluding Remarks

This report includes the results of the evaluation modelling programme of the TBT experiment performed by the group coordinated by ENRESA. The definition of the models and the parameters used in the computations follow the guidelines of the document by Clay Technology (2004).

The modelling work has been divided in two tasks: on the one hand it was required to understand what happened at Rings 9 & 10, which showed an unexpected cycle of suction and stresses. On the other hand, the temporal evolution of main THM variables along different scan-lines in the geometry was required.

Three cases have been considered in the analyses. First case refers to a simulation using a flux of water applied at the bottom of the sand shield as boundary condition. It is believed that this measurement is more reliable than the record of water pressure in that sand shield. Second case refers to an analysis using the water pressure as boundary condition. Both cases have been used not only for the simulation of the behaviour of Rings 9 & 10, but also for the prediction exercise. Case number 3 was computed between December 2004 and March 2005 and used a mixed boundary condition, applying first a fixed flux, and after 456.5 days a pore water pressure boundary condition, combining, therefore, cases 1 & 2.

The analysis of all cases regarding Rings 9 and 10 indicates that the cycle of suction and stresses was due to the lack of water available to saturate the bentonite after day 100^{th} approximately. This is the most consistent explanation that we can present so far. Prediction of the THM variables has been included and all cases give similar trend. Case 3 provides with a complete picture of the field experiment, whereas cases 1 & 2 are more appropriate for a particular period of time, i.e., Case 2 seems to be more appropriate for long term behaviour (i.e. day 900^{th}), and the cycle of suction/stress has been well reproduced with Case 1.

The difficulties found when interpreting the test suggest that a careful dismantling of the experiment would be necessary, in order to check some of the assumptions considered in the analyses. During the period of time remaining before dismantling, it would be convenient to keep all controlling variables constant (i.e. heat power, water pressure, etc.).

From the figures of section 3 it becomes evident that at 900 days (and even before) the bentonite reaches a very high degree of saturation. That result should be checked with "in situ" measurements, in order to decide when to stop the test (in other experiments the final stages of saturation of the bentonite have been slower than the predictions).

The laboratory experiments being performed at CEA and at Ciemat constitute an important source of information as far as the behaviour of bentonite at high temperatures is concerned. The numerical simulation of those experiments will help in the development and understanding of the fundamental laws that are required for improving the analysis of the experiment in the near future.

References

Clay Technology (2004) – (H. Hökmark, B. Fälth, M. Åkesson). TBT – Evaluation Modeling Program, Step 2, proposal for September – November 2004. August.

Clay Technology AB

Ideon Research Center

Lund, Sweden

TBT – Evaluation Modeling Step 2

-

Mechanical behaviour of Ring 9 and 10

December 2004

Mattias Åkesson

Harald Hökmark

Contents

1 Introduction and background

1.1 TBT experiment

ANDRA is performing a Temperature Buffer Test in granitic rock at Äspö Hard Rock Laboratory, Sweden. The main objective is to improve the understanding of the Thermo-Hydro-Mechanical properties and behaviour of bentonite-based buffer materials during the saturation process, in particular in the high temperature range above 100°C. The experiment includes two individually powered heaters, stacked on top of each other but separated by a 0.5 m ring-shaped bentonite block. The design is shown in Figure 1-1 below.

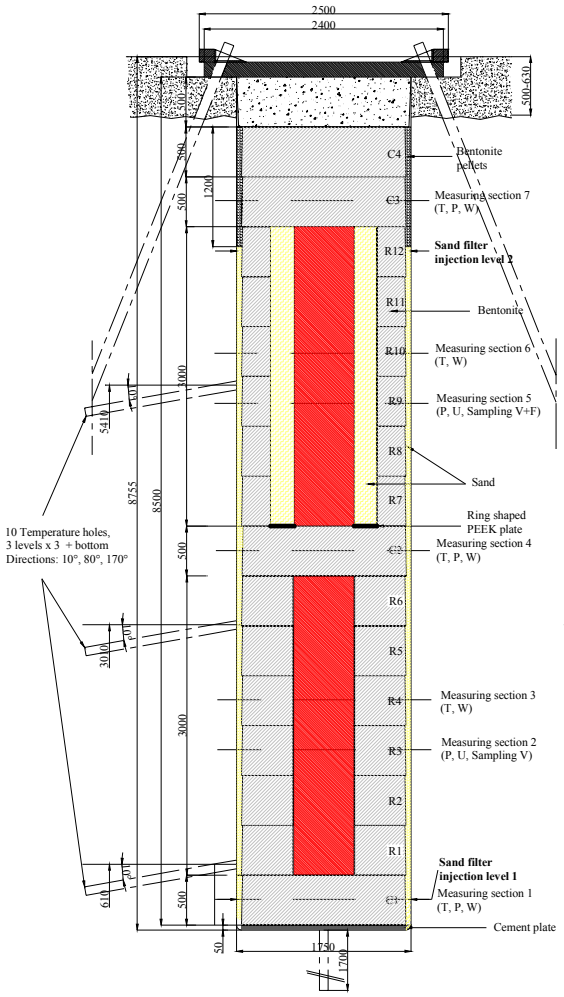

Figure 1-1. *Design of TBT*

The experiment includes an extensive instrumentation to monitor temperatures, total pressures, pore pressures, relative humidities, etc. /Goudarzi et al., 2003/

1.2 Modeling

1.2.1 General

The TBT experiment has well-defined boundary conditions and is extensively instrumented. In particular the horizontal sections at mid-height of the two heaters provide convenient test grounds for conceptual and numerical THM models. Prior to test start, a Predictive Modeling Program was specified /Hökmark and Fälth, 2002/. Clay Technology and other modeling teams made blind predictions based on the specifications in that program /Hökmark et al, 2004/. The present report regards a set of evaluation calculations made when some of the trends of the test have been documented.

1.2.2 Evaluation modeling phase

The experiment (heat generation) started in March 2003 and has been producing data for about 500 days up to the present day. In April 2004 an evaluation modeling phase was initiated and an evaluation modeling program was specified /Hökmark, Fälth, Åkesson, 2004a/. As a first step, predictions of the effects of a possible 750 W increase in upper heater thermal output were asked. The first step results indicated that the effects (for instance on the speed of buffer resaturation) would not be clear enough to be useful with regard to the general test objectives. The modelling teams recommended that the conditions should be kept as constant as possible.

A second version of the program was issued August 2004 / Hökmark, Fälth, Åkesson, 2004b/. The August program focused on the hydro-mechanical behavior around the upper heater, where disturbances in the evolution of stress and suction had been observed. The present report regards modeling work performed in response to that modeling program.

2 Objectives

The main issue is to reproduce the behavior of the hydro-mechanical behavior of the bentonite in rings 9 and 10.

- Analysis of radial stress development in Ring 9. This point should include a suggestion of qualitative description of the hydro-mechanical sand-bentonite interaction as well as actual attempts to reproduce the experimental findings shown in Fig. A30 and Figs. A37-A39.
- Prediction of temperature, saturation, RH, porosity, stresses and displacements on scan-line A1-A4.

Scan-line output should be given for the following days after TBT start:

60, 120, 300, 450, 600, 900

Figure numbers given above refer to the modeling guidelines /Hökmark et al., 2004/.

3 Model description

3.1 General

The modeling work was performed with the finite element program, Code_Bright version 2.2. For the specific problem, an axi-symmetric 1D geometry was applied. The problem constitutes a fairly complex THM process. In order to simplify the numerical treatment, HM and TH-models where analyzed separately.

The modelling approach used here is based on the assumption that the variation in stress and suction observed in rings 9 and 10 was a consequence of disturbances in the supply of water to the sand filter. The uncertainties regarding the hydraulic pressure conditions the sand filter was represented by a "dry period" from day 234 to day 373. During this intermediary period the liquid pressure in the sand filter was fixed at a specified negative value (models No 1- No4 and models No 6 and No 7, c.f. Table 3-7), or alternatively, the hydraulic boundary was kept close, so that the liquid pressure was handled as a free parameter (model No 5, c.f. Table 3-7).

3.2 Geometry

The model geometry is shown in Figure 3-1. The shield, buffer and filter were divided into 20, 25 and 5 elements respectively.

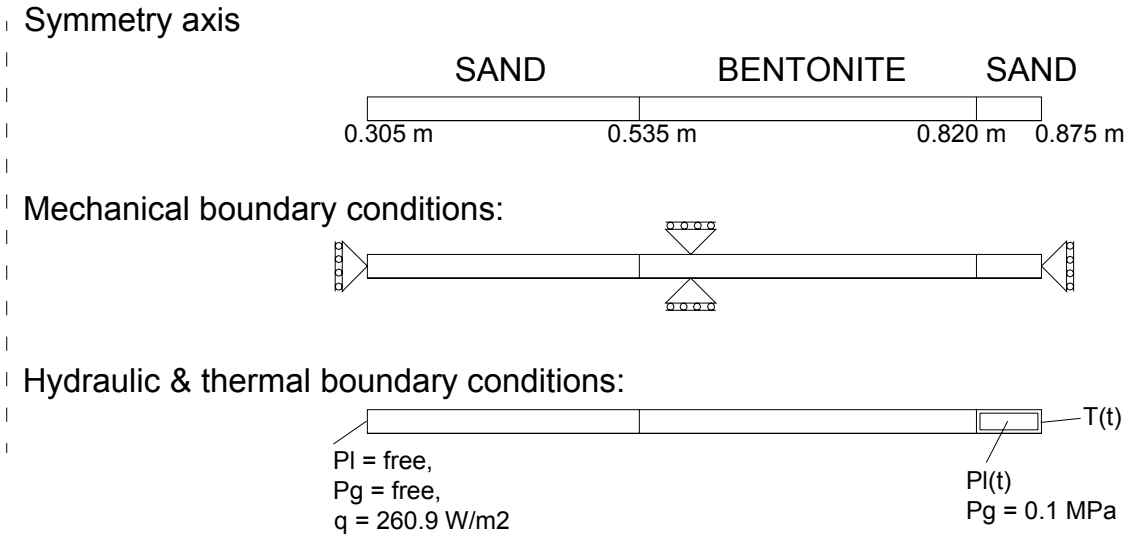

Figure 3-1. *1D-model geometry.*

3.3 Initial and boundary conditions

The initial conditions are presented in Table 3-1. The liquid pressure, -45 MPa, corresponds to a degree of saturation of 85 % in the bentonite.

Table 3-1. Initial conditions.

Material	Temperature	Liquidpressue	Gas pressure	Stresses	Porosiy
Sand – shield	20 °C	-45 MPa	0.1 MPa	-0.5/-0.5/-0.5 MPa	0.30
Sand – filter					0.36
Bentonite					0.368

The mechanical boundaries consisted of roller boundaries (zero normal displacement) above and below the geometry as well as at the heater and at the rock wall.

The only hydraulic boundary was applied as a surface condition over the sand filter. The reason for choosing a surface boundary condition was mainly numerical, in order to eliminate the problem of water transport in the filter with artificially low permeability (see below). This simplification can by justified by the notion that the main part of water transport into the filter occur axially.

The hydraulic boundary history was divided into four periods (see Figure 3-2): the first with dry conditions, the second with saturated conditions, the third period with dry conditions and finally a fourth period with saturated conditions. Different versions of the dry period have been investigated: either with constant liquid pressure (-45 or –8 MPa) or with closed boundary so that the liquid pressure is a free parameter.

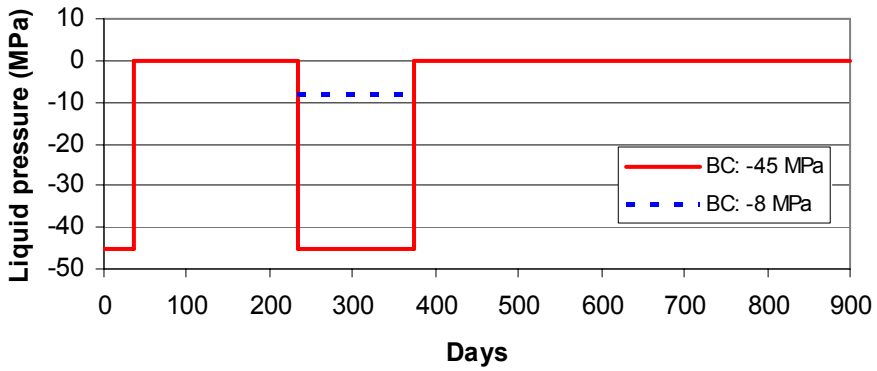

Figure 3-2. *Hydraulic boundary condition over sand filter.*

Two thermal boundary conditions were applied: a constant heat load of 260.9 W/m^2 at the inner side of the sand shield; and a varying temperature at the outer side of the sand filter (see Figure 3-3). This development was derived through an analytical solution of the heat transport. This method was previously described by /Hökmark and Fälth, 2003/.

Finally, a boundary condition for gas was also applied over the sand filter by keeping the gas pressure constant at atmospheric pressure. The only exception was the model with closed hydraulic boundary. During the dry period both liquid and gas pressure were treated as free parameters.

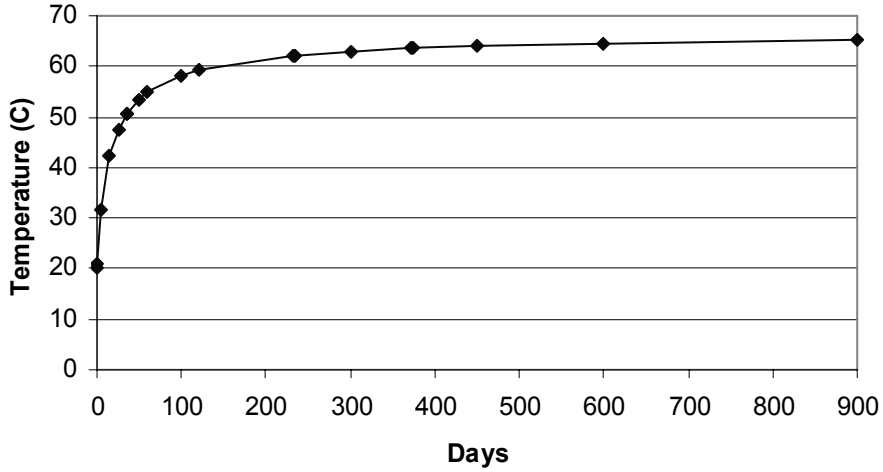

Figure 3-3. *Thermal boundary condition at the rock wall.*

3.4 Material properties

The retention, thermal and hydraulic properties of the modeled materials is presented in Tables 3-2 and 3-3. These values follow previous modeling tasks of the TBT experiment performed by Clay Technology /Fälth and Hökmark, 2004/. It should be noted that the permeability is kept constant even if the porosity is changing.

Table 3-2. Retention properties.

Material	Law	P_0	λ	P_m	λ_m
Sand – shield	$S_r = \left\{1+\left(\frac{P_g - P}{P_0 \cdot \left(\frac{\sigma}{\sigma_0}\right)}\right)^{\frac{1}{1-\lambda}}\right\}^{-\lambda} \left\{1-\frac{P_g - P}{P_m}\right\}^{\lambda_m}$	0.01	0.6	700	1.1
Sand – filter		0.005	0.6	700	1.1
Bentonite		100	0.5	800	1.2

Table 3-3. Thermal & hydraulic properties.

Material	Solid phase density [kg/m^3]	Intrinsic permeability* [m^2]	Liq rel. perm. $k_{rl} = S_r^{\delta_l}$	Vap. tourt.	Solid phase spec. Heat [J/kgK]	Heat cond. [W/mK] $\lambda = \lambda_{dry}(1-S_r) + \lambda_{sat} S_r$	
			δ_l			λ_{dry}	λ_{sat}
Sand – shield	2650	$1 \cdot 10^{-19}$	3	0.6	800	0.5	1.7
Sand – filter	2650	$1 \cdot 10^{-19}$		0.6	800	0.5	1.7
Bentonite	2780	$1.6 \cdot 10^{-21}$		0.6	800	0.3	1.2

* Constant permeability

Estimates of the mechanical properties for the sand and the bentonite are shown in Tables 3-4, 3-5 and 3-6.

The sand was modeled as a linear elastic material with a Young modulus of 25 MPa and a Poisson's ratio of 0.4. The choice of the linear elastic law is possibly rather simplistic, therefore preliminary attempts have also been made with a porous elastic description of the sand. In this case, a κ_i-value of 0.1 has been chosen.

Table 3-4. Mechanical properties of sand.

ν	E / κ_i
0.4	25 MPa / 0.1

The bentonite was modeled as an elastoplastic material in accordance with the Barcelona Basic Model. The choices of elastic parameters was mainly based on results from compression tests, free swelling and saturated swelling pressure tests with MX80. The plastic parameters, however, were generally taken from one of the Code_Bright tutorial examples. One exception, though, was the critical state line parameter M. In three of the HM-models (see below), a realistic low value of 0.36 was used. This value is derived from results from triaxial tests with MX80.

Table 3-5. Elastic properties of bentonite.

κ_{i0}	α_i	κ_{s0}	α_{ss}	p_{ref}	α_{sp}	K_{min}	ν
0.25	-0.022	0.28	0	0.1	-0.15	10	0.2/0.4

Table 3-6. Plastic properties of bentonite.

$\lambda(0)$	r	β	ρ	k	p_{s0}	p^c	M	α	e_0	p_0^*
1.5	0.75	0.05	0	0.1	0	0.1	1.5/0.36	0.194	0.582	16/8

3.5 Model versions

In order to capture as many characteristics as possible without employing a fully coupled model, a series of simpler models, either MH or TH, have been analyzed (Table 3-7). The first three versions simulated the hydro-mechanical processes with constant temperature and constant gas pressure. The two subsequent versions simulated the thermo-hydrodynamic processes only. Finally, two additional HM-models with new types of variations were analyzed.

The alternative settings of the hydraulic boundary were described in section 3.3 above. Four other aspects with implication for the mechanical processes have been varied: (1) the Poisson's ratio (ν), (2) the yield surface extension of the bentonite, (3) the temperature and (4) the elastic property of the sand.

Reported values of ν for MX80 varies between 0.14 /Kalbantner and Johanesson, 2000/ and 0.4 /Börgesson et al., 1995/. Results indicate also that ν may increase with increasing degree of saturation. Two different values of ν were therefore applied in this study.

Two different extensions of the bentonite yield surface were tested: one far reaching surface, with a high critical state line parameter (M) and a high apparent preconsolidation mean stress (p_0^*). The reason for extending the surface to such unrealistic levels is simply to avoid plastic conditions. In model No 3, 6 and 7, however, a reasonable extension was modeled, even though the value of p_0^* should be viewed as a guess.

The HM models were executed at isothermal conditions and the default temperature was set to 20 °C. However, since the temperature affects the water viscosity, and thereby the rate of hydration and the buildup of stresses, the latter models were run at a more realistic level of 70 °C.

Finally, the effects of the mechanical properties of the sand were tested as described in section 3.4 above.

Table 3-7. Model compilation with variations.

Model	Processes	Dry period p_l BC	Bentonite v	Bentonite yield surface	Sand
No 1	HM (T = 20°C)	-45 MPa	0.4	p_0^* = 16 ; M = 1.5	E=25 MPa
No 2	HM (T = 20°C)	-8 MPa	0.2	p_0^* = 16 ; M = 1.5	E=25 MPa
No 3	HM (T = 20°C)	-8 MPa	0.2	p_0^* = 8 ; M = 0.36	E=25 MPa
No 4	TH	-8 MPa	-	-	-
No 5	TH	Closed	-	-	-
No 6	HM (T = 70°C)	-8 MPa	0.2	p_0^* = 8 ; M = 0.36	E=25 MPa
No 7	HM (T = 70°C)	-8 MPa	0.2	p_0^* = 8 ; M = 0.36	κ_i=0.1

4 Results

4.1 Stress and displacement developments

Calculated developments of stresses in model No 1 – No 3 and No 6 – No 7 are compared with experimental results in Figure 4-1 – Figure 4-5, respectively. The radial distances of the shown model results correspond to sensor positions. Radial, axial and tangential stresses are displayed separately.

Model displacements at the inner and outer sand/bentonite interfaces in model No 1 – No3 and No 6 – No 7 are shown in Figure 4-6.

Details of plastic conditions in model No 3 are illustrated in Figures 4-7 through 4-9. Figure 4-7 shows how plasticity has occurred, disappeared and recurred along the scan line. Stress paths in the (p,q, s) – space for two points are shown in Figure 4-8. The inner point, at r = 0.635, corresponds to an experimental position with stress sensors measuring in all three directions. The calculated stress path can therefore be compared with experimental results in the (p,q) plane (Figure 4-9).

4.2 Suction, RH and saturation developments

Calculated developments of suction values in model No 4 – No 6 are compared with experimental results in Figures 4-10 through 4-12, respectively. The radii of the shown model results correspond to sensor positions. Among the HM models, suction data is only presented for model No 6. Models executed for 20 °C give significantly higher suction values due to restrained hydration.

Calculated developments of relative humidity values in model No 4 – No 5 are compared with experimental results in Figure 4-13 – Figure 4-14, respectively. The radial distances of the shown model results correspond to sensor positions. Results from the HM models are omitted due to the isothermal conditions in these models.

Calculated developments of degrees of saturation in model No 3, No 4 and No 6 are shown in Figure 4-15 – Figure 4-17.

4.3 Thermal developments

Temperature scan-lines for model No 4 are compared with experimental results from ring 10 in Figure 4-18.

4.4 Scan-lines

Figures 4-19 through 4-24 show stresses, porosity and suction along the radial scan-line.

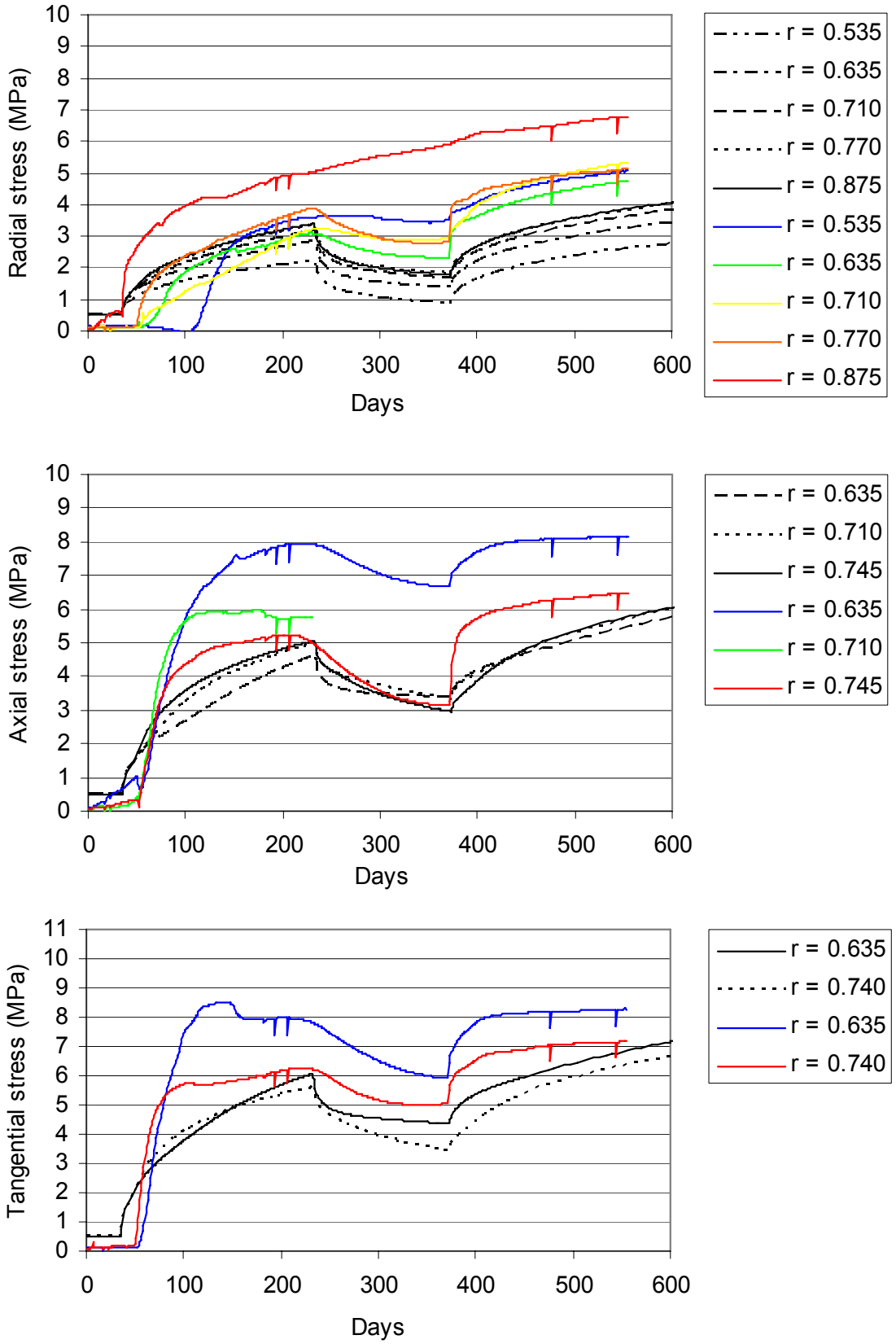

Figure 4-1. *Stress data from HM-model No 1 (black) and measured stresses (colored).*

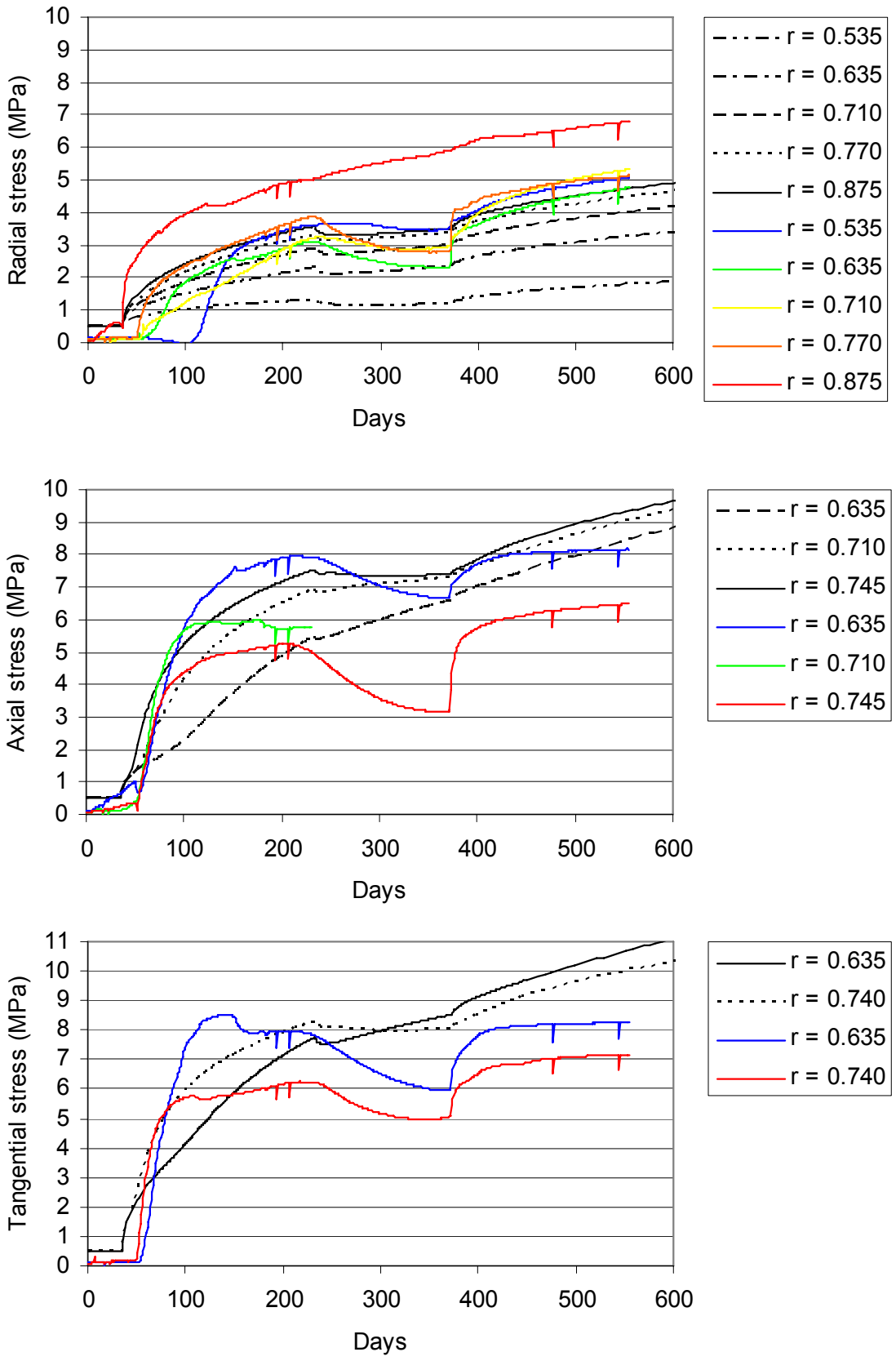

Figure 4-2. *Stress data from HM-model No 2 (black) and measured stresses (colored).*

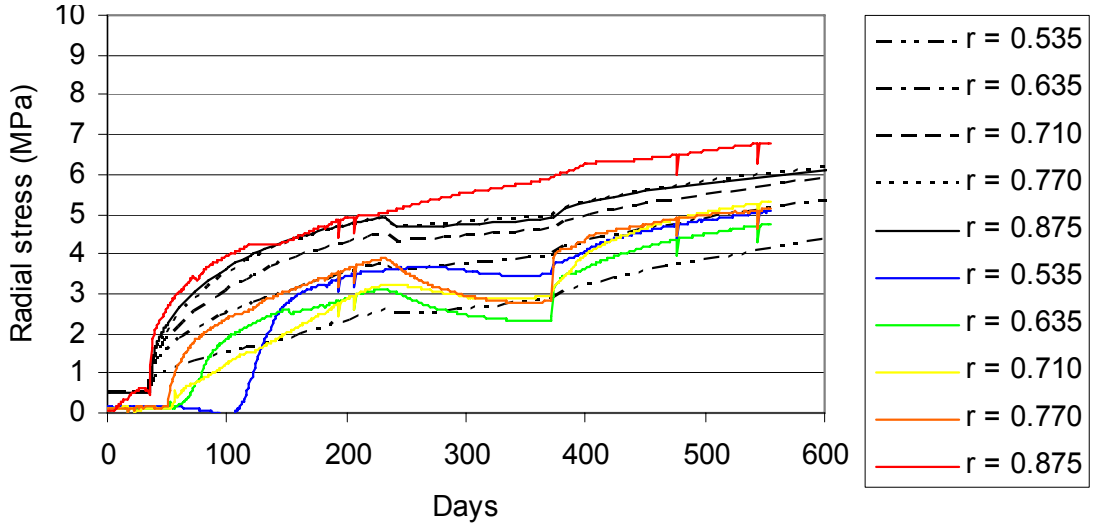

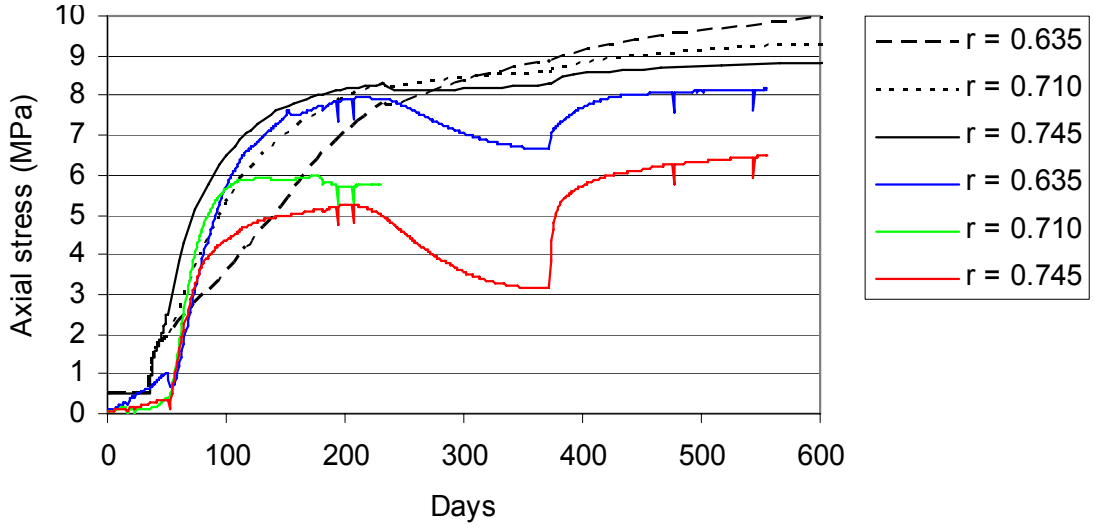

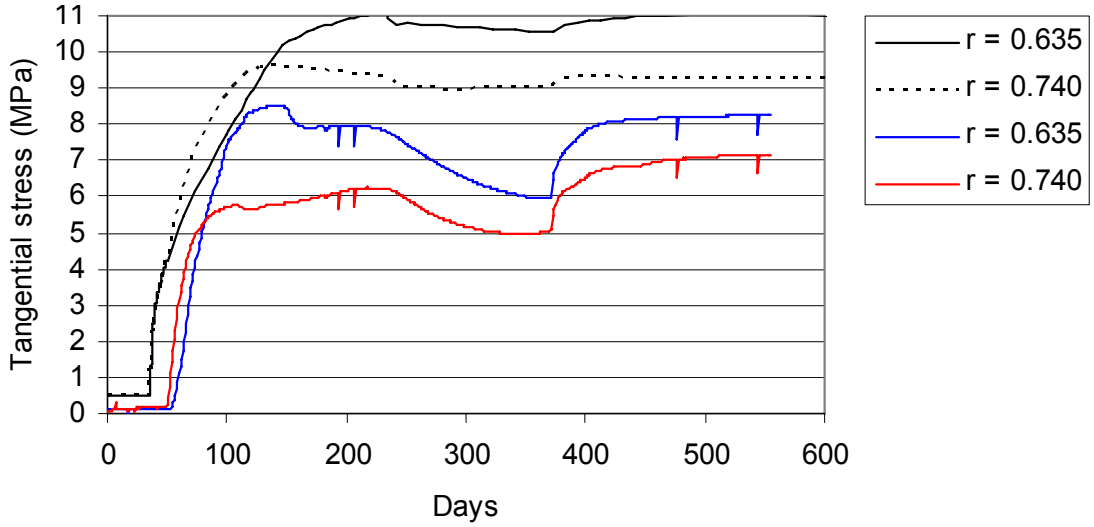

Figure 4-3. *Stress data from HM-model No 3 (black) and measured stresses (colored).*

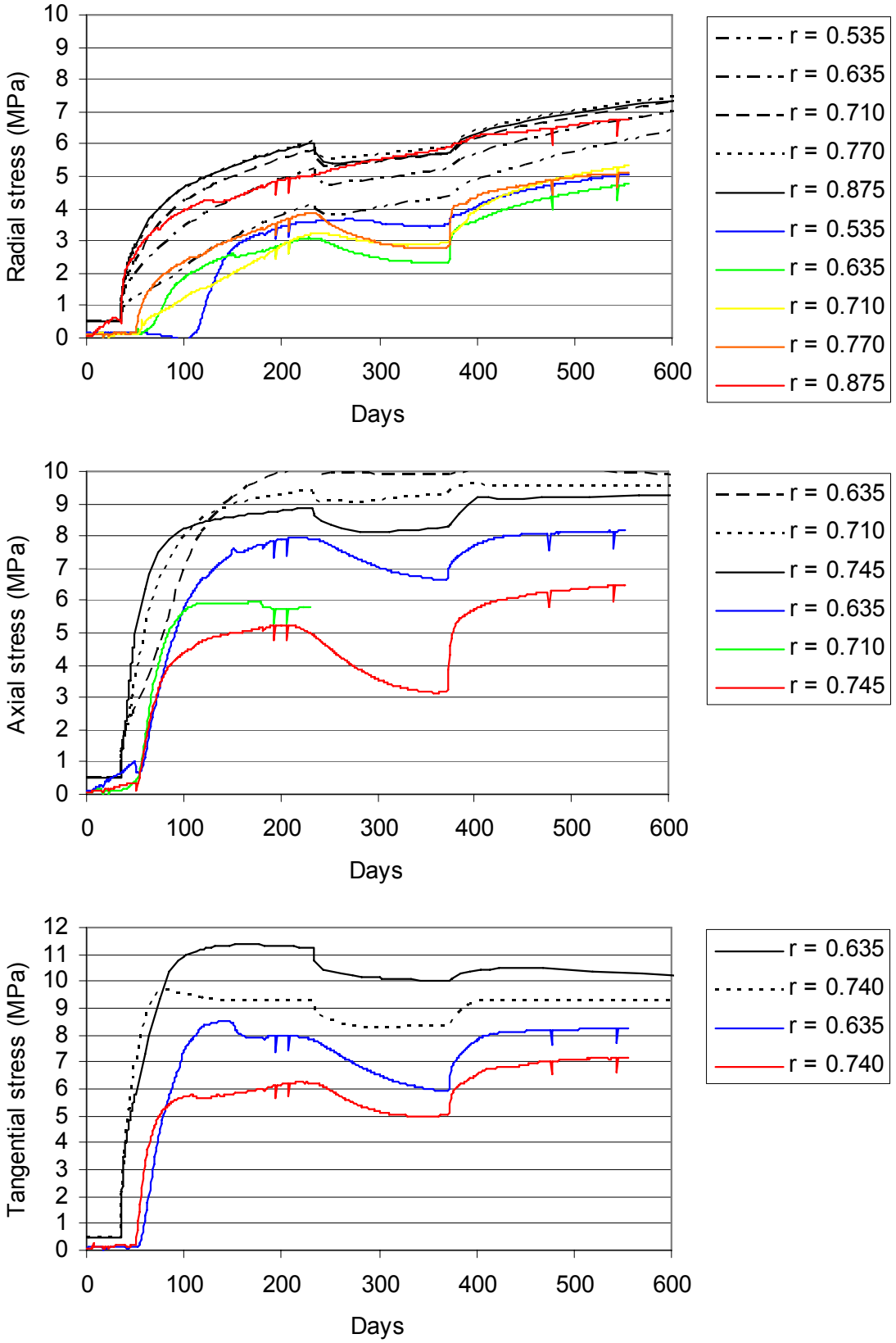

Figure 4-4. *Stress data from HM-model No 6 (black) and measured stresses (colored).*

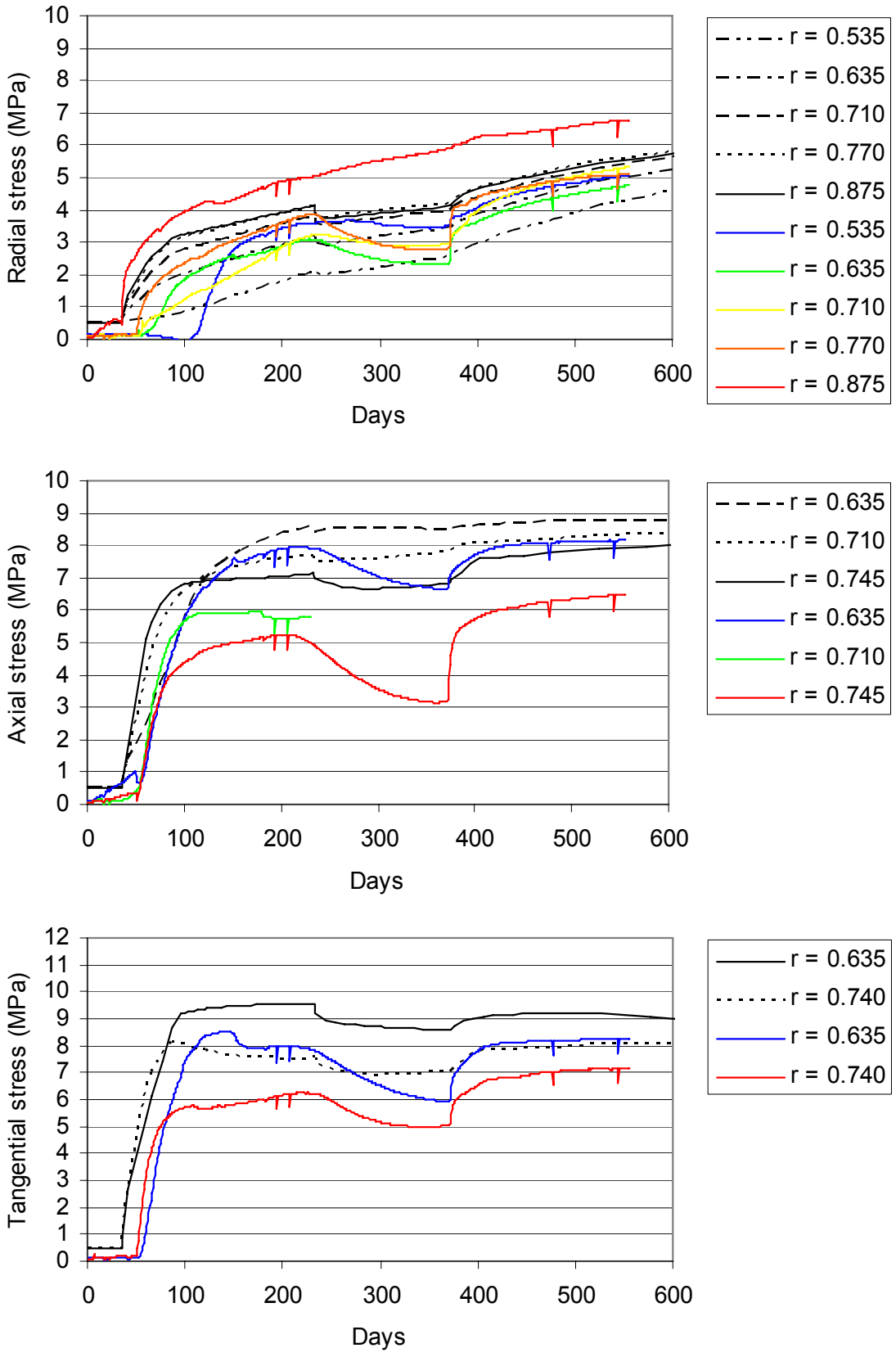

Figure 4-5. *Stress data from HM-model No 7 (black) and measured stresses (colored).*

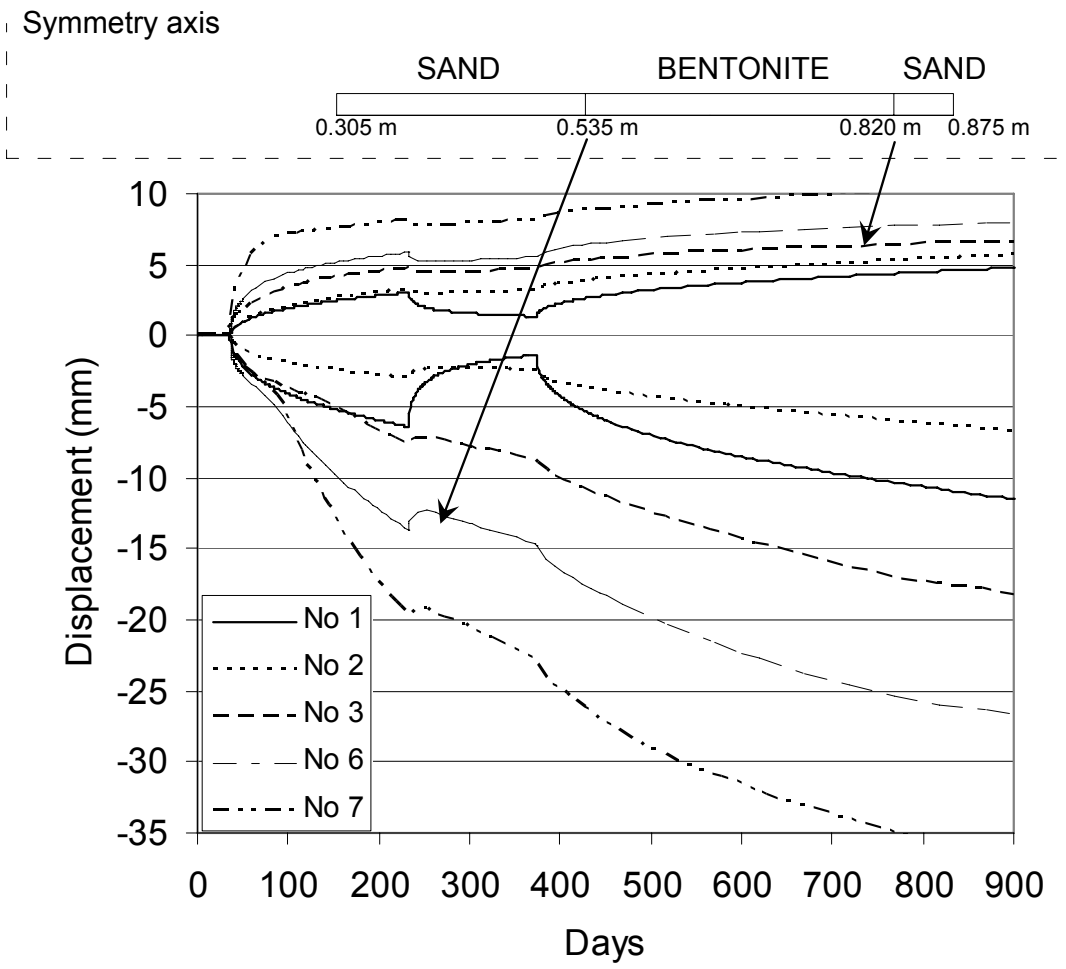

Figure 4-6. *Calculated displacements at inner and outer sand/bentonite interface.*

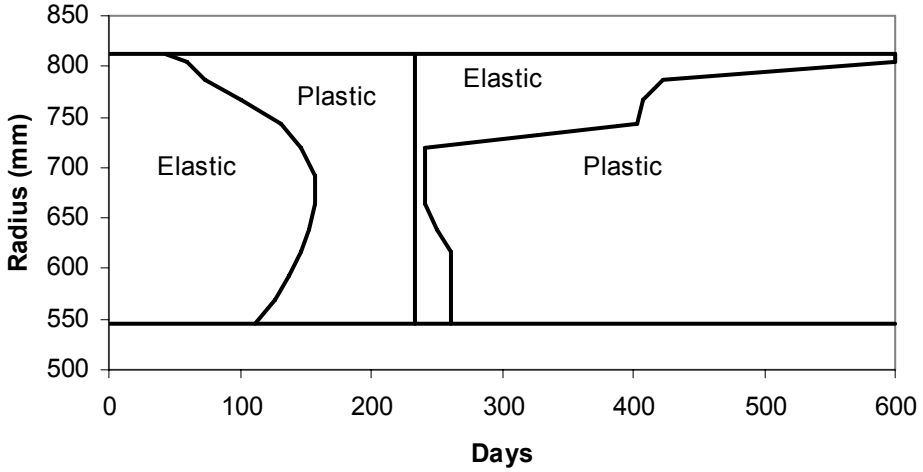

Figure 4-7. *Occurrence of elastic and plastic conditions in HM-model No 3.*

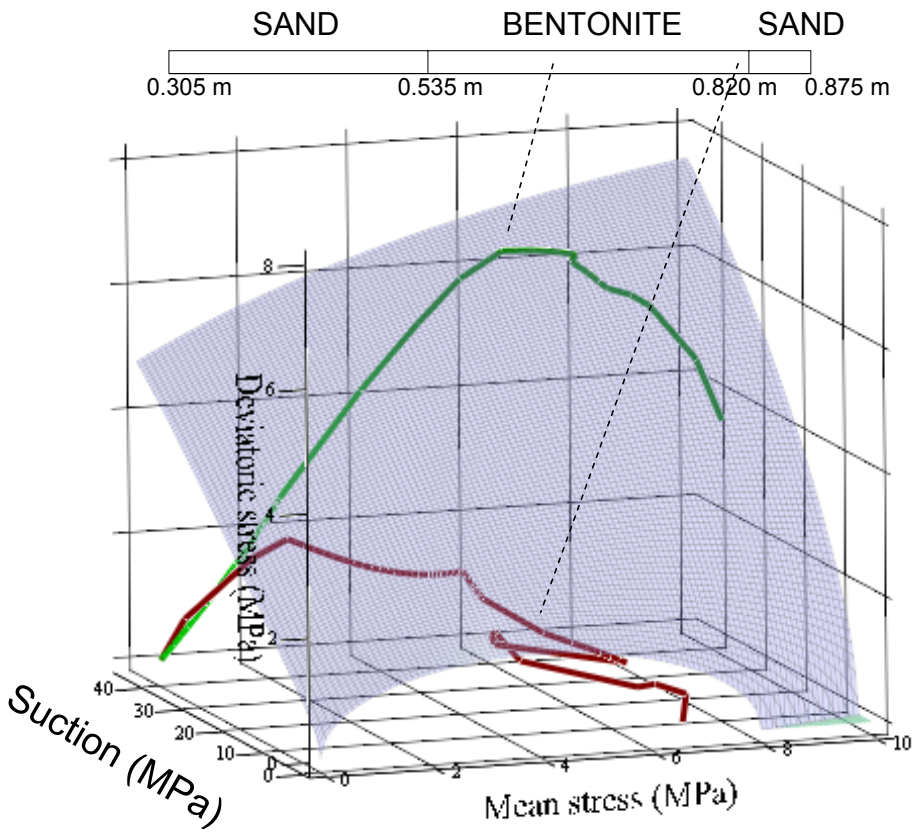

Figure 4-8. *Stress paths for HM-model No 3 in (s,p,q)-space with initial yield surface.*

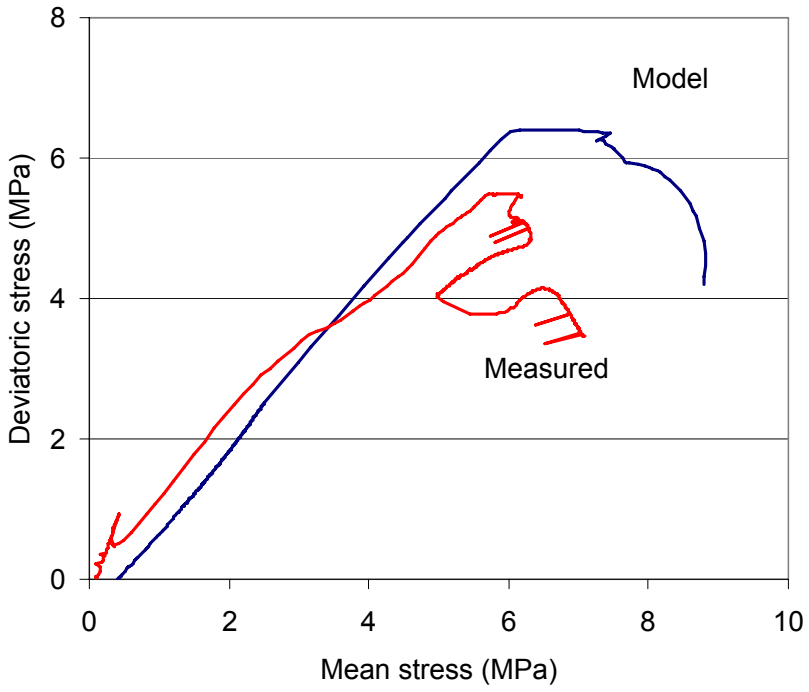

Figure 4-9. *Measured and calculated (No 3) stress path in (p,q)-plane at r= 0.635 m.*

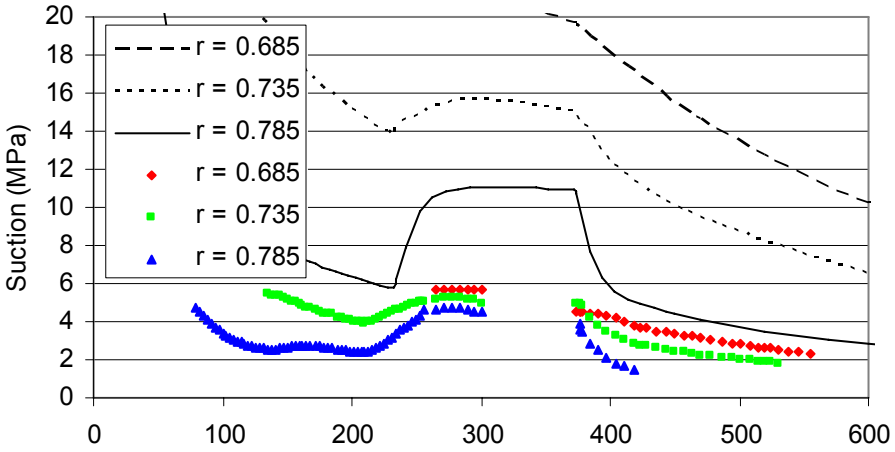

Figure 4.10. *Suction data from HM-model No 6 (black) and measured values (colored).*

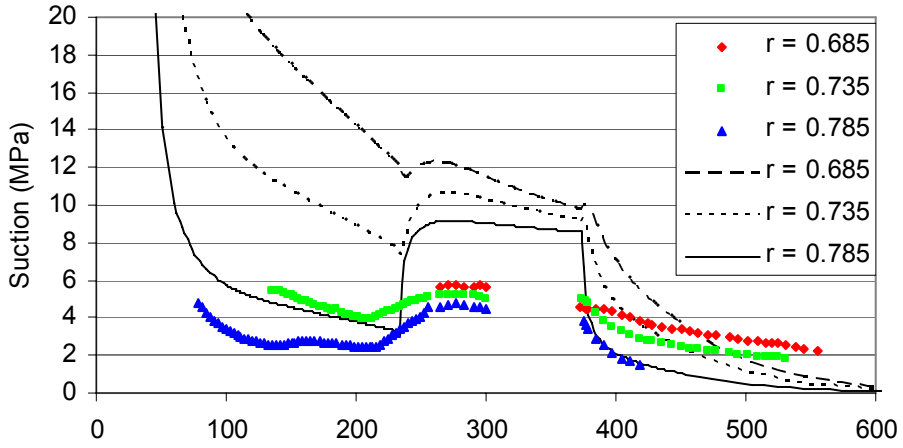

Figure 4-11. *Suction data from TH-model No 4 (black) and measured values (colored).*

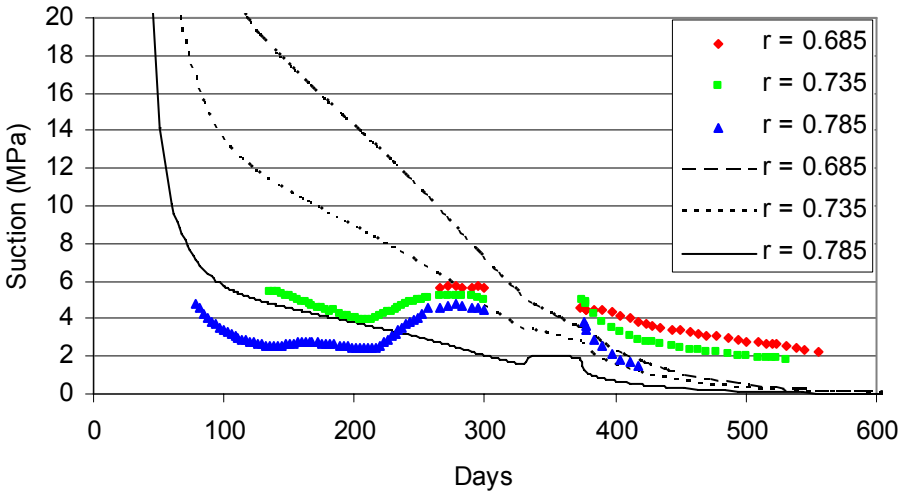

Figure 4.12. *Suction data from TH-model No 5 (black) and measured values (colored).*

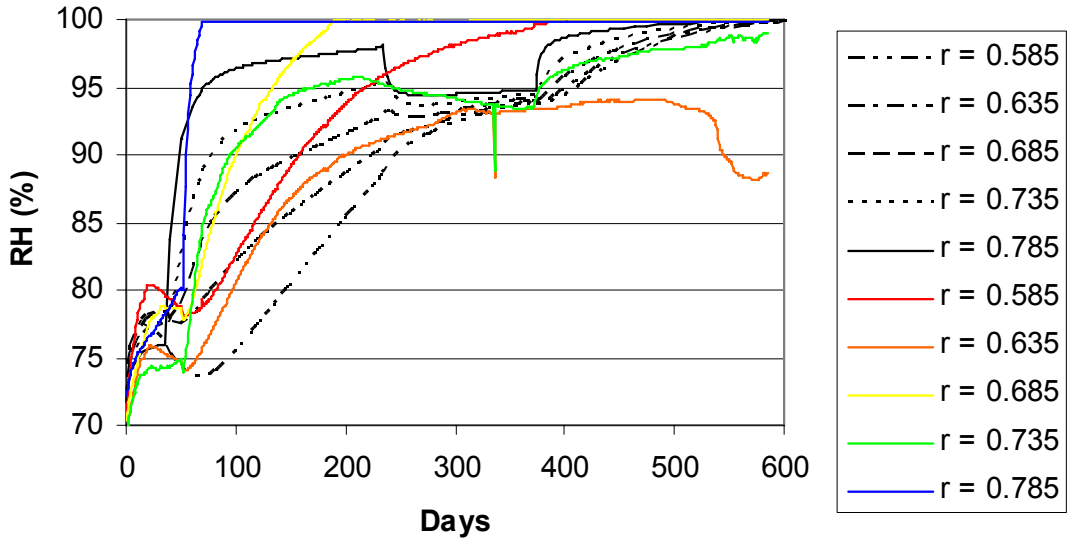

Figure 4-13. *Relative humidity data from TH-model No 4 (black) and measured values (colored lines).*

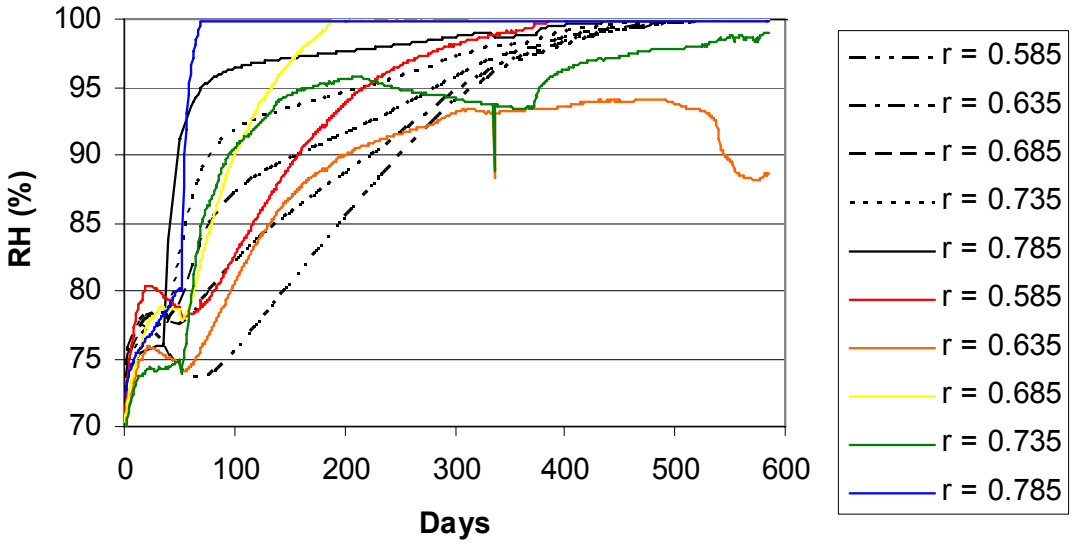

Figure 4-14. *Relative humidity data from TH-model No 5 (black) and measured values (colored lines).*

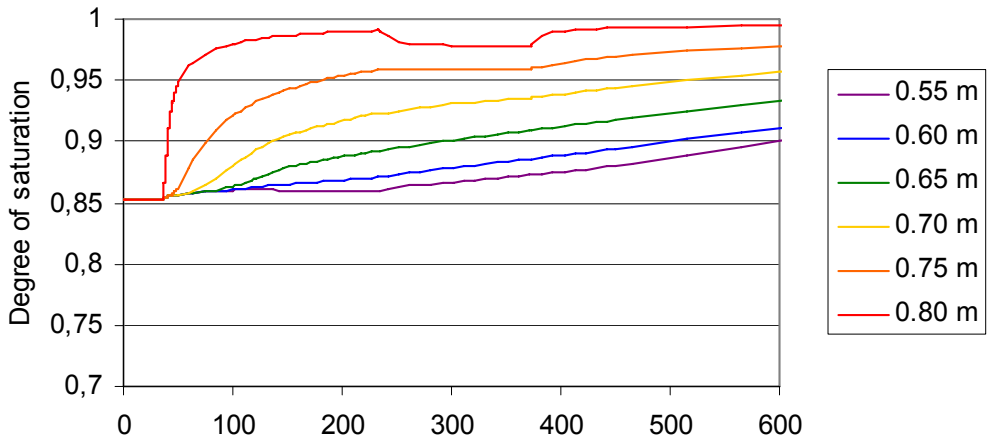

Figure 4-15. *Development of degree of saturation in HM-model (No 3).*

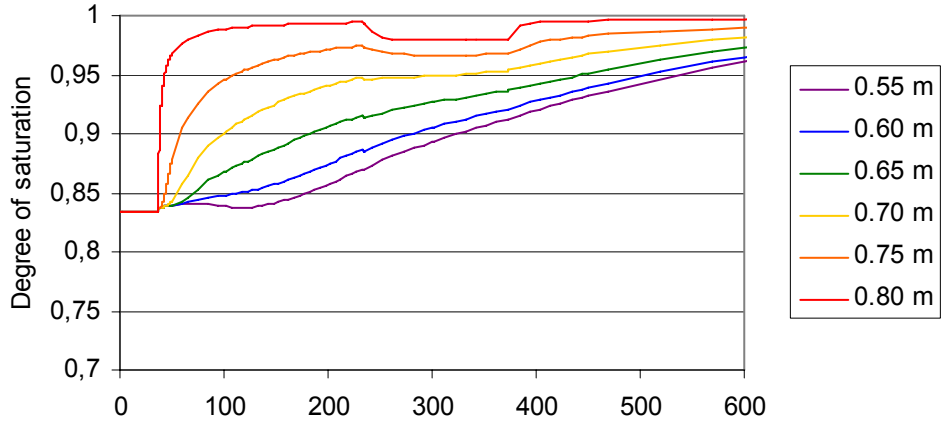

Figure 4-16. *Development of degree of saturation in HM-model (No6).*

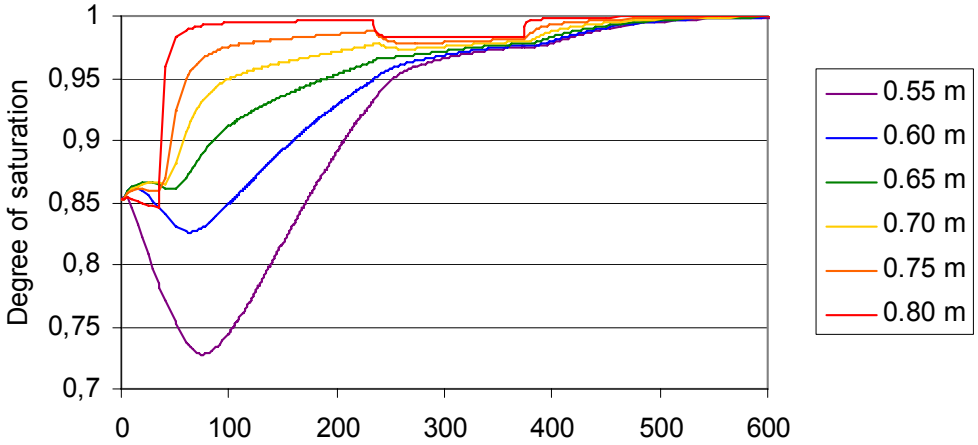

Figure 4-17. *Development of degree of saturation in TH-model (No 4).*

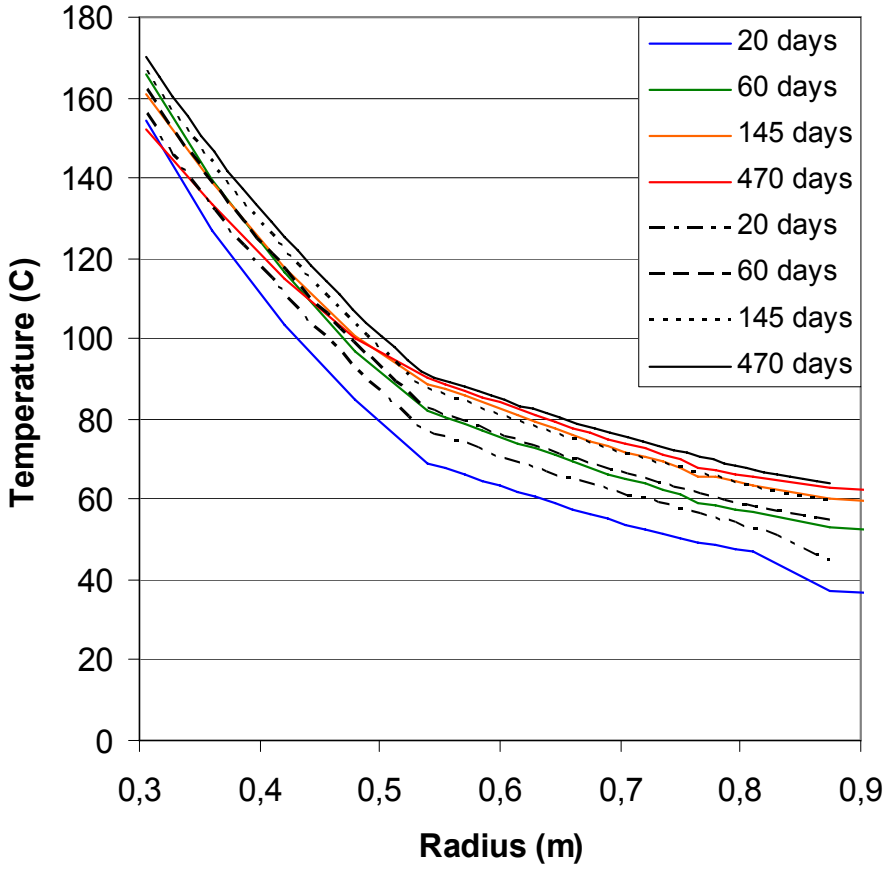

Figure 4-18. *Temperature scan lines TH-model No 4 (black) and experimental results (colored).*

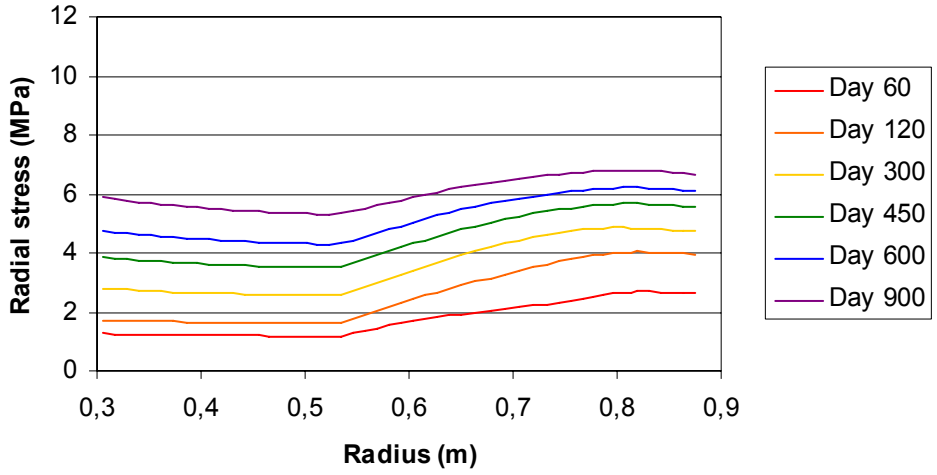

Figure 4-19. *Scan lines of radial stresses in HM-model No 3.*

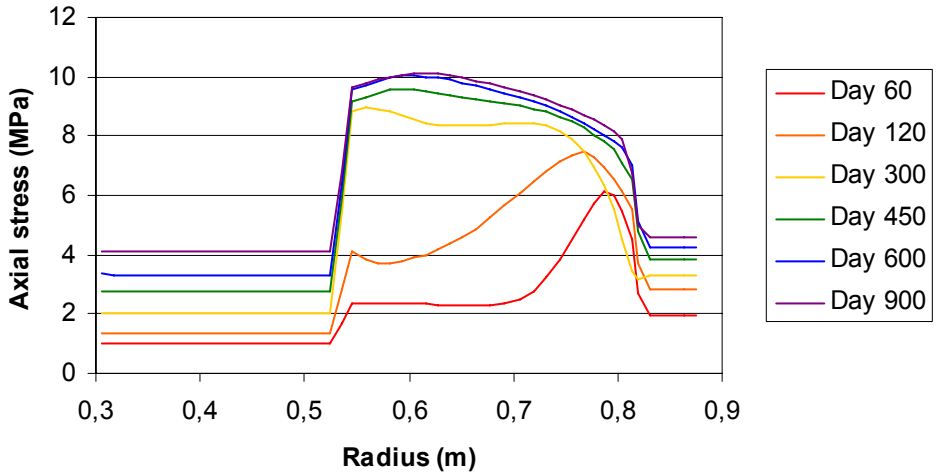

Figure 4-20. *Scan lines of axial stresses in HM-model No 3.*

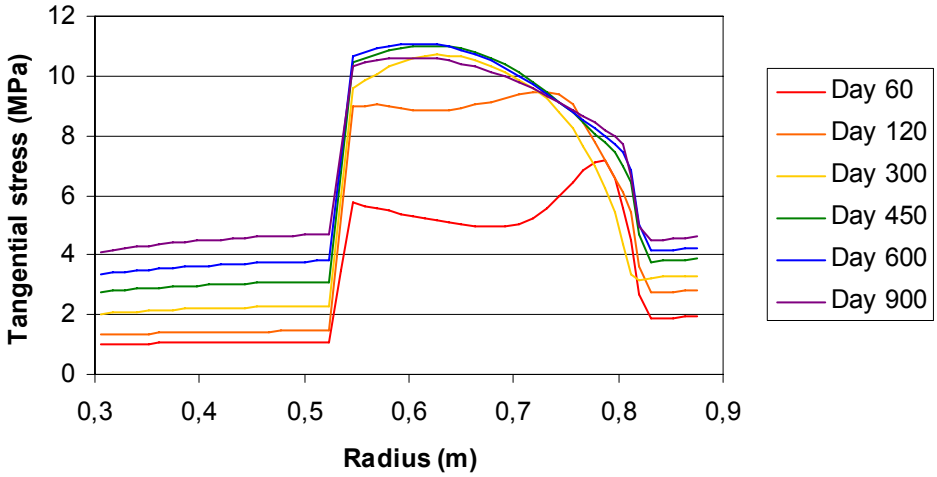

Figure 4-21. *Scan lines of tangential stresses in HM-model No 3.*

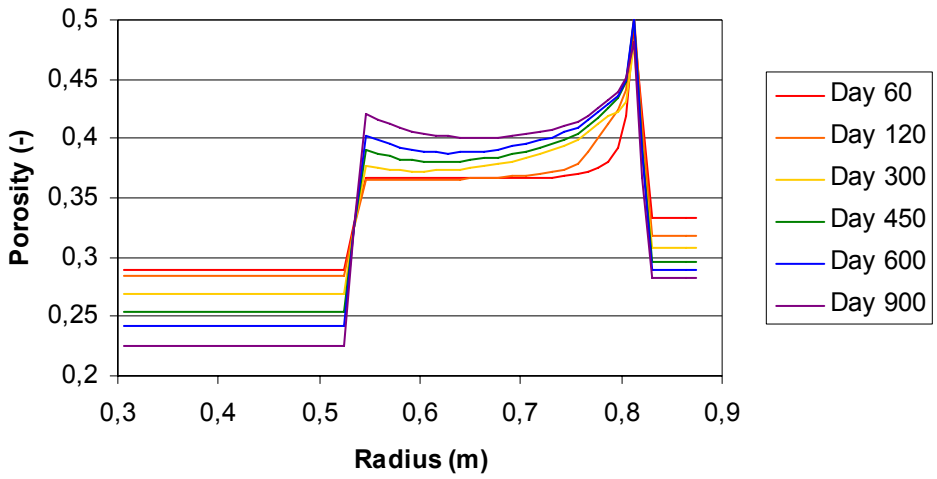

Figure 4-22. *Scan lines of porosity in HM-model No 3.*

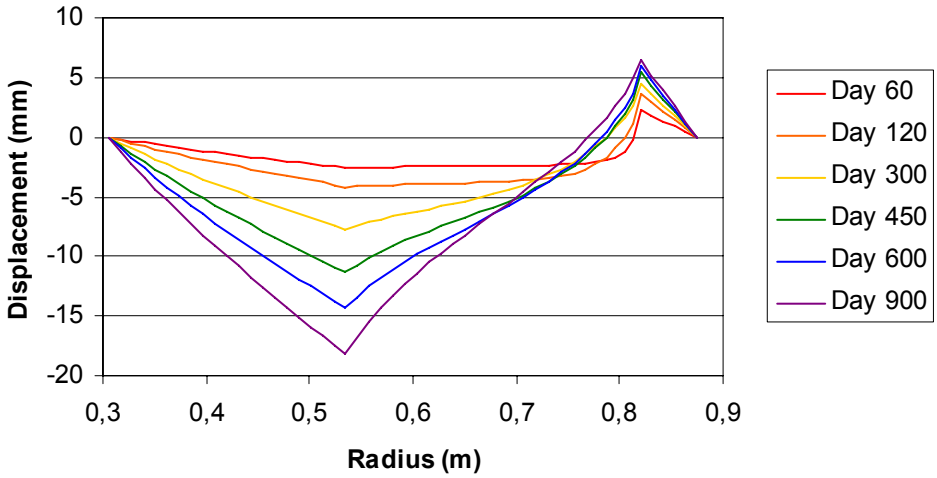

Figure 4-23. *Scan lines of radial displacements in HM-model No 3.*

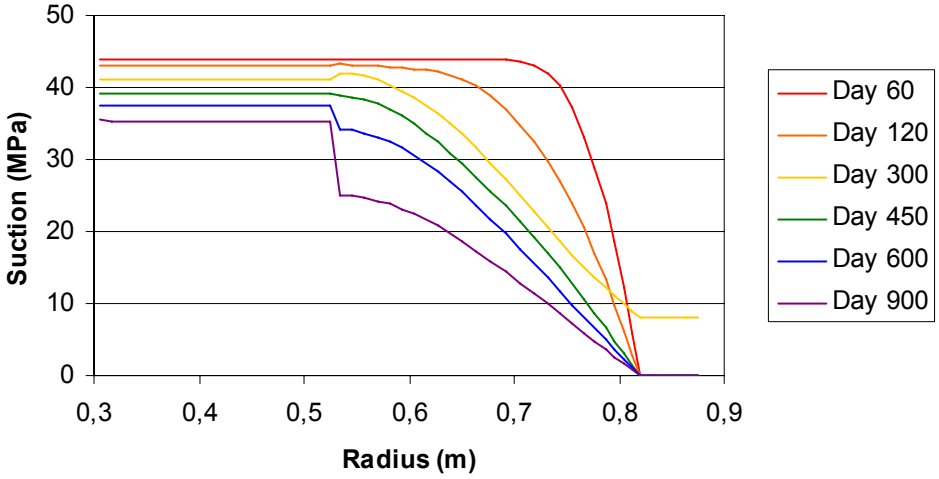

Figure 4-24. *Scan lines of suction in HM-model No 3.*

5 Conclusions & discussion

5.1 General

The phenomenon studied here was the loss of stresses and increase in suction observed in the bentonite surrounding the sand-shield around the upper heater from day 234 to day 373.

The stress/suction disturbance has recently been verified to be a result of the high flow resistance of the sand filter in general and the region around the lower injection points in particular. When the upper injection points were engaged around day 373, the stresses began to recover. From day 234 to day 373 the injected water did, apparently, not suffice to keep the upper parts of the sand filter saturated, i.e. at a pore pressure larger than atmospheric.

The decrease in boundary pressure at the level of rings 9 and 10 was translated into a hydraulic boundary conditions for two types of models: TH models without account of mechanical aspects and MH models without account of heat and gas transport.

Below, results obtained from the different types of models are discussed and compared.

5.2 Thermo-hydrodynamic processes

The TH models appear to capture the general outline of the experimental results regarding heating (Figure 4-18) and hydration (Figure 4-11 through 4-14). Some minor differences exist, e.g. regarding the temperature gradient in the shield and the apparent saturation of the outer parts. The thermal results could certainly be improved through calibration of the thermal conductivity of the shield. The three outer RH sensors indicate complete saturation during the first 400 days. This is not reproduced in the models, although the differences in RH are quite small.

The hydration in the HM models run at 20 °C differs significantly from the corresponding process in the TH models (compare Figure 4-15 and Figure 4-17). This difference can be reduced to some extent by increasing the temperature to the more realistic level of 70 °C (Figure 4-16). The effect on the speed of saturation should mainly be a result of the reduced water viscosity. Much of the remaining discrepancy can probably be attributed to thermal expansion of water in the TH models.

An important observation is that the bentonite around the upper heater at present (after about 600 days) appears to be close to full saturation (at heater mid-height). This is supported by both experimental and TH model data.

The intermediary dry period was first model as a liquid pressure boundary at -45 MPa. However, the TH models show, together with experimental suction results, that this boundary condition exaggerates the drying. Comparisons between calculated and measured suction values (Figure 4-11 and Figure 4-12) indicate that water is indeed lost from the model domain during the dry period, although even the level of 8 MPa sand filter suction is somewhat high. The most realistic boundary pressure level would perhaps be approximately 4 MPa of suction.

5.3 Mechanical processes

The hydro-mechanical models reproduced the *general development of stresses* fairly well. Among the HM models run at 20 °C these are best captured in model No 3 with a low value of Poisson's ratio and with a low yield surface that gives plastic deformations soon after test start (c.f. Figure 4-7). Examples are the pronounced trends with a rapid buildup and a subsequent cut-off of tangential stresses found in that model. The general level of radial stresses and the order of precedence with highest levels at the largest radius are also mimicked (see Figure 4-3).

These features are also found in the HM models run at 70 °C (No 6 and No 7), although model No 6 overestimates the level of stresses to some extent (see Figure 4-4). The last model analyzed (No 7) with a porous elastic sand model comes quite close to the measured level and trends (see Figure 4-5).

As noted by Ledesma *et al* /2004/, the measured stress paths in ring 9 indicate the development of plastic shear strains. The plasticity model used in models No 3, No 6 and 7 appears to reproduce this behaviour (see Figure 4-9) and therefore it seems to be clear that the plastic conditions play an important role in the hydro-mechanical evolution of the buffer around the sand shield.

Reductions of stresses during the dry period are best reproduced in model No 1, in which the "dry period" suction in the sand filter is set to 45 MPa (Figure 4-1). As described above, this level is probably too high. The stress reduction in the subsequent HM models, run at 8 MPa of sand filter suction, is much less pronounced. Indeed, in model No 2 and No 3, it is almost non-detectable. However, some improvement is obtained in the last models, run at 70° C, especially in model No 6.

The magnitude of stress reduction should be related to the degree of saturation, since, according to the laws of the thermo-elasto-plastic model used here, the suction-induced strain (in this case the shrinkage) is proportional to the ds/(s+0.1)-ratio. A more extensive saturation (such as in the TH models) would thus lead to a lower suction level and more suction-induced strain. It therefore seems that it would be possible to obtain realistic stress-losses with a fully coupled THM-model.

None of the models is capable of reproducing the observed *successive development of radial stresses*, with a rapid buildup in the outer parts and a delayed development in the inner parts. The closest resemblance is given by the model with a porous elastic sand model (No 7), although the measured abrupt buildup is not captured. The experimental results indicate that the evolution is different in different radial directions. An alternative approach could therefore be to extend the model to a plane horizontal 2D geometry and apply different hydraulic boundary conditions in different parts of the filter. This would be consistent with the notion of uneven supply of water around the sand filter.

The calculated *displacements* such as those presented in Figure 4-6 cannot be compared with empirical data until the experiment has been dismantled and spatial variations in void ratio have been examined. In general, the displacement magnitudes appear to be consistent with compression data given for the sand /Hökmark and Fälth, 2002/. The extensive narrowing of the ring during the dry period, especially the one found in model No 1, does however not seem to be relevant.

6 Final remarks

A number of unexpected results and events have been observed in the TBT experiment, especially around the upper heater:

- The difficulty of injecting water into the sand filter was first noticed and acted upon in April 2004. Obstructions appear to have emerged as early as day 100 when the rate of inflow was significantly reduced.
- From day 234 to day 373, the recorded developments of stresses and suction levels in Ring 9 reversed, with decreasing stresses and increasing suction levels.
- Finally, the recorded development of radial stresses in Ring 9 was distributed in time and did not coincide as in other sections.

A relationship between the first two points seems to be fairly well confirmed through the present work. It should therefore be clear that it was the limited access of water in the sand filter that caused the stress/suction disturbance in the bentonite.

The third point, i.e. the delayed successive development of radial stresses was not persuasively reproduced in any of the studied models. One explanation for this discrepancy can probably be that the used geometry is too simplified. The possibility that the chosen parameter values, or the conceptual models, differ from the actual processes should however not be excluded.

The models imply that water is lost from the problem domain during the period with stress/suction disturbance. This is modeled as a boundary condition in the sand filter with negative liquid pressure. The water is therefore forced to be lost outwards in the radial direction. An additional moisture escape route may be upwards into the less saturated bentonite above the studied section. Water would in that case move also in the axial direction. In order to capture this, the model would have to be extended considerably axially and probably have to include portions above and below the heater. With regard to the effects on stress, suction and saturation, such an approach would probably not differ qualitatively from the present work.

Finally, a few notes concerning the conceptual models. The TH processes have previously been investigated in detail and nothing new has in principle been included in this study. Mechanical processes, however, have not been modeled with Code_Bright on this scale previously at Clay Technology. It should be noted that apparently correct stresses do not necessarily imply relevant strains. Empirical data for displacements will however not available until the experiment is dismantled. The question of the validity of the mechanical parameter values and the conceptual models should therefore be addressed in more detail when information from the dismantling is available.

References

Börgesson L., Johannesson L.-E., Sandén T., Hernelind J., 1995. Modeling of the physical behaviour of water saturated clay barriers. Laboratory tests, material models and finite element application. SKB TR 95-20.

Goudarzi R., Börgesson L., Sandén T., Barcena I., 2003,2004. Temperature Buffer Test. Sensors data report (Period 030326-031001). Report No:1. SKB IPR-04-02

Hökmark H., Fälth B., 2002. Predictive Modeling Program. Clay Technology AB. Lund.

Hökmark H., Fälth B., 2003. Thermal dimensioning of the deep repository. Influence of canister spacing power, rock thermal properties and nearfield design on the maximum canister surface temperature. SKB TR-03-09.

Hökmark H., Fälth B., Åkesson M., 2004. TBT - Evaluation Modeling Program. Clay Technology AB. Lund.

Fälth B., Hökmark H., 2004. TBT - Evaluation Modeling. Clay Technology AB. Lund.

Kalbantner P., Johannesson L.-E., 2000. Hållfasthetsberäkningar för bentonitbuffert bestående av enaxligt kompakterade bentonitkroppar. SKB R-00-42.

Ledesma A., Chen G.J., Jacinto A., Velasco M., Huertas F., 2004. Temperature Buffer Test. Evaluation Modelling Performed by ENRESA.